#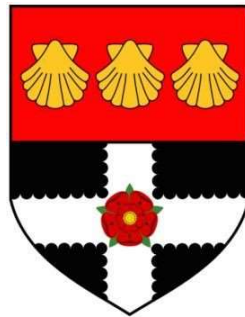 Developing a novel 3D platform for investigating the osteogenic differentiation and the anti-inflammatory potential of human mesenchymal stem cells and their secretome

Mesude Bicer

Thesis submitted for the Degree of Doctor of Philosophy

School of Chemistry, Food and Pharmacy
Department of Pharmacology

University of Reading

June 2021

To MH(TB)^2

Declaration of original authorship

I confirm that this is my own work and that the use of all material from other sources has been properly and fully acknowledged.

Mesude Bicer

Abstract

Osteoporosis and osteoporosis-associated fractures are one of the most prevalent global public health problems due to the rising population age. These diseases result in a large economic burden. The use of autologous mesenchymal stem cells (MSCs) is a potential therapeutic approach in in orthopaedics and dentistry as well in treatment of osteoporosis and osteoporotic fractures. However, both the number and the osteogenic potential of MSCs decrease with age. Recent research has suggested that osteogenic potential of MSCs can be positively affected by combining electrical stimulation (ES) and cultivation in 3D. Moreover, 3D cell culture has been shown to increase viability of MSCs and reduce cellular senescence.

Adipose-derived stem cells (ASCs) are an easily accessible and readily available type of MSCs and represent promising candidates for cell-based therapies for bone regeneration. This thesis investigated how cultivation of MSCs in different 3D scaffolds in combination with ES affects proliferation, osteogenic potential, as well as the anti-inflammatory potential of ASCs. To assess the optical properties of different scaffolds, absorbance spectra of different concentrations of anionic nanofibrillar cellulose (aNFC) were compared to other commonly used scaffolds, such as alginate and fibrin. Biocompatibility was studied by assessment of cellular viability using XTT and live/dead assays. Data analysis revealed that aNFC is highly biocompatible with ASCs whilst having low autofluorescence and light absorption allowing for easy monitoring of osteogenic differentiation using colorimetric and fluorescence-based methods. In subsequent experiments, the osteogenic potential of ASCs in aNFC was evaluated using RT-PCT, assessment of alkaline phosphatase (ALP) activity, analysis of calcification by Alizarin Red S staining and immunocytochemical staining against the osteogenic markers osteopontin (OPN) and osteocalcin (OCN). As an additional read-out, osteogenic differentiation was assessed by analysing intracellular calcium oscillation patterns. Osteogenic differentiation of ASCs in 3D aNFC resulted in a robust induction of osteogenesis related transcripts and down-regulation of stem cell marker expression. Moreover, ASCs subjected to differentiation in 3D showed high levels of mineralisation and an increased expression of OPN and OCN at protein level.

To study the impact of a combination of 3D cell culture and ES, ASCs in osteogenic and

standard media were exposed to electric fields for up to 21 days followed by analysis of osteogenic differentiation. When exposed to ES in 3D, ASCs showed high ALP activity and an increased calcium deposition evidenced by Alizarin Red S staining. Furthermore, exposure of ASCs to ES in 3D aNFC resulted in an increased expression of the osteogenic markers OPN and OCN and a rearrangement and alignment of the actin cytoskeleton.

Since the regenerative potential of ASCs at least partly depends on paracrine factors, the impact of the combination of ES and 3D cell culture on the anti-inflammatory potential of ASC-secretomes was assessed. The anti-inflammatory potential of ASCs secretomes in 3D was investigated by analysing the nuclear translocation of p65 in human fibroblasts exposed to tumour necrosis factor (TNF-α) using immunocytochemistry and confocal imaging. Additionally, luciferase reporter assays were performed to quantify TNF-α induced NF-κB activity in an established reporter cell line exposed to secretomes from 3D cultured ASCs with and without ES. 3D cell culture combined with ES resulted in an increase on the anti-inflammatory potential of ASCs secretomes from 3D aNFC.

Taken together, this thesis suggests that cultivation of ASCs in 3D aNFC can increase their viability without interfering with their osteogenic potential. Moreover, levels of osteogenic differentiation can be increased if 3D cultivation is combined with ES. Finally, both cultivation of ASCs and ES has positive effects on the anti-inflammatory potential of the ASC-secretome. The results presented in this thesis could pave the way for developing improved MSC-based strategies for bone regeneration in multiple clinical scenarios including but not limited to osteoporosis, osteoporotic fractures, regenerative dentistry, and regenerative orthopaedics. Future studies should investigate optimal experimental parameters (e.g., ES prior or after differentiation, alternative hydrogels) and include *in vivo* experiments (e.g., critical size defects in rodents and large animal models) to validate the promising *in vitro* findings presented in this thesis."

Following publications originated within the scope of the conferral of a doctorate:

*Included in this dissertation

1.*

Jonathan J. Sheard, Mesude Bicer, Yiming Meng, Alessia Frigo, Rocío Martínez Aguilar, Thomas M. Vallance, Donata Iandolo and Darius Widera (2019). Optically transparent anionic nanofibrillar cellulose is cytocompatible with human adipo tissue-derived stem cells and allows simple imaging in 3D. Stem Cells International Volume 2019, Article ID 3106929, 12 pages; https://doi.org/10.1155/2019/3106929

2.*

Mesude Bicer, Jonathan J. Sheard, Donata Iandolo, Samuel Y. Boateng, Graeme S. Cottrell and Darius Widera (2020). Electrical Stimulation of Adipose-Derived Stem Cells in 3D Nanofibrillar Cellulose Increases their Osteogenic Potential. Biomolecules 2020, 10(12), 1696; https://doi.org/10.3390/biom10121696

3.*

Mesude Bicer, Graeme S. Cottrell and Darius Widera (2021). Impact of 3D cell culture on bone regeneration potential of mesenchymal stromal cells. Stem Cell Research & Therapy 12, Article number: 31; https://doi.org/10.1186/s13287-020-02094-8

4.*

Enrico C. Torre, Mesude Bicer, Graeme S. Cottrell, Darius Widera and Francesco Tamagnini (2021). Adipogenic but not osteogenic differentiation progressively reduces intracellular calcium oscillations in mesenchymal stem cells

(in preparation)

Acknowledgement

I would first like to thank and acknowledge my supervisors, Dr Darius Widera and Dr Graeme Cottrell for not only giving me the opportunity to conduct this work, but also for guiding me through this project. I wish to thank them for helping me to take ownership of my work and form my own thoughts, as I continue to learn during this PhD. It has been a pleasure to work in their lab. I was lucky to have both supervisors who always had time to help me brainstorm and support me both personally and academically with the research. I would not have succeeded without your wisdom, knowledge and dedication, so I am truly grateful to have worked in your team. I have had so many opportunities to share my research with the public due to publications. Those opportunities were exciting and rewarding parts of my PhD so many thanks for your effort and help me to share science with others.

I would like to say a huge thank you to Dr Graham Luke who have contributed his time to give me excellent training for the vital knowledge, skills and techniques. I am also very grateful for the support from all other members of Widera Lab. All of them are a creation of the corner therapy and been a sounding board for my ideas to my research throughout my PhD. I thank Jonathan Sheard and Enrico Torre for their contribution to the papers as well as Karin Müller from the Cambridge Advanced Imaging Centre (CAIC) for her technical support with the scanning electron microscopy. I would also like to say a huge thank you to my colleagues and friends in the Hopkins and Harborne buildings, who each made the University of Reading a happy place to work.

I would like to say the excessive thank you of all to my wonderful family Mr. and Mrs. Bicer for their endless love and emotional support throughout. I wish to thank my dear Fatih Caliskan for always being there, cheering and supporting me on. I also wish to express my deep gratitude to the Ministry of National Education of the Republic of Turkey for the funding to complete my research. Without which, this would not have been possible. Finally, it is so easy to look back on things with rose-tinted glasses. So, I have put this acknowledgement because it will remind me of what looking forward in the future whenever I look this dissertation with reached triumph step by step.

Table of Contents

List of Figures

List of Tables

List of Supplemental Information

List of Abbreviations

2D	Two-dimensional
3D	Three-dimensional
AF-MSCs	Amniotic fluid-derived mesenchymal stem cells
ALP	Alkaline phosphatase
aNFC	Anionic nanofibrillar cellulose
ANOVA	Analysis of variance
ASCs	Human adipo-derived mesenchymal stem cells
bFGF	Basic fibroblast growth factor
BMP	Bone morphogenetic protein
BSA	Bovine serum albumin
BSP	Bone sialoprotein
$CaCl_2$	Calcium chloride
Calcein AM	3',6'-Di(O-acetyl)-2',7'-bis [N, N-bis (carboxymethyl) aminomethyl] fluorescein, tetraacetoxymethyl ester
cDNA	Complementary deoxyribonucleic acid
CHACC	Coralline hydroxyapatite/calcium carbonate
cm	Centimetre
CM	Conditioned media
CPC	Calcium phosphate cements
DAPI	4',6 diamidino-2-phenylindole
DMEM	Dulbecco's modified Eagle's media
DNA	Deoxyribonucleic acid
dNTP	2'-deoxynucleoside 5'-triphosphate
DPBS	Dulbecco's phosphate buffered saline
DPHC	Diphlerothohydroxycarmalol
ECM	Extracellular matrix
EDTA	Ethylenediaminetetraacetic acid
ERK	Extracellular signal-regulated protein kinase
FBS	Foetal bovine serum
FGF	Fibroblast growth factor

FITC	Fluorescein isothiocyanate
G	Gauge (needle gauge)
GAPDH	Glyceraldehyde 3-phosphate dehydrogenase
GFP	Green fluorescent protein
H	Hour (s)
HA	Hydroxyapatite ($Ca_{10}(PO_4)_6(OH)_2$)
hESC	Human embryonic stem cell
HEPES	N-(2-hydroxyethyl) piperazine-N-(2-ethane sulfonic acid)
HGF	Hepatocyte growth factor
hUCMSC	Human umbilical cord mesenchymal stem cell
Hz	Hertz
ICC	Immunocytochemistry
IFNγ	Interferon γ
IGF	Insulin-like growth factor
IgG	Immunoglobulin G
InsP3R	Inositol-1,4,5-trisphosphate receptor
iPSC	Induced pluripotent stem cell
JNK	c-Jun N-terminal kinase
kHz	Kilohertz
MAPK	Mitogen activated protein kinase
$MgCl_2$	Magnesium chloride
min	minute (s)
mL	Millilitre
mM	Millimolar
mRNA	Messenger ribonucleic acid
MSCs	Mesenchymal stem cells
NFκB	Nuclear factor kappa-light-chain-enhancer of activated B cells
NFC	Nanofibrillar cellulose
NHDF	Normal human dermal fibroblast
Nm	Nanometre
nM	Nanomolar
OCN	Osteocalcin

ONJ	Osteonecrosis of the jaw
OPN	Osteopontin
Pa	Pascal
PBS	Phosphate buffered saline
PCR	Polymerase chain reaction
PDGF	Platelet-derived growth factor
PEG	Poly (ethylene glycol)-based
PFA	Paraformaldehyde
PG	Prostaglandins
PLGA	Poly (lactic-co-glycolic acid)
PPARγ	Peroxisome proliferator-activated receptor gamma
PRP	Platelet-rich plasma
PTH	Parathyroid hormone
RANKL/M-CSF	Receptor activator of nuclear factor kappa-B ligand/macrophage colony- stimulating factor
RNA	Ribonucleic acid
RNase	Ribonuclease
rpm	Rotations per minute
RT	Reverse transcription
Runx2	Runt-related transcription factor 2
s	Second(s)
SDF	Stromal cell-derived factor
SEM	Scanning Electron Microscope
SOST	Sclerostin antibody
TGF-β	Transforming growth factor beta
UV	Ultraviolet
V	Volt
VEGF	Vascular endothelial growth factor
μg	Microgram
μL	Microlitre
μm	Micrometer
μM	Micromolar

v/v   Volume per volume

w/v   Weight per volume

Chapter 1

Introduction

1.1. General Introduction

As populations age across the world, osteoporosis and osteoporosis-related fractures are becoming the most prevalent degenerative bone diseases (Loeser et al., 2012). More than 75 million patients suffer from osteoporosis in the US, the EU and Japan (Iandolo et al., 2020). Furthermore, it is anticipated that the number of patients affected by osteoporosis will increase by a third by 2050 (Iandolo et al., 2020). Bone regeneration is a desired clinical outcome in patients with skeletal abnormalities (Einhorn, 1998, Cho et al., 2002). Bone regeneration is also important in orthopaedic surgery and in oral and maxillafacial surgery, as well as in skeletal reconstruction of large bone defects created by trauma, infection and tumour resection. In addition, efficient strategies for bone regeneration are required in conditions where fracture healing and regenerative processes are compromised, such as avascular necrosis, atrophic non-unions, and osteoporosis (Dimitriou et al., 2011a).

Although conventional therapies including calcitonin and oestrogen-like drugs can be used to treat bone degenerative diseases, they can be associated with some side-effects including the development of oesophageal cancer, ocular inflammation and severe musculoskeletal pain (Kennel and Drake, 2009). As an alternative therapeutic agent, parathyroid hormone therapy (PTH) and bisphosphonates have recently been developed to increase bone mineral density and to reduce the risk of bone fracture. Despite their positive effects on the osteoblast-mediated bone formation, PTH therapy leads to drawbacks including headaches, injection-site tenderness and nausea (Lou et al., 2019), and bisphosphonates also cause the osteonecrosis of the jaw (Kennel and Drake, 2009). However, these side effects are not very common and can be avoided.

Stem-cell therapy is a cell-based therapy option for bone defects because stem cells have abilities to different into multiple lineages including bone cells (McClelland Descalzo et al., 2014). As of July 2020, more than 1100 clinical trials utilising MSCs have been registered on ClinicalTrials.gov with a wide indication profile including cardiovascular diseases, diabetes and musculoskeletal symptoms. However, of these, only three clinical trials have been registered with the indication 'osteoporosis'. Notably, as one Phase 2 clinical trial is recruiting, one trial terminated and only one Phase 1 trial

completed, there are not enough data available to evaluate the efficacy and safety of MSCs in this clinical scenario.

In addition to autologous bone grafts, stem cell therapy can equally be involved in other surgical approaches including allograft implantations and free fibula vascularised grafts (Spin-Neto et al., 2011). Even though the use of autologous stem cells is currently seen as a promising technique, there are still some drawbacks including an intervention-induced inflammation and a high risk of morbidity (Pape et al., 2010). Another alternative approach is to mobilize endogenous stem cells for enhancing tissue regeneration. A rapidly mobilization of endogenous stem cells is an effective strategy for delivery of stem cells to home to the site of injury for bone fracture healing (Toupadakis et al., 2013). Notably, osteoporosis can cause a decrease in the numbers of MSCs and lower their osteogenic differentiation potential (Saito et al., 2018, Tan et al., 2015, Wang et al., 2014c). To overcome this problem, stem cells have recently been combined with biomaterials to improve their viability and to boost their osteogenic potential. In this context, a variety of substrates have been developed including natural, synthetic, metal and nanoparticle-based materials (Fernandez-Yague et al., 2015, Hussey et al., 2018). In this opening chapter, the current 3D cell culture techniques used to expand and differentiate MSCs and assess how 3D cultivation affects their osteogenic differentiation potential will be discussed.

1.2. Overview of bone remodelling

1.2.1. Bone degeneration

Bone remodelling is a continuous cycle of degeneration and regeneration involving osteoblasts (bone-forming cells) and osteoclasts (cells which absorb bone tissue) (Figure 1.1) (Chang et al., 2019). If the balance between bone formation and bone resorption is lost, the bone becomes vulnerable to osteoporosis (Jimi et al., 2012).

Figure 1.1. Bone remodelling and degeneration. The dynamic relationship between osteoblasts and osteoclasts is primarily regulated by a fine balance between bone formation and bone resorption. With increasing age, the balance shifts towards higher levels of osteoclast activation with reduced osteoblast differentiation, thereby impairing the regenerative potential of the bone resulting in structural deterioration of the bone tissue and reduced bone strength.

Osteopenia is a condition involving low bone mass and it is strongly associated with increased bone resorption combined with reduced bone regeneration (Li et al., 2016a) and mostly affects postmenopausal women (Johnell and Kanis, 2006). A T-score based on bone density levels is recommended by the World Health Organization. Differences between a bone mineral density and that of the healthy norm are measured. A T-score between -1 and -2.5 SD indicates low bone mass. A T-score of -2.5 SD or lower indicated an increased risk of osteoporosis. Osteoporosis does not only affect postmenopausal women, but also other patient groups. Factors that increase the risk of developing osteoporosis in both female and male include cigarette smoking, excessive alcohol and caffeine consumption, lack of exercise, vitamin D deficiency and long-term use of corticosteroids (Ross, 1996).

The modulation of oestrogen/hormone therapy is an intriguing method for suppressing apoptosis of osteoblasts as oestrogen plays an active role in the osteoblast-osteoclast coupling. Specifically, oestrogen regulates osteoblast survival and suppresses cellular apoptosis (Bradford et al., 2010). The onset and development of osteoporosis are related to the life span of osteoblasts. Oestrogen plays a role in the reduction of apoptotic gene expression in osteoblasts (Bradford et al., 2010). In conjunction with the direct effects of oestrogens on bone-forming osteoblast, oestrogen contributes to the acute inhibition of caspase-3 activity via intrinsic and extrinsic pathways (Boehning et al., 2004). Oestrogen can also suppress apoptosis-related genes, including the type 1 inositol-1,4,5-trisphosphate receptor (InsP3R) (Li et al., 2007, Orrenius et al., 2003). Nuclear oestrogen receptors (ERα and ERβ) and androgen receptors (AR) are likely to be directly related to the process of bone remodelling, as well as indirectly via modulating the levels of interleukin-6 (IL-6) (Galien and Garcia, 1997). Interestingly, in women with post-menopausal osteoporosis, osteoblasts express higher levels of the inflammatory receptor Fas, which can induce Fas ligand-induced cell death (Xing and Boyce, 2005).

Within the bone remodelling cycle, osteoclasts are regulated by several hormones and by local factors (Demontiero et al., 2012). For example, in secondary hyperparathyroidism, calcium and vitamin D deficiency can trigger bone loss (Demontiero et al., 2012). Vitamin D plays an essential role for calcium absorption in bone mineralisation. Vitamin D binds to vitamin D receptors thereby increasing expression levels of the receptor activator for nuclear factor kappa-B ligand (RANKL) in the plasma membrane. This in turn increases uptake of calcium into the cells and improves its absorption (Holick, 2006, Khosla, 2001). RANKL is also a critical mediator in bone homeostasis, which is involved in both bone formation and bone resorption. RANKL is released by osteoblasts and plays important role to stimulate RANK on the surface of stem cells and thus, promote bone resorption by releasing osteoclasts (Ray, 2018). The decrease in calcium absorption promotes a high level of parathyroid hormone (PTH) secretion, which is responsible for osteoclastic activity with cortical bone loss (Lips, 2001). Moreover, oestrogen deficiency and low levels of gonadal sex steroid result in an increasing PTH level in aging people (Khosla et al., 2001). Oestrogen has two potential roles in regulating osteoclasts. Briefly, it decreases osteoclast cell

differentiation by suppressing the receptor activator of nuclear factor kappa-B ligand/macrophage colony-stimulating factor (RANKL/M-CSF) signalling (Mitnick et al., 2001) and indirectly blocks the production of the bone-resorbing cytokines IL-1β, IL-6, tumour necrosis factor-α (TNF-α), M-CSF and prostaglandins (PG) (Charatcharoenwitthaya et al., 2007).

A number of studies have shown that growth factors, including transforming growth factor (TGF-β), Wnt3a and Indian hedgehog (Ihh), and signalling molecules such as Smad3, β-catenin and Hypoxia-inducible factor (HIF)-2α play important roles in cartilage degeneration in osteodegenerative diseases (Yang et al., 2001, Zhu et al., 2009, Lin et al., 2009, Saito et al., 2010). The loss of TGF-β signalling correlated with Smad3 promotes increased bone defects in osteoarthrosis patients (Valdes et al., 2010). β-catenin is a significant molecule supported by the canonical Wnt signalling pathway and the loss of β-catenin from preosteoblasts also leads to decreased bone mass induced by the wnt/ β-catenin signalling pathway (Assis-Ribas et al., 2018). Consistent with Smad3 and β-catenin, HIF-2α expression encourages the upregulation of nuclear factor kappa-light-chain-enhancer of activated B cells (NFκB) signalling for bone destruction (Yang et al., 2010). Ihh signalling is associated with induced cartilage degradation and Ihh inhibitor can be used a therapeutic agent to prevent this (Lin et al., 2009). Ihh signalling is essential in endochondral ossification and osteoblast differentiation in the perichondrium. The interaction between Ihh and Wnt signalling promotes endochondral bone formation and synovial joint formation. When Ihh signalling is disrupted, bone diseases such as progressive osseous heteroplasia can occur (Yang et al., 2015).

Amyloid β peptide (Aβ) is another pathological hallmark in osteoporotic bone fracture, correlating with osteoclast activation (Li et al., 2014a). RANKL activates NFκB and promotes calcium oscillations for osteoclast activation (Asagiri and Takayanagi, 2007). NFκB activation is an early signalling step in osteoclastogenesis (Abu-Amer, 2013) whereas calcium oscillations induce bone resorption by stimulating osteoclast differentiation (Kajiya, 2012). The extracellular signal-regulated protein kinases (ERKs) are both isoforms, ERK1 and ERK2, and are implicated in the activation of osteoblast-lineage (Kim et al., 2019). Aβ induces osteoclast differentiation through NFκB, ERK

signalling and calcium oscillation (Li et al., 2016a). Given the complex nature of osteoporosis, therapeutic interventions represent a major clinical need.

1.2.2. Current therapeutic options and their limitations

The prevention of osteoporosis is supported by maximising bone health. Nonpharmacological management of disease includes adequate calcium and vitamin D intake, smoking cessation, weight-bearing exercise, limitation of alcohol and caffeine consumption (Office of the Surgeon, 2004, Tosteson et al., 2008, Das and Crockett, 2013). In recent years, alternative approaches to treating bone degeneration have been developed. These techniques range from systemic pharmacological approaches to surgical procedures.

The main aim of pharmacological therapy is to reduce the risk of bone fractures (Office of the Surgeon, 2004). Bisphosphonates (BPs) are recommended as a first-line option for the treatment of osteoporosis in postmenopausal women and men (Camacho et al., 2016, Watts et al., 2012). BPs are commonly used for the treatment of osteoporosis as they have the potential to suppress osteoclast formation (Kwak et al., 2009, Nishikawa et al., 1996), which can disrupt osteoblast/osteoclast coupling. The action of BPs promotes apoptosis of osteoclastic cells that induce bone resorption. BPs can bind to hydroxyapatite (HA) binding sites to restrain the osteoclast accumulation and inhibit the breakdown of HA, and thus suppressing bone resorption (Drake et al., 2008). However, a negative effect of BPs is that they rarely cause osteonecrosis of the jaw (ONJ) (Florencio-Silva et al., 2015, Sims and Martin, 2015).

Prior to 2002, one of the most common therapies prescribed for osteoporosis was hormone replacement therapy (HRT). In 2002, however, it was reported that HRT increases the risk of breast cancer and heart disease and as a result fewer people have been prescribed HRT (Isaksson et al., 2002). In addition to prescribing HRT for female patients with osteoporosis, post-menopausal women were advised to take oestrogen to prevent the loss of bone density (Demontiero et al., 2012).

Currently, the main therapeutic agents for treating osteoporosis include anti-resorptives such as HRT, selective oestrogen-receptor modulators (SERMs) and RANKL antibodies (Table 1.1). An ideal pharmacological intervention for treating bone loss should suppress osteoclastic activity and enhance osteoblast-mediated bone formation (Demontiero et al., 2012). A humanised monoclonal antibody (denosumab) has recently been developed to inhibit osteoclastic differentiation by preventing RANKL from binding to its receptor (Demontiero et al., 2012). Long-term administration of denosumab has been shown to have a positive effect not only on the prevention of fragility fracture, but also on the amelioration of joint damage in osteoporotic patients (Cummings et al., 2009). However, denosumab is also linked to a risk of hypocalcaemia and a risk of ONJ (de Sales Lima et al., 2018).

Table 1.1. Current pharmacological approaches to treating osteoporosis

Compound	Advantages	Adverse effects	Osteogenic differentiation	Reference
Bisphosphonates	Decrease fractures	Gastrointestinal tract symptoms (nausea, esophagitis)	↑	(Cosman et al., 2014)
Selective oestrogen-receptor modulators (SERMs)	Decrease fractures, Increase bone mineral density (BMD)	*Urogenital symptoms, Deep vein thrombosis, Cardiovascular diseases*	No effect	(MacLean et al., 2008)
Parathyroid hormone (PTH)	Decreases fractures	*Injection donor reaction, leg cramps, dizziness, nausea*	↑	(Cosman et al., 2014)
Calcitonin	Decreases fractures, Prevents BMD loss	*Epistaxis, Rhinitis*	No effect	(Muñoz-Torres et al., 2004)
Oestrogen/Hormone therapy	Decreases BMD loss, Decreases fractures	Increases the risk of venous thromboembolism and cardiovascular disease after menopause	↑	(Cosman et al., 2014)
Vitamin D supplementation	Decreases bone turnover, Decreases fractures, Increases BMD	Increases the risk of cardiovascular disease	↑	(Lips and van Schoor, 2011)
Denosumab	Reduces the risk of fracture, Increases BMD at the lumbar spine	Gastrointestinal tract symptoms, Dermatitis, Back and Limb pain, Hypercholesterolemia, Rash, Headache, Hypocalcaemia,	No effect	(Cummings et al., 2009)
Cathepsin K inhibitor	Increases bone mass, bone microarchitecture, strength	Increases the number of cells of osteoclast lineage	No effect	(Duong le et al., 2016)
Sclerostin (SOST) antibody	Bone density and strength, Fracture risk reduction	-	↑	(Ominsky et al., 2017)
Interferon γ	Increases bone mass, Bone strength	Gastrointestinal tract symptoms	↑	(Duque *et al.*, 2011)

As an alternative pharmacological treatment option, PTH has been explored for treating severe osteoporosis in post-menopausal women and men with osteoporosis. A systematic review of PTH for the treatment of osteoporosis showed that PTH increases bone mineral density and reduces the risk of fractures by decreasing osteoblast apoptosis and enhancing the differentiation of osteoblasts from pre-osteoblasts thereby inducing new bone deposition (Cranney et al., 2006). Despite this, the disadvantages of PTH therapy include headaches, injection-site tenderness and nausea in osteoporotic patients (Lou et al., 2019).

A sclerostin (SOST) antibody and interferon γ (IFNγ) also have potential therapeutic uses to promote osteoblastic differentiation (Demontiero et al., 2012). SOST antibody plays a pivotal role in modulating osteoblastic activity and bone formation by inhibiting Wnt/β-catenin signalling (McClung, 2017). Currently, SOST is being evaluated multiple preclinical studies and multiple published clinical trials for management of osteoporosis (MacNabb et al., 2016). At present, SOST-binding monoclonal antibody (Romosozumab) is in clinical use in four countries such as Japan, South Korea, Australia and Canada. In Europe, the approval of Evenity that is the registered trade name of romosozumab, is still pending the final decision of the European Medicines Agency (Kerschan-Schindl, 2020). IFNγ can be used as an effective anabolic treatment for osteoporosis, as IFNγ is secreted in the bone microenvironment by MSCs to promote osteogenic differentiation (Duque et al., 2011). However, there are some risks and disadvantages of local interferon therapy for bone loss, such as gastrointestinal tract symptoms (Duque et al., 2011).

In addition to these pharmacological options, surgical procedures are recommended to be used in the clinical management of osteoporosis (e.g., treatment of bone fracture). These surgical techniques include autologous bone grafts, allograft implantations and free fibula vascularised grafts (Spin-Neto et al., 2011). In surgical practice, the different types of autologous bone grafting including cancellous bone graft, cortical bone graft, autologous bone marrow aspirates and vascularized cortical bone graft, are used in the management of certain bone defects and non-unions. Although the biologic properties of bone grafting are essential for new bone formation, there are still concerns about the

donor-site morbidity, technical difficulties of implantation, increased surgical time and length of hospital stay. As a result of its excellent combination of biological and mechanical properties, autologous bone graft may be a superior treatment in the future, as a graft source in terms of osteogenic, osteoinductive and osteoconductive potential (Spin-Neto et al., 2011). Artificial bone materials such as HA, are a well-established method for treating osteo-degenerative diseases (Jimi et al., 2012). HA, a calcium phosphate material, promotes autogenous bone regeneration and supports guided bone regeneration and platelet-rich plasma (PRP) (Sanchez et al., 2003).

1.2.3. Emerging therapies based on natural products

Natural products are a therapeutic option under development. It has been suggested that natural compounds can avoid the side effects of anti-osteoclast BPs (Ihn et al., 2017). Among various herbal medicines, diphlerothohydroxycarmalol (DPHC) is an important component for inhibiting osteoclast differentiation (Ihn et al., 2017). As shown in Figure 1.2, the activation of NFκB pathways is stimulated by RANKL promoting osteoclast differentiation. DPHC-mediated suppression of osteoclast differentiation is suggested to play a major role in the inhibition of these signalling pathways, including the p38, ERK1/2, c-Jun N-terminal kinase (JNK), AKT and NFκB pathways (Ihn et al., 2017). Ihn et al. (2017) reported that DPHC extracted from marine brown algae inhibits osteoclast differentiation for bone resorption by suppressing the NFκB signalling pathways.
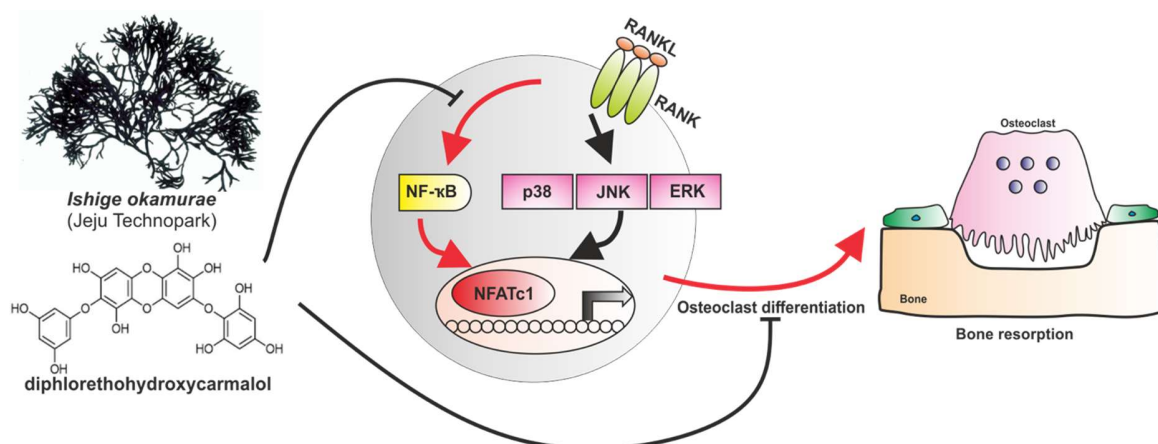
Figure 1.2. Diphlerothohydroxycarmalol (DPHC)-mediated suppression of osteoclast differentiation. DPHC extracted from *Ishige okamurao* (marine brown

algae) inhibits the activation of NFκB pathways to promote osteoclast differentiation through p38, ERK1/2, c-Jun N-terminal kinase (JNK) and NFκB pathways. The transcription factor NFATc1 is activated by p38, ERK1/2, JNK and NFκB pathways to promote bone resorption.

Importantly, pharmacological treatment options remain first line therapies for osteoporosis. However, there are some side effects of pharmacological agents, thus autologous bone grafts can also be preferred as a surgica technique that would need to be performed when a patient has an insufficient amount of healthy natural bone. Autologous bone grafting has long been considered a gold standard therapy among graft materials. Compared to other augmentation techniques, autologous bone grafting has several advantages including suitable bone quality, low costs, short healing time, a lack of disease transmission and the repair of larger defects (Misch, 2010). Even though autologous bone grafting is currently seen as a gold standard therapy, this technique still has drawbacks in terms of a high risk of morbidity (Pape et al., 2010) and intervention-induced inflammation (Rosetti et al., 2009). Thus, safe and predictable therapies for osteoporosis are an unmet clinical need.

1.3. Regenerative engineering: stem cell therapy as a new direction to treating bone degeneration

In the light of the limitations of conventional therapies discussed above, the use of stem cells has been explored in the context of bone healing. Because of their wide availability, the minimally invasive isolation procedures required to obtain them and their high osteogenic differentiation capability, MSCs are considered the most feasible stem cell type to be used in osteoporosis treatment (Simão et al., 2010). Stem cell therapies also offer benefits including an effective cure, faster healing and returning to mobility. Importantly, MSCs have been shown to contribute to bone regeneration *in vitro* and *in vivo* (Singh et al., 2015, Tortelli et al., 2010). Tortelli et al. (2010) demonstrated the impact of tissue-engineered bone in porous ceramic scaffolds embedded into murine MSC and detected the formation of bone via the activation of endochondral ossification performed by the implanted cells into scaffolds in immunocompromised mice (Tortelli et al., 2010). They also observed the high level of vascularization in MSC implants (Tortelli

et al., 2010). Some researchers have reported that bone formation at sites of bone defects has been stimulated through the implantation of BM-MSCs (An et al., 2012, Vulcano et al., 2013). In 2015, the potential of MSCs to mediate the regeneration of oral bone was investigated in a randomised clinical trial (Padial-Molina et al., 2015) in which a total of 190 records were evaluated for quality and 51 articles were determined as relevant by means of full-text assessment. Among these, only 28 articles met the inclusion criteria: nine case series, ten case reports and nine randomized controlled clinical trials. Padial-Molina et al. (2015) reported the paper selection process including the application of MSCs in 290 patients in 342 interventions. A meta-analysis was not consistent because of the high viability in different variables (Padial-Molina et al., 2015). In addition to oral bone regeneration, safety and efficacy of MSC transplantation has been assessed in clinical trials. Although Phase 1 studies showed that MSC transplantation is safe and indicated that stem cell therapies could also potentially have added benefits including an effective cure, faster healing and returning to mobility, data from Phase 2 and 3 clinical trials for the use of MSCs in osteoporosis are not yet available.

In addition to differentiation and functional integration, MSCs are widely believed to contribute to regeneration via paracrine factors. As bystander cells, MSCs modulate endogenous regeneration which includes soluble factors such as cytokines and growth factors, and extracellular vesicles carrying miRNAs affecting the molecular signalling pathways involved in bone regeneration (Chaparro and Linero, 2016). Growth factors and cytokines secreted by MSCs have numerous effects on healing bone tissue defects in terms of immunomodulation, anti-apoptosis, angiogenesis, supporting the growth and differentiation of stem cells and chemo-attraction, as shown in Table 1.2. The immunomodulatory effects of MSCs involve suppression of the proliferation of CD8$^+$ and CD4$^+$ lymphocytes, natural killer (NK) cells, dendritic cells (DCs), regulatory T cells and immunoglobulin production by plasma cells (Meirelles Lda et al., 2009). In addition, MSCs possess immunomodulatory capabilities affecting the majority of immune cells (Kyurkchiev et al., 2014). In respect to bone healing, this intrinsic property of MSCs has been suggested to contribute to bone regeneration (Medhat et al., 2019). Despite this high clinical potential, MSC-based approaches to tackling osteoporosis are limited by the fact that osteoporosis has a negative impact on the number and osteogenic

differentiation potential of MSCs (Saito et al., 2018, Tan et al., 2015, Wang et al., 2014c). So, increasing the viability, proliferation rate and osteogenic differentiation capacity of MSCs are still essential steps, which need to be optimized in order to deliver a successful and reliable stem cell-based therapy for osteoporosis.

Table 1.2. Paracrine effects of the MSC secretome on bone regeneration

Target	Paracrine factors	References
Immunomodulation	prostaglandin E2, human leukocyte antigen-G molecules, hepatocyte growth factor, inducible nitric oxide synthase, transforming growth factor -β and interleukin-10	(Di Nicola et al., 2002, Krampera et al., 2003, da Silva Meirelles et al., 2009, Meirelles Lda et al., 2009)
Anti-apoptosis	vascular endothelial growth factor, hepatocyte growth factor, insulin-like growth factor-1, stanniocalcin-1, macrophage colony-stimulating factor and transforming growth factor -β	(Di Nicola et al., 2002, Krampera et al., 2003, da Silva Meirelles et al., 2009, Meirelles Lda et al., 2009)
Angiogenesis	vascular endothelial growth factor, insulin-like growth factor-1, placental growth factor, monocyte chemoattractant protein-1, fibroblast growth factor and interleukin-6	(Kinnaird et al., 2004, Hung et al., 2007, Meirelles Lda et al., 2009)
Support of growth and differentiation of stem cells	macrophage colony-stimulating factor, leukemia inhibitory factor, macrophage colony-stimulating factor, stromal cell-derived factor -1 and angiopoietin-1	(Haynesworth et al., 1996, Majumdar et al., 1998, Ohab et al., 2006, Meirelles Lda et al., 2009)
Chemoattraction	chemokine (C-C motif) ligands 2,3,4,5,6,20,26 and chemokine (C-X-C motif) ligand 5,11,1,2,8,10,12	(da Silva Meirelles et al., 2008, Meirelles Lda et al., 2009)
Anti-fibrosis	hepatocyte growth factor, fibroblast growth factor and adrenomedullin	(Suga et al., 2009, Li et al., 2009)

1.3.1. Biochemical factors affecting osteogenic differentiation of MSCs

Several physical, chemical and biological factors have been reported to stimulate osteogenic differentiation. Among the biological factors, the effects of fibroblast growth factors (FGFs), BMPs, platelet-derived growth factors (PDGFs) and insulin-like growth factors (IGFs) have been widely reported (Kempen et al., 2010). BMP2 and BMP7 induce osteogenic differentiation, followed by up-regulating alkaline phosphatase (ALP) and osteocalcin (Rutherford et al., 2002). FGFs are another stimulator of bone healing (Behr et al., 2010); FGF-2 treatment of MSCs stimulates osteogenic differentiation (Behr et al., 2010). There are five known signalling pathways for osteogenic differentiation: the

TGF-β, BMP, Wnt, Nell-1 and Ihh signalling pathways (Liu et al., 2018). The Ihh pathway induces anti-adipogenic differentiation by reinforcing BMP signalling with Smad lineage (Caplan, 2010).

Studies have also shown the importance of lamin A/C regulators in the osteogenic differentiation of MSCs (Pajerowski et al., 2007). Lamins are intermediate filament proteins located in nuclear lamina and matrices (Li et al., 2011). A decrease in the level of lamin A expression is related to the decrease of bone mass seen in patients suffering from osteoporosis, osteolysis and bone fracture (Rodrigues et al., 2002). Serum leptin is another mediator regulating fat mass and bone mass and can inhibit adipogenic differentiation (Thomas et al., 1999). Serotonin also has a curative effect on bone fracture in humans (Modder et al., 2010). Nam et al. (2016) reported the positive impact of serotonin on osteoblast differentiation and subsequent bone regeneration using both rat calvarial cell cultures *in vitro* and a rat critical-sized calvarial defect model *in vivo* (Nam et al., 2016). Increasing levels of reactive oxygen species (ROS) and oxidative stress in ageing are also correlated to age-related bone loss through transcription factors such as forkhead homeobox type O (FOXO), Wnt and peroxisome proliferator-activated receptor gamma (PPARγ) (Almeida et al., 2009). Kim et al. (2018) found that the function of FoxOs in cells of osteoblast lineage is to promote bone formation by inhibiting Wnt signalling (Kim et al., 2018). FoxOs also tend to decrease bone resorption by means of the effect of antioxidants on osteoclast. However, the FoxOs' action in osteoclast lineage effects bone resorption (Kim et al., 2018).

In addition to growth factors, MSC differentiation is promoted by physical and chemical factors (Chen et al., 2016). ECM components such as osteopontin (OPN) and fibronectin stimulate the adipo-osteogenic differentiation of MSCs by binding to integrin receptors (Chen et al., 2014). OPN-integrin interaction shifts MSCs to an osteogenic differentiation pathway (Chen et al., 2014).

1.3.2. Biophysical factors and osteogenic differentiation of MSCs

Physical factors such as mechanical force, electrical and electromagnetic stimulation and nanotopology also promote osteogenic differentiation and subsequent fracture healing on bone regeneration (Huang et al., 2018).

Favourable mechanical forces such as cyclic strain and fluid shear stress are significant for bone homeostasis of ASCs (Bodle et al., 2011). For instance, the magnitude of tensile strain was reportedly associated with the suppression of adipogenic differentiation to promote osteogenic differentiation (Hanson et al., 2009). Electrical stimulation (ES) has been proven to effect cell proliferation and migration, as well as bone regeneration both *in vitro* and *in vivo* (Itoh et al., 2006, Nakamura et al., 2010). Itoh et al. (2006) reported the effect of polarized HA ceramics with ES after implantation into the right or left femoral condyle of rabbits. Their findings demonstrated increased osteogenic differentiation after three weeks (Itoh et al., 2006). ES also modulated the expression of adenosine A2a receptor and integrin β molecules to improve anti-inflammatory effects and osteogenic differentiation potential (Adey, 1993). Furthermore, pulsed electromagnetic fields (PEMFs) can have an effective role in lumbar vertebral osteoporosis by regulating Wnt3a/LRP5/β-catenin and OPG/RANKL/RANK signalling pathways in order to alleviate bone resorption (Lei et al., 2018). Ehnert et al. reported that low-frequency PEMFs (10-90.6 Hz) induced osteogenic differentiation in an ERK1/2-dependent manner (Ehnert et al., 2017, Ehnert et al., 2015). Ultrasound (US), a well-established physical stimulus, has been reported to improve bone repair when combined with growth factors (for example calcium-regulating hormones, BMP2 and BMP7) (Ito et al., 2000, Kim et al., 2012, Lee et al., 2013). Some studies have shown that low-intensity pulsed US stimulation accelerates rat femoral fracture healing by means of various cellular reactions such as inflammation, angiogenesis and early osteogenesis (Azuma et al., 2001). Shock wave treatment also stimulated osteogenic differentiation and was associated with the induction of TGF-β1 expression (Hofmann et al., 2008). Hofmann et al. (2008) also evaluated changes in the proliferation and differentiation of human osteoblasts after shock wave treatment (500 impulses of energy flux densities of 0.06 mJ/mm, 0.18 mJ/mm, 0.36 mJ/mm and 0.5 mJ/mm). According to their findings, shock wave treatment on human osteoblasts between 0.18 mJ/mm and 0.5 mJ/mm showed an increase in ALP activity (Hofmann et al., 2008).

Another biophysical factor is the effect of nanotopography on the osteogenic differentiation of human stem cells. Recent studies have reported that nanopores of 30 nm induced the osteogenic differentiation of human stem cells on the surface of collagen type I fibres but also other topological factors (Greiner et al., 2019b). It was found that scaffolds coated with SiO_2 nanoparticles with 30 nm pores showed a high performance for bone reconstruction at damaged site (Greiner et al., 2019b). Hwang et al. (2017) investigated nanotopological pillars with a size gradient through the activation of a transcriptional coactivator with a PDZ binding motif (TAZ) (Hwang et al., 2017). A nanotopological plate 70 nm in diameter showed the highest regulation of osteogenic differentiation of MSCs by regulating TAZ to mediate actin reorganization (Hwang et al., 2017). A polycaprolactone growth surface engineered with 120 nm diameter dots (NSQ50) was evaluated using human MSCs. By controlling the stiffness and nanoscale topography, the surface increased the osteogenic differentiation potential of human MSCs and pushed them towards chondrogenic, osteogenic and adipogenic lineages (Wang et al., 2014a). Moreover, Song et al. (2013) reported the effect of MSCs cultured on nanoporous alumina to investigate the interaction gap between the nanoscale topography of the scaffolds (20 nm and 100 nm) and the cellular response in regard to cellular proliferation and osteogenic differentiation (Song et al., 2013). Cell viability measured by an MTT assay showed a decrease on scaffolds with 100 nm pore size and enhanced the osteogenic potential for bone mineralisation (Song et al., 2013). Gauthier et al. (1998) evaluated microporous biphasic calcium phosphate (MBCP) ceramics and the macroporosity percentage on bone ingrowth. A total of 60 spherical MBCP ceramics were transplanted into a femoral site of 30 rabbits. Analysis of the implanted surface with MBCP ceramics with 565 μm pore size was performed by backscattered electron imaging and the ceramics showed an increased bone formation in deep and peripheral pores compared with ones with 300 μm (Gauthier et al., 1998). Taken together, these results show that cellular behaviour showed variations on MSCs grown on the engineered scaffold with different topological factors.

1.3.3. The importance of physical signals to promote osteogenic differentiation in bone health

Previous studies have reported that physical exercise or sports can effectively increase the level of bone mass and prevent bone resorption without pharmacological intervention by the use of steroids (Wohl et al., 2000). In such cases, WHO recommends weight-bearing exercise as a physical therapy to treat osteoporosis and osteoporotic-fractures with no side effects (Kohrt et al., 2004). Physical signals promote osteogenic differentiation via different mechanisms including mechanical loading, cell signalling pathways and noncoding RNAs as well as hormones and cytokines. Some studies have showed that mechanical loading (e.g., compression, strain and fluid shear) promotes osteoblast differentiation and mineralization, which results in the increased level of bone density (Klein-Nulend et al., 2012). In contrast, a report by Lang et al. also showed that due to lack of mechanical stimuli, astronauts in space have a 2% lower bone mass than age-matched controls (Lang et al., 2004). Several studies have reported that physical exercise plays a role in improving bone remodelling through the multiple signalling pathways including Wnt/β-catenin, BMP and OPG/RANKL/RANK signal pathways and promote osteoblast differentiation and suppress osteoclast activity (Yuan et al., 2016, Yuan et al., 2017). Recent studies have reported that noncoding RNAs induced by exercise promote bone formation. Noncoding RNAs (e.g., siRNA, microRNAs, lncRNA and circRNA) could be an efficient agent to promote osteoblast differentiation as well as cell proliferation in the bone metabolism (Yuan et al., 2017). Further, *in vitro* findings by Yehya and Shyu et al demonstrated that mechanical stress regulates the expression of microRNAs (e.g., miR208a, miR-32, miR-466c, miR-466b, miR-375, miR-378, miR-347, miR-15b and miR-154) which could be potential therapeutic candidates for the treatment of bone disorders (Yehya et al., 2012, Shyu et al., 2013). Another key mechanism in bone remodelling aree hormones and cytokines including estrogen, parathyroid hormone and glucocorticoids, all of which are induced by exercise (Krum, 2011, Gardinier et al., 2015). Bentz et al. indicated that physical exercise increases the secretion of estrogen (estradiol) in premenopausal women and is accompanied by the increase of bone mass (Bentz et al., 2005).

1.4. Impact of 3D cell culture on the osteogenic differentiation of MSCs

Recent advances in biomedical research have improved cell-based treatments to provide a simple, cost-effective and fast approach. Most cell-based assays currently use the traditional two-dimensional (2D) cell culture, but this monolayer cell culture approach has some drawbacks, including phenotypic changes and a low level of compatibility in living organisms (McKee and Chaudhry, 2017), and 3D techniques have been developed to address some of the monolayer cell culture problems. As shown in Table 1.3, the advantages of 3D construction take precedence over the 2D culture system in spite of the drawbacks of 3D cell culture, such as the limitation of diffusional transport and alterations in gene expression (Edmondson et al., 2014).

Table 1.3. The benefits and drawbacks of 2D and 3D cell culture systems (Katt et al., 2016, Edmondson et al., 2014).

	2D CELL CULTURES	3D CELL CULTURES
BENEFITS	+ less expensive and easier to maintain	+ more reflective of *in vivo* response
	+ well-established	+ more similar to *in vivo* behaviour
	+ easier environmental control	+ reduce the involvement of animals
	+ plenty of literature available	+ more physiologically relevant
	+ easier observation and measurement for analysis	+more accurately copy the actual microenvironment
DRAWBACKS	- misleading and non-predictive data for *in vivo* responses	- challenges in microscopy and measurement due to larger size
	- low level of compatibility in living organisms	- not suitable for drug development and research
	- lack of clinical efficacy and unacceptable toxicity	- limited diffusional transport
		- alteration in gene expression

1.4.1. Physical properties needed in a bone graft/scaffold for bone regeneration

In order to improve the differentiation of stem cells, 3D scaffolds for stem cell-based bone regeneration need to mimic the structure of bone ECM, thereby stimulating cell proliferation and differentiation. Moreover, they need to be biodegradable, biocompatible, bioactive, non-cytotoxic, printable and osteo-conductive-inductive *in vivo* (Qu et al., 2019). An ideal biomaterial for this purpose should also be designed taking stiffness and surface topography into consideration. Mechano-physical cues are efficient factors for the fate of stem cells, which is including surface stiffness, presence of micro-

and nanoscale pores, pillars and pit-like structures at microscale and nanoscale (Moghaddam et al., 2019). It is important to note that substrate stiffness can influence the osteogenic potential of MSCs in 2D and 3D (Engler et al., 2006). It has been reported that 2D micropores of 60 and 550 μm provide a positive effect on osteogenic differentiation (Gauthier et al., 1998). Interestingly, nanopores with a diameter of 30 nm within elastic with collagen (Greiner et al., 2019b) and rigid with titanium (Schürmann et al., 2014) have been suggested as a strong cue to improve osteogenic potential. Notably, nano- and micro- and macropore profiles of scaffolds could contribute to the increased osteogenic potential of MSCs in 3D. Moreover, physical properties of substrates with an elasticity of 20kPa showed an increase in the expression of anti-inflammatory potential of stem cells, compared to scaffolds with an elasticity of 2 kPa (Seib et al., 2009).

Designing these scaffolds helps us to understand how to deliver the seeded cells in the body (Langer and Tirrell, 2004) and their anti-inflammatory and cytotoxicity abilities *in vivo* (Langer and Tirrell, 2004).

1.4.2. 3D scaffolds supporting 3D differentiation of MSCs

Four different generations of biomaterials for 3D scaffolds have been developed, as shown in Figure 1.3 (Yu et al., 2015). The first generation of biomaterials was developed in the 1960s (Ratner et al., 2013) and comprised metals (titanium), synthetic polymers (PMMA and PEEK) and ceramics (alumina and zirconia). Second generation biomaterials had biodegradability *in vivo* and included synthetic and natural polymers (for example, collagen, calcium phosphate, calcium carbonate, calcium sulphate and bioactive glasses). The third generation of biomaterials were created to promote beneficial biological responses (Jandt, 2007, Murugan and Ramakrishna, 2005). Finally, the fourth-generation biomaterials are also referred as biomimetic biomaterials and include tissue-engineered scaffolds (Jandt, 2007, Murugan and Ramakrishna, 2005).
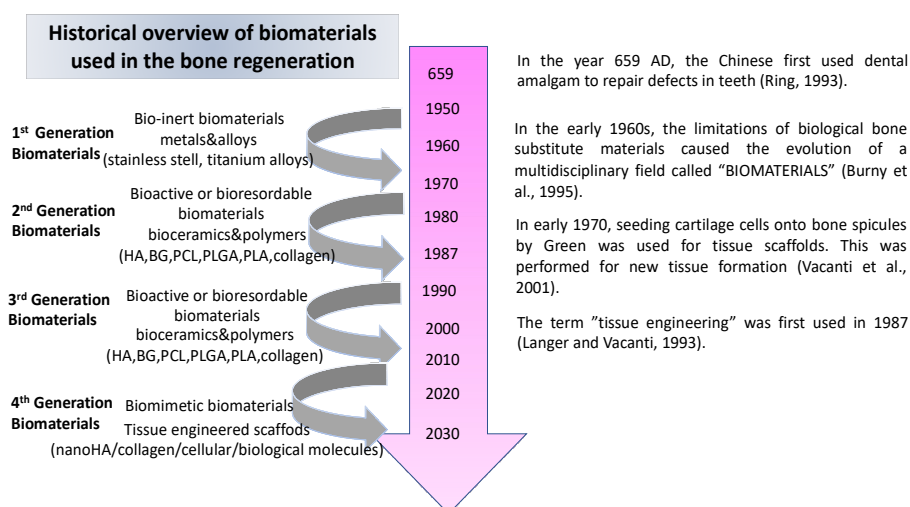
Figure 1.3. The evolution of biomaterials in bone regeneration.

In 2001, the first successful implantation of a cell-seeded porous biomaterial was reported in the context of bone regeneration (Quarto et al. 2001). The implantation repaired a large bone defect (4-8 cm) using a custom-made porous hydroxyapatite scaffold seeded with autologous bone marrow-derived MSCs (BM-MSCs) (Quarto et al. 2001). Allogenic cells combined with specific biomaterials are accepted as more favourable materials among the commercial products (Mason and Dunnill, 2009). In 2004, *in vivo* osteogenic differentiation of adult stem cell-seeded apatite-coated PLGA scaffolds in critical-size defects was reported in mice (Cowan et al. 2004). The results of implanting apatite-coated PLGA scaffolds demonstrated new bone formation at the damaged site of 25%, 80%, 70% and 85% after two, four, eight and twelve weeks of bone reconstruction respectively.

The first clinical use of hASC-fibrin glue was reported by Lendeckel et al. (2004), who described how extensive craniofacial injury in a seven-year-old girl was treated using hASC-fibrin glue (Lendeckel et al., 2004). After two years, the initial injuries at the calvarial defects were repaired by using autologous stem cells in fibrin glue. Some researchers have evaluated magnesium scaffolds coated with ß-tricalcium phosphate for bone tissue engineering (Chen et al., 2014) and found that these scaffolds are capable of stimulating the osteogenic differentiation of MSCs, being supported with an anti-inflammatory M2 macrophage phenotype (Zhang et al., 2017).

1.4.3. The advantages and disadvantages of stem cells to support *in vitro* and *in vivo* osteogenic differentiation potential

Stem cells are categorised into pluripotent stem cells and adult stem cells. Pluripotent stem cells include embryonic stem cells (ESCs) and induced pluripotent stem cells (iPSCs). Although the advantages of iPSCs is their ability to differentiate into all cell types in bone, there are still drawbacks including ethical and safety concerns and a risk of teratoma formation when transplanted *in vivo.* As an adult stem cell type, MSCs are particularly promising due to their higher osteogenic potential for bone repair and regeneration. Moreover, adipose-derived stromal vascular fraction (SVF) has been also determined as an efficient source for regenerating vascularized bone tissue (Yousefi et al., 2016). The advantages and disadvantages of various stem cell sources are listed in Table 1.4 (Mizuno, 2009, Coutu et al., 2012). Jiang et al., have reported that designing scaffolds with nanoscale topographical features and micro and macro scale gradient structures have been incorporated into living cells and/or growth factors (Jiang et al., 2015). Some of the recent studies making use of MSC-seeded 3D scaffolds have been suggested to improve cell proliferation and osteogenic differentiation potential as well as cell adhesion (Grayson et al., 2011).

Table 1.4. The advantages and disadvantages of stem cell sources for bone tissue engineering (Mizuno, 2009, Coutu et al., 2012).

Stem cell sources	Advantages	Disadvantages
Embryonic stem cells (ESCs)	- Pluripotency for differentiating into all cell types in bone	- Ethical and regulatory issues - Risk of teratoma formation when transplanted *in vivo*
Induced pluripotent stem cells (iPSCs)	- Pluripotency for differentiating into all cell types in bone	- Reprogramming efficiency is low - Safety concerns due to limited clinical applications
Bone marrow-derived mesenchymal stem cells (BM-MSCs)	- Higher osteogenic potential - Studied extensively	- Limited expansion ability *in vitro*
Adipose-derived mesenchymal stem cells (ASCs)	- Osteogenic characteristics similar to that of BM-MSCs - Easy to surgically obtain large numbers of multipotent stem cell	- No widely used protocol *in vitro* - More studies are required to test in bone regeneration
Umbilical cord blood MSC	- High availability, proliferation and	- More difficult to be isolate

(hUCMSC)	differentiation potential - Higher *in vivo* safety than ESCs due to genomic stability	- More studies are required to test bone regeneration potential
Adipose-derived stromal vascular fraction (SVF)	- Easily harvesting by liposuction -Availability for the formation of vascularized bone	- Cell population varies among donors - Multistep isolation process including 2-3-hour

Bone tissue engineering also includes the use of MSC-seeded 3D scaffolds to generate new bone by osteoinductive cues (Grayson et al., 2011). An important requirement for tissue-engineered bone graft is the integration capacity with the host tissue. The design of 3D scaffolds including scaffold composition and surface properties play a fundamental role in MSC proliferation and differentiation (Taboas et al., 2003). Extensive research has been devoted to different stem cell sources in combination with appropriate 3D scaffolds. Day et al. (2018) assessed the osteogenic potential of hUCMSC seeded on coralline hydroxyapatite/calcium carbonate (CHACC) microparticles. They evaluated osteogenic differentiation potential in human MSCs isolated from bone marrow and umbilical cord matrix when seeded onto 200-300 µm CHACC granules. Their findings showed that MSCs derived from bone marrow exhibited more potential for osteogenic differentiation compared with cells from the umbilical cord matrix (Day et al., 2018). The developments in bone regeneration have been assessed using different stem cell types seeded into calcium phosphate cements (CPCs) (Wang et al., 2014b). These stem cell types include hUCMSC, BM-MSC, human ESCs and iPSC. Wang et al. (2014b) concluded that hUCMSCs, ESC-MSCs and iPSC-MSCs seeded onto CPC blood vessels were similar to those of BM-MSCs, whereas ESC-MSCs and iPSC-MSCs cultured onto CPC had greater two- to three-fold osteogenic differentiation potential than those of the CPC control (Wang et al., 2014b).

A recent study reported the impact of co-delivering autologous PRP and autologous BM-MSCs embedded into macroporous CPC for bone healing in minipigs (Gengtao et al., 2017). The report showed that a CPC scaffold with autologous BM-MSC-PRP provided a two-fold increase in osteogenic potential for bone regeneration in minipigs compared with a CPC control (Gengtao et al., 2017). Mohammed et al. (2019) compared the regenerative potential of amniotic fluid-derived mesenchymal stem cells (AF-MSCs) and

BM-MSCs *in vivo* and found that AF-MSCs seeded into gel-foam scaffolds showed a higher level of bone recovery than BM-MSCs *in vivo* (Mohammed et al., 2019). In addition, ASCs loaded onto bioactive glass or β-TCP scaffolds supplemented with BMP-2 promoted bone healing in ten out of thirteen cases of cranio-maxillofacial hard-tissue damage (Sandor et al., 2014). In another study using bioglass-based scaffolds, the osteogenic differentiation of ASCs seeded onto bioglass-based scaffolds exhibited higher potential compared with a control (Rath et al., 2016). Furthermore, BM-MSCs embedded onto nanocomposite bioactive glass/gelatin scaffolds led to higher levels of osteogenic differentiation compared with ASCs seeded onto bioglass-based scaffolds both *in vitro* and *in vivo* (Kargozar et al., 2018).

1.4.4. The advance of 3D cell culture on osteogenic differentiation of human MSCs

When preparing 3D scaffolds for cells, it is worth noting that cells should be embedded within a biocompatible microenvironment, i.e., 3D scaffolds should resemble their native extracellular matrix (ECM). A variety of scaffolds and their potential fabrications are activated to promote osteogenic differentiation of human MSCs, as listed in Table 1.5. Microfibre polymer scaffolds modified by either jet-spraying or electrospinning have been evaluated for cell viability and osteogenic differentiation of human BM-MSCs *in vitro* (Brennan et al., 2015). That study reported that MSCs distributed on jet-sprayed scaffolds displayed a more intense actin filament staining and osteogenic potential compared with cells on scaffolds modified by electrospinning (Brennan et al., 2015).

A fibre-based scaffold designed with 3D weaving from poly (lactic acid) PLA represented a good platform for the osteogenic differentiation of BM-MSCs *in vitro* (Persson et al., 2018). Another study has reported that the culture of BM-MSCs in 3D dynamic spinner flasks enhanced the osteogenic differentiation and cell proliferation on porous Poly (D, L-lactic-co-glycolic acid) (PLGA) scaffolds compared with cells cultured under static conditions (Stiehler et al., 2009). A recently developed bioactive glass enriched with strontium and magnesium was produced in the form of granules and results showed that the bioactive granules induced the osteogenic differentiation of BM-MSC (Bellucci et al., 2019).

Recently, Haussling et al. (2019) developed poly (2-hydroxyethyl methacrylate) cryogels containing composite HA to mimic the inorganic bone matrix and examined the osteogenic differentiation potential. These cryogels were supplemented with a variety of proteins, including PRP, immune cells-conditioned media, collagen and RGDSP (Arg-Gly-Asp-Ser-Pro) peptides. ASCs cultured in collagen and PRP cryogels showed a higher potential for osteogenic differentiation for cultivation at 14 days, compared with those with RGDSP peptides (Haussling et al., 2019). Furthermore, Heo et al. (2019) investigated encapsulated spheroids of human MSCs in collagen/fibrin hydrogel and found that the incorporation of human umbilical vein endothelial cells (HUVECs) into MSC spheroids exhibited increased osteogenic potential and bone mineral deposition compared with a control (Heo et al., 2019).

Hydrogel scaffolds are designed to provide a fine 3D network in terms of their mechanical, biological and physio-chemical features (El-Sherbiny and Yacoub, 2013). Pore size and porosity are additional criteria considered in the design of scaffolds since an inadequate pore size might hinder neo-vascularisation, inhibit osteogenic differentiation and potentially drive MSCs in an undesired direction (El-Sherbiny and Yacoub, 2013). Hydrogel-based scaffolds have a natural adhesive capacity as well as biocompatibility and are likely to promote high cell viability and cell differentiation (Langhans, 2018). On the other hand, cellulose and chitosan are the most common sources of natural polymers for osteogenic differentiation (del Valle et al., 2017). Generally, cellulose-based scaffolds in a 3D network present strong support for *in situ* implantation for bone repair due to their mechanical properties and high porosity, which allow them to be used in tissue engineering approaches (Abeer et al., 2014). Aggarwal and Pittenger (2005) reported that MSCs seeded in hydrogel scaffolds showed increased cell viability compared with MSCs encapsulated in non-degradable PEG hydrogels or conjugated with the adhesive ligand RGDSP peptides.

The optimisation of 3D scaffolds has shown variations in MSC differentiation (McKee and Chaudhry, 2017). For instance, 3D scaffolds containing chitosan and mechanically strong polysaccharides are likely to induce MSC osteogenic differentiation, whilst those containing HA more readily promote differentiation to a chondrogenic lineage (Kim et al., 2013a). In addition, stiffer substrates promote osteogenic differentiation by binding

integrin (Huebsch et al., 2010). Young's modulus of cortical bone is 6-23 GPa and its tensile strength is 80-150 MPa (Rho et al., 1998, Reilly and Burstein, 1975). Natural biomaterials demonstrate lower values of strength and toughness than natural bone, but composite biomaterials have excellent toughness compared with single-natural polymers (Wegst et al., 2015). In order for nanocomposites or biodegradable polymers to be effective, their mechanical properties should be arranged to match those of natural bone. Figure 1.4 shows the mechanical properties of a range of biomaterials (Wegst et al., 2015).

Table 1.5. The categorization of 3D scaffoldings with their proliferation and osteogenic differentiation potential

3D scaffold type	Cell type	Species	Impact of 3D on the viability/proliferation of MSCs	Impact of 3D on the osteogenic potential of MSCs	Reference
Micro-fibre polycaprolactone (PCL) scaffold	Bone-marrow MSCs	Human	positive	positive	(Brennan et al., 2015)
Poly (D, L, -lactic-co-glycolic acid) (PLGA)	Bone-marrow MSCs	Human	positive	positive	(Stiehler et al., 2009)
Poly (lactic acid) & hydroxyapatite (PLA/HA)	Bone-marrow MSCs	Human	positive	positive	(Persson et al., 2018)
Poly (D, L, -lactic-co-glycolic acid) (PLGA)	Stem cells of apical papilla and periodontal ligament stem cells	Human	positive	positive	(Jafar et al., 2019)
Apatite-wollastonite glass ceramic (A-W) 3D scaffolds	heterogeneous plastic adherence MSCs and CD271-enriched MSC	Human	positive	positive	(Muller et al., 2019)
Gelatin-methacryloyl (GelMA) hydrogels	Adipose-derived MSCs (ASCs)	Human	positive	positive	(Kirsch et al., 2019)
Poly-e-caprolactonetri-calcium-phosphate (PCL-TCP) scaffolds	Fetal MSCs	Human	positive	positive	(Goh et al., 2013)
Photocrosslinked methacrylated gelatin	MSCs	Human	positive	positive	(Romero-López et al., 2020)
PLGA–PEG–PLGA triblock copolymers (Thermosensitive hydrogel)	Stem cells from apical papilla (SCAPs)	Human	positive	positive	(Deng et al., 2020)
Nanohydroxyapatite/chitosan (HA/C) scaffolds	Amniotic MSCs (AF-MSCs)	Human	positive	positive	(Mohammed et al., 2019)
Strontium-Enriched Bioactive Glass (BGMS10)	Bone-marrow MSCs	Human	-	positive	(Bellucci et al., 2019)
Poly (2-hydroxyethyl methacrylate) cryogels	Adipose-derived MSCs (ASCs)	Human	constant	positive	(Haussling et al., 2019)
HA/β-TCP scaffolds	Bone-marrow MSCs	Human	constant	positive	(Zheng et al., 2019)
Biodegradable light polycaprolactone microcarriers (LPCL) (MCs)*	MSCs	Human	-	positive	(Lam et al., 2019)
Collagen/fibrin hydrogels	MSCs, Human Umbilical Vein Endothelial Cells (HUVEC)	Human	positive	positive	(Heo et al., 2019)
Injectable double-network (DN) hydrogel based on glycol chitosan (GC) and calcium alginate (Alg)	Bone-marrow MSCs, Vascular Endothelial cells	Human	positive	positive	(Yang et al., 2018)
Poly(urea-urethane) (PUU) nanohybrid scaffolds	Bone-marrow MSCs	Human	positive	positive	(Wu et al., 2018)
3D printed polycaprolactone/β-tricalcium phosphate scaffold ((PCL/TCP)	Adipose-derived MSCs (ASCs) Bone-marrow MSCs	Human	-	positive	(Park et al., 2018)
Devitalized ECM from human osteoblast differentiated MSCs	Bone-marrow MSCs	Human	positive	positive	(Baroncelli et al., 2018)
3D printed porous poly-ε-caprolactone/hydroxyapatite (PCL/HA) scaffolds	MSCs	Human	positive	positive	(Zheng et al., 2017)
Methacrylated hyaluronic acid (MeHA) hydrogel	Bone-marrow MSCs	Human	negative	positive	(Poldervaart et al., 2017)
PCL scaffolds enriched with 5% tricalcium phosphate (TCP)	Adipose-derived MSCs (ASCs)	Human	positive	positive	(Ruminski et al., 2018)

Continuation of Table 1.5. The categorization of 3D scaffoldings with their proliferation and osteogenic differentiation potential

Performing 3D scaffolds	Cell type	Species	Impact of 3D on the viability/proliferation of MSCs	Impact of 3D on the osteogenic potential of MSCs	Reference
Calcium phosphate ceramic (CaP)	Adipose-derived MSCs (ASCs)	Human	positive	positive	(Urquia Edreira et al., 2016b)
3D scaffolds including spherical spatial boundary conditions	MSCs	Human	positive	positive	(Lo et al., 2016)
Poly (Ethylene Glycol)– Poly (Dimethylsiloxane) Hybrid Hydrogels	MSCs	Mouse	-	positive	(Munoz-Pinto et al., 2012)
Matrigel	Adipose-derived MSCs (ASCs)	Canine	positive	positive	(Kang et al., 2012a)
Synthetic polymer poly (propylene fumarate) (PPF)	Bone-marrow MSCs	Human	constant	positive	(Ferlin et al., 2016)
Polyethylene glycol (PEG)-alginate	3T3 fibroblasts, D1 cells, clonally derived bone-marrow MSCs	Human, Mouse	positive	positive	(Chaudhuri et al., 2016)
Cytodex 3 gelatin-coated dextran microcarriers	Fetal MSCs	Human	positive	positive	(Shekaran et al., 2015)
3D porous poly (epsiloncaprolactone) scaffolds	Bone-marrow MSCs	Human	-	positive	(Mehr et al., 2015)
Coralline hydroxyapatite/calcium carbonate (CHACC)	Bone-marrow MSCs	Human	positive	positive	(Day et al., 2018)
Poly (ethylene glycol)-Poly (L -alanine- co - L -phenyl alanine) (PEG-PAF) Thermogel	Tonsil-tissue-derived mesenchymal stem cells (TMSCs)	Human	-	No effect	(Park et al., 2014)
3D porous chitosan scaffolds	MSCs	Human	positive	positive	(Teixeira et al., 2014)
Collagen hydrogels	Bone-marrow MSCs	Mouse	-	positive	(Klumpers et al., 2013)
Collagen hydrogels	MSCs	Rat	positive	positive	(Han et al., 2012b)
Poly (e-caprolactone) (PCL) nanofibre scaffold	Bone-marrow MSCs	Pig	positive	positive	(Rampichová et al., 2013)
Collagen hydrogels	Bone-marrow MSCs	Rat	positive	positive	(Oh et al., 2011)
3D porous scaffolds (degradable polyurethane foam (EF PU foam))	Chorion mesenchymal cells (CMCs)	Human	-	positive	(Bertoldi et al., 2010)
Biodegradable electrospun poly(εcaprolactone) (PCL) scaffolds*	MSCs	Rat	-	positive	(Mountziaris et al., 2010)
3D thixotropic gel (PEG-silica gel)	Bone-marrow MSCs	Human	negative	positive	(Pek et al., 2010)
Novel Melt-Based Chitosan/Polyester 3D Porous Scaffolds	Mesenchymal stem cell line (BMC9)	Mouse	positive	positive	(Costa-Pinto et al., 2008)
3D fibrin matrices	Bone marrow MSCs	Human	positive	positive	(Martino et al., 2009)
Electrospun Poly (D, L-lactide-co-glycolide) (PLGA) nanofibre scaffold	Bone marrow MSCs	Human	positive	positive	(Xin et al., 2007)

In order to combine the advantages of both types of scaffold, blends of hydrogels and stiff biomaterials have been explored in combination with different cell types. In this context, a blend of PEDOT:PSS and collagen type I has recently been reported to support the osteogenic differentiation of human neural crest-derived stem cells (Iandolo et al., 2020). In future studies, a similar approach should be explored in combination with MSCs. Several studies have reported that MSCs can be affected by substrate properties such as stiffness, surface roughness, chemistry and energy to commence the differentiation for specific lineages (Seib et al., 2009, Xue et al., 2013, Her et al., 2013) and the stiffness of the substrate can contribute to stem cell differentiation (Zhang et al., 2018b, Viswanathan et al., 2015). Many reports have shown that metal and polymer substrates are correlated to the higher or the lower moduli for bone regeneration compared with the natural moduli of bone ((Wegst et al., 2015, Hench and Polak, 2002, Rezwan et al., 2006).
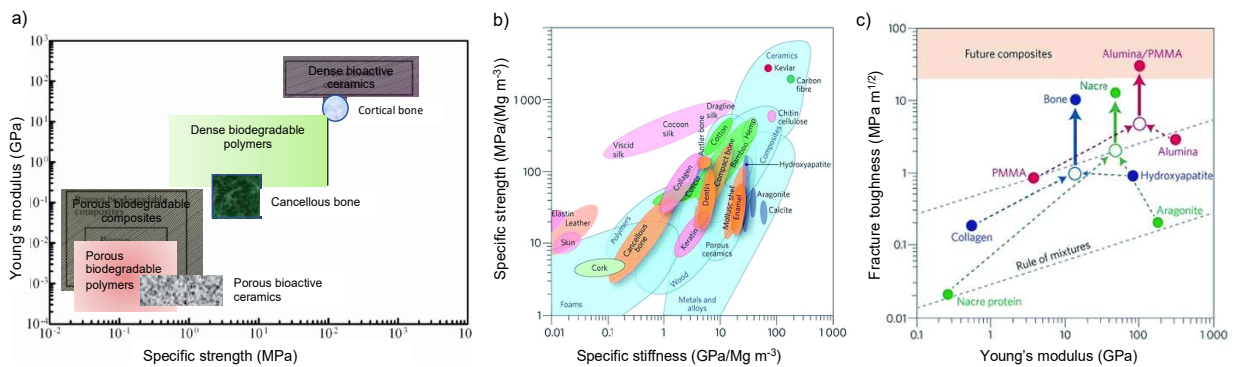
Figure 1.4. Young's modulus and specific strengths of natural and synthetic materials: (a) the mechanical properties of biodegradable polymers, bioactive ceramics and composite scaffolds with high porosity and pore structure; (b) an Ashby chart of stiffness and strength for natural and synthetic polymers; (c) the calculation for natural and synthetic polymers (Wegst et al., 2015, Hench and Polak, 2002, Rezwan et al., 2006).

Few studies, however, have found that osteogenic differentiation is sensitive to or dependent on stiffness and chemistry (Olivares-Navarrete et al., 2017). Surface properties affect the expression of particular integrins (such as $\alpha5\beta1$ and $\alpha2\beta1$) on titanium and this in turn affects differentiation and proliferation (Keselowsky et al., 2007, Olivares-Navarrete et al., 2008). Olivares-Navarrete *et al*. (2017) developed a series of polymer substrates with a variety of stiffnesses and found that a high stiffness (850 MPa) promoted osteogenic differentiation for osteoblast-like MG63 cells (Olivares-Navarrete et al., 2017). Their results showed that the organisation of

cytoskeletal filaments was affected by substrate stiffness and that MSCs embedded in a MA-MMA copolymer surface were more viable on the less elastic modulus with 40MA stiff surface (Olivares-Navarrete et al., 2017).

Improving the performance of biomaterials will be the next step in the interaction between substrate stiffness and bone tissue engineering.

1.5. The focus of the current research

The evidence from the literature indicates the need for further assessment of 3D cell culture platforms supporting the mechanisms of MSCs differentiation *in vitro*. This current study explored different approaches to MSC-based, bioactive molecules and various scaffolds in bone regeneration. It is clear that the impact of 3D cell culture on osteogenic differentiation ensures innovation in the regenerative, anti-inflammatory and immunomodulatory potential of human MSCs and their secretome. This modulatory potential has an integral role in the treatment of bone defects. Effective bone healing depends on determining the best approach for triggering osteogenic differentiation. There are a variety of 3D scaffolds that show great promise for treating bone defects in disease conditions ranging from osteoporosis to skeletal disorders. Furthermore, composite biomaterials in particular have received a great deal of attention for the generation of biomedical materials as their strength and toughness are similar to those of natural bone. All these biomaterials, in part or together, are likely contribute to the osteogenic differentiation of stem cells directly or provide a more appropriate environment for bone healing indirectly. A better understanding of stem cell therapies combined with biomaterials will offer the best therapeutic applications to reinforce bone repair. Further studies of the combination of stem cell therapies and appropriate 3D scaffold materials will be of considerable benefit for patients suffering from osteoporosis and osteoporosis-associated bone fracture.

A better understanding of the mechanisms of cell signalling in *in vitro* 3D cell culture systems could be a guide for performing in the *in vivo* environment (Tibbitt and Anseth, 2009, Merryweather and Roach, 2017). Previous studies using 3D biomaterials have shown that a variety of scaffolds can be fabricated to promote the osteogenic differentiation of human MSCs. Micro-fibre polymer scaffolds modified by

either jet-spraying or electrospinning have been evaluated for cell viability and the osteogenic differentiation of human BM-MSCs *in vitro* (Brennan et al., 2015). That study reported that MSCs distributed on jet-sprayed scaffolds displayed a more intense actin filament staining and osteogenic potential compared with cells on scaffolds modified by electrospinning (Brennan et al., 2015). ES has promoted cell proliferation and differentiation both *in vitro* and *in vivo* to treat damaged bone (Itoh et al., 2006, Nakamura et al., 2010). Some researchers have reported that ES showed positive effects on the left and right femoral condyle of rabbits when implanted with polarized hydroxyapatite ceramics (Itoh et al., 2006). Their findings demonstrated an increased osteogenic differentiation after three weeks.

The primary goal of this PhD study was to generate a novel 3D platform using aNFC hydrogels to investigate the impact of 3D cell culture methods on bone regeneration mediated by ASCs and, in particular, optimization using electric fields. The development of the 3D platform was intended to overcome the limitations of 2D systems by introducing a stem cell-derived source into the novel 3D platform. In the current project, ASCs were incorporated into 3D hydrogels to promote osteogenic differentiation through biophysical factors such as mechanical force, electrical and electromagnetic stimulation and nanotopology. The ability to introduce stem cells into the scaffold was a significant characteristic of the 3D platform since the cells embedded into 3D biomaterials constituted a more versatile 3D platform, which could be adjusted for further experiments.

1.5.1. Objectives of the experimental chapters

- Chapter 3: 'Assessment of the optical properties of anionic nanofibrillar cellulose for 3D imaging, biocompatibility and viability with human adipose-derived mesenchymal stem cells' outlines different 3D biomaterials with a particular focus on the biocompatibility of the scaffolds for ASCs. The work addresses two different aspects: the best performing hydrogel and the best solid substrate for ASC culture.

- Chapter 4: 'Evaluation of the osteogenic differentiation of human adipose-derived mesenchymal stem cells within 3D anionic nanofibrillar cellulose' presents an analysis of osteogenic differentiation of ASCs in 3D. Among the analysed 3D models, aNFC hydrogel was evaluated to understand its effects on the osteogenic differentiation of ASCs.

- Chapter 5: 'Performing electrical stimulation of adipose-derived mesenchymal stem cells in anionic nanofibrillar cellulose to promote their osteogenic potential' describes the development of an *in vitro* protocol, which optimized ES treatment to promote cell mineralization in 3D aNFC. The impact of ES treatment in 3D was evaluated in regard to the osteogenic potential of ASCs.

- Chapter 6: 'The impact of 3D cell culture combined with electrical stimulation on the anti-inflammatory and immunomodulatory potential of human adipose-derived mesenchymal stem cells and their secretome' explores the effects of different 3D cell culture systems on the immunomodulatory and anti-inflammatory potential of ASCs.

Chapter 2
Materials and Methods

2.1. Materials

All reagents, histochemical stains and general laboratory chemicals were obtained from Sigma-Aldrich (Dorset, UK) unless otherwise stated. All tissue culture media and reagents were obtained from Invitrogen (GIBCO; Paisley, UK) and Thermo-Fisher, unless otherwise stated. Antibodies used in the specification of cell differentiation are listed in Supplement 2.1, in Appendix I and those used for other applications are remarked within relevant sections. Primers used for gene expression analysis (Supplement 2.2, Appendix I) were commercially synthesised by Invitrogen (Paisley, UK) or Sigma-Aldrich. The source of all other materials is indicated in the relevant sections.

Cell culture plastics such as a non-adherent 96 well plates (Sarstedt-83.3992), tissue culture treated plates (Sarstedt-83.3924), 6-well tissue culture treated non-pyrogenic polystyrene plates (Corning Incorporated Costar REF 3516) and TC cell culture inserts (24 well format, $\varnothing 3.0 \mu M$, Sarstedt, 83.3932.300) were purchased from Sarstedt and Corning Incorporated.

2.2. Hydrogels and Cellulase solutions

2.2.1. Anionic Nanofibrillar Cellulose (aNFC)

aNFC hydrogel (GrowDexT®, GDxT) and NFC hydrogel (GrowDex®, GDx) were kindly provided by UPM Biochemicals, Helsinki, Finland.

2.2.2. 100 mM CaCl$_2$/10 mM HEPES buffer

CaCl$_2$ (final concentration 100 mM, Sigma-Aldrich, C1016) and 1 M HEPES buffer (final concentration 10 mM, Sigma-Aldrich, H3375) were added to DPBS without calcium and magnesium (Thermo-Fisher, Cat. No. 12037539) to prepare the cross-linking solution. The resulting solution was then filtered with a 0.2 μm filter Luer lock (Sarstedt, 83.1826.001).

2.2.3. 0.9% (w/v) Alginate, 0.1% (w/v) Gelatin Solution

Alginic acid sodium salt from brown algae (1 g, Sigma-Aldrich, Cat. No. 71238-250G) or Alginic acid, sodium salt (1 g, Acros Organics, code 17775000)) (Two molecular weights of alginate: low molecular weight, low viscosity alginate (100 Pa) and high

molecular weight, high viscosity alginate (500 Pa)) was dissolved in DPBS without calcium and magnesium (Thermo-Fisher, Cat. No. 12037539) or DMEM (as appropriate) to prepare 1% (w/v) alginate.

Gelatin (1 g, Sigma-Aldrich, Cat. No. G1393) was mixed in 100 mL sterile water (tissue culture grade, BioReagent, suitable for cell culture) to prepare 1% (w/v) Gelatin beads.

To prepare the 0.9% (w/v) Alginate, 0.1% (w/v) Gelatin bead solution, 1% (w/v) Alginate (900 µL) was mixed with 1% (w/v) Gelatin solution (100 µL). ASCs were then seeded in the 0.9% (w/v) Alginate and 0.1% (w/v) Gelatin beads to generate a cell-alginate paste, which was then extruded through a 21G needle into a bath of 100 mM $CaCl_2$/10 mM HEPES buffer to allow cross-linking.

2.2.4. TrueGel3D Polymer

TrueGel3D Polymer modified for fast gelling (FAST-DEXTRAN) (Sigma Aldrich, Cat. No. TRUEDEXF) is a natural degradable polymer functionalized with maleimide thiol-reactive groups, which react rapidly with crosslinkers (PEG or CD cell-degradable crosslinker) to form biomimetic hydrogels. The chemically defined hydrogel formed from FAST-DEXTRA polymers allows complete control over gel stiffness. The polymers are transparent and mimic the natural ECM environment. FAST-DEXTRAN polymers are used when cells need to obtain appropriate media within a few minutes, or when the application requires fast gelatin, as in the case of bioprinting. A TrueGel3D polymer working solution was prepared by mixing FAST DEXTRAN (170 µL, Sigma Aldrich, Cat. No. TRU-FDE), water (175 µL, Sigma Aldrich, Cat. No. TRUWA) and TrueGel3D buffer (34.5 µL, Sigma Aldrich, Cat. No. TRUBUF-55PH).

2.2.5. Blood plasma

Blood from a healthy volunteer was collected in an autologous blood bag and stored on ice. To prepare a plasma, the blood (50 mL) was gently poured into a 50 mL tube and centrifuged (3000 *g*, room temperature, 20 min, no decelerating brake). The upper clear yellow layer of plasma was then carefully removed using a 20 mL syringe. Plasma was stored at -20°C until required for experimentation.

2.2.6. Cellulase solution (GrowDase™)

Cellulase solution (GrowDase™, GDase) was provided by UPM Biochemicals, Helsinki, Finland. A working solution was prepared according to the manufacturer's instructions. The volume of GDase required for the number of seeded cells was calculated as follows:

1) well volume (μL) x [% aNFC or NFC] / 100 = mg GDxT/well

2) [mg aNFC or NFC/well] x 600 μg/mg = μg GDase enzyme

3) μg GDase/GDase stock (10 μg/μl) = μL of GDase stock

2.2.7. Collagenase and Dispase I protease solution

The retrieval of cells from NFC and aNFC was performed by enzymatic digestion with collagenase and dispase I solution including 200 U/mL of dispase I protease (10 μL, 10 U/mg, Cat. No. D4818-2MG, Sigma-Aldrich), type1 collagenase 125 CDU (collagen digestion units) (100 μL, 5 U/mL, Cat. No. C0130-1G, Sigma-Aldrich) and DPBS with $CaCl_2$, $MgCl_2$ (Gibco, Thermo Fisher Scientific 31966-021) (890 μL) for 4 h at 37°C. In order to obtain collagenase 125 CDU/mg working solution, collagenase 5 U/mL (Sigma C0130-1G) was diluted in 10 mL DPBS with $CaCl_2$, $MgCl_2$ (Gibco, Thermo Fisher Scientific 31966·021). In order to obtain dispase I protease 10 U/mg, dispase I 200U/mL (Sigma D4818-2MG) was diluted in 200 μL DPBS with $CaCl_2$, $MgCl_2$ (Gibco, Thermo Fisher Scientific 31966-021).

2.3. Kits and Solutions

2.3.1. Freezing media

90% FBS (Gibco, Thermo Fisher Scientific 10270·106) and 10% Dimethyl sulphoxide (DMSO) (BDH Chemicals 103234L).

2.3.2. Collagenase digestion solution

Collagenase 5 U/mL (Sigma C0130-1G) was diluted in 10 mL DPBS with $CaCl_2$, $MgCl_2$ (Gibco, Thermo Fisher Scientific 31966·021) to obtain collagenase 125 CDU (collagen digestion units)/mg solid working solution.

2.3.3. Dispase I solution

Dispase I 200 U/mL (Sigma D4818-2MG) was diluted in 200 μL DPBS with CaCl2, MgCl2 (Gibco, Thermo Fisher Scientific 31966-021) to obtain dispase I 10 U/mg activity (Gibco, Thermo Fisher Scientific 31966-021).

2.3.4. Fixation solution (4% Paraformaldehyde, PFA)

4% PFA (w/v) (Sigma Aldrich P6148) in 1 x DPBS solution was prepared by adding 80 mL of DPBS 1x into a glass beaker in a ventilated hood and heated to 60°C. PFA powder (4 g) was added to the heated solution and the pH adjusted to 6.9 by adding 1 N NaOH with a Pasteur pipette. DPBS 1x was added to complete 100 mL of DPBS 1x. The solution was aliquoted and stored at -20°C.

2.3.5. DEPC-treated water

1 mL of DEPC (diethyl pyrocarbonate) were mixed with 1000 mL of sterile water in a screw-cap glass bottle. The mixture was incubated for 2 h at room temperature in a fume hood with occasional swirling and autoclaved to store at room temperature for up to 12 months.

2.3.6. Cell proliferation Kit II

Cell proliferation Kit II (Sigma-Aldrich) was prepared according to the manufacturer's guidelines.

2.3.7. LIVE/DEAD® Viability/Cytotoxicity Kit for mammalian cells

4 μM EthD-1 working solution comprises of 20 μL of the supplied 2 mM EthD-1 stock solution to 10 mL of sterile, tissue culture-grade DPBS. 2 μM calcein AM working solution consists of 5 μL aliquot of the supplied 4 mM calcein AM stock solution to the 10 mL of 4 μM EthD-1 solution. Subsequently, 5 μL of 2 μM calcein AM working solution and 20 μL of 4 μM EthD-1 working solution were added in 10 mL DMEM.

2.3.8. Oil Red O stock solution

300 mg Oil Red O powder in 100 mL 99% isopropanol.

2.3.9. Oil Red O working solution

4 parts water to 6 parts oil red O stock solution, incubated for 10 min at room temperature and filtered through a 0.2 μm filter Luer lock (Sarstedt, 83.1826.001). Stable for 2 h.

2.3.10. Alizarin Red S working solution

1 mg/mL Alizarin Red S stain (Sigma-Aldrich A5533) made up in sterile water, adjusted to pH 5.5 with ammonium hydroxide (Sigma-Aldrich 320145), and filtered through a 0.2 μm filter Luer lock (Sarstedt, 83.1826.001).

2.3.11. Alkaline phosphatase, Diethanolamine Detection Kit

The kit contains sufficient reagents for 100 assays (1 mL volume each) (Sigma-Aldrich AP0100). The reaction buffer (500 mL, Catalogue number A5987) is provided as a ready-to-use solution. 0.67 M pNPP solution: 247 mg/mL of pNPP (Catalogue number P4744) was prepared in ultrapure water. Alkaline phosphatase solution (enzyme control): the alkaline phosphatase (Catalogue number P6774) was diluted to ~0.15 units/mL in cold reaction buffer. The calculation of the units/mL solution was followed as shown in the below. df=Dilution Factor, V_F=Volume (in mL) of assay, 18.5=Millimolar extinction coefficient of pNPP at 405 nm, V_E=Volume (in mL) of sample solution used.

$$[(\Delta A_{405nm}/min\ Test - \Delta A_{405nm}/min\ Blank)\ (df)\ (V_F)] / (18.5)\ (V_E)$$

2.3.12. Crystal violet staining solution

The different amount of crystal violet (0.5%, 0.01% and 0.05% v/v) in sterile water for 20 min, 5 min and 2 h, respectively. (50 μg crystal violet powder in 10 mL sterile water to prepare 0.5% working solution)

2.3.13. DAPI (4',6-Diamidino-2-phenylindole dihydrochloride) working solution

DAPI working solution (0.5 μg/mL) was prepared from a stock (1 mg/mL) (Sigma-Aldrich, D9542) by diluting it 1:2000 in sterile DPBS.

2.3.14. Phalloidin staining solution

Phalloidin working solution (0.2 nM) from a stock (10 nM) by diluting the stock with the DAPI working solution.

2.3.15. Permeability buffer

DPBS containing 0.02% Triton X100 (Sigma-Aldrich) and %5 normal goat serum (Stratech Scientific Unit, Suffolk, UK).

2.3.16. TNFα treatment

10 ng/mL human recombinant TNFα (PeproTech EC Ltd., London, UK) was diluted in 0.1% BSA (cell culture grade, Sigma-Aldrich) in DPBS (Sigma-Aldrich).

2.3.17. Fluorescein Isothiocyanate Isomer I (FITC/dextran)

The stock solution of 1 mg/mL FITC/dextran was diluted in DMSO to a final concentration of 6 µg/mL.

2.3.18. Mowiol

Mowiol (Mowiol 4.88, Carbiochem catalogue number 475904) was prepared by dissolving Mowiol (2.4 g) in glycerol (6 g) and distilled water (6 mL) for 2 h at room temperature. 2 M Tris/HCl (12 mL, pH 8.5) was then added into the mixture, followed by sodium azide (0.02%). The solution was incubated in hot water (50-60°C) for 10 min to dissolve the Mowiol and centrifuged at 5000 g for 15 min to remove any undissolved solids and then stored in 1 mL aliquots at -20°C.

2.3.19. 0.1% p-phenylenediamine (1,4-Benzenediamine hydrochloride) (PPD) (w/v) aqueous solution

0.1 g PPD (Sigma-Aldrich, P1519) was dissolved in 100 mL distilled water to prepare 0.1% PPD aqueous solution. The solution was aliquoted in 1 mL microcentrifuge tubes, wrapped in aluminium foil and stored at -20°C.

2.3.20. Fluorescent mounting media

Mounting media was prepared by mixing the Mowiol and 0.1% PPD (w/v) aqueous solution at a 9:1 ratio.

2.4. Cells

2.4.1. Cell Isolation

2.4.1.1. Human adipose-derived mesenchymal cells (ASCs)

ASCs were purchased from Lonza, Slough, United Kingdom. Fully characterised human ASCs were obtained from five non-diabetic adult donors lipoaspirates in Lonza (ASCs 34331, ASCs 28183, ASCs 30039, ASCs 29738; Slough, United Kingdom). StemPro® Human Adipose-Derived Stem Cells (Life Technologies 510070), lot number 2117 obtained from a 49-year-old female donor. All ASCs were characterised immunocytochemically and by tri-lineage differentiation assay as detailed by the manufacturer and as recommended by The International Society for Cellular Therapy (Dominici et al., 2006b). All cell lines were stored in cryovials in liquid nitrogen.

2.4.1.2. Fibroblasts

Fibroblasts were purchased from Lonza (Slough, United Kingdom). Fibroblast used in this study is normal human dermal fibroblast adult skin (NHDF 29750). The cell line was derived were obtained from five non-diabetic adult donors by Lonza.

2.4.1.3. U251-NFκB-GFP-Luc cells

The U251-NFκB-GFP-Luc cells were generated previously in this laboratory by transducing U251 cells (Cell Line Service, Eppelheim, Germany) with lentivirus produced using the pGreenFire-NFκB-Puro plasmid (System Biosciences, Palo Alto, CA, USA). NFκB-dependent firefly luciferase activity and NFκB-independent Renilla luciferase activity were assessed using Dual-Luciferase® Reporter Assay system (Promega Corporation) (Zeuner et al., 2017). Luciferase activity of U251-NFκB-GFP-Luc cells was analysed using firefly luciferase assay system (Promega Corporation) (Zeuner et al., 2017).

2.4.2. Cell Culture

2.4.2.1. Cultivation of cells in 2D monolayers

ASCs and fibroblasts were cultured in DMEM high glucose (Sigma Aldrich, lot: RNBH5598) containing 2 mM L-glutamine, 1% penicillin/streptomycin (100U penicillin with 100 µg/mL streptomycin (all from Sigma-Aldrich)), 20% heat-inactivated FBS (Sigma Aldrich, lot: 8204188981) and 1 ng/mL basic fibroblast growth factor (bFGF) (Peprotech, UK) All cells were used between passages 2-15.

U251-NFκB-GFP-Luc cells were cultivated in DMEM high glucose (Sigma Aldrich, lot: RNBH5598), 10% heat inactivated FBS (Sigma Aldrich, lot: 8204188981), 2 mM L-glutamine solution (Sigma Aldrich, lot: RNBH7479), 1% 100U penicillin with 100 µg/mL streptomycin (all from Sigma-Aldrich) and puromycin (5 µg/mL).

All cells were grown in a humidified incubator at 37°C with 10% CO_2 and the media was changed every 2-3 days. Although other studies use low glucose DMEM, high glucose DMEM was preferred in this study due to a greater potential for cell proliferation and cell attachment.

2.4.2.2. Cultivation of cells in aNFC 3D matrix

In order to cultivate ASCs in 3D, cell suspensions were mixed with 1.0% aNFC hydrogel to obtain a desired hydrogel concentration of 0.1%, 0.2%, 0.4% and 0.5% (w/v) aNFC with cell densities of 1×10^5 cells/100 µL. After incubation (30 min, 37°C), standard culture media was added to a final volume of 150 µL on top of the hydrogel/cell mixture.

2.4.3. Revival of cells from liquid nitrogen storage

All cell culture protocols including the preparation culture media prior to the thawing of cells were carried out under in a Class 2 laminar flow hood. In order to revive cells from liquid nitrogen storage, cells were quickly thawed by placing in a water bath at 37°C. As soon as the cells were thawed, they were carefully transferred into a sterile collection tube (15 mL) containing pre-warmed culture media (5 mL). Cells were then centrifuged (300 g, 10 min), the supernatant discarded, and the pelleted cells re-suspended in culture media (1 mL). Cells were then counted using a haemocytometer and seeded into T75 tissue culture-treated flasks (5×10^3 cells/cm^2) in a final volume of 10 mL of fresh media. After seeding, cells were cultured in a humidified incubator (37°C, 90% air, 10% CO_2). Any non-adherent cells were removed by replacing the media the next day. The media was exchanged every 3 days and cells were grown to approximately 80% confluency before sub-culturing.

2.4.4. Sub-culturing of cells

At approximately 80% confluency, cells were passaged and re-seeded or prepared for storage in liquid nitrogen. Briefly, the adherent monolayer was washed with DPBS (calcium- and magnesium-free), incubated with trypsin-EDTA solution (4 mL, Sigma-

Aldrich, T3924) for 10 min at 37°C. The trypsin was inactivated with a standard cultivation media (containing FBS) and the cell suspension was then centrifuged (300 g, 10 min). After centrifugation, supernatant was removed, and the cell pellet was resuspended in fresh media (1 mL) and counted using a haemocytometer and seeded at 5×10^3 cells/cm^2.

2.4.5. Counting cells using a haemocytometer

Cell suspensions obtained from cell passaging (1 mL) were diluted in standard cultivation media (1:100) in a microcentrifuge tube. After cleaning the haemocytometer with 70% of ethanol, 10 μL of the diluted cell suspension was added under the coverslip. A 4x objective (EVOS XL Cell Imaging System, Thermo Fisher) was used to find the grids on the haemocytometer, then switched to 10x objective to count the cells in each of the four corners. The number of cells was then averaged and the number of cells in 1 mL of stock cell suspension was calculated using the following calculation: the number of cells in 1 mL of stock cell suspension = the corner average x 10^4 x 1 mL).

2.4.6. Preparation of cells for long-term storage in liquid nitrogen

Dissociated cells were counted, centrifuged (300 g, 10 min) and then re-suspended (1×10^6 cells/mL) in FBS containing 10 % v/v dimethyl sulphoxide (BD Biosciences) for long-term storage in liquid nitrogen. The cells were pipetted into 1.8 mL cryovials and cooled at a rate of 1°C per minute using a Mr Frosty™ freezing container (Thermo Fisher Scientific 5100-0001) at -80°C overnight. Cryovials were then transferred from -80°C to a liquid nitrogen dewar for long-term storage.

2.4.7. Preparation of nitric acid-treated coverslips for cell culture

Coverslips were treated with 65% (v/v) nitric acid overnight with gentle agitation. Coverslips were then washed three times with sterile water for 30 min each with gentle agitation and washed a further time in 70% ethanol in a new glass beaker. Under aseptic conditions, coverslips were carefully laid out on a layer of clean tissue under a laminar flow hood. Coverslips were autoclaved after drying.

2.4.8. Absorbance Assay

Alginate, NFC and aNFC were diluted to 0.9%, 0.2% and 0.2% using DPBS. In order to perform the absorbance assay, dilutions of aNFC and NFC were made using Dulbecco's Phosphate Buffered Saline (DPBS) (Sigma-Aldrich. Irvine, UK). The samples were transferred into a 96-well plate in triplicate. Total light absorbance was measured between 240-800 nm using the Spectra Max ID3 plate reader (Molecular Devices, Wokingham, United Kingdom). All readings were corrected by subtracting the average from DPBS control values.

2.4.9. Liberation Assay

Liberation Assay was performed to liberate and visualise ASCs from aNFC with GDase (stock concentration 10 mg/mL). ASCs ($1x10^5$) embedded in 0.2% aNFC or 0.2% NFC (100 μL) were placed into non-adherent 96 well plates (Sarstedt, 83.3992). After 72 h incubation, the volume of GDase for the seeded cells was calculated and added to each well to incubate at overnight (12-18 h). The dispase/collagenase mixture was prepared and added to 100 μL for each well to incubate for 4 h. After taking images from an inverted microscope (EVOS XL Cell Imaging System, Thermo Fisher), all contents together with the retrieved cells were transferred into microcentrifuge tubes, one well corresponding to one tube. 50 μL of trypsin was added into the wells for 30 m and then transferred to microcentrifuge tubes. All contents in the microcentrifuge tubes were then centrifuged (400 g, 10 min). The pellet was then re-suspended in DPBS (100 μL) and cells were counted using a Countess^{TM} cell counting chamber slide and a Countess Automated Cell Counter. The number of cells retrieved was expressed as a percentage relative to the number of cells seeded.

2.4.10. Cell Viability Assay (XTT)

An XTT viability assay was performed to examine the viability of ASCs when seeded within aNFC. $1x10^5$ of ASCs seeded into 0.2% aNFC hydrogels per well were cultivated in a non-tissue culture treated 96 well plate (Sarstedt, 83.3924.500) as triplicate for each condition and controls. ASCs were also seeded into a tissue culture treated plate (Sarstedt, 83.3924) and cells with and without aNFC were incubated for 72 h at 37°C with 10% CO_2. After placing XTT labelling reagent (1 mL) into a microcentrifuge tube, electron coupling reagent (20 μL) was added and mixed

thoroughly. XTT solution (100 μL) was transferred to each well. Absorbance of the XTT metabolite was measured using an excitation wavelength of 490 nm and a reference wavelength of 650 nm on a Spectra Max ID3 plate reader (Molecular Devices, Wokingham, United Kingdom). Measurements were taken after 30 min, 1 h, 2 h, 3 h and 4 h. Values were corrected using the reference value (650 nm).

2.5. Media for Generation of Conditioned Media from Cells

2.5.1. Media for human ASCs

The media was prepared with DMEM high glucose (Sigma Aldrich, lot: RNBH5598) containing 20% heat inactivated FBS (Sigma Aldrich, lot: 8204188981), 2 mM L-Glutamine solution (Sigma Aldrich, lot: RNBH7479), 1% of 100U penicillin with 100 µg/mL streptomycin (all from Sigma-Aldrich) and 5 ng/mL bFGF (Peprotech, UK).

2.5.2. Media for fibroblasts

The media was prepared with DMEM high glucose (Sigma Aldrich, lot: RNBH5598) containing 20% heat inactivated FBS (Sigma Aldrich, lot: 8204188981), 2 mM L-Glutamine solution (Sigma Aldrich, lot: RNBH7479), 1% 100U penicillin with 100 µg/mL streptomycin (all from Sigma-Aldrich) and 5 ng/mL bFGF (Peprotech, UK).

2.5.3. Media for U251-NFκB-Luc-GFP cells

A specific U251 complete media was prepared with DMEM high glucose (Sigma Aldrich, lot: RNBH5598) containing 10% heat inactivated FBS (Sigma Aldrich, lot: 8204188981), 2 mM L-Glutamine solution (Sigma Aldrich, lot: RNBH7479), 1% 100U penicillin with 100 µg/mL streptomycin (all from Sigma-Aldrich) and 100 μL of puromycin from 2.5 mg/mL stock ([Final] 5 µg/mL).

2.5.4. Media for U251-NFκB-Luc-GFP cells

A specific U251 antibiotic free media was prepared with DMEM high glucose (Sigma Aldrich, lot: RNBH5598) containing 10% heat inactivated FBS (Sigma Aldrich, lot: 8204188981) and 2 mM L-Glutamine solution (Sigma Aldrich, lot: RNBH7479).

2.5.5. Serum free media for U251-NFκB-Luc-GFP cells

A specific U251 serum free media was prepared with DMEM high glucose (Sigma Aldrich, lot: RNBH5598) containing 2 mM L-Glutamine solution (Sigma Aldrich, lot: RNBH7479).

2.5.6. Differentiation of human ASCs to an adipogenic and osteogenic lineage using conditioned media

Following standard cultivation, human ASCs were prepared for the adipogenic and osteogenic differentiation in a 6-well tissue culture treated non-pyrogenic polystyrene plate (cell growth area of 9.5 cm^2 approximately) by seeding at density of 1.5x10^5 cells per cm^2 and cultured until 90% confluent. The standard media in the wells was replaced with StemPro® Adipogenesis basal media (Life Technologies A10410-01) and StemPro® Osteocyte/Chondrocyte basal media (Life Technologies, Thermo Fisher Scientific A10069-01) whereas a control group continued to be cultured in a standard media. StemPro® Adipogenesis Supplement (Life Technologies, Thermo Fisher Scientific A10065-01) and StemPro® Osteogenesis Supplement (Life Technologies, Thermo Fisher Scientific A10066-01) were prepared as the manufacturer's instructions. Cells were cultured for 21 days with a differentiation media and the media was exchanged every 3 days. After 21 days, cells were gently washed in DPBS to avoid disruption to a confluent cell layer. Cells were then fixed in 4% PFA (section '2.3. Kits and Solutions') for 30 min, washed three times with ultrapure deionised water (dH$_2$O). For adipogenic differentiation, ASCs were washed with 60% (v/v) isopropanol for 5 min and then air-dried and incubated at room temperature in a working solution of Oil Red O stain (section '2.3. Kits and Solutions') for 30 min with gentle agitation. Following staining, excess dye was removed by four washes with dH$_2$O (each for 5 min) and cells were allowed to air dry. Cells were visualized and imaged using a brightfield microscope at a high magnification (40x). A successful differentiation of ASCs towards an adipogenic lineage was identified by positive Oil Red O staining of oil droplets. For osteogenic differentiation, cells were incubated at room temperature in a working solution of Alizarin Red S stain for 30 min with gentle agitation. Following the staining, as per the osteogenic differentiation protocol, cells were washed with dH$_2$O, air-dried and imaged using a bright field microscope (for example, 10x or 20x

objectives). A successful differentiation of ASCs towards an osteogenic lineage was identified by positive Alizarin Red S staining of calcium deposits within cells.

2.6. Differentiation of Cells

2.6.1 Differentiation assays

The monolayer cultures were grown to confluency in an appropriate media and were induced to the adipogenic and osteogenic lineages by an addition of specific differentiation cocktails as described in the relevant sections.

2.6.1.1 Adipogenic and osteogenic differentiation

After cells were grown to confluency, cells were cultured in an adipogenic differentiation media including StemPro® Adipogenesis basal media (Life Technologies A10410·01) supplemented with StemPro® Adipogenesis Supplement (Life Technologies, Thermo Fisher Scientific A10065·01). For osteogenic differentiation, cells were cultured in a StemPro® Osteocyte/Chondrocyte basal media (Life Technologies, Thermo Fisher Scientific A10069-01) and a StemPro® Osteogenesis Supplement (Life Technologies, Thermo Fisher Scientific A10066-01). The cells were fed every 3 days with freshly prepared adipogenic and osteogenic differentiation medias for up to 21 days.

2.6.2 Staining protocols for assessment of cultivation and differentiation

2.6.2.1 Crystal Violet staining

ASCs were cultivated in 0.2% aNFC at 1×10^5 cells/mL within TC cell culture inserts (24 well format, $\varnothing3.0\mu M$, Sarstedt, 83.3932.300) for 72 h. Following cell culture, the cells were fixed with 4% PFA for 5 min at room temperature. ASCs were stained with crystal violet (0.05% v/v) at 4°C for 2 h. After incubation with the Crystal Violet dye, the cells were washed five times with DPBS. Images were collected using bright field microscopy on an inverted microscope (EVOS XL Cell Imaging System, Thermo Fisher).

2.6.2.2 Oil Red O staining

Oil Red O dye (Sigma Aldrich, Lot: SHBL 1039) was prepared with 300 mg Oil Red O in 100 mL 99% isopropanol (Sigma Aldrich). After allowing the crystals to dissolve for

1 h, a working solution was prepared in a distilled water and then filtered through a 0.2 μm filter Luer lock (Sarstedt, 83.1826.001). After 21 days of adipogenic differentiation, cells were carefully washed with DPBS and fixed in 4% PFA for 30 min at room temperature. Cells were washed three times with DPBS, and Oil Red O staining solution was then added to the cells for 5 min. After staining the cells, the dye solution was removed and washed twice with DPBS to remove unbound dye. Under microscope, intense red droplets with no background were seen by using the EVOS imaging system. Stained cells were covered with DPBS and either stored at 4°C or quantified for adipogenesis.

For spectrophotometric determination, the absorbance was measured at 540 nm. After staining and washing, 100 μL of 2-propanol was added and incubated for 10 min to extract the stain from the cells. The extracted dye was then transferred into a 96-well Greiner black and glass bottom plate. The optical density was measured at a wavelength of 540 nm using on a Spectra Max ID3 plate reader with SoftMax Pro7 (Molecular Devices, Wokingham, United Kingdom). The amount of extracted dye was normalised to undifferentiated cells as a negative control and differentiated adipocytes as a positive one. Dye recovery was determined using a standard curve. Based on the calibrated OD_{540nm} value of the Oil Red O standard, a standard curve was made by plotting absorbance (540 nm) as a function of Oil Red O concentration. The equation and R^2 value of the trend line were determined. The Oil Red O concentration in the samples was calculated using the standard curve (Supplement 5.2., Appendix III).

For the quantification of adipogenic differentiation, lipid droplets stained with Oil Red O dye were visualised under 40x magnification of bright field microscopy on an inverted microscope (EVOS XL Cell Imaging System, Thermo Fisher), per three random fields of view per well. The number of adipocytes formed was expressed as an average of the three wells.

2.6.2.3 Alkaline phosphatase (ALP) activity

The osteogenic differentiation was assayed using an Alkaline Phosphatase Diethanolamine Detection Kit (Sigma Aldrich, Lot: SLCB6272) following the manufacturer's protocol. For 2D culture, $5x10^5$ of ASCs were assayed in 24-well formats in triplicate. For 3D culture, $1x10^5$ of ASCs seeded into 0.2% aNFC were assayed into TC cell culture inserts (24 well format, ∅3.0μM, Sarstedt, 83.3932.300)

in triplicate. At the end of 7 days, two different protocols were followed for 2D and 3D cell culture. For 2D culture samples, 30 µL of Lysis buffer including 50 mM Tris and 0.1% Triton X-100 was added to each well which was then waited at 4°C for 30 min. After pipetting into each well, 2 µL per sample was put in a 96-well plate, and then added reaction buffer supplemented with the pNPP substrate including 96 µL of reaction buffer and 2 µL of pNPP substrate. For 3D test samples, the growth media was taken off the insert and ASCs seeded into 0.2% aNFC were kept on the bottom. 100 µL of reaction buffer was pipetted in the insert to mix ASCs embedded into 0.2% aNFC, and then all contents were transferred to a 96-well plate. Subsequently, the reaction buffer supplemented with the pNPP substrate including 98 µL of reaction buffer and 2 µL of pNPP substrate were added into the same 96-well plate. The enzyme control cuvette was prepared by mixing 2 µL of diluted Alkaline Phosphatase solution and reaction buffer supplemented with the pNPP substrate including 96 µL of reaction buffer and 2 µL of pNPP substrate. For blank cuvette, 98 µL of reaction buffer was pipetted to a 96-well plate, and then added 2 µL per sample. Subsequently, the wells were equilibrated to 37°C for 5 min. The yellow colour developed from the phosphatase reaction was measured at 405 nm in triplicate. The increase in A_{405nm} was recorded to obtain the maximum linear rate (ΔA_{405nm}/min) for the test, blank and control. The amount of ALP enzyme was deduced from the standard curve drawn from 1 mL each of six p-nitrophenol concentration, ranging from 30 μg to 0.75 μg. The absorbance in a spectrophotometer at 405 nm was measured at different intervals (from first minute until 30 min). Using pNPP calibration curve of concentration, the concentration of p-nitrophenol at each time period was calculated and the results was graphed with time on the *x*-axis and p-nitrophenol on the *y*-axis (Supplement 5.3., Appendix III).

2.6.2.4 Osteogenesis: Alizarin Red S staining

After 21 days of osteogenic differentiation, calcium deposition was assessed by using 2% w/v Alizarin Red S solution. 2 g Alizarin Red S was dissolved in 100 mL sterile water, and pH was adjusted to 4.1-4.3 with 0.1% NH_4OH. The solution was filtered through a 0.2 μm filter Luer lock (Sarstedt, 83.1826.001). The cell monolayers were carefully washed with DPBS with $CaCl_2$, $MgCl_2$ (Gibco, Thermo Fisher Scientific 31966·021). The cell monolayer was subsequently fixed in 4% PFA for 30 min at room temperature, washed twice with sterile water and stained with Alizarin Red S

solution (pH 4.1-4.3) for 45 min at room temperature in the dark. Unincorporated dye was then aspirated, and cells washed three times with sterile water. The cells were counterstained with DAPI to visualise nuclei and incubated for 30 min at room temperature in the dark. After the staining procedure, cells were covered with DPBS with $CaCl_2$, $MgCl_2$ (Gibco, Thermo Fisher Scientific 31966·021) and observed using bright field microscopy on an inverted microscope ((EVOS XL Cell Imaging System, Thermo Fisher). Undifferentiated ASCs in the control group were slightly reddish, whereas the differentiated ASCs with extracellular calcium deposits were bright orange red.

Alizarin Red S dye extraction was quantified using the EVOS imaging system. All images were analysed using GraphPad Prism software (GraphPad, La Jolla, CA, USA). Using the protocol adapted from (Gregory *et al.*, 2004), the dye was recovered by acetic acid extraction. Briefly, 400 µL of 10 % v/v acetic acid (Thermo Fisher) was added to each well and incubated for 30 min while shaking at room temperature. Using a wide-mouthed pipette, the loosely attached cells were scraped and transferred to a 1.5 mL tube and vortexed for 30 s. The slurry obtained was covered with mineral oil and heated for 20 min at 85°C. The tubes were then iced for 5 min and centrifuged (accuSpin™ Micro) at 20 000 rpm for 15 min. A volume of 500 µL of the supernatant was transferred to a fresh tube containing 100 µL of 10 % v/v ammonium hydroxide and the pH measured to ensure a range of between 4.2-4.3. Aliquots of 100 µL were read in triplicate in a 96-well Greiner black and glass bottom plate. The optical density was measured at a wavelength of 405 nm using ID3 spectrophotometer with SoftMax Pro7. Dye recovery was determined using a standard curve. Based on the calibrated OD_{405nm} value of the standard, a standard curve was made by plotting absorbance (405 nm) as a function of Alizarin Red S concentration. The equation and R^2 value of the trend line were determined. According to the equation of the trend line, the Alizarin Red S concentration in the samples were calculated (Supplement 5.1., Appendix III).

2.6.2.5 Fluorescent Dye staining

Phalloidin Atto 555 (Sigma-Aldrich-19083) and AlexaFluor™ 647 (ThermoFisher-A22287) were used to label the actin filaments of ASCs seeded in 0.2% aNFC at 1×10^5 cells/mL within TC cell culture inserts (24 well format, $\varnothing 3.0 \mu M$, Sarstedt,

83.3932.300) for 7 days at 37°C with 10% CO_2. Following cell culture, the cells were fixed with 8% PFA for 45 min at room temperature (section '2.3. Kits and Solutions'). ASCs were gently washed with DPBS (5 min) and then incubated with DPBS/0.1% Triton X-100 (100 μL per well) for 30 min at room temperature. After the DPBS/0.1% Triton X-100 was carefully removed, cells were washed once DPBS for 5 min before 100 μL of Phalloidin/DAPI staining solution (section '2.3. Kits and Solutions') was added to the cells and incubated overnight at 4°C. Following an overnight incubation, the staining solutions were removed, and the cells were washed once with DPBS. Following the final wash, DPBS was replaced with DPBS/0.02% Sodium azide and the samples were imaged using the Nikon A1-R inverted confocal microscope.

2.7. Immunocytochemistry

2.7.1. Immunocytochemistry staining for 2D and 3D cell culture

After 7, 14 and 21 days of an osteogenic differentiation, ASCs in 2D culture were washed gently with DPBS. Fixation stage with 4% PFA was carried out for 20 min at room temperature, followed by further washing stages with DPBS. Cells were incubated with a PBS/0.02% Triton-X 100 including 5% horse serum for 30 min. Osteocalcin antibody (G-5) (Santa Cruz Biotechnology, sc-365797) and osteopontin antibody (AKm2A1) (Santa Cruz Biotechnology, sc-21742) were used as primary antibodies. The primary antibody (pre·diluted in DPBS/0.02% Triton X-100 with 5% horse serum at room temperature for 30 min) was added and incubated for 90 min at room temperature. The sample was washed three times in DPBS to remove any unbound primary antibody and the secondary antibody (pre-diluted in DPBS/0.02% Triton-X 100 with 5% horse serum at room temperature for 30 min in the dark) was added and incubated for 1 h at room temperature in the dark. The sample was washed three times in DPBS to remove any unbound secondary antibody. DAPI (1:2000 in DPBS) was then performed on the cells for 15 min, followed by further washing stages, three times with DPBS. Finally, cells were mounted onto a glass microscope slide and covered with a cover slip affixed with mounting media for analysis. Samples were imaged using a Zeiss AxioImager A1 fluorescent microscope and Axiovision software (v4.0). Immunofluorescence negative controls were fixed and stained under the same conditions.

ASCs embedded into 0.2% aNFC within TC cell culture inserts (24 well format, $\varnothing 3.0\mu M$, Sarstedt, 83.3932.300) were cultured for 7, 14 and 21 days at 37°C with 10% CO_2. Following the osteogenic differentiation of ASCs in 3D aNFC, the cells were washed with DPBS, followed by a fixation using 4% PFA for 20 min at room temperature (section '2.3. Kits and Solutions'). Following fixation, 4% PFA was removed and cells were gently washed twice with DPBS. The DPBS was replaced with 100 μL DPBS/0.02% Triton-X 100 with 5% horse serum for 1 h at room temperature. The DPBS/0.02% Triton-X 100 with 5% horse serum was removed carefully without disturbing the scaffold of cells before washing with DPBS for 5 min. 100 µL of primary antibodies (osteocalcin antibody (G-5) (Santa Cruz Biotechnology, sc-365797) and osteopontin antibody (AKm2A1) (Santa Cruz Biotechnology, sc-21742)) staining solution (1:100) (as detailed in the Appendix II) was added to the inserts and incubated for 3 days at 4°C. Following 3 days incubation, the staining solutions were gently removed, and the cells were washed once with DPBS. Following the final wash, the DPBS was replaced with secondary antibodies (1:300) (Donkey α-mouse 555 Alexa Fluor) for 2 days at 4°C. After washing with the DPBS, the cells were counterstained with DAPI in DPBS (1:2000 Sigma Aldrich) and incubated for overnight at 4°C. Following the final washing, the DPBS was replaced with 0.02% DPBS-Sodium Azide and the samples were imaged using the Nikon A1-R inverted confocal microscope.

2.8. Live/Dead Cytotoxicity Assay

The LIVE/DEAD® Viability/Cytotoxicity Assay Kit (Invitrogen, Molecular Probes) provides a two-colour fluorescence cell viability assay. It allows the simultaneous determination of live and dead cells with two probes to measure different parameters of cell viability such as intracellular esterase activity and plasma membrane integrity. Live cells are determined by the presence of ubiquitous intracellular esterase activity with the enzymatic conversion of the nonfluorescent cell-permeant calcein AM to the fluorescent calcein. The dye calcein produces an intense uniform green fluorescence in live cells (ex/em ~495 nm/515 nm). Ethidium homodimer-1 (EthD-1) affects the damaged cells by 40-fold improvement of fluorescence in dead cells (ex/em ~495 nm/635 nm). ASCs were cultured in 0.2% aNFC at $5x10^4$ cells/100 μL for 21 days within TC cell culture inserts (24 well format, $\varnothing 3.0\mu M$, Sarstedt, 83.3932.300). The

dye was reconstituted according to the manufacturer's protocol (Thermo Fisher) and the cells were stained with a Live/Dead viability/cytotoxicity kit for 45 min. Cells were then fixed in 4% PFA for 30 min and counterstained with DAPI (Sigma-Aldrich) for 15 min. All images were taken using the Nikon A1-R inverted confocal microscope with the Nikon Plan Apo VC 20x DIC N2 optic lens, running NIS Elements AR. DAPI was imaged at an excitation/emission of 405/450 nm, calcein 494/517 nm and EthD-1 at 528/617 nm. 3D reconstructions were created with z-stack depths of 200 μm (z-plane) for all the channels using the NIS Elements AR software (v4.0).

2.9. Calcium Imaging

ASCs were seeded in 0.2% aNFC at 1×10^7 cells/mL and plated within cell culture chambers (Sarstedt) and incubated for 72 h. ASCs were also seeded at density of 1×10^5 cells per cm^2 in a 6-well plate (Corning Incorporated Costar REF 3516). To induce osteogenic differentiation, cells were cultured in the osteogenic differentiation media for 7, 14 and 21 days with fresh differentiation media changes every 3 days. After 3, 7, 14 and 21 days, cells were gently washed with DPBS and incubated with 1x HBSS supplemented with 2.5 μM Fluo-4 (Molecular Probes, Eugene, OR USA) and 1x HBSS supplemented with 2.5 mM Probenecid (25 mM HEPES Buffer and 2.5 mM Probenecid) for 45 min at 37°C. Subsequently, the cells were rinsed twice in DPBS and incubated with HBSS supplemented with 2.5 mM Probenecid (25 mM HEPES Buffer, 2.5 mM Probenecid and pH 7.4) for 15 min at room temperature.

For the quantification of calcium imaging of ASCs in 3D aNFC, the chamber was visualized on an inverted fluorescence microscope (EVOS FL, AMG, WA, USA). The images of cytosolic calcium (Ca^{2+}) were obtained in real time through a 4x/0.13 numerical aperture (NA) objective using a CCD camera (Sony ICX285AQ, Tokyo, Japan). Ca^{2+} oscillations were recorded every 10 s for 340 s and images were analysed using ImageJ software (Schneider et al., 2012). For the quantification of ASCs in 2D, cells were visualized on a 2-Photon microscopy. Average fluorescence quantification of calcium imaging for each condition was determined and analysed using an OriginLab software. All images used in current thesis were designed using ImageJ software.

2.10. Gene expression analysis

2.10.1. Ribonucleic acid (RNA) extraction

Total RNA was extracted using TRIzol reagent (1 mL, Invitrogen) according to the manufacturer's guidelines. Briefly, TRIzol reagent was added to the cells followed by chloroform (200 µL). The tube was shaken to mix the contents and was centrifuged (12000 g, 15 min, 4°C). The aqueous phase (top layer) was carefully transferred to a fresh tube. The RNA was precipitated by mixing with 2-propanol (500 µL), followed by incubation on ice for 10 min. RNA was collected by centrifugation (12000 g, 20 min, 4°C). DEPC-treated water was prepared (section '2.3. Kits and Solutions'). The supernatant was carefully removed, and the RNA pellet was washed with a 70% ethanol/ 30% DEPC-treated water (1 mL). The pellet was collected via a centrifugation (7500 g, 10 min, 4°C). Finally, the RNA pellet allowed to air dry for 2 min and then was suspended in DEPC-treated water (20 µL). The RNA was then quantified using a Nanodrop 2000 Spectrophotometer (Thermo Scientific) and stored at -80°C.

2.10.2. Removal of Genomic DNA

RNA (0.5 µg) was diluted to a final volume of 8 µL using DEPC-treated water. Following then, 10x reaction buffer with MgCl$_2$ (1 µL) and RNase-free DNase I () (IU) (1 µL) were added to a final volume of 10 µL. After a brief vortex, the reaction was collected by pulsing in a centrifuge. The reaction was then incubated in a thermal cycler (37°C, 30 min). EDTA (1 µL, 50 mM) was added to the reaction and incubated at 65°C (10 min). This product was used as a template for cDNA synthesis.

2.10.3. cDNA synthesis

For cDNA synthesis, a First Strand cDNA Synthesis Kit (Thermo Scientific) was used following the manufacturer's protocol. Briefly, RNA (11 µL, after genomic DNA removal) was added to DEPC treated water (0.5 µL), and then random hexamer primer (1 µL, Thermo Scientific, SO142) was added into the mixture to incubate for 5 min at 65°C. Following this step, 10 mM dNTP mix (2 µL, Thermo Scientific), RevertAid H Minus M-MuLV reverse transcriptase (200 U/µL) (1 µL, Thermo Scientific, K1632), Ribolock RNase inhibitor (20 U/µL) (0.5 µL, Thermo Scientific) and 5x reaction buffer (4 µL, Thermo Scientific) were added and incubated for 5 min at

25°C. The first strand cDNA synthesis was carried out for 1 h at 42°C, and the reaction was inactivated for 5 min at 70°C. Subsequently, the reaction was stored at -20°C.

2.10.4. Polymerase Chain Reaction (PCR) amplification

PCR screens were executed using PCR Thermal Cycler. A typical 25 µL reaction was set up with a final concentration of reagents as follows: Dream Taq PCR mastermix (2x) (12.5 µL, Thermo Scientific, K1071), each primer (1 µL) and DEPC-treated water (9.5 µL). DNase-free PCR tubes were placed on ice, and then cDNA (1 µL) was added into the tubes. The respective mastermix (24 µL) was added into the tubes (including cDNA (1 µL)) to total product (25 µL), and then followed by flicking the tubes and centrifuge shortly. The PCR conditions used for gene screening were 95°C for 2 min, 35 cycles of (95°C for 30 s, *x* for 30 s, 72°C for 30 s), then 72°C for 10 min, where *x* refers to the annealing temperature used for specific primer pair. Information on the annealing temperatures and primer pairs used for each gene is listed in Supplement 2.2., Appendix I.

2.10.5. Agarose gel electrophoresis

PCR products were separated on 2% w/v agarose gels with 0.005% SYBR™ Safe DNA Gel Stain (Thermo Fisher Scientific S33102) for DNA visualisation. PCR samples were mixed with DNA loading buffer (6x stock concentration: Bromophenol Blue/Glycerol), electrophoresed for typically 1 h and visualised on Uvitec™ transilluminator imaging system. Agarose was dissolved in 1x Tris-acetate-EDTA (1xTAE, 100 mL) to make a 2% (mini) gel containing SYBR safe DNA gel stain (Thermo Fisher Scientific S33102), with care taken to avoid creating air bubbles. Once set, the gel was submerged in TAE buffer in the electrophoresis chamber, the combs were removed, and samples were loaded into wells along with loading buffer (Thermo Fisher Scientific R0631; for example, loading dye (2 µL) was added to PCR reaction product (18 µL)). The first well of each row, however, was loaded with 100 bp DNA ladder (1 µL, Promega G2101) and following a 40-minute electrophoresis run at 80 V. The presence and sizes of bands were visualized and imaged using an ultraviolet (UV) transilluminator system, were used to determine the genotypes of differentiated ASCs for osteocalcin, osteopontin, osterix, BMP2 and RunX2, respectively. Primers were designed using the primer designing tool on the NCBI

Blast website and the primers listed in Supplement 2.2., Appendix I. All data were normalised to the housekeeping gene, GAPDH.

2.11. Biological sample preparation for critical point drying and scanning electron microscopy (SEM) EMLAB (Electron Microscopy Laboratory) protocol

aNFC (0.5%) with and without cells ($1x10^6$ cells/mL) were fixed with 2% formaldehyde and 2% glutaraldehyde in 0.05 M cacodylate buffer for 24 h. The aNFC was then washed twice with deionised water and placed on 10 mm $\varnothing$ melinex coverslips (mesh-side down). The samples were then frozen by submersion in liquid nitrogen-cooled ethane and freeze-dried overnight (EMITECH K775X liquid nitrogen-cooled freeze dryer, Quorum Technologies).

Using silver-DAG (TAAB), the melinex coverslips were mounted on aluminium SEM stubs. In order to secure the sample on the coverslip and ensure conductivity, silver-DAG around the bottom rim of the mesh/sample was performed. An EMITECH K575X sputter coater (Quorum Technologies) then coated samples with 35 nm gold and 15 nm iridium particles. The samples were imaged with a FEI Verios 460 scanning electron microscope, which includes a probe current of 50 pA and an accelerating voltage of 2 keV. SEM imaging was carried out secondary electron mode via an Everhart-Thornley detector (ETD) or immersion mode through a Through-Lens detector (TLD). ImageJ Fiji was performed to measure the fibre diameter and pore sizes on the SEM imaging (Schindelin et al., 2012). The more than 280 fibres and pores were measured for data analysis.

2.12. Statistical analysis

Using GraphPad Prism software (GraphPad version 8.4.3), statistical analysis was performed (GraphPad, La Jolla, CA, USA). Data were compared using one-way analysis of variance (ANOVA) with Bonferroni correction (confidence interval 95%) or Student's t-test (two-tailed, confidence interval 95%), where appropriate. Standard error of the mean (SEM) was represented with error bars to indicate the results and values were shown as means±SEM. At least three independent experiments were performed in triplicate. ***$P<0.0001$, **$P<0.01$ and *$P<0.05$ were considered to be statistically significant.

Chapter 3

Assessment of the optical properties of anionic nanofibrillar cellulose for 3D imaging, biocompatibility and viability with human adipose-derived mesenchymal stem cells

3.1. Introduction

Stem cells are important in various fields including tissue engineering and regenerative medicine due to their capacity to self-renew and differentiate into specialized cell types. A requirement for efficient clinical approaches to stem cell treatment is large-scale expansion and homogenous differentiation. Generally, there are two methods used for the maintenance and expansion of cells: 1) traditional methods including 2D culturing techniques on plastic culture plates and 2) modern three-dimensional 3D cell culture which mimics the *in vivo* environment (McKee and Chaudhry, 2017). The generation of stem cells in 2D culture as a monolayer might necessitate xenogeneic materials including cytokines, growth factors and serum. However, xenogeneic media might be a risk for transmitting pathogens and might limit reproducibility (McKee and Chaudhry, 2017). Furthermore, MSC cultivation and cellular transformation in 2D culture might lead to an increased risk of chromosomal aberrations, loss of multipotency and cellular senescence. MSC expansion in 2D culture can also give rise to phenotypic changes such as converting from a spindle shape to a broad, flattened morphology (McKee and Chaudhry, 2017). Due to these limitations of 2D culture methods, 3D techniques have been developed to address the drawbacks of the 2D culture system (McKee and Chaudhry, 2017).

3D culture systems such as spheroids/organoids, multi-layered tissue-like models and scaffold models have recently been developed with a variety of biomaterials (Shamir and Ewald, 2014). 3D tissues are commonly built by means of hydrogel-based biomaterials (for example Matrigel and PuraMatrix) (Huerta et al., 2015, Li et al., 2014b). Although these biomaterials have a satisfactory degree of mechanical softness, the use of hydrogel-based biomaterials can be hindered by drawbacks related to the cost and heterogeneity of the biomaterials (Hughes et al., 2010). Multi-layer models can be used for biomedical applications including skin toxicology measurement, but multi-layer models are not favoured for complex tissues such as those related to vasculature (Rozman et al., 2009). Notwithstanding the putative benefits of 2D monolayer culture, 3D culture systems have paid great attention to the biocompatibility of scaffold materials which integrate microfabrication techniques (Shin et al., 2012).

The need for biomedical treatments has driven the development of tissue engineering techniques that support expansion and differentiation (del Valle et al., 2017). For example, Baraniak and McDevitt (2012) developed 3D culture methods supporting the formation of multicellular spheroids (Baraniak and McDevitt, 2012). They seeded tissue-specific cells into 3D scaffolds which mimic the natural extracellular matrix (ECM) of the targeted tissues (El-Sherbiny and Yacoub, 2013). The design of biomaterials seeks to promote the correct distribution of the seeded cells in the body, interaction between cells and biomaterials, improvement of cell proliferation-differentiation and increased anti-inflammatory and cytotoxicity properties *in vivo* (Langer and Tirrell, 2004). Some results are consistent with those of a previous study in which 3D interactions between cells and ECM without additional substrates have improved osteogenic differentiation and subsequently bone regeneration (Baraniak and McDevitt, 2012). As a scaffold model, the use of an artificial ECM for cellular therapy has actually been shown to improve the osteoconductive properties for bone formation (Egger et al., 2018). Takewaki et al. (2017) reported that ECM-MSC transplantation had been performed for periodontal bone regeneration in seven dogs. The ECM-MSC complex (without any artificial substrates) induced cellular functions *in vitro* and improved bone healing following transplantation into the damaged area. MSCs cultivated in ECM-scaffolds have shown a greater potential for bone recovery than cell therapy alone (Takewaki et al., 2017).

3.2. Objectives

The objectives in this chapter are to examine different 3D biomaterials with a particular focus on the biocompatibility of the scaffolds for ASCs. The work focused on two different aspects: the best performing hydrogel and the best solid substrate for ASC culture. First, different hydrogel-based scaffolds were examined for their absorbance using a visible light spectrum. Next, the viability of ASCs in 3D scaffolds was compared with cells grown in conventional 2D culture. The hypothesis was that 3D anionic nanofibrillar cellulose (aNFC) hydrogels would have superior biocompatibility and improve the viability and osteogenic differentiation potential of ASCs. The latter could then be explored for bone regeneration and tissue repair.

The objectives therefore were

To assess the optical properties and biocompatibility of ASCs with different hydrogel scaffolds

- The absorbance spectrums of different concentrations of alginate, dextran-based scaffold and serum-free fibrin were compared with nanofibrillar cellulose (NFC) and aNFC hydrogels to assess their optical properties.
- XTT assays and live/dead cytotoxicity tests were conducted to assess cell viability.
- Liberation assays were conducted to retrieve cells from aNFC and NFC.
- Calcium imaging in 3D culture was evaluated in ASCs to examine unsynchronized Ca^{2+} oscillations.

To combine the best performing hydrogel with the best solid substrate

- In order to increase stiffness, the biocompatibility of magnesium with the best performing hydrogel was evaluated using calcofluor white staining and epifluorescent microscopy.

3.3. Results

3.3.1. aNFC demonstrated a low level of absorbance over the whole light spectrum

In order to determine the compatibility of aNFC with 3D imaging techniques, the optical properties of aNFC (0.2%, 0.4% and 1.0%) were evaluated using different wavelengths of light (240-800 nm) and compared with 0.9% alginate hydrogel (Figure 3.1B). Compared with the 0.9% alginate hydrogel, all concentrations of aNFC exhibited a lower absorption over the whole spectrum. The absorption of all concentrations of aNFC was lower at wavelengths between 240-300 nm and 0.9% alginate and aNFC showed an increase with increasing concentrations.

Next, the optical properties of 0.2% NFC, 0.9% alginate, TrueGel3D, 0.2% aNFC and 10% blood plasma were compared (Figure 3.1C). 0.2% NFC, 0.9% alginate, TrueGel3D, 0.2% aNFC and 10% blood plasma exhibited similar optical properties between 500-800 nm, all demonstrating low absorbance. However, both 0.2% NFC and 0.2% aNFC showed superior optical properties (lower absorbance) in the lower wavelengths (240-400 nm), with TrueGel3D and 10% blood plasma displaying the

poorest optical properties (higher absorbance). Overall, aNFC demonstrated the lowest absorbance over the whole spectrum, with its highest absorbance between 240-350nm (Figure 3.1B-C).

To determine the distribution of cellulose fibres, aNFC was stained with calcofluor white in order to visualise the mesh-like cellulose content (Figure 3.2, left panel). Fluorescence imaging with calcofluor white showed that aNFC formed a mesh-like structure with high and low content of cellulose (Figure 3.2, left panel). Crystal violet staining showed ASCs embedded in 0.2% aNFC (Figure 3.2, right panel).
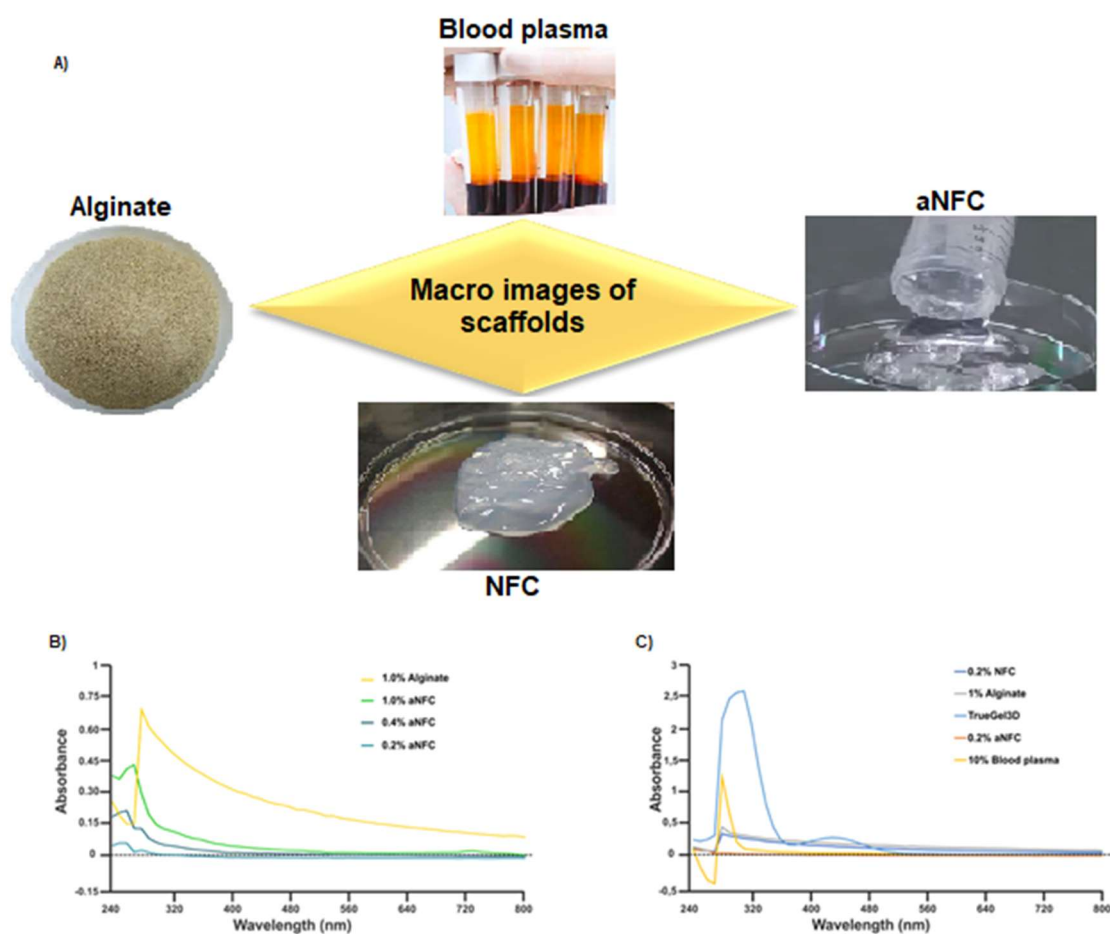
Figure 3.1. Hydrogel-based scaffolds showed superior optical properties with light absorbance spectrum. (A) Macro images of the aNFC and other scaffolds. Macro images of aNFC hydrogel and other scaffolds are obtained from Widera Lab at the University of Reading. (B) A light absorbance spectrum of 0.2% aNFC was compared with 0.4% and 1% aNFC, and 0.9% alginate. 0.2% aNFC had the lowest absorbance in other scaffolds. (C) A light absorbance spectrum of 0.2% aNFC, 0.2% NFC, 0.9% alginate, TrueGel3D and 10% blood plasma showed that 0.2% aNFC had the lowest absorption between 240-800 nm.
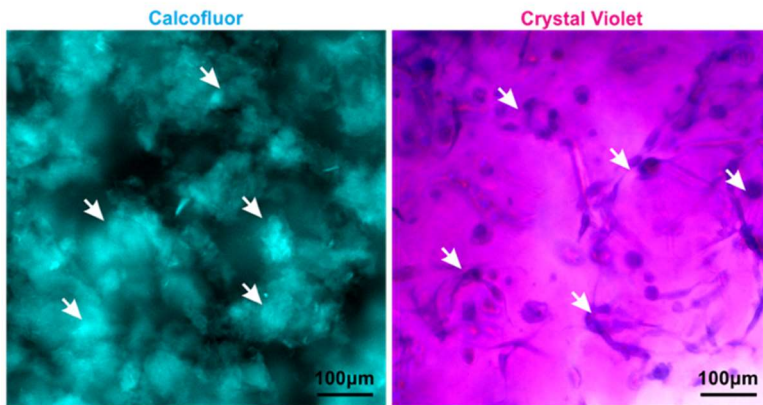
Figure 3.2. The distribution of 3D aNFC hydrogel was visualised with calcofluor white staining. Fluorescence microscopy showed a mesh-like cellulose network (shown by the arrows). Bright field microscopy of crystal violet staining showed intensely stained, evenly distributed ASCs in an aNFC matrix (shown by the arrows). 0.2% (w/v) aNFC with cell densities of 1×10^5 cells/100µL. Scale bar: 100 µm.

3.3.2. aNFC demonstrated a higher level of fluorescence emission spectra over the whole light spectrum

In order to determine the compatibility of aNFC with fluorescence-based techniques (such as fluorescence microscopy), fluorescence emission was measured for each substrate (DAPI and FITC-dextran) with excitation wavelengths of 405 nm (DAPI) and 488 nm (FITC-dextran) and emission was recorded for 485-750 nm, as shown in Figure 3.3. The results showed a higher level of fluorescence emission in aNFC than in other scaffolds. aNFC was therefore proved to be compatible with the fluorescence-based techniques.
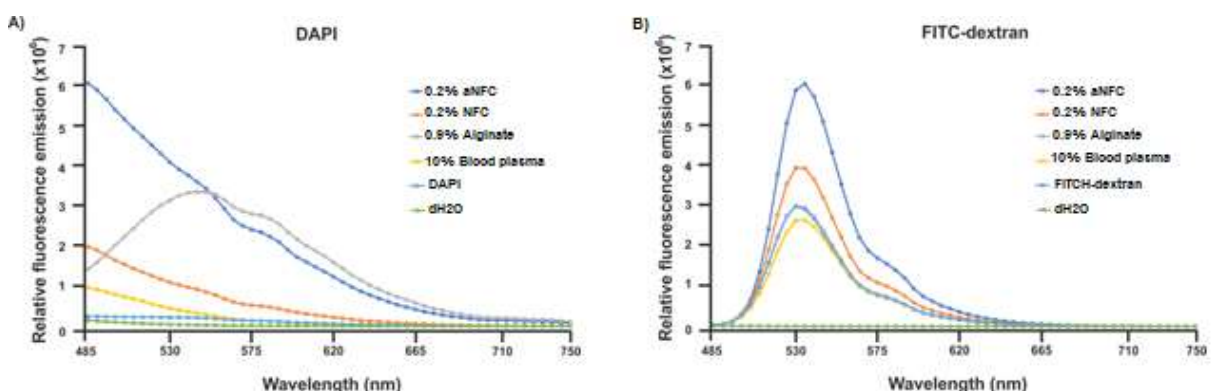
Figure 3.3. Hydrogel-based scaffolds showed a high level of fluorescence emission by light microscopy. (A-B) The fluorescence spectra from different

substrates (aNFC, NFC, alginate and blood plasma) were measured with a spectral scanning plate reader, with excitation wavelengths at 405 and 488 nm in terms of DAPI and FITC-dextran respectively. The excitation wavelengths were selected to reflect usual biological imaging. The fluorescence spectra of aNFC showed higher emission at the excitation wavelength of commonly used molecular probes (405 and 488 nm) compared with NFC and alginate.

3.3.3. aNFC formed a dense mesh-like network with heterogeneous pore sizes

To further analyse the structure of the aNFC hydrogel, scanning electron microscopy (SEM) was employed. Image analysis showed that aNFC was a dense mesh-like structure of cellulose that formed nano-scale fibres ranging from 10-70 nm with a mean fibre diameter of 28.8 ± 0.6 nm (Figure 3.4A-B). aNFC hydrogels also contained heterogeneous pores ranging from 1-100 μm^2 with a mean size of 10.5 ± 0.9 μm^2 (Figure 3.4C-D). The images shown in the Figure 3.4A were acquired at the Cambridge Advanced Imaging Centre (CAIC) using scanning electron microscopy.
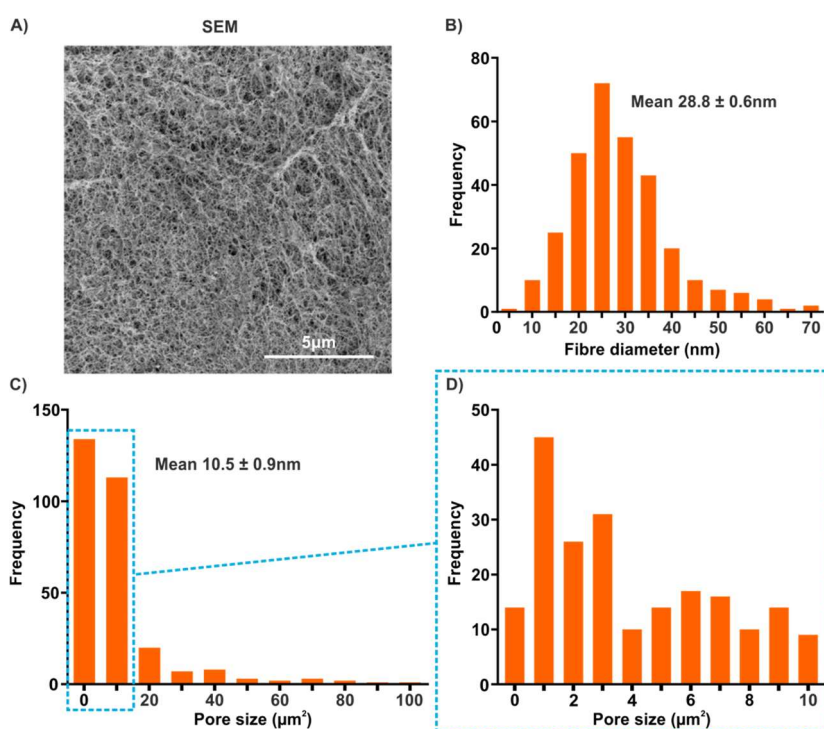
Figure 3.4. Scanning Electron Microscopy showed the structural organization of the 3D aNFC. (A) A dense mesh-like structure of cellulose was visualized with SEM. Scale bar: 5 μm. (B) Analysis of SEM imaging showed a mean fibre diameter of 28.8 ± 0.6 nm. (C-D) A heterogeneous pore size of aNFC was shown ranging from 1-100 μm and a mean size of 10.5 ± 0.9 μm^2.

3.3.4. Magnesium substrate failed to adhere to aNFC

In order to make hydrogels containing ASCs suitable for transplantation *in vivo*, the stiffness of the hydrogel must be increased by combining it with stiff materials, such as magnesium scaffolds. So, in order to examine and visualize the adhesion of aNFC hydrogel with magnesium scaffolds, 0.2% aNFC hydrogel was combined with magnesium substrate. After leaving the magnesium and aNFC together for 2, 24 and 48 h, the samples were stained using calcofluor white and visualised using epifluorescent microscopy (Figure 3.5A-D). Image analysis showed that aNFC did not adhere to the magnesium substrate.
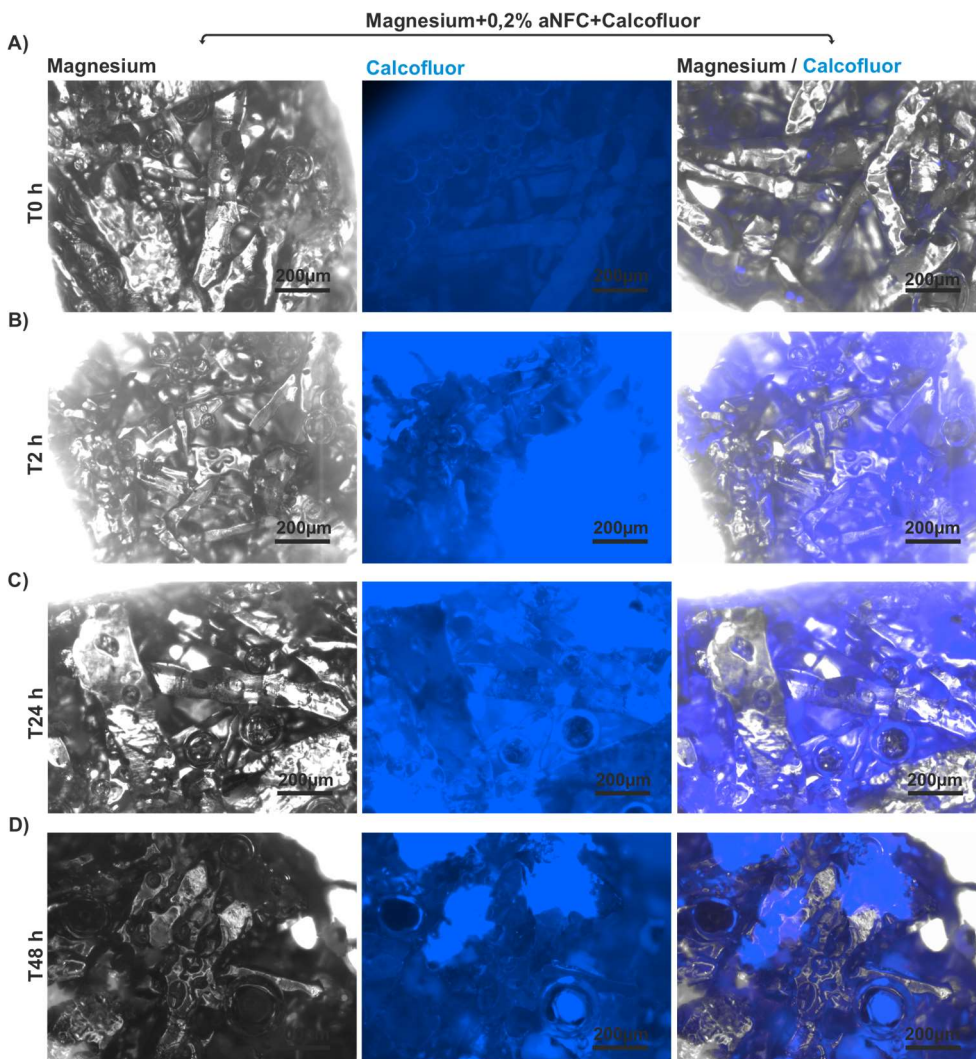
Figure 3.5. aNFC hydrogels did not attach to magnesium scaffolds. (A) A magnesium scaffold combined with 0.2% aNFC hydrogel was stained with calcofluor white staining and visualized with epifluorescent microscopy to detect the compatibility of aNFC. (B-D) After leaving the magnesium and aNFC together for 2, 24 and 48 h, the aNFC was visualised with calcofluor white. The images showed that

there was no adhesion of the magnesium scaffold with 0.2% aNFC compared with images stained with calcofluor in the middle. Scale bar: 200 µm.
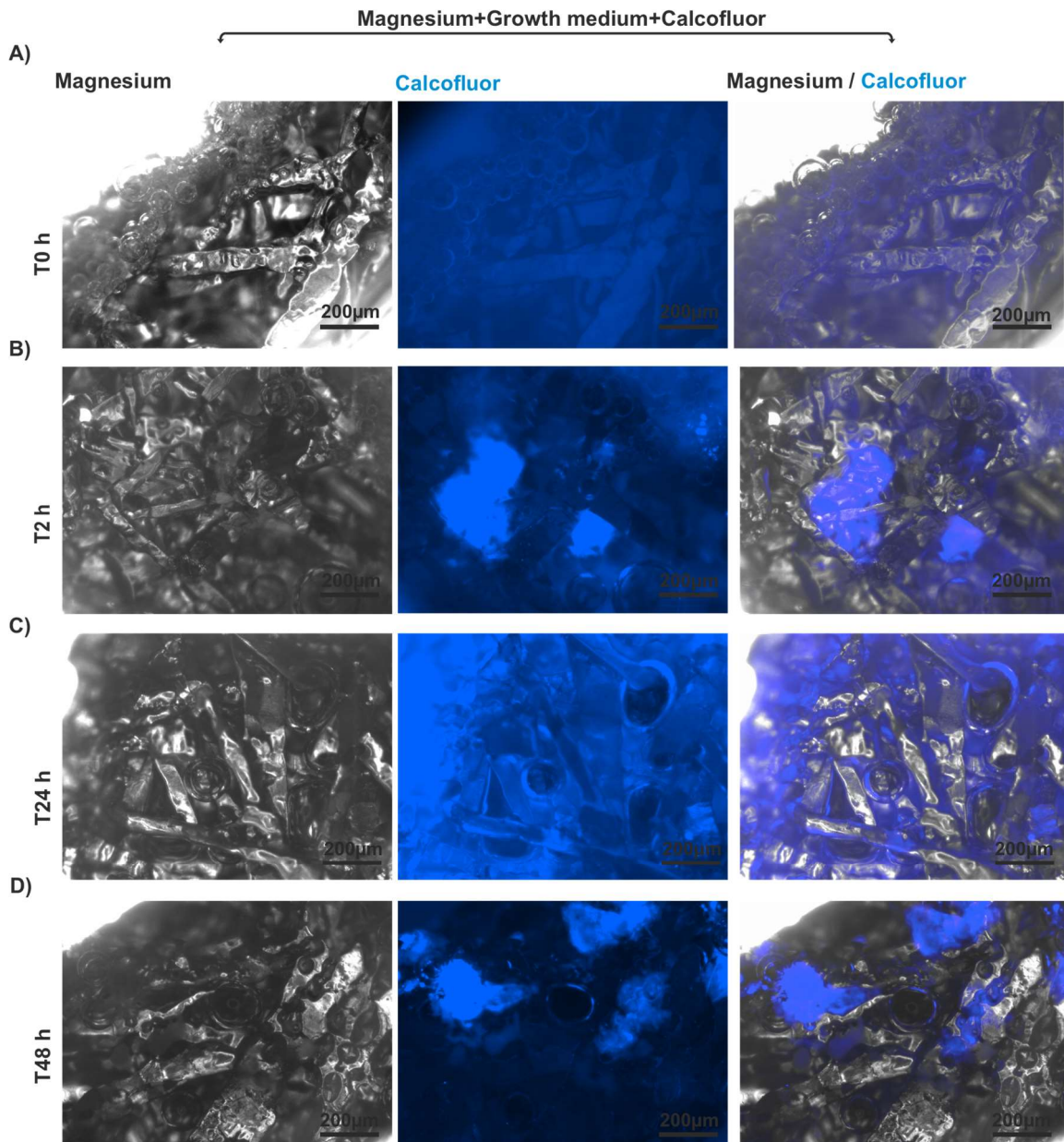
Figure 3.6. aNFC hydrogels did not attach to magnesium scaffolds in a standard culture media. (A) A magnesium scaffold cultivated in a standard media was stained with calcofluor white and visualized using epifluorescent microscopy to detect the compatibility of the standard media. Scale bar 200 µm. (B-D) After leaving the magnesium and standard media together for 2, 24 and 48 h, there was not enough adhesion. There was a lack of attachment of the standard media with magnesium compared with the images stained with calcofluor in the middle. Scale bar: 200µm.

Magnesium scaffolds were combined with aNFC in a standard growth media and stained with calcofluor white to visualise the aNFC. Even in the presence of a growth media, the aNFC did not attach to the magnesium scaffold (Figure 3.6A-D). After leaving the magnesium and standard media together for 2, 24 and 48 h, there was not enough adhesion or diffusion due to the lack of attachment of the standard media with calcofluor white staining (Figure 3.6B-D). Due to the poor adherence of magnesium to aNFC, it was decided to use aNFC alone combined with ASCs for future experimentation.

3.3.5. ASCs were biocompatible with aNFC hydrogels in 3D

The biocompatibility of ASCs cultivated in different concentrations of aNFC hydrogel was evaluated using bright field and SEM microscopy. The bright field microscopy images showed that ASCs embedded in 0.2% aNFC hydrogel exhibited a good adhesion and presented a typical, fibroblast-like morphology (Figure 3.7A). Furthermore, SEM revealed that ASCs seeded into 0.5% aNFC hydrogel formed direct interactions with the matrix, with multiple cell-matrix anchor points (Figure 3.7B). Spinning disk imaging of ASCs in 0.2% aNFC hydrogel stained with PKH67 (a green fluorescent membrane dye) and calcofluor white showed an homogenous cell distribution at both low (Figure 3.7C) and high magnification (Figure 3.7D). ASCs demonstrated 'nodule-like' cell aggregates under high magnification (Figure 3.7D).
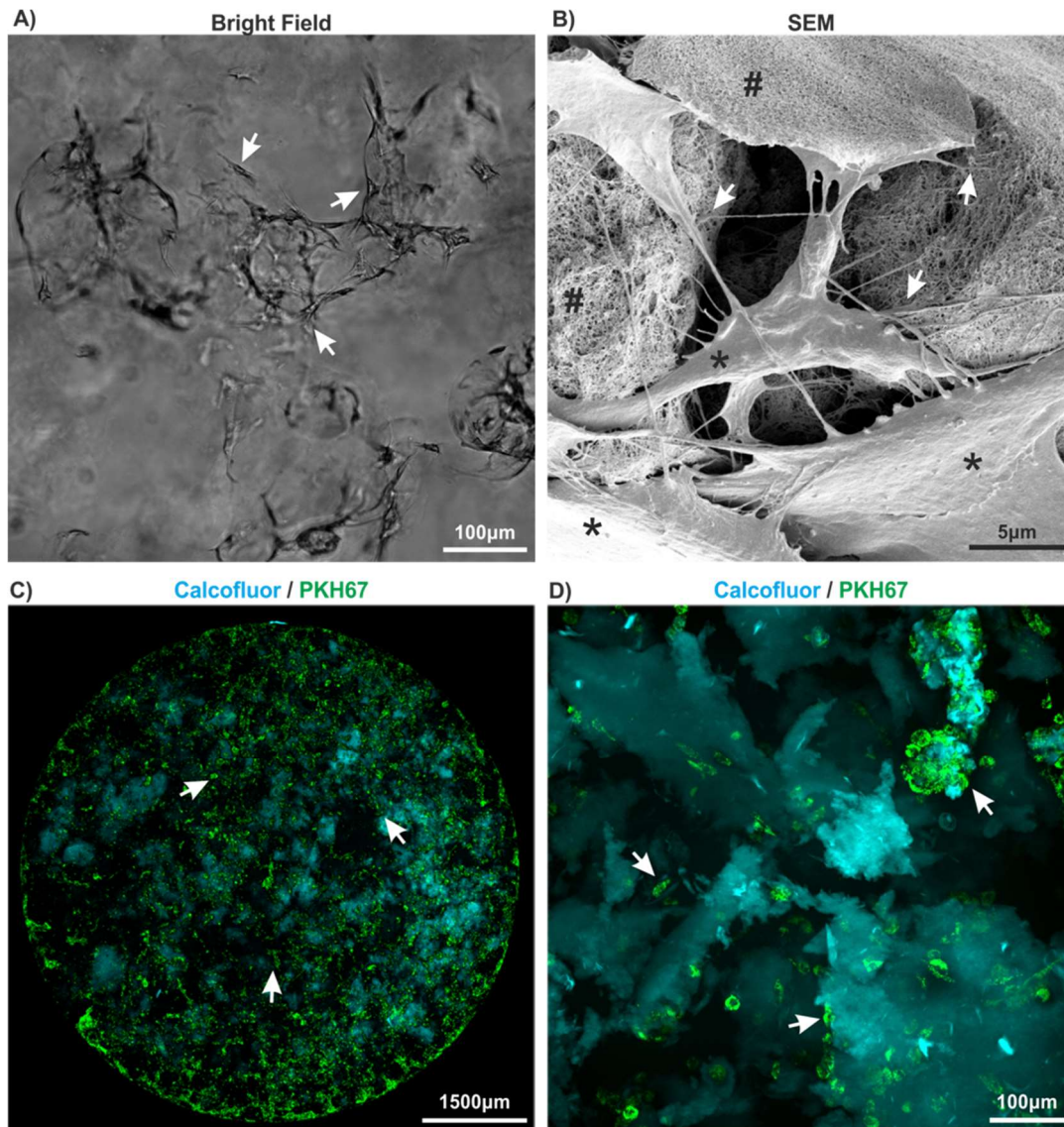
Figure 3.7. ASCs cultivated in different concentrations of aNFC hydrogels had an homogenous distribution. (A) ASCs were seeded into 0.2% aNFC hydrogel and imaged using bright field microscopy. ASCs in 0.2% aNFC hydrogel showed a typical, fibroblast-like morphology (shown by the arrows). 0.2% (w/v) aNFC with cell densities of $1x10^5$ cells/100μL. Scale bar: 100μm. (B) SEM imaging showed that ASCs (*) cultured in 0.5% aNFC hydrogel (#) showed multiple cell-matrix anchor points (shown by the arrows). 0.5% (w/v) aNFC with cell densities of $1x10^5$ cells/100μL. Scale bar: 5 μm. (C-D) ASCs were stained with PKH67 (green) and cultivated in aNFC hydrogel labelled with calcofluor (cyan). Spinning disk imaging at low (2.6x) and high (40x) magnification revealed an homogenous distribution of cells. 0.1% (w/v) aNFC with cell densities of $5x10^5$ cells/mL. (C) Scale bar: 1500 μm. (D) Scale bar: 100 μm.

3.3.6. Interactions of ASCs with aNFC hydrogels in 3D were revealed by fluorescence microscopy

ASCs embedded into 0.2% aNFC hydrogel were stained with primary antibodies against the cytoskeletal protein, β-actin, intermediate filament protein and nestin filament and co-stained with calcofluor white (aNFC). Single section images and 3D reconstructions were performed to examine the location of human ASCs within aNFC (Figure 3.8A-B).
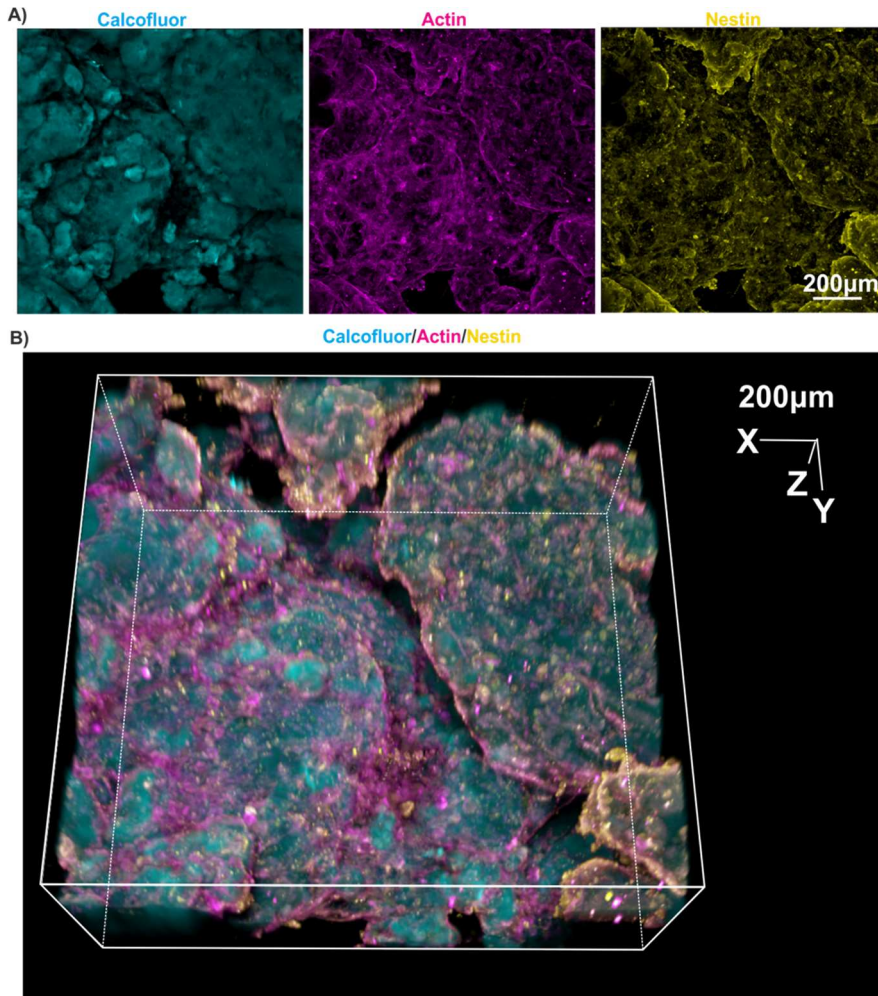
Figure 3.8. Actin cytoskeleton in ASCs showed compatibility with 3D aNFC. In order to examine the regulation of the assembly of intermediate filaments and the function of the actin cytoskeleton, ASCs embedded into aNFC were stained with primary antibodies (nestin and actin) followed by counter-staining with calcofluor. (A) Single sections were imaged by showing β-actin (magenta), nestin (yellow) and aNFC hydrogel (cyan) (B) A 3D reconstruction of single sections was visualised with the distribution of ASCs within aNFC. 0.2% (w/v) aNFC with cell densities of 1x10^5 cells/mL. Scale bar: 200μm. No primary antibody controls for Alexa Fluor 488 and Alexa Fluor 555 are shown in the Appendix II, as supplement figure 3.1.

The regulation of the assembly of intermediate filaments and the function of the actin cytoskeleton of ASCs cultivated in 0.2% aNFC were evaluated using confocal microscopy. Cells combined with 0.2% aNFC hydrogel were fixed and stained with CellTracker™ Green CMFDA dye and phalloidin and counterstained with calcofluor (Figure 3.9A). Confocal laser-scanning microscopy showed the interaction between intermediate filaments of ASCs and 3D aNFC. The actin filaments were also evaluated in ASCs embedded into 0.2% aNFC counterstained with calcofluor white (Figure 3.9B).
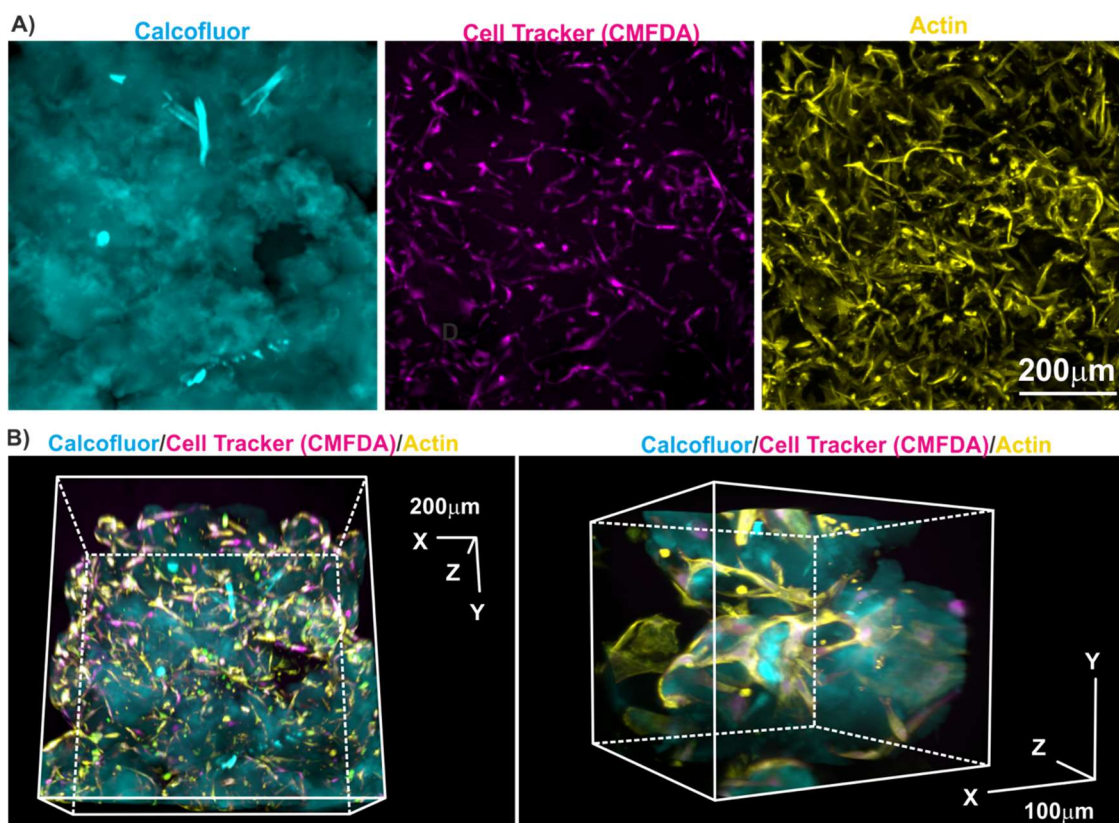
Figure 3.9. The morphological appearance of ASCs in 3D aNFC visualised with 3D reconstruction of multiple fluorescence microscopy-based assays. In order to examine the structure of the actin filament in live ASCs in 3D, cells seeded into 0.2% aNFC were stained with cell tracker CMFDA (magenta) and phalloidin (yellow) and counterstained with calcofluor white (cyan). (A) ASCs in 0.2% aNFC were then visualised with a maximum intensity projection using confocal laser-scanning microscopy, which showed an homogenously morphological appearance of ASCs in aNFC. Scale bar: 200 μm. (B) 3D reconstruction of single section images was imaged with confocal laser-scanning microscopy to assess the compatibility of aNFC with ASCs. 0.2% (w/v) aNFC with cell densities of 1×10^5 cells/mL. Scale bar (left): 200 μm and scale bar (right): 100 μm.

3.3.7. ASCs were viable in 0.2% aNFC hydrogel

The viability of ASCs cultivated in 0.2% aNFC hydrogel was evaluated using live/dead cytotoxicity and XTT viability assays. For the live/dead viability assay, ASCs embedded into 0.2% aNFC were stained with calcein for living cells and ethidium homodimer-1 for dead cells and counterstained with DAPI (Figure 3.10A-B). The majority of the cells stained positive for calcein, indicating that ASCs were viable in the 0.2% aNFC hydrogel (Figure 3.10A-B). Only a few cells were ethidium homodimer 1-positive, again indicating a high viability of ASCs in the 0.2% aNFC hydrogel (Figure 3.10B).

The viability of ASCs cultivated in different hydrogels (0.2% aNFC, 0.2% NFC and 0.9% alginate hydrogel) and in a traditional 2D culture was assessed using an XTT viability assay. It was found that ASCs embedded in 0.2% aNFC showed greater viability than ASCs grown in 0.2% NFC, 0.9% alginate and in a traditional 2D culture. Moreover, the viability of cells in alginate was lower than in 2D culture.
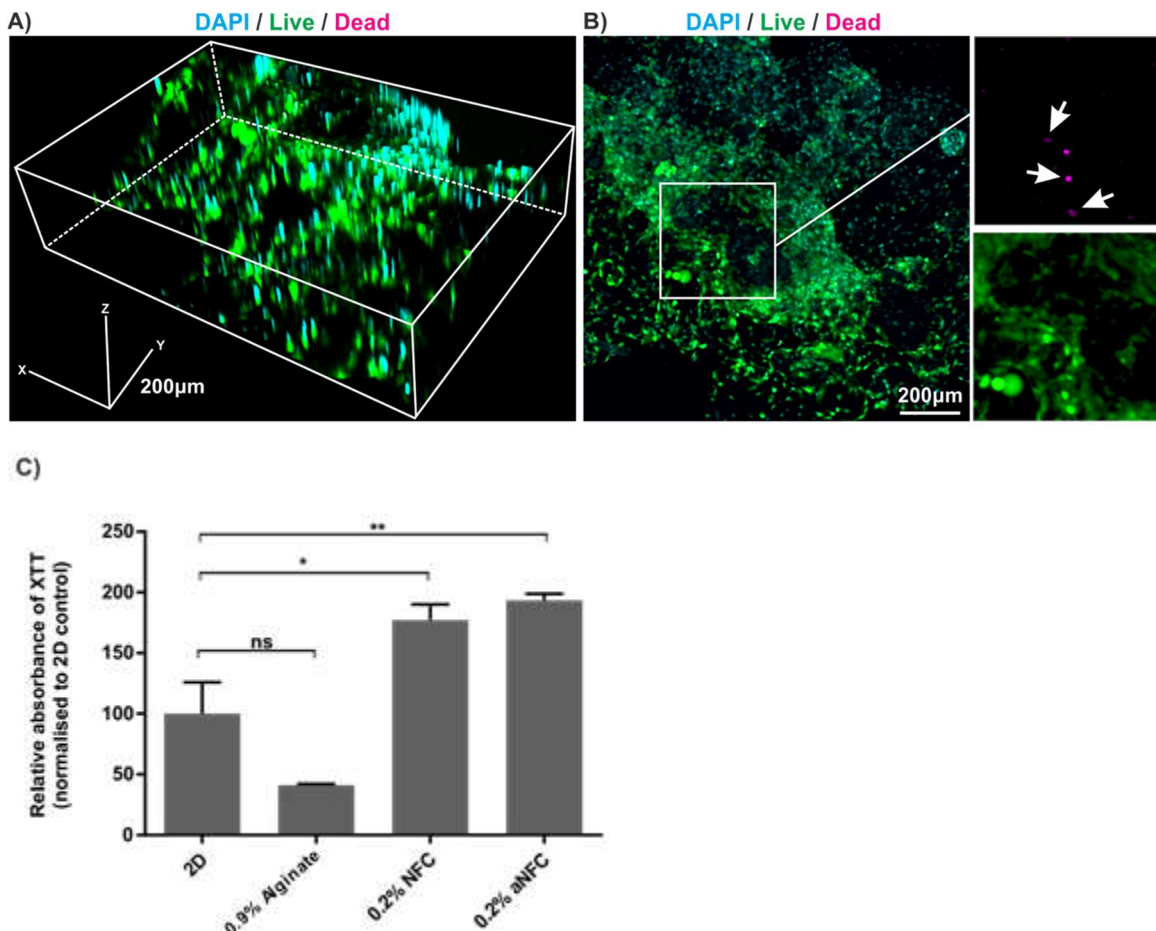
Figure 3.10. ASCs were viable in 0.2% aNFC hydrogel. (A) 3D reconstruction of ASCs showed an homogeneous distribution of live cells in all dimensions of the

aNFC hydrogel. Scale bar: 200 µm. (B) Using confocal laser-scanning microscopy, ASCs cultivated in 0.2% aNFC hydrogel were stained with calcein (living cells, green), ethidium homodimer-1 (dead cells, magenta) and counterstained with DAPI (nucleus). The majority of the cells were stained as positive for calcein (green), indicating viable cells. Only a few non-viable cells were found (top right panel, magenta, shown by the arrows). Scale bar: 200 µm. (C) Cell viability was determined using a XTT viability assay. ASCs embedded into different hydrogels including 0.9% alginate, 0.2% NFC and 0.2% aNFC were examined by XTT viability assay, normalised to 2D control. Values are shown as means ± standard errors of three independent experiments using GraphPad Prism software (GraphPad, La Jolla, CA, USA). Data were compared using a one-way ANOVA with Bonferroni correction (CI 95%). At least three independent experiments were performed. The results are presented as mean ± SEM with n=3. $^{**}P<0.01$ and $^{*}P<0.05$ were considered to be statistically significant. 0.2% (w/v) aNFC with cell densities of $1x10^5$ cells/100µL.
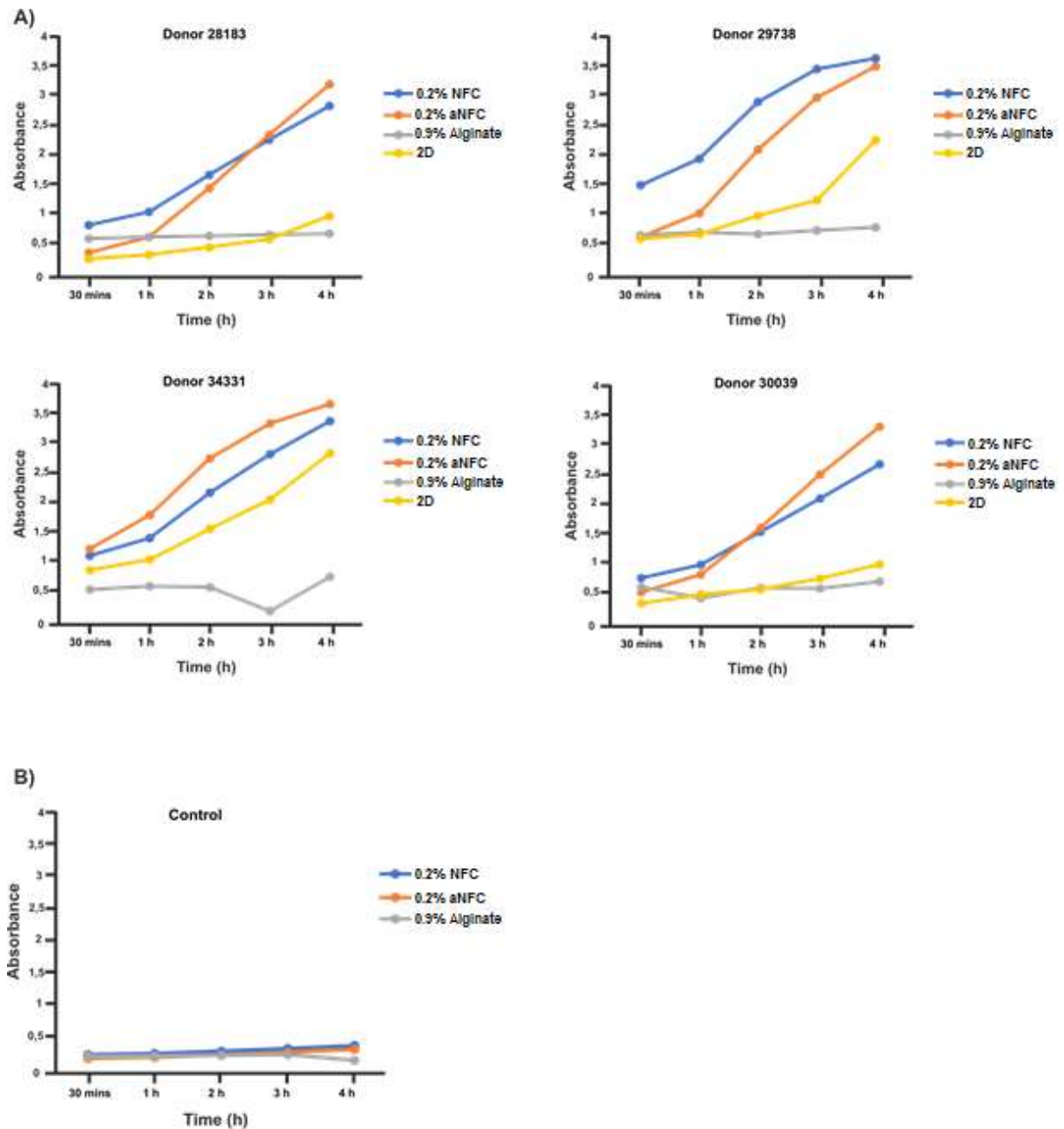
Figure 3.11. ASCs were more viable in aNFC hydrogel compared with other scaffolds. (A) The viability of ASCs embedded into 0.9% alginate, 0.2% NFC and 0.2% aNFC were compared with a 2D control. XTT reaction was allowed to proceed for 4 h in cells embedded into 0.2% aNFC compared with cells cultured onto other scaffolds for four different donors (ASCs 28183, ASCs 29738, ASCs 34331 and ASCs 30039). At least three independent experiments were performed. 0.2% (w/v) aNFC with cell densities of 1×10^5 cells/100μL. (B) Different hydrogels including 0.9% alginate, 0.2% NFC and 0.2% aNFC were evaluated as a control without cells: no viability was seen in the scaffolds.

3.3.8. ASCs can be successfully retrieved from 3D aNFC hydrogels

In order to determine whether viable cells could be retrieved from NFC and aNFC hydrogels, ASCs were cultured for 72 h in hydrogels and then enzymatically retrieved and counted (Figure 3.12). Bright field images showed that cells were successfully liberated from the 0.2% aNFC (Figure 3.12). Figure 3.12A shows that 0.2% aNFC were digested using GDase with an overnight incubation. ASCs were retrieved from 0.2% aNFC hydrogel (Figure 3.12B). Using a collagenase and dispase I mixture for 4 h, ASCs were retrieved from 0.2% aNFC hydrogel (Figure 3.12C). The numbers of retrieved ASCs from 0.2% aNFC and 0.2% NFC hydrogel were compared with the number of cells seeded. The number of retrieved viable ASCs from the 0.2% aNFC hydrogel was approximately 2×10^5 cells (Figure 3.12D). In comparison with the retrieved cells from 0.2% NFC hydrogel, 200% of viable ASCs were retrieved from the aNFC hydrogel relative to the number of cells seeded at 1×10^5 (Figure 3.12E).
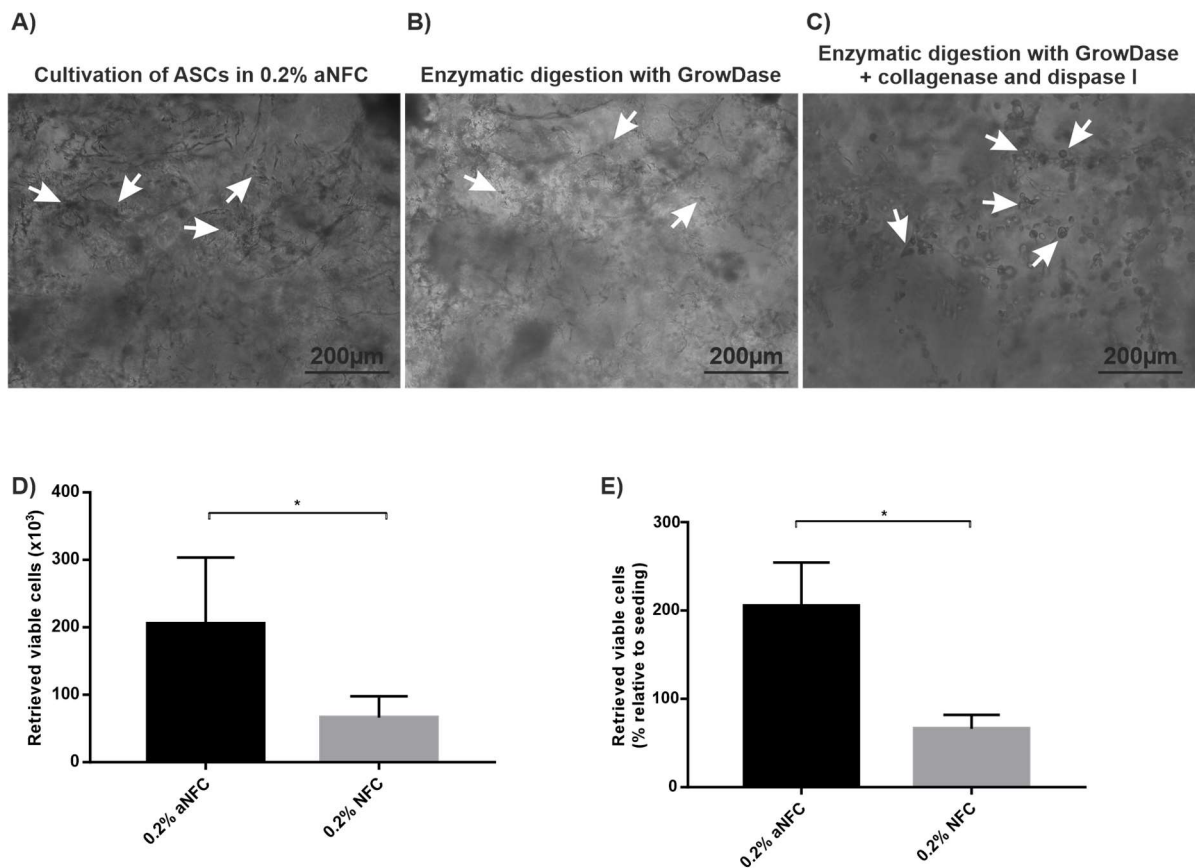
Figure 3.12. The retrieval of ASCs from the 0.2% aNFC was greater than from 0.2% NFC hydrogels. (A) Bright field images of ASCs embedded in 0.2% aNFC hydrogel cultured for 72 h. Scale bar: 200µm. (B) Bright field images of ASCs embedded in 0.2% aNFC hydrogel after enzymatic digestion with GrowDase (overnight). ASCs were retrieved from 0.2% aNFC hydrogel. Scale bar: 200 µm. (C)

Bright field images of ASCs embedded in 0.2% aNFC hydrogel after enzymatic digestion with collagenase and dispase I mixture (4 h). This digestion resulted in a single cell suspension (shown by the arrows). Scale bar: 200 µm. (D) After enzymatic digestion with GrowDase and collagenase/dispase I, $2x10^5$ cells were retrieved from 0.2% aNFC hydrogel and compared with the retrieved nearly $1x10^5$ cells into 0.2% NFC hydrogel. (E) The percentage of retrieved cells showed that 200% of cells were retrieved relative to the number of cells seeded. Values are shown as means ± standard errors of three independent experiments using GraphPad Prism software (GraphPad, La Jolla, CA, USA). Data were compared using a student t-test with unpairedt test Welch's correction. At least three independent experiments were performed. The results are presented as mean ± SEM with n=3. $^*P$<0.05 were considered to be statistically significant. 0.2% (w/v) aNFC with cell densities of $1x10^5$ cells/100µL.

3.3.9. Fluorescence time-lapse imaging demonstrated cytosolic Ca^{2+} oscillations in ASCs in grown in 3D

Ca^{2+} oscillations are a fundamental characteristic of undifferentiated ASCs undergoing osteogenic differentiation (Hanna et al., 2017, Sun et al., 2007). ASCs were grown for 3 days embedded in 0.2% aNFC ($1x10^7$ cells/ml), labelled with Fluo-4 dye and spontaneous cytosolic Ca^{2+} oscillations were recorded using epifluorescent microscopy (Figure 3.13). The fluorescence intensity of ASCs embedded into 3D aNFC was quantified once every 10-second for a time period of 6 min (Figure 3.12B). The undifferentiated ASCs exhibited unsynchronized Ca^{2+} oscillations with increased Ca^{2+} spike patterns compared with the differentiated cells.
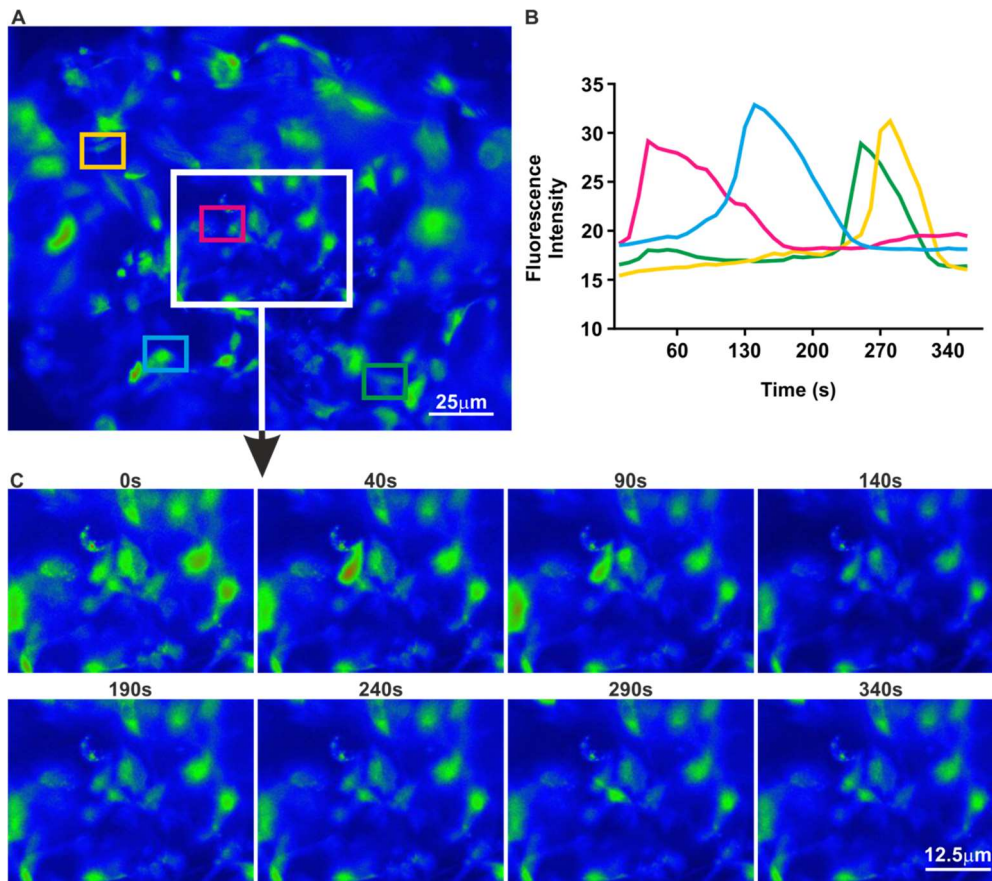
Figure 3.13. Calcium imaging of ASCs showed unsynchronized Ca2+ oscillations in 3D aNFC. (A) ASCs embedded into 0.2% aNFC were incubated with HBSS, 2.5 µM Fluo-4 and 2.5 mM Probenecid. Fluorescence time-lapse images were recorded for 340 s for spontaneous cytosolic calcium oscillation in cells in 3D. Unsynchronized Ca^{2+} spike patterns were observed in real time. Scale bar: 25 µm. (B) The fluorescence intensity of ASCs embedded into 3D aNFC was quantified once every 10-second for a time period of 6 min. The average fluorescence intensity for Ca^{2+} oscillations was analysed using Image J software. (C) Consecutive images of the cytosolic Ca^{2+} were recorded for a time period of 340 s (at 0, 40, 90, 140, 190, 240, 290 and 340 s. 0.2% (w/v) aNFC with cell densities of $1x10^7$ cells/mL. Scale bar: 12.5 µm.

3.4. Discussion

In recent years, 3D cell culture scaffolds have been introduced in many fields of cell-based research (Bhattacharya et al., 2012). Compared with standard 2D culture, 3D cell culture better resembles the ECM for the physiological microenvironment and more closely mimics *in vivo* tissue (Bowers et al., 2010, Dutta and Dutta, 2009).

Bone-graft substitutes include natural and synthetic biomaterials such as collagen, hydroxyapatite (HA), β-tricalcium phosphate (β-TCP), calcium phosphate cements and glass ceramics. These biomaterials promote the migration, proliferation and differentiation of bone-forming cells (Finkemeier, 2002). To ameliorate injured cells, cylindrical metallic or titanium scaffolds have also been used to bind to autologous-allograft bone or another biomaterial (Dimitriou et al., 2011a). Calcium phosphate-based scaffolds including HA and β-TCP are used as the main materials for bone healing (Becker et al., 2012). HA, a commonly used ceramic material, has advantages in terms of osteoconductivity and is similar to bone structure (Becker et al., 2012). Moreover, β-TCP, which is a synthetic calcium phosphate-based material, has been shown to increase cell growth, cell proliferation and bone formation (Tarafder et al., 2013).

Hydrogels are emerging materials for 3D cell culture as the interconnected pores inside hydrogels have promising features including high water retention and the efficient transport of oxygen and nutrients (Drury and Mooney, 2003). In this chapter, various types of biomaterials were evaluated in terms of their absorbance and fluorescence emission. aNFC was found to be the best performing hydrogel in terms of its optical properties (Figure 3.1). However, as cell viability and biocompatibility are more important parameters for their clinical use, these were evaluated in chapter 3. Bhattacharya et al. (2012) determined the absorbance spectrum and fluorescence emission of NFC hydrogels and measured the UV-visible absorbance of 0.5% NFC in the range 300-550 nm (Bhattacharya et al., 2012). They also determined the fluorescence emission of NFC hydrogel using a spectral scanning-plate reader at different excitation wavelengths of 405, 488 and 560 nm. Their results showed that NFC hydrogels exhibited no autofluorescence and also did not absorb visible or UV light (420 to 700 nm) (Bhattacharya et al., 2012). These findings are in general accordance with those of the present study showing that autofluorescence was shown relatively low based on the data presented by the absorbance spectrum and quantified by GraphPad Prism software. A higher level of fluorescence emission was also detected using aNFC hydrogel with excitation wavelengths of 405 and 488 nm (DAPI and FITC respectively) (Figure 3.3). DAPI and FITC were embedded in the aNFC hydrogels and the fluorescence emission was measured. aNFC was found to be compatible with fluorescence-based techniques due to a greater signal of

fluorescence emission for DAPI and FITC in the aNFC hydrogel compared with others (Figure 3.3).

The adhesion of aNFC was evaluated when loaded onto magnesium (Mg^{2+}). However, there was not enough adhesion to the Mg^{2+} (Figure 3.5). Because of the poor adherence of Mg^{2+} to aNFC, it was decided to use aNFC alone combined with ASCs for all future experimentation (Figures 3.5 and 3.6). One potential explanation for the failure of aNFC to adhere to magnesium could be the fact that the magnesium used in the experiments was a modified resorbable form. As an alternative, non-modified magnesium could be used. Alternatively, the failure of adhesion of aNFC could be addressed in future experiments by coating of the magnesium with poly D lysin. Moreover, titanium could be used with or without coating. Other alternative could be the use of poly (3,4-ethylenedioxythiophene) polystyrene sulfonate (PEDOT: PSS). In a recent study, a blend of collagen hydrogels and stiff PEDOT:PSS scaffold has been successfully used for cultivation and differentiation of human neural crest-derived stem cells (Iandolo et al., 2020). By combining PEDOT: PSS with collagen components, the authors have developed a highly biomimetic, electroactive scaffold. Future work could also explore blending aNFC with PEDOT:PSS to generate a substrate with a stiffness closed to that of the bone. Schurmann et al. (2014) reported that neural crest-derived stem cells (NCSCs) were evaluated on titanium with different pore sizes in terms of the cell viability and osteogenic differentiation. Titanium with a flat version and 30 nm pores showed increased proliferation on the cultivated NCSCs for 4 days (Schürmann et al., 2014). Together with its proliferative ability, titanium with pores with a diameter of 30 nm also increased the osteogenic differentiation (Schürmann et al., 2014). These findings are in accordance with those of Park et al. (2017) showing the cultivation of MSCs on titanium nanotubes with lateral spacing of 15-30 nm for 4 days. They demonstrated increased mineralization and focal adhesion kinase (FAK) phosphorylation (Park et al., 2007). In an earlier study, Oh et al. (2009) had reported that MSC cultivation on titanium nanotubes (100 nm pores) promoted an increase in osteoinductive effects (Oh et al., 2009).

The viability of cells was evaluated in 3D cell culture. ASC viability after cultivation in 0.2% aNFC was assessed using a live/dead cytotoxicity assay. The vast majority of the cells stained positive for calcein, indicating that ASCs were viable in the 0.2%

aNFC hydrogel (Figure 3.10A-B). The viability of ASCs cultivated in different hydrogels was also evaluated using an XTT viability assay. The viability of ASCs cultivated in 0.2% aNFC, 0.2% NFC and 0.9% alginate hydrogel were compared with a 2D control to measure the number of viable cells (Figure 3.10C). Currently, there is no consensus regarding the effects of 3D cultures on viability and proliferation of MSCs. While some studies have reported that 3D culture promotes an increase in viability, others have observed the opposite effects (reviewed in (Edmondson et al., 2014). This can be at least partly attributed to the nature of the 3D cell culture method. Our data showed that ASCs embedded in 0.2% aNFC showed greater viability than cells grown in 0.2% NFC, 0.9% alginate and in a traditional 2D culture. In contrast to aNFC, the viability of cells in alginate was lower than in the 2D culture (Figure 3.10C). In fact, 3D cell culture methods including MSC cultivation as scaffold-free spheroids have a negative effect on cellular proliferation and viability, which have often been associated with a decrease in cellular viability (Tsai et al., 2015). Despite spheroid cultures, 3D hydrogels are able to represent an equal or superior performance compared with 2D cultures (reviewed in (Mirbagheri et al., 2019). In the light of the reports, the effect of 3D culture on scaffolds and in hydrogels seem to be much more complex.

Aggarwal and Pittenger found that MSCs seeded in hydrogel scaffolds have an increased viability when encapsulated in non-degradable PEG hydrogels or conjugated with adhesive ligands RGDSP (Arg-Gly-Asp-Ser-Pro) (Aggarwal and Pittenger, 2005). A recent study from the Widera lab showed that low concentrations (0.2%) of NFC did not negatively affect the proliferation of bone-marrow MSCs (BM-MSCs), ASCs or palatal MSCs, whereas a higher concentration (0.5%) significantly reduced cellular viability and proliferation compared with 2D controls (Azoidis et al., 2017). Notwithstanding the putative benefits of NFC on cell viability and proliferation, a follow-up study showed that an anionic form of NFC significantly increased the viability of human ASCs (Sheard et al., 2019). Similarly, Yin et al. (2020) recently reported that 3D cultivation of ASCs in a nanofibrous polysaccharide hydrogel increased their proliferation and viability (Yin et al., 2020b).

In contrast to these findings, 3D printed polycaprolactone/tricalcium phosphate did not affect the viability of human ASCs and BM-MSCs in a recent study (Park et al., 2018). Interestingly, Brennan et al. (2015) had previously shown that sprayed micro-

fibre polycaprolactone scaffolds increase human BM-MSC proliferation whilst electrospun variants of the same scaffold decreased proliferation compared with 2D controls (Brennan et al., 2015). In general accordance with this finding, woven biodegradable composite fibres from poly-L-lactic acid substituted with hydroxyapatite had an overall positive effect on BM-MSC viability, whereas growth from poly-L-lactic acid alone reduced viability (Persson et al., 2018). Conversely, Nguyen et al. (2012) reported that electrospun scaffolds significantly reduced the proliferation of human MSCs as early as 7 days after seeding on nanofibrous scaffolds composed of poly-L-lactic acid and type I collagen (Nguyen et al., 2012). Some 3D scaffolds including gelatin, poly lactic-co-glycolic acid and chitosan showed no effect on the viability and the proliferation of MSCs (Lo et al., 2016). In contrast, collagen seems to have different effects depending on the preparation of the collagen and the source of MSCs. In this context, Lo et al. did not observe any significant changes in the cell viability or proliferation of collagen-embedded human MSCs (Lo et al., 2016), whereas rat BM-MSCs have been reported to increase their proliferation on collagen-based scaffolds (Han et al., 2012a). Other reports have also suggested that small differences in the scaffold composition and even in the technique can be decisive for the outcome. Rampichová et al. (2013) suggested that 3D cultivation of mini pig MSCs in electrospun 3D polycaprolactone increases both their proliferation and their viability (Rampichova et al., 2013).

Mg^{2+} is a fundamental mineral in the human body and positively affects MSC proliferation and inflammatory/immune responses (da Silva Lima et al., 2018). MSCs cultivated with different concentrations of Mg^{2+} (0-5 mM) were investigated to evaluate the effect of Mg^{2+} on cell viability and proliferation (da Silva Lima et al., 2018). Cell viability was assessed using an MTT assay and the results showed that MSCs cultured in Mg^{2+} showed a higher cell viability compared with MSCs in a culture without Mg^{2+} (da Silva Lima et al., 2018). Gold nanoparticles (GNPs) have also been examined (Heo et al., 2014) who reported that photo-curable gelatine hydrogels (Gel) loaded with GNPs improved bone healing in male New Zealand rabbits with regard to the levels of proliferation and differentiation (Heo et al., 2014). In addition, their findings showed that ASCs embedded into Gel-GNPs hydrogels exhibited an increased osteogenic differentiation behaviour which was dependent on the p38 mitogen-activated protein kinase (MAPK) pathway (Heo et al., 2014).

3.5. Conclusion

In this chapter, I have explored different scaffolds in terms of the optical and spectral properties of the hydrogels. The results obtained in this chapter have identified the most suitable hydrogel tested in terms of its optical properties, biocompatibility and similarity to native ECM. However, since only a limited range of hydrogels have been tested, future research should explore the use of other hydrogels and blends of hydrogels with stiff substrates. It is clear that there are a variety of 3D culture methods, which show great promise in bone healing in disease conditions ranging from osteoporosis to skeletal disorders. Among all the scaffolds, aNFC hydrogels have received special attention for the generation of biomedical materials due to their biocompatibility, biodegradability and structural similarities to natural ECM. Furthermore, these hydrogels based on cellulose have been shown to be the best options for use in physiological environments because of their bioactive properties, which enhance cell proliferation and bone healing. Understanding the interactions between ASCs and aNFC hydrogels will provide further insights into the best therapeutic applications to promote bone regeneration.

Chapter 4

Evaluation of the osteogenic differentiation of human adipose-derived stem cells within 3D anionic nanofibrillar cellulose

4.1. Introduction

Due to rising life expectancy and increasing numbers of injuries from trauma and disease in the elderly, there is an increasing worldwide demand for bone replacement (Li et al., 2020). Bone tissue engineering is an attractive option for treating bone damage without the side effects associated with current treatment strategies (Li et al., 2020). Human mesenchymal stem cells (MSCs) have huge potential in these approaches because of their self-renewing ability, osteogenic differentiation potential and the possibility to be used for autologous therapy (Leventhal et al., 2012). Adipose-derived stem cells (ASCs) are a readily available and abundant subtype of MSCs. Traditionally, two-dimensional (2D) cell culture on flat plastic or glass surfaces is still widely used in basic stem cell research. However, 2D culture of MSCs and ASCs is known to result in a loss of multipotency and premature cellular senescence (Turinetto et al., 2016). Moreover, 2D cell culture conditions have been linked to the accumulation of chromosomal aberrations within the MSC genome (Ben-David et al., 2011, Bara et al., 2014). To overcome these drawbacks of 2D cell culture, MSCs have been exposed to a wide range of 3D cell culture methods and substrates including alginates (Ho et al., 2016), collagen (Lund et al., 2009), Matrigel (Yamaguchi et al., 2014) and different formulations of cellulose (Favi et al., 2013, Cochis et al., 2017, Azoidis et al., 2017, Sheard et al., 2019). The use of 3D hydrogels has often been associated with increases in cellular proliferation and viability compared with 2D cultures (reviewed in (Mirbagheri et al., 2019). In some cases, 3D cell cultures have resulted in reduced cellular proliferation and viability due to the prolonged culture time (Luca et al., 2013).

In contrast to the controversial impact of 3D culture on MSC viability and MSC proliferation, there are multiple reports suggesting that 3D cultivation might increase osteogenic differentiation. Nguyen et al. (2012) used a blended scaffold composed of collagen and electrospun poly (L-lactic acid) to study the influence of 3D cell culture on the differentiation of human MSCs of undefined origin and found that differentiation in 3D significantly increases the expression of OCN and OPN and increases the levels of calcification compared with cells differentiated in 2D (Nguyen et al., 2012). A 2008 report provided evidence that 3D nanofibrillar scaffolds prepared from rat tail collagen increased the expression of osteogenic markers including type I

collagen, OPN and osteonectin in human ASCs compared with differentiation conducted in 2D. Although Alizarin Red S staining in that report suggested that calcification could also be increased, the significance of the data was not assessed (Sefcik et al., 2008). Similar effects on the expression levels of osteocalcin OCN and OPN in rat bone marrow MSCs (BM-MSCs) were observed when purified collagen was used to create a 3D scaffold (Han et al., 2012a). Notably, von Kossa staining revealed a statistically significant increase of calcification. On the other hand, the use of pure poly (L-lactic acid) scaffolds as a substrate showed similar increases in the expression of pro-osteogenic markers compared with human BM-MSCs differentiated in 2D (Persson et al., 2018). This was accompanied by a significant increase in Ca^{2+} deposition demonstrated by von Kossa and Alizarin Red S staining. In addition to collagen, Matrigel, a hydrogel mainly composed of type IV collagens, entactin, perlecan and laminin have been shown to increase the osteogenic differentiation potential compared with 2D cell culture. When differentiated within a Matrigel scaffold, human BM-MSCs showed higher activity alkaline phosphatase (ALP) (an early marker of osteogenesis) than the 2D counterparts (Yu et al., 2018). In addition, Alizarin Red S staining revealed higher Ca^{2+} deposition in cells differentiated in 3D.

In this chapter, the effects of hydrogels on osteogenic differentiation of ASCs in 3D cultures were assessed using a multitude of assays including conventional PCR, immunocytochemical staining for OCN and OPN, Alizarin Red S staining to visualise calcium deposition.

4.2. Objectives

Despite progress in developing efficient strategies for osteogenic differentiation in traditional cell culture, little has been achieved in establishing optimal conditions for differentiating MSCs in 3D. Data indicating in Chapter 3 have examined that aNFC is biocompatible with ASCs and represents a promising scaffold for the differentiation of MSCs in 3D.

Hence, the focus of this chapter is the analysis of the osteogenic differentiation of ASCs in 3D aNFC hydrogels. Among the analysed 3D models, aNFC hydrogel has been investigated to understand its effects on the osteogenic differentiation of ASCs. aNFC can represent a promising 3D scaffold for the osteogenic differentiation of ASCs as well as cell proliferation and cell morphology. By using different

approaches, the potential of osteogenic differentiation of ASCs was investigated in 3D culture.

As a proof of principle, osteogenic differentiation in 2D was first evaluated. The osteoblast-related gene expression of ASCs was determined using conventional PCR analysis in 2D and 3D. The reason for this is that when cells are differentiating, the first molecular event is a change of expression of osteogenic genes at RNA level. Briefly, PCR analysis was used to examine the expression of osteogenic genes at RNA level in 2D and 3D. The next step was the up-regulation of osteogenic markers at protein level. The ability of ASCs to differentiate into bone cells was also tested using immunocytochemical staining for OCN and OPN in 2D and 3D. In order to assess osteogenic differentiation at a functional level, ALP activity and then calcium deposition as an indicator of mineralisation were analysed using assessment of ALP activity and Alizarin Red S assay. The differentiated cells subjected to Alizarin Red S staining showed a significantly higher signal than cells in a standard media in both 2D and 3D. This part of the project provided information about the best performing hydrogel for the osteogenic differentiation of ASCs in 3D. In addition, 2-Photon microscopy and calcium imaging of ASCs in 2D were used to examine oscillatory patterns such as spikes and waves. Finally, to visualize potential changes of the actin cytoskeleton structure, ASCs embedded in aNFC were stained with phalloidin after 21 days of differentiation of cultivation in a standard media.

4.3. Results

4.3.1. Osteogenic induction of ASCs cultured in 2D results in the up-regulation of osteogenesis-related transcription

ASCs were differentiated towards the osteogenic lineage in 2D. These cells were collected on days 3, 14 and 21 to analyse the expression of osteogenesis-related genes at RNA level using conventional PCR. PCR products were evaluated using electrophoresis. For quantification, the expression levels of osteogenic markers were normalised to the corresponding levels of the housekeeping gene GAPDH. Figure 4.1A shows the order of activation of the analysed genes during osteogenic differentiation (Li et al., 2014c, Hauschka and Wians, 1989, Karsenty, 2001). Vimentin is a stem cell marker and BMP2, RunX2, osterix, OCN and OPN are

osteogenic genes that are expressed in the early, middle and late stages of osteogenic differentiation, respectively.
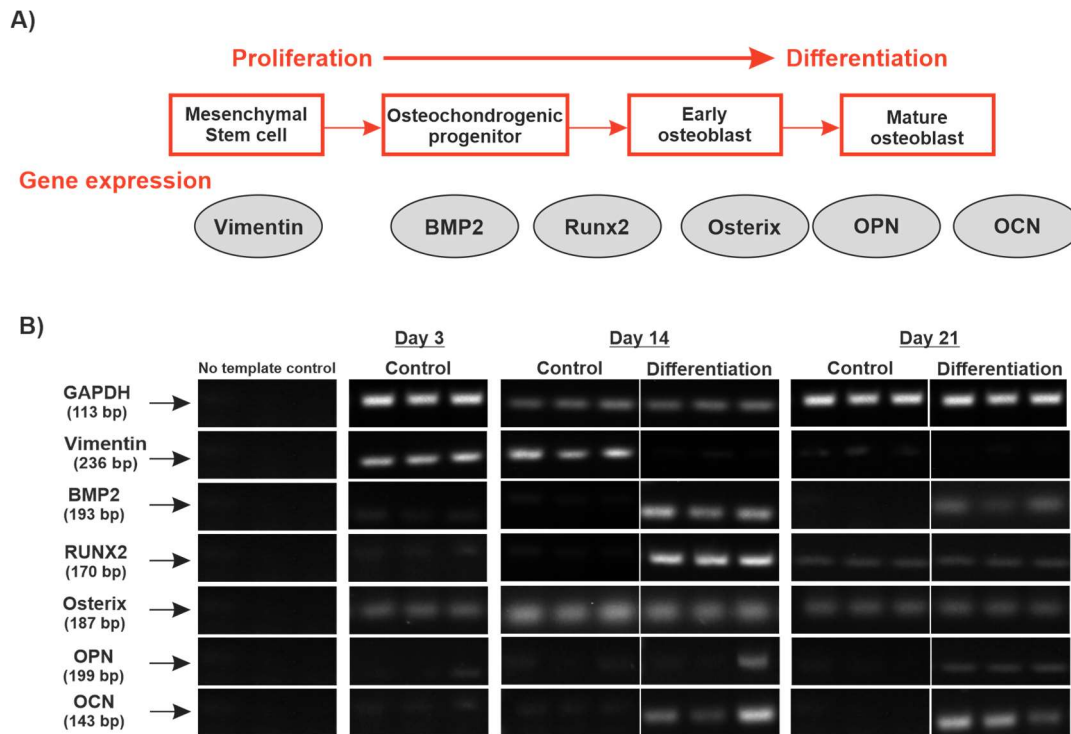
Figure 4.1. Osteogenic induction of ASCs cultured in 2D resulted in up-regulation of osteogenesis-related transcription. (A) Expression time frame of osteoblast-related genes during osteogenic differentiation; (B) Images of conventional PCR product bands were analysed using electrophoresis to determine the level of reverse-transcribed cDNA. The sizes of the PCR products (GAPDH, Vimentin, BMP2, RUNX2, Osterix, OCN and OPN) were 113 bp, 236 bp, 193 bp, 170 bp, 187 bp, 143 bp and 199 bp, respectively. GAPDH was used for normalization of the quantitative analysis of the gel images. The no template controls did not amplify any products as shown in panel B.
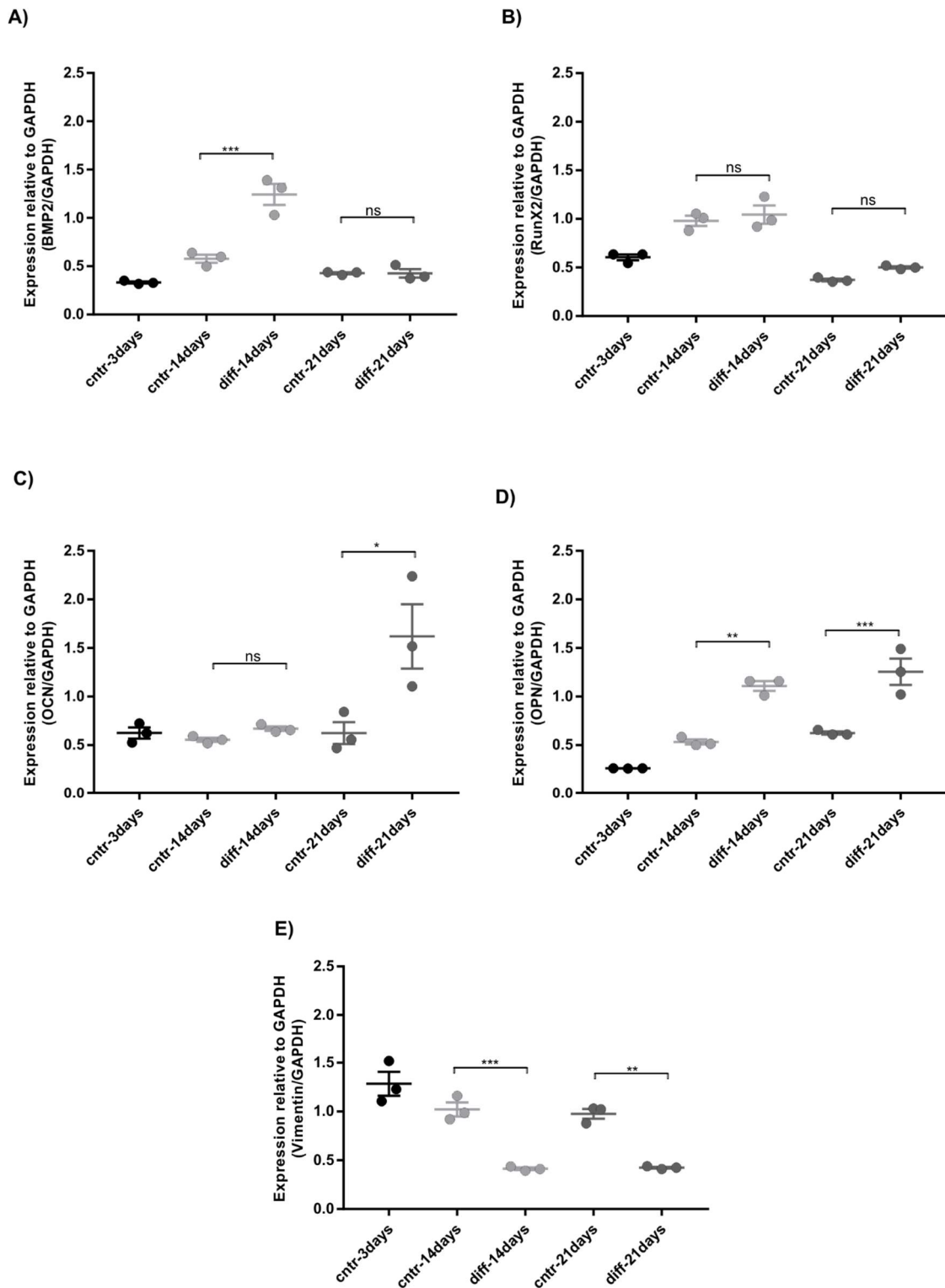
Figure 4.2. Expressions of osteogenesis-related genes on ASCs cultured in 2D for 3, 14 and 21 days. (A-E) The expression level of BMP2, RunX2, OCN, OPN and Vimentin were quantified by employing an image acquisition and analysis system in ImageJ software; (A-B) The expression level of BMP2 and RunX2 showed increased upregulation in ASCs in a differentiation media at day 14; (C-D) The expression level of OCN and OPN in the differentiated cells was significantly higher than in the control groups when cultured in 2D for 21 days; (E) The expression level of Vimentin in

ASCs in a standard media was significantly higher than that of the differentiation groups when cultured in 2D for 14 and 21 days. GAPDH was used to normalize the relative expression for each gene. Values are shown as means ± standard errors of three independent experiments using GraphPad Prism software (GraphPad, La Jolla, CA, USA). Data were compared using one-way analysis of variance (ANOVA) with Bonferroni correction (CI 95%). At least three independent experiments were performed. The results are presented as mean ± SEM with n=3. $^{***}P<0.0001, ^{**}P<0.01$ and $^{*}P<0.05$ were considered to be statistically significant.

Semi-quantitative PCR was performed, and the image analysis of gene expression of ASCs cultured in 2D for 3, 14 and 21 days was quantified using GAPDH expression for normalization. As demonstrated in Figure 4.2, the expression levels of BMP2 and RunX2 were higher in ASCs under osteogenic differentiation conditions at 14 days compared with cells in a standard media. The expression levels of OCN and OPN showed that the increased upregulation in ASCs in the differentiation media was significantly higher than in the control groups when cultured in 2D for 21 days. In addition, the expression level of Vimentin in ASCs in a standard media was significantly higher than in the differentiation groups when cultured in 2D for 14 and 21 days. GAPDH was used to normalize the relative expression for each gene. Notably, quantitative RT-PCR would provide a more accurate picture of the potential changes of the expression levels compared to semi-quantitative PCR and should be used in future experiments.

4.3.2. Osteogenic differentiation in 2D results in the increased expression of selected osteogenic markers

Osteogenic differentiation of ASCs was visualized using a Zeiss AxioImager A1 fluorescence microscope. As Figures 4.3A-B show, the expression of OCN and OPN protein in ASCs was higher in the osteogenic differentiation media compared with cells in a standard cultivation media. Figure 4.3C shows that the fluorescence intensity was quantified and the increased expression of OCN was significantly increased in the cells undergoing osteogenic differentiation compared with the control group ($^{*}P<0.005$). Figure 4.3D shows that the fluorescence intensity of OPN was examined to detect the effect of chemical stimulation on the osteogenic potential of ASCs cultured in differentiation media. The results showed no significant differences

in protein expression between differentiated and undifferentiated cells. The late osteogenic proteins were only expressed in differentiated ASCs.
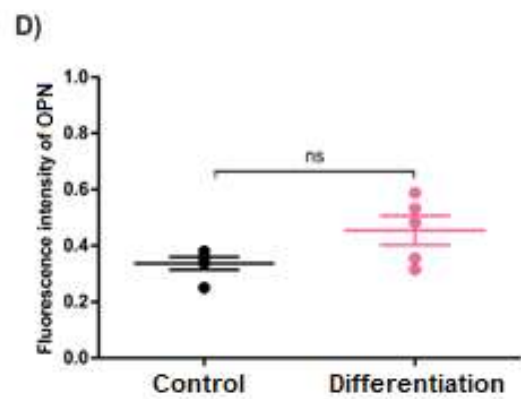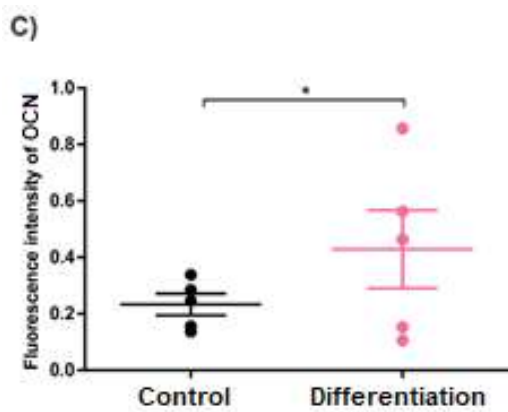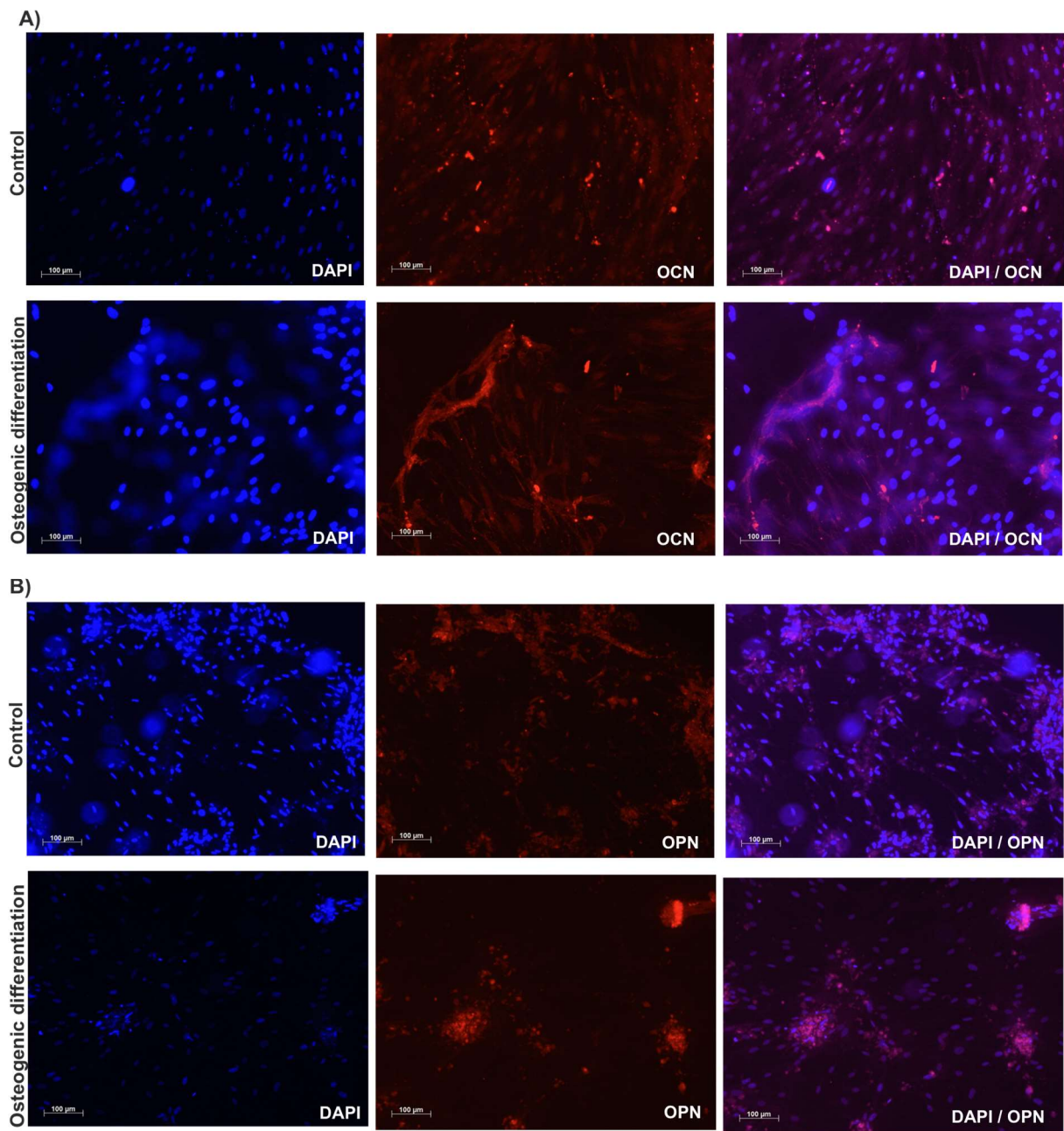
Figure 4.3. The expression of late osteogenic proteins of ASCs in 2D was higher in osteogenic differentiation media at 21 days. A and B: Immunocytochemical staining of differentiated and undifferentiated cells performed using monoclonal antibodies against OCN and OPN at 21-days: scale bar: 100µm. C and D: Quantification of fluorescence intensity. The fluorescence intensity for mature osteoblast markers (OCN and OPN) was analysed using ImageJ software. The expression of OCN was significantly higher in the cells in the osteogenic differentiation media compared with the control group. The fluorescence intensity of OPN showed no significant differences in ASCs in osteogenic and standard medias. Data were compared using student t-test with unpaired t test Welch's correction. At least three independent experiments were performed. *P<0.05 was considered to be statistically significant.

4.3.3. Osteogenic differentiation of ASCs in 2D results in increased mineralisation

Osteogenic and adipogenic differentiation in a 2D cell culture were evaluated. As shown in Figure 4.4A, calcium deposition in ASCs after 21 days of exposure to chemical stimulation with an osteogenic differentiation media resulted in a higher Alizarin Red S signal compared with cells cultivated in a standard media. After differentiation, cells subjected to Alizarin Red S showed a significantly higher signal compared with cells in the control group. Figure 4.4B shows that the quantification of Ca^{2+}-depositions was performed using Alizarin Red S dye and subsequent confocal laser scanning microscopy. Statistical analysis showed that the chemical stimulation increased the Alizarin Red S signal in the differentiated cells in the osteogenic media. The differentiated cells in the osteogenic lineage were proof of multipotency.
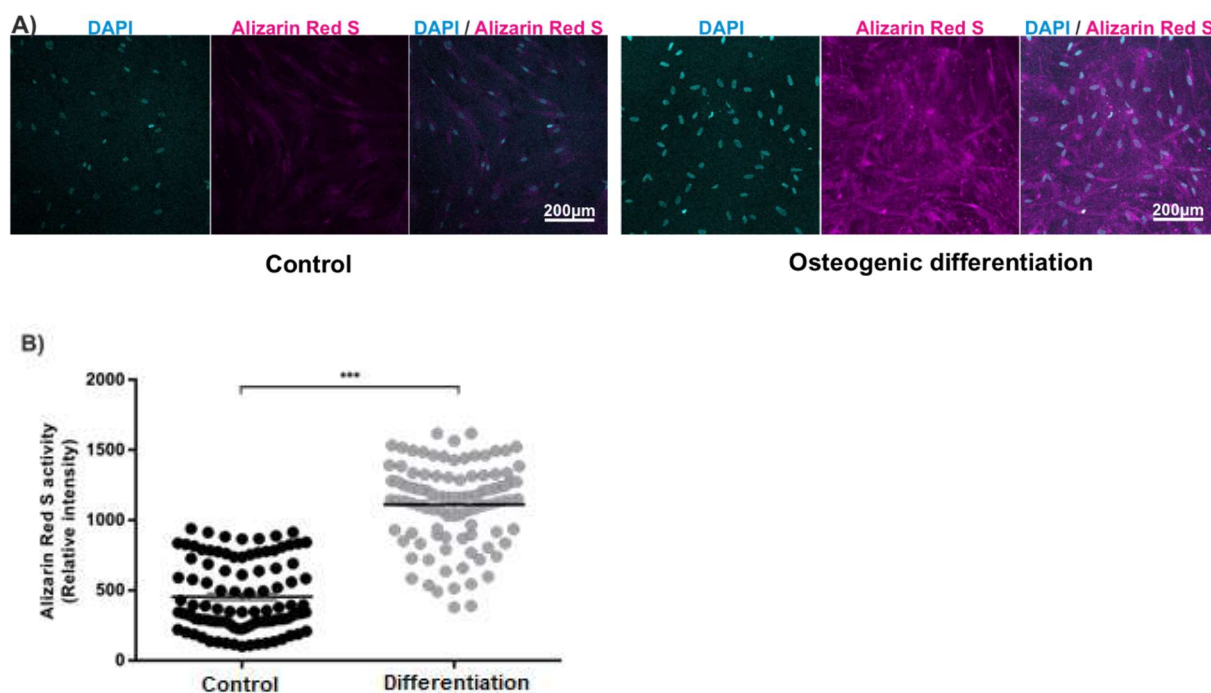
Figure 4.4. Alizarin Red S staining revealed a higher level of calcium deposition in the differentiated cells. (A) ASCs exposed to chemical stimulation in the osteogenic differentiation media at 21 days were compared with cells cultivated in a growth media. Confocal laser scanning microscopy clearly revealed the presence of nuclei in close proximity to the Alizarin Red S signal. Scale bar: 200µm. (B) Quantification of Ca^{2+}-depositions was performed using Alizarin Red S dye in confocal laser scanning microscopy. Alizarin Red S activity was measured using ImageJ software. Higher Alizarin Red S values suggest a higher level of calcium deposition in cells cultivated in the osteogenic differentiation media compared with the control. Statistical evaluation was performed using student t-test with unpaired t test Welch's correction. At least three independent experiments were performed. ***$P<0.0001$ was considered to be statistically significant.

4.3.4. Osteogenic differentiation of ASCs in 2D decreases the frequency of calcium oscillations

In this section, the calcium (Ca^{2+}) oscillation profiles in ASCs were characterized with and without subjecting the cells to the osteoinductive factors. To evaluate the different Ca^{2+} oscillation characteristics in the undifferentiated ASCs, the Ca^{2+} dynamics were recorded in ASCs for 30 min at 10-second intervals and the averaged FLUO-4 fluorescence intensities were plotted as a function of time. In contrast to the undifferentiated cells, the differentiated ASCs demonstrated an irregular Ca^{2+} spike pattern and a decreased number of Ca^{2+} spikes at 7, 14 and 21 days (Figure 4.5B-D-

F). The results showed that the calcium spikes decreased rapidly with osteogenic differentiation (Figure 4.5B-D-F).
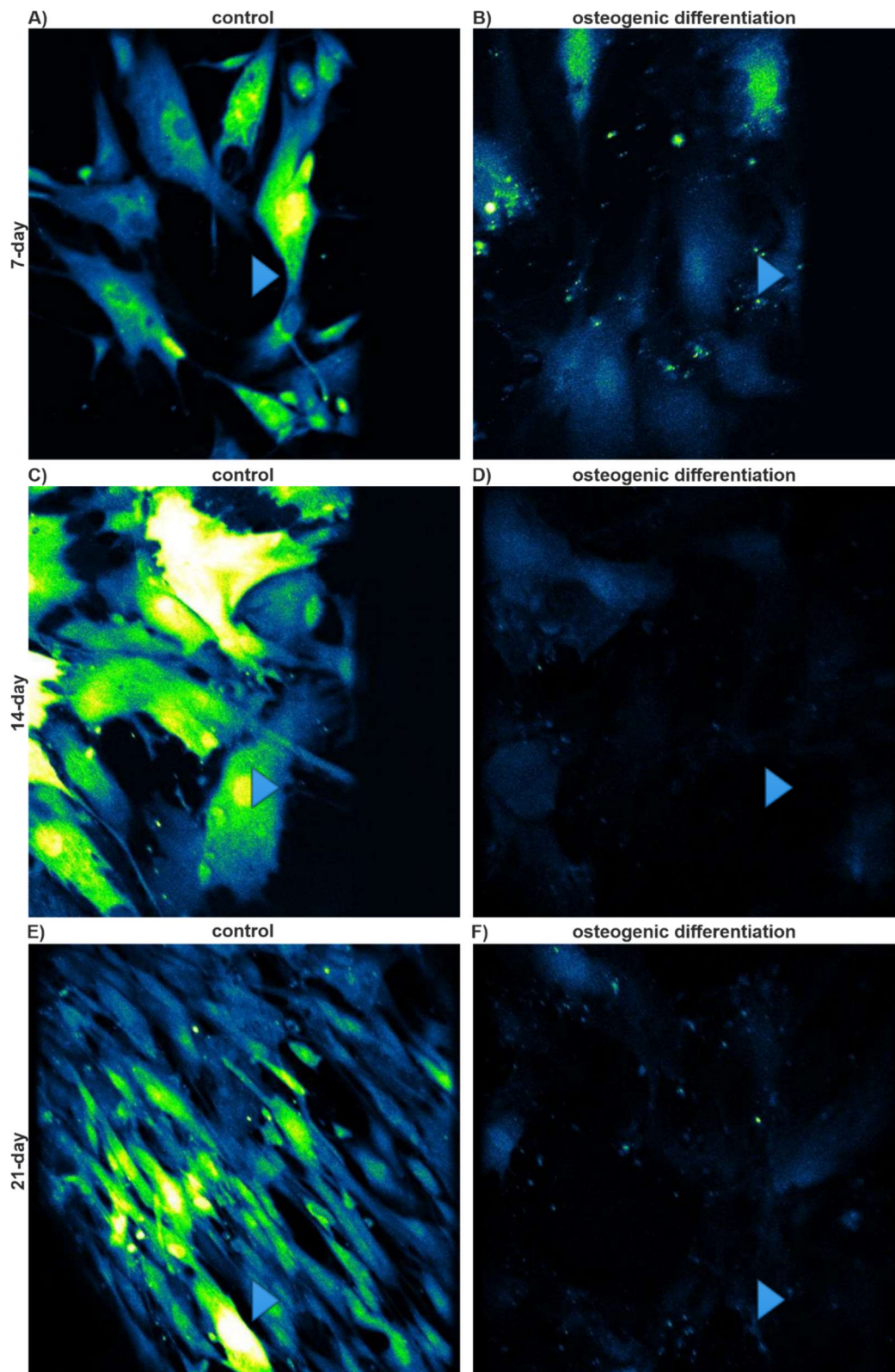
Figure 4.5. Images of spontaneous Ca2+ oscillations in ASCs in 2D cultivated in standard and osteogenic media. (A-F) Osteogenic differentiation showed a

decrease of calcium spikes in ASCs in 2D under osteogenic differentiation media, compared with cells in standard media for 7, 14 and 21 days. ASCs cultivated in the standard media displayed more intense Ca^{2+} spikes compared with cells in an osteogenic differentiation media.

Figure 4.6(A-C) shows that regular and multiple Ca^{2+} spikes were observed in the undifferentiated ASCs cultured in 2D for 7, 14 and 21 days. Treatment of ASCs with osteogenic differentiation supplementation is likely to not only alter the calcium oscillations but also serve the differentiation potential.
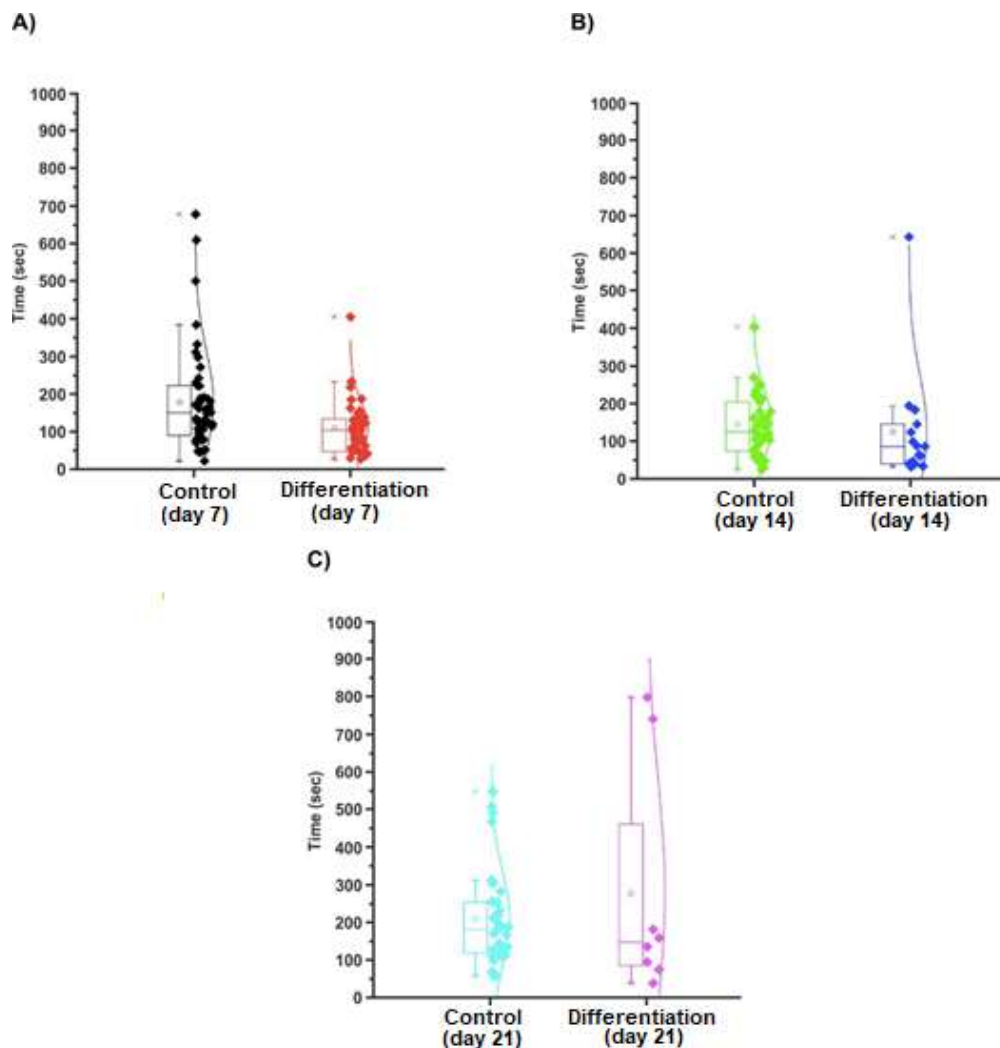
Figure 4.6. Comparison of oscillation patterns of ASCs treated with osteogenic media for 7, 14 and 21 days. (A-C) Frequency of Ca^{2+} spikes decreased rapidly with osteogenic differentiation in terminally differentiated human osteoblasts, compared with undifferentiated cells after 7, 14 and 21 days.

4.3.5. Osteoblast-related gene expressions of ASCs in 3D increases under osteogenic differentiation conditions

After performing proof-of-principle experiments in 2D, the effects of osteogenic differentiation were assessed on the expression of osteogenic genes at RNA level in human ASCs embedded in 3D aNFC (Figure 4.7). The osteogenic treatment was applied to ASCs cultured in 3D. These cells were collected on days 3, 14 and 21 to analyse their osteogenesis-related genes using conventional PCR. Expression of osteogenesis-related gene products was evaluated using electrophoresis and normalised to the corresponding levels of the housekeeping gene GAPDH. Vimentin is known as a stem cell marker whilst BMP2, RunX2, osterix, OCN and OPN are the osteogenic genes which mainly express in the early, middle and late stages. Notably, additional markers of mineralisation could also have been used to monitor osteogenic differentiation. These could include bone sialoprotein (BSP), collagen type I and osteonectin. A more complete analysis of osteogenic markers would allow a more complete view of the osteogenic differentiation in future research.

The image analysis of gene expressions of ASCs cultured in 3D for 3, 14 and 21 days was quantified as shown in Figure 4.8. The expression levels of OCN and OPN in ASCs in the osteogenic differentiation media were higher than those of cells in the standard media when cultured in 3D aNFC for 21 days. The expression level of BMP2 in the differentiated cells was higher than in the control groups when cultured in 3D for 14 days. The expression level of RunX2 in the differentiated cells for 21 days was higher when differentiated in 3D for 21 days. The expression level of Vimentin showed a decrease in the differentiated groups. GAPDH was used to normalize for each gene.
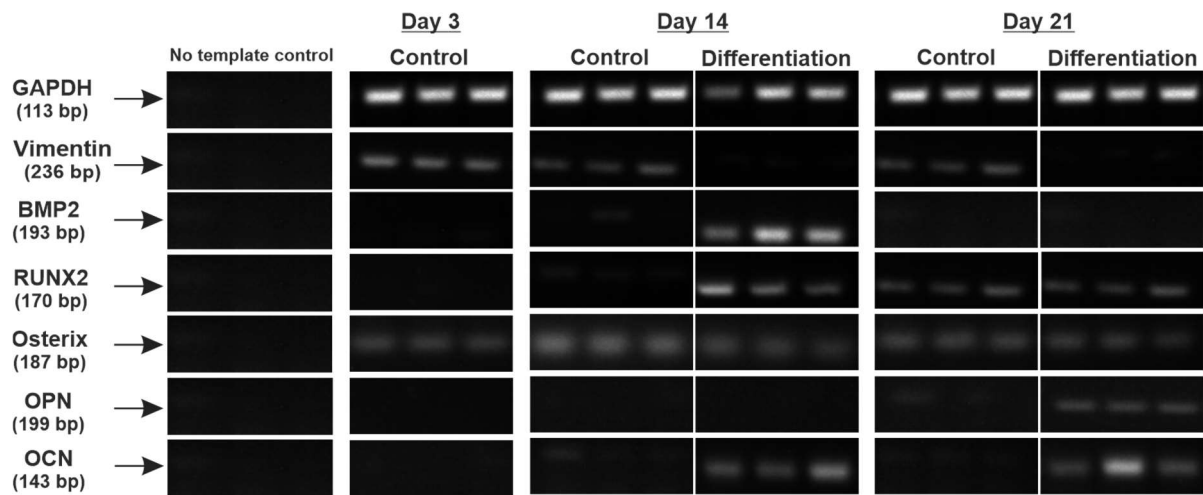
Figure 4.7. Osteogenic induction of ASCs cultured into 3D resulted in up-regulation of osteogenesis-related transcripts. Images of conventional PCR product bands were analysed using electrophoresis to determine the level of reverse-transcribed cDNA. The size of the PCR products (GAPDH, Vimentin, BMP2, RUNX2, Osterix, OCN and OPN) in the Figure was 113 bp, 236 bp, 193 bp, 170 bp, 187 bp, 143 bp and 199 bp respectively. GAPDH was applied for normalization to adjust the concentrations of cDNA before the electrophoresis analysis. The no template controls did not amplify any products as shown in the panel.
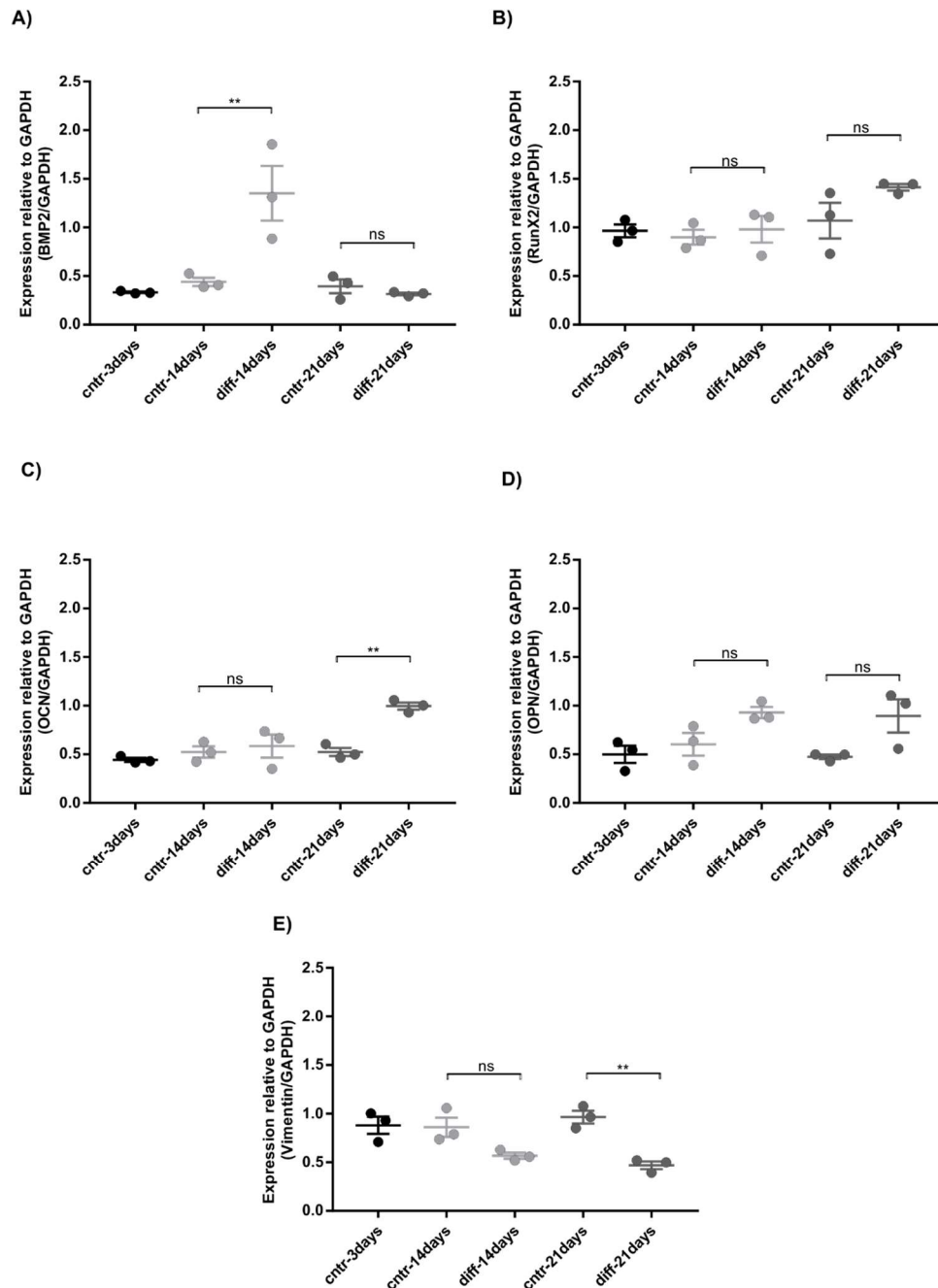
Figure 4.8. Expressions of osteogenesis-related genes normalised to GAPDH in ASCs cultured in 0.2% aNFC for 3, 14 and 21 days. (A-E) The expression levels of BMP2, RunX2, OCN, OPN and Vimentin were quantified and normalised to GAPDH. (A) ASCs in 3D aNFC showed an increase in the expression level of BMP2 in an osteogenic differentiation media compared with cells in 3D in a standard media for 14 days. (B) The expression level of RunX2 was higher in ASCs in 3D aNFC under the osteogenic media for 21 days compared with cells in the standard media. (C-D) The expression levels of OCN and OPN in ASCs in the osteogenic differentiation media were higher than those of cells in the standard media when cultured in 3D aNFC for 21 days. (E) The expression level of Vimentin showed a

decrease in ASCs in the osteogenic differentiation media. GAPDH was used to normalize the relative expression for each gene. The results are presented as mean ± SEM. At least three independent experiments were performed. Data were compared using one-way ANOVA with Bonferroni correction (CI 95%). $^{**}P<0.01$ was considered to be statistically significant.

4.3.6. Osteogenic differentiation in 3D aNFC results in the increased expression of selected osteogenic markers

Using confocal laser scanning microscopy, the expression levels of OCN and OPN were detected. The expression of OCN significantly increased in ASCs embedded into 0.2% aNFC with exposure to chemical stimulation in an osteogenic differentiation media compared with cells in a standard media for 21 days. Furthermore, ASCs embedded into 0.2% aNFC hydrogel showed an increased expression of OPN in the osteogenic differentiation media after 21 days compared with cells in the standard media.

Figure 4.9 shows that image-based confocal microscopy revealed a higher level of OCN expression in ASCs cultivated in 3D aNFC under osteogenic conditions compared with cells in ASCs in 3D NFC in a standard media for 21 days. The fluorescence intensity of the late osteogenic marker OCN was significantly higher in ASCs seeded into 3D aNFC cultured in the osteogenic differentiation media for 21 days compared with cells in the standard media (Figure 4.9C). Confocal laser scanning microscopy was also used to visualise late osteogenic markers (such as OPN) in ASCs embedded in 3D aNFC in an osteogenic differentiation media (Figure 4.10). The fluorescence intensity of the late osteogenic marker OPN was significantly higher in ASCs embedded into 3D aNFC cultured in the osteogenic differentiation media for 21 days (Figure 4.10C) compared with the OCN expression of the differentiated cells in 3D aNFC (Figure 4.9C). These results show that aNFC works obviously much better in differentiated cells in terms of the late osteogenic markers (such as OCN and OPN).

In these experiments, more pronounced differences were observed in the expression levels of OPN compared to OCN. This could be explained by different temporal expression pattern of these two markers. As a late osteogenic differentiation marker, OCN leads to the downregulation of early osteoblast markers including ALP and

RUNX2 and the expression of transcription factors for osteoblstic bone formation. Thus, high OCN levels can only be detected at late stages of differentiation. In contrast, OPN is an early marker of differentiation and changes in its expression levels can be detected already early in the process of osteogenic differentiation.
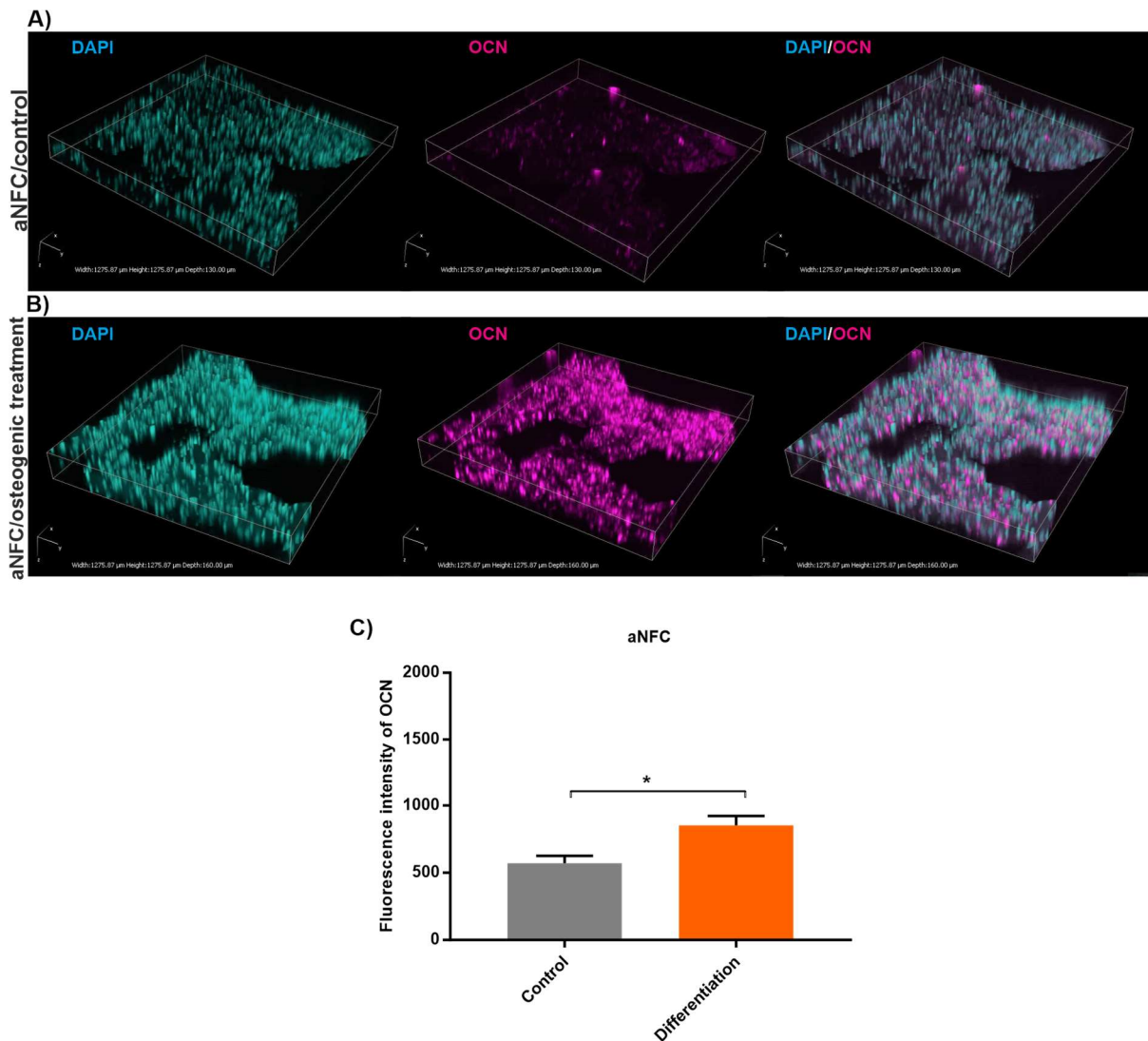
Figure 4.9. Image-based analysis revealed a higher level of OCN expression in ASCs in 3D under osteogenic conditions. (A-B) Confocal microscopy was used to visualise and quantify the OCN in the differentiated ASCs embedded in 0.2% aNFC compared with the undifferentiated cells. (C) The fluorescence intensity of the late osteogenic marker OCN was significantly higher in ASCs embedded into 3D aNFC in the osteogenic differentiation media for 21 days compared with cells in the standard media. No primary antibody control for Alexa Fluor 555 was shown in the Appendix II, as supplement figure 3.1.
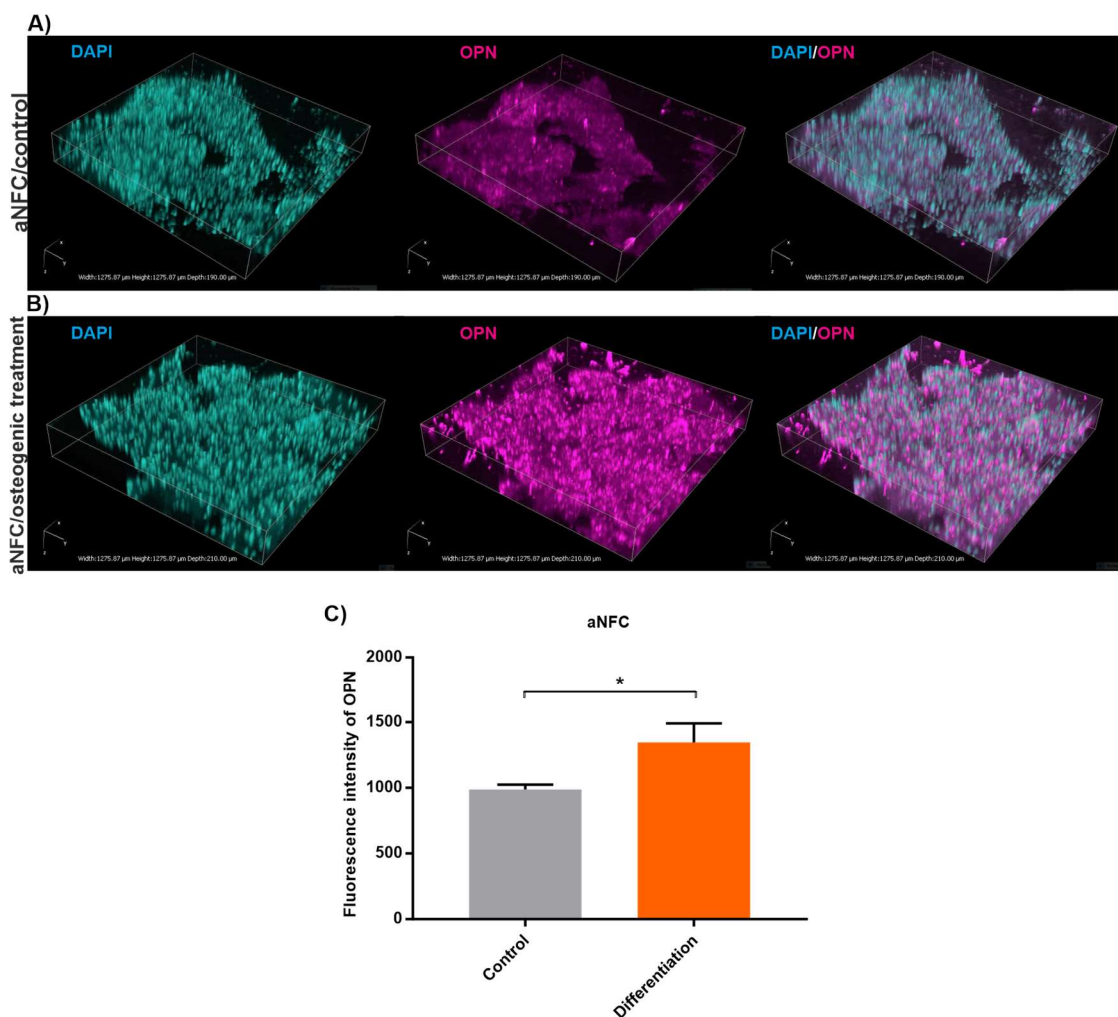
Figure 4.10. Image-based analysis revealed a higher level of OPN expression in ASCs in 3D under osteogenic conditions. (A-B) Confocal microscopy was used to visualise and quantify the OPN in the differentiated ASCs embedded in 0.2% aNFC compared with the undifferentiated cells. (C) The fluorescence intensity of the late osteogenic marker OPN was significantly higher in ASCs embedded into 3D aNFC in the osteogenic differentiation media for 21 days compared with cells in the standard media. Compared with the results shown in Figure 4.9C, OPN works obviously better in the differentiated cells cultivated into 3D aNFC in terms of the higher level of fluorescence intensity of OPN under confocal microscopy. The reason is that OPN and OCN are osteoblast markers, but only OCN is suggested as an osteogenic differentiation marker. No primary antibody control for Alexa Fluor 555 was shown in the Appendix II, as supplement figure 3.1.

4.3.7. Osteogenic induction increases calcium deposition in 3D aNFC

To determine the effects of 3D cell culture on calcium deposition, ASCs embedded into 3D aNFC were evaluated by Alizarin Red S staining after 21 days. ASCs embedded into 0.2% aNFC were cultivated in the osteogenic differentiation media for

21 days and then assessed by Alizarin Red S staining. Using confocal microscopy, image-based analysis was used to examine and quantify calcium deposition.

As shown in Figure 4.11, ASCs cultivated in 3D aNFC showed an intense mineral deposition in an osteogenic differentiation media at 21 days compared with cells in a standard media. The fluorescence intensity of Alizarin Red S was evaluated by ImageJ software. ASCs in 3D aNFC showed the increased fluorescence intensity of Alizarin Red S under osteogenic differentiation conditions compared with cells in 3D in a standard media after 21 days (Figure 4.11D). Statistical analysis revealed a higher expression of calcium deposits in differentiated cells embedded into 3D compared with cells in a standard cultivation media.
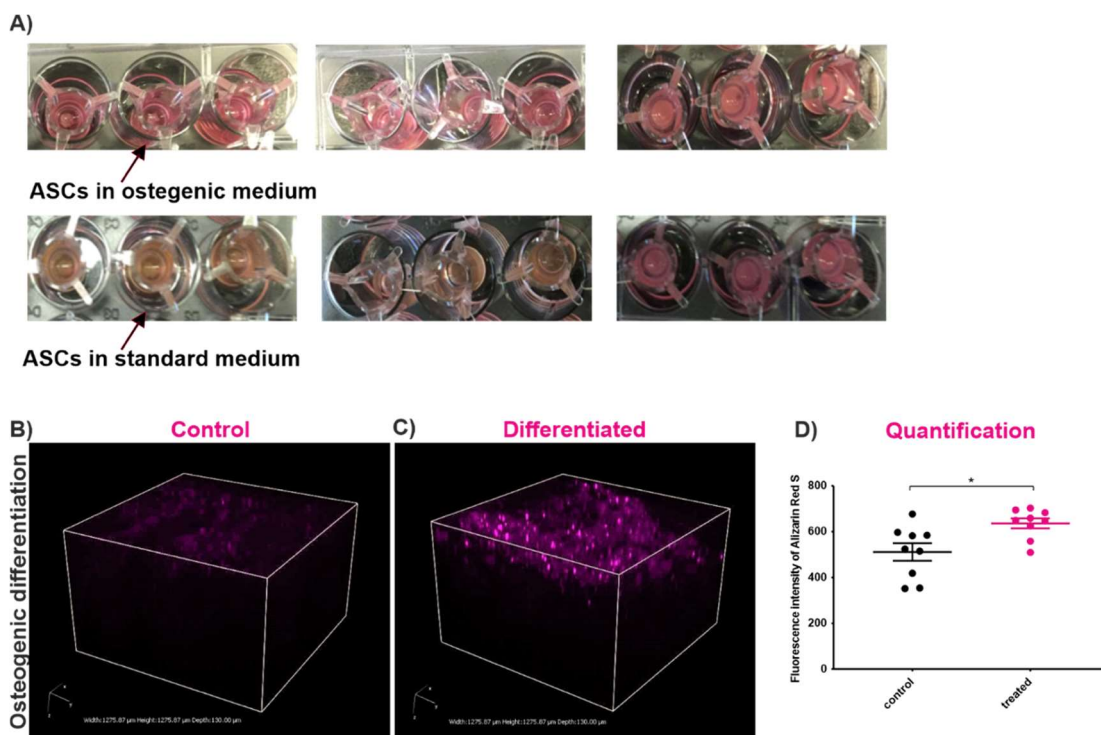
Figure 4.11. ASCs can undergo osteogenic differentiation in 3D aNFC hydrogels. (A) ASCs in 0.2% aNFC were subjected to osteogenic differentiation for 21 days and subsequently stained with Alizarin Red S to examine calcium deposition; (B-D) ASCs in 3D aNFC showed a higher level of mineralisation when subjected to osteogenic differentiation media for 21 days compared with cells in a standard media. A significant difference was observed between cells subjected to osteogenic differentiation and a standard media.

4.3.8. A denser actin cytoskeleton was observed in ASCs in 3D aNFC under osteogenic differentiation conditions

The alignment of actin fibres in the cell periphery and increased actin polymerization with perinuclear actin bundles are notable criteria of osteogenic differentiation (Titushkin and Cho, 2007), reviewed in (Khan et al., 2020). To visualise the actin cytoskeleton, ASCs embedded in 0.2% aNFC under standard and osteogenic differentiation medias were fixed and stained with phalloidin at day 21. Using confocal microscopy, image-based analysis demonstrated a denser F-actin texture subjected to osteogenic differentiation conditions in 3D aNFC (Figure 4.12A).

On this point, osteogenic differentiation can affect morphological changes in the cell cytoskeleton when cultured into aNFC. The arrangement of dense actin bundles was related to the increased osteogenic differentiation (Treiser et al., 2010).
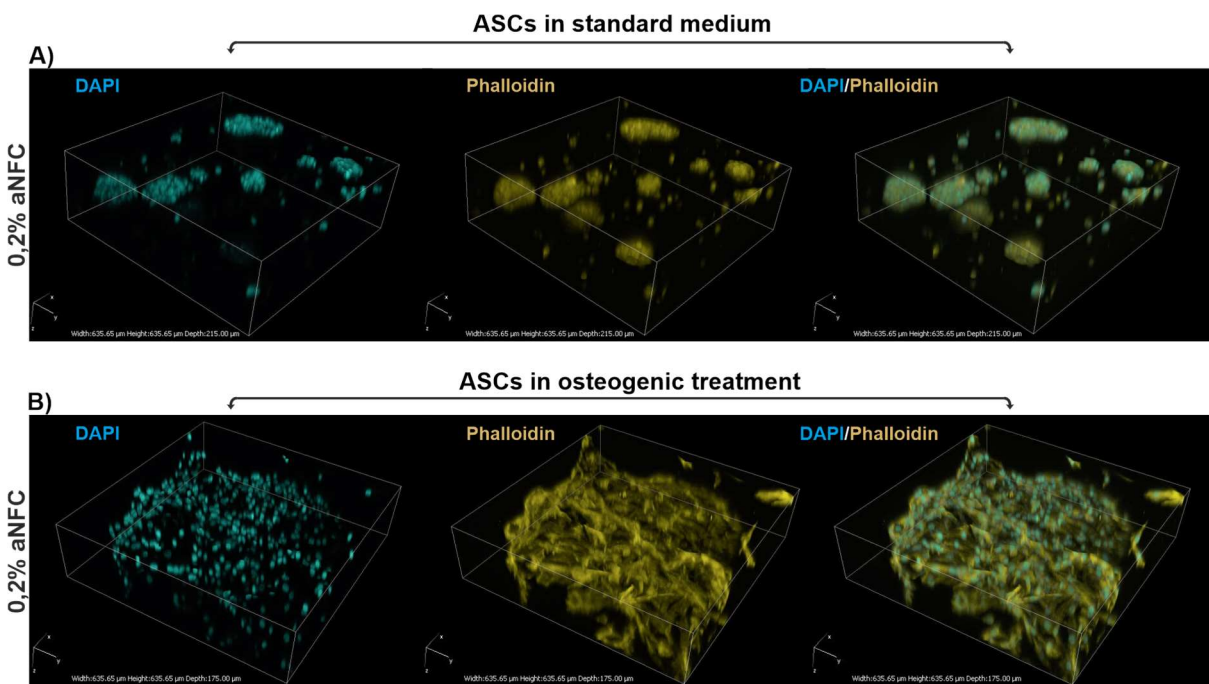
Figure 4.12. ASCs exposed to osteogenic differentiation displayed a highly arranged actin cytoskeleton and formation of cell-free pores within the 3D hydrogels. Confocal microscopy was used to visualise actin filaments in ASCs in 0.2% aNFC exposed to osteogenic treatment for 21 days. Magnification=20x. Image analysis showed that the actin cytoskeleton is more aligned in ASCs in 3D aNFC subjected to osteogenic differentiation. F-actin filament showed increased actin polymerization in ASCs in 3D aNFC.

4.4. Discussion

The first study to assess the osteogenic differentiation of rat MSCs was published almost fifty years ago (Friedenstein et al., 1974). Following that discovery, MSCs from numerous species and tissue origins have been demonstrated to undergo differentiation into osteogenic cells. Notably, in a key position statement, the International Society for Cellular Therapy defined the ability to give rise to bone cells *in vitro* as one of the minimal criteria for defining MSCs (Dominici et al., 2006a). In addition to *in vitro* differentiation, even more stringent evidence for the osteogenic potential of MSCs has been provided by several *in vitro* studies in different small and large animal models including rats (Kotobuki et al., 2008), sheep (Shang et al., 2001) and pigs (Stockmann et al., 2012). Furthermore, these promising *in vitro* and *in vivo* results motivated several clinical trials designed to assess the feasibility, safety and efficacy of MSCs in oral bone regeneration (Rickert et al., 2011, Kaigler et al., 2013, Sauerbier et al., 2010). Although several individual trials suggested that the transplantation of MSCs is safe and is associated with improved oral bone regeneration, a more recent meta-analysis did not reveal a significant increase in vital bone mass (Padial-Molina et al., 2015).

In this chapter, the osteogenesis-related gene expressions of ASCs cultured in 2D have been analysed. Osteogenic induction resulted in up-regulation of osteogenesis-related transcripts (such as OCN and OPN) (Figures 4.1 and 4.2). Castrén et al. (2015) reported that OCN mRNA level in 2D increases until day 21, which is in general accordance with the findings of the current study. I have also shown that the osteogenic differentiation of ASCs in 2D cell culture resulted in a higher expression of OCN and OPN at protein level. In contrast, although I found an increased up-regulation of Runx2 until day 14, Castrén et al. demonstrated a lower level of Runx2 mRNA at day 14. Compared with the differences between 2D and 3D cultures, Runx2 levels showed an increase at day 14 in MSCs cultivated in FCS in 2D cultures but were found to be low in PLP (human platelet lysate and plasma) cultures in 2D under osteogenic differentiation potential (Castrén et al., 2015). However, the mRNA profiles in 3D cultures showed differences from those obtained in 2D cultures since the highest level of Runx2 mRNA in PLP and FCS-differentiated cultures was found on day 14 (Castrén et al., 2015). Moreover, the differentiation potential of ASCs in 2D was evaluated by analysing calcium deposition as proof of mineralization by using

Alizarin Red S staining. ASCs subjected to osteogenic differentiation showed a significantly higher Alizarin Red S signal compared with cells in a control media (Figure 4.4). These findings are in general accordance with the study by Castrén et al. (2015), which showed that calcium deposition is higher in cells in an osteogenic differentiation media.

Spontaneous calcium oscillation of the undifferentiated ASCs was compared with cells treated with osteogenic differentiation for 7, 14 and 21 days. Osteogenic differentiation resulted in a decrease in the frequency of calcium oscillations with Ca^{2+} spikes compared with cells in the standard media for 7, 14 and 21 days. Sun et al. (2007) reported changes of Ca^{2+} oscillation in undifferentiated bone marrow MSC and exhibited unsynchronized Ca^{2+} oscillations in undifferentiated human MSCs (Sun et al., 2007). These findings are in general accordance with those of the current study showing that regular and multiple Ca^{2+} spikes were observed in ASCs cultured in a standard media in 2D for 7, 14 and 21 days (Figures 4.5 and 4.6). Sun et al. (2007) also evaluated the effect of intracellular Ca^{2+} dynamics on differentiated human osteoblasts in response to osteoinductive factors and found that the frequency of Ca^{2+} spikes decreased in response to osteoinductive factors present in the osteogenic differentiation media (Sun et al., 2007).

NFC is a highly promising hydrogel for bone regeneration since it is generally biocompatible with MSCs. I examined the expression of osteogenic genes associated with early and mature osteoblasts at RNA level (for example, Bmp2, Runx2, OCN and OPN) in 3D (Figure 4.8). Importantly, OCN is secreted by mature osteoblasts to promote the mineralization of calcium deposits (Lian et al., 1998). This corresponds with the increased expression of osteogenesis-related proteins visualized by specific monoclonal antibodies (such as OCN and OPN) after 21 days of osteogenic induction of ASCs in 3D aNFC. Some expression observed in cells cultured in a standard media. Other markers of mineralisation could also have been used to be proved. Bone sialoprotein (BSP) is an important mineralised tissue associated marker. The overexpression of BSP promotes the increased level of osteoblast-related gene expression. The expression of OCN significantly increased in ASCs into aNFC under osteogenic conditions (Figure 4.9). In contrast, OCN expression was decreased in ASCs embedded into NFC when subjected to osteogenic differentiation conditions. Furthermore, the expression of OPN demonstrated a significantly higher

signal in cells within 3D aNFC compared with cells in both a standard media and 3D NFC (Figure 4.10). In addition, Matrigel, a hydrogel mainly composed of type IV collagens, entactin, perlecan and laminin, has been shown to increase the osteogenic differentiation potential compared with a 2D cell culture. When cells were cultured within a Matrigel scaffold under osteogenic conditions, human BM-MSCs showed higher activity alkaline phosphatase (an early marker of osteogenesis) than the 2D counterparts (Yu et al., 2018). As alternative scaffolds, different polycaprolactone-based substrates have been explored in the osteogenic differentiation of MSCs. An elastic 3D poly (ε-caprolactone) has been shown to increase the expression of bone sialoprotein and OCN in minipig BM-MSCs subjected to differentiation on 3D (Rampichova et al., 2013). As a consequence of that finding, polycaprolactone-tricalcium phosphate scaffolds and jet sprayed microfibre polycaprolactone scaffolds were suggested to possess similar osteoinductive effects in human foetal and adult BM-MSCs (Shekaran et al., 2015, Brennan et al., 2015). There have also been reports of increased osteogenic differentiation of ASCs and BM-MSCs in 3D when gelatin and blends of gelatin and alginate are used as a scaffold (Lo et al., 2016, Wang et al., 2016b).

In addition to the effects on the expression of osteogenic genes at RNA level and the up-regulation of osteogenic markers at protein level, ASCs in 3D aNFC also demonstrated more intense mineral deposition under osteogenic conditions at 21 days compared with cells in a standard media (Figure 4.11). Sheard et al. (2019) showed a high level of Alizarin Red S signal after osteogenic induction in human MSCs seeded into aNFC (Sheard et al., 2019). a more stringent test by the additional determination of specific signals was applied on the differentiated cells as the detection of Alizarin Red S might lead to the risk of overestimation because of false-positive signals produced by cell debris. The results therefore demonstrated the expression levels of OCN and OPN are readily detectable in ASCs in 3D aNFC cultured in an osteogenic differentiation media for 21 days, whereas the expression was undetectable in cells cultured in a standard media. However, real-time RT-PCR should be performed in future experiments to validate these results. Park et al. (2007) reported that MSCs on a vertically oriented titanium surface resulted in increased mineralization and a high level of OCN (Park et al., 2007). A 2008 report provided evidence that 3D nanofibrillar scaffolds prepared from rat tail collagen increased the expression of osteogenic markers including type I collagen, OPN and

Osteonectin in human ASCs compared with differentiation conducted in 2D. Although Sefcik et al. (2008) reported increased calcification by means of Alizarin Red S staining, they did not assess the significance of the data (Sefcik et al., 2008). Similar effects on the expression levels of OCN and OPN in rat BM-MSCs were observed when purified collagen was used to create a 3D scaffold (Han et al., 2012a). Notably, von Kossa staining revealed a statistically significant increase of calcification. Nguyen et al. (2012) used a blended scaffold composed of collagen and electrospun poly (L-lactic acid) to study the influence of 3D cell culture on the differentiation of human MSCs of undefined origin and found that differentiation in 3D significantly increased the expression of OCN and OPN and the levels of calcification in human MSCs (Nguyen et al., 2012). On the other hand, the use of pure poly (L-lactic acid) scaffolds as a substrate showed similar increases in the expression of pro-osteogenic markers in human BM-MSCs under osteogenic conditions (Persson et al., 2018). This was accompanied by a significant increase in Ca^{2+} deposition demonstrated by von Kossa and Alizarin Red S staining.

In order to investigate potential differences in actin cytoskeleton architecture and the formation of cell-free pores, ASCs cultivated in aNFC and NFC hydrogels were evaluated at 21 days of osteogenic differentiation and were directly subjected to fluorescent phalloidin staining. The reorganization of the actin filament in cells showed denser actin bundles, which were cultivated into aNFC under an osteogenic differentiation media (Figure 4.12). These results are consistent with those of Chen and Jacobs (2013) indicating a rearrangement of the cytoskeleton during osteogenic differentiation (Chen and Jacobs, 2013). Okumura et al., (2001) found that the osteogenic differentiation of cells orientated with a nanoporous titanium surface was directly associated with the reorganization of the actin cytoskeleton (Okumura et al., 2001) and those results were consistent with those of Treiser et al. (2010) which implied the arrangement of dense actin bundles supported by osteogenic differentiation (Treiser et al., 2010). Increased actin polymerization with perinuclear actin bundles framing the nucleus and the alignment of actin fibres in the cell periphery are well characterized hallmarks of osteogenesis ((Titushkin and Cho, 2007), reviewed in (Khan et al., 2020)).

4.5. Conclusion

In recent years, the impact of 3D cell culture has been evaluated on the osteogenic differentiation of ASCs. By comparison with cells cultivated in a 2D culture, ASCs in 3D aNFC showed an increased osteogenic differentiation potential. NFC hydrogels allowed an increase in osteogenic differentiation. ASCs embedded in aNFC hydrogels demonstrated an increase in the expression of osteoblast-related genes (OCN and OPN) at RNA level at day 21 under osteogenic differentiation media. The expression level of OCN and OPN in ASCs in an osteogenic media was significantly higher than that of cells in a standard media when cultured in both 2D and 3D for 21 days. ASCs in 3D aNFC hydrogels showed an increase in the expression of BMP2 in an osteogenic differentiation media compared with other genes tested at day 14. After exposure to osteogenic differentiation conditions, ASCs showed an up-regulation of osteogenic markers (OCN and OPN) at protein level at day 21. In addition, the results of functional assays supported the increased osteogenic differentiation in human ASCs. Following osteogenic differentiation, cells subjected to Alizarin Red S showed a significantly higher signal in 3D compared with cells in the standard media. The cytoskeleton re-arrangement of ASCs demonstrated a more intense actin filament in 3D aNFC hydrogel. In summary, therefore, aNFC hydrogel could be effectively used in bone tissue engineering to support cell growth and osteogenic differentiation.

Chapter 5

Electrical stimulation of adipose-derived mesenchymal stem cells in anionic nanofibrillar cellulose increases their osteogenic potential

5.1. Introduction

Over 2.2 million bone graft procedures are performed each year to treat bone defects and fractures (Kinaci et al., 2014). In the European Union, the economic burden of bone fractures in 2010 was €37 billions of which of 66% was due to accidental fractures, 29% to long-term fracture care and 5% to pharmacological preventions (Ferrari et al., 2016). The worldwide economic burden of bone fracture treatment is expected to reach nearly €46 billions in 2025 (Hernlund et al., 2013). Although various procedures, including allografting, autografting and xenografting, are commonly used to treat bone defects, these applications can result in many drawbacks, such as donor morbidity, lack of tissue supply and immune rejection, respectively (Zhang et al., 2016, Dimitriou et al., 2011b). The gold standard treatment is autografting, but it is not entirely beneficial because of its drawbacks, including donor site morbidity, the limited number of donors and the risk of infection. Allografting, which is used in clinical applications, has also raised some concerns, such as disease transmission and immune rejection (Liu et al., 2013).

To address the limitations of bone grafting, MSCs are widely used for bone regeneration, especially in combination with various scaffolds (Zhang et al., 2012b). Osteogenic differentiation of MSCs can be stimulated through biophysical factors including nano- and macro-topology (Greiner et al., 2019a, Vordemvenne et al., 2020), substrate stiffness (Olivares-Navarrete et al., 2017), fluid shear stress (Yourek et al., 2010), nanovibration-induced displacement (Tsimbouri et al., 2017, Orapiriyakul et al., 2020) and electrical stimulation (ES) (Eischen-Loges et al., 2018, Chen et al., 2019). Electricity has become increasingly popular for modulating the regeneration capacity of numerous tissues (McCaig et al., 2009). ES has been administered clinically to heal bone fractures for over 40 years (Aleem et al., 2016). The impact of ES on cells has a profound effect on cellular proliferation and osteogenic differentiation (Leppik et al., 2020). ES treatments have been performed to induce bone matrix formation followed by bone healing (Song et al., 2009). Yonemori et al. (1996) reported that ES resulted in higher improvement in bone regeneration compared with control groups in rabbits (Yonemori et al., 1996). A greater level of understanding of ES functions in tissue engineering relies on studies which explore the changes in stem cell behaviours stimulated with and without an electrical field (Titushkin and Cho, 2007). Many studies have recently reported that

stem cells stimulated by daily ES showed an increase in osteogenic differentiation in terms of alkaline phosphatase (ALP) activity and the fluorescence intensity of OPN (Balint et al., 2013, Mobini et al., 2016). Some studies have also reported that changes in cytoskeleton reorganization are linked with osteogenic differentiation when exposed to an electrical field (Titushkin and Cho, 2007, Titushkin and Cho, 2009). Clinical studies have reported that ES has been shown to be an effective treatment for osteoarthritis and bone defects (Maziarz et al., 2016). Even though pulsed electromagnetic stimulation has been found to support the improvement of osteogenic differentiation in MSCs (Schwartz et al., 2008, Teven et al., 2012, Kaivosoja et al., 2015, Ongaro et al., 2014), a few researchers have reported that cells exposed to ES have shown lower cell viability and osteogenic differentiation (Zhu et al., 2017, Kumar et al., 2016, Li et al., 2016b).

Many studies have evaluated the osteogenic differentiation of MSCs performed on flat 2D substrates that can cause a loss of multipotency, accumulation of chromosomal aberrations and premature cellular senescence (Ben-David et al., 2011, Bara et al., 2014, Turinetto et al., 2016). In contrast, 3D cell culture can positively affect MSC differentiation as well as mimicking the 3D structure of the bone tissue (Yin et al., 2020a). MSCs have been successfully cultivated in different solid 3D scaffolds and hydrogels such as calcium phosphate ceramic (Urquia Edreira et al., 2016a), poly(ε-caprolactone) (Guarino et al., 2014), alginate (Ho et al., 2016), Matrigel (Yamaguchi et al., 2014), collagen (Lund et al., 2009), bacteria-derived cellulose (Favi et al., 2013) and methylcellulose (Cochis et al., 2017). Moreover, conductive polymers can be applied as ES treatments due to their biocompatibility and easy modification (Guo and Ma, 2018). Among these conductive polymers, poly(3,4-ethylenedioxythiophene), polystyrene sulphonate (PEDOT: PSS) (Guex et al., 2017), polypyrrole (PPy), (Luculescu et al., 2018, Liu et al., 2017) and polyaniline (PANI) (Pournaqi et al., 2017) have been used in combination with ES to induce osteogenic differentiation. However, direct observation of cells in these materials is unfeasible due to their opaque properties. Attempts to optimize ES conditions can therefore be difficult. To overcome this disadvantage, NFC hydrogels with good optical properties have been successfully fabricated, as described in the previous chapters. These biomaterials are light-transparent so the surface of the cells can be directly visualised.

In the previous chapters, hydrogels based on NFC and aNFC, which represent scaffolds biocompatible with ASCs allowing their osteogenic differentiation were evaluated. aNFC promoted a significant increase in cell viability and osteogenic differentiation compared with NFC and 2D controls. These data are consistent with those reported in previous studies in which NFC and aNFC hydrogels showed a positive effect on the expansion and osteogenic differentiation of ASCs in 3D (Sheard et al., 2019, Azoidis et al., 2017). Azoidis et al. (2017) found that NFC did not negatively affect the proliferation of ASCs whereas Sheard et al. (2019) found that aNFC significantly increased their viability compared with 2D controls. In this chapter, I hypothesize that combining 3D cultivation of ASCs in aNFC hydrogels with ES can promote their osteogenic differentiation.

5.2. Objectives

The results presented and discussed in Chapter 4 showed that cultivation in 3D aNFC hydrogels resulted in an increase of the osteogenic differentiation potential of ASCs. The focus of this chapter is on developing an *in vitro* ES protocol to optimise cell mineralization in 3D aNFC. Although there are many different parameters published, an electric field of 0.1V/cm at a frequency of 10 Hz and 0.4 ms pulse width alternating current was determined to provide the best balance between viability and osteogenic differentiation. Even though both short-term electrical stimulation (Eischen-Loges et al., 2018) and ES over 21 days (Zhang et al., 2016) have been both reported to have pro-osteogenic effects in MSCs, the impact of long term ES in 3D on both osteogenic differentiation and viability of the cells has not yet been assessed. Optimization experiments were performed (Supplement Fig. 5.4, Supplement Fig. 5.5, Supplement Fig. 5.6 and Supplement Fig. 5.7) to determine the best balance between viability and osteogenic differentiation. Two different voltages (0.1V/cm and 0.3V/cm) have been tested for optimization. Whereas 0.3V/cm of ES resulted in a decrease in the cell viability, ES with 0.1V/cm evidently showed no negative effect on cell viability after 21 days as well as an increase in the osteogenic differentiation of ASCs in 3D aNFC. To explore the impact of ES treatment in 3D, osteogenic potential was evaluated in ASCs exposed to an electric field of 0.1V/cm at a frequency of 10Hz and 0.4ms pulse width alternating current. The changes in the cytoskeleton reorganization of ASCs were investigated under control and osteogenic differentiation conditions in response to directly applied ES.

ES parameters were set up for delivering direct current to cells through a specially built cell-culture chamber. The chamber worked in conjunction with IonOptix C-Dish™ Culture Dish Electrode Assemblies. U-shaped platinum electrodes, 22 mm apart, were secured to the lid of a 6-well cell-culture plate and connected to a standard DC power supply. The electrodes were in contact with the bottom of the plate and were fully covered by culture media. The electrodes were connected to a standard multi-channel stimulator designed for chronic stimulation of cultured cells in incubators (for example, C-Pace EP) (Figure 5.1). Using digital adjustment of frequency (0.010-99 Hz), pulse duration (0.4-24 ms) and voltage (up to +/-40V and 240 mA), the cells were exposed to 0.1V/cm chronic stimulation for 30 min a day for 7, 14 or 21 days using a standard electrical power supply.
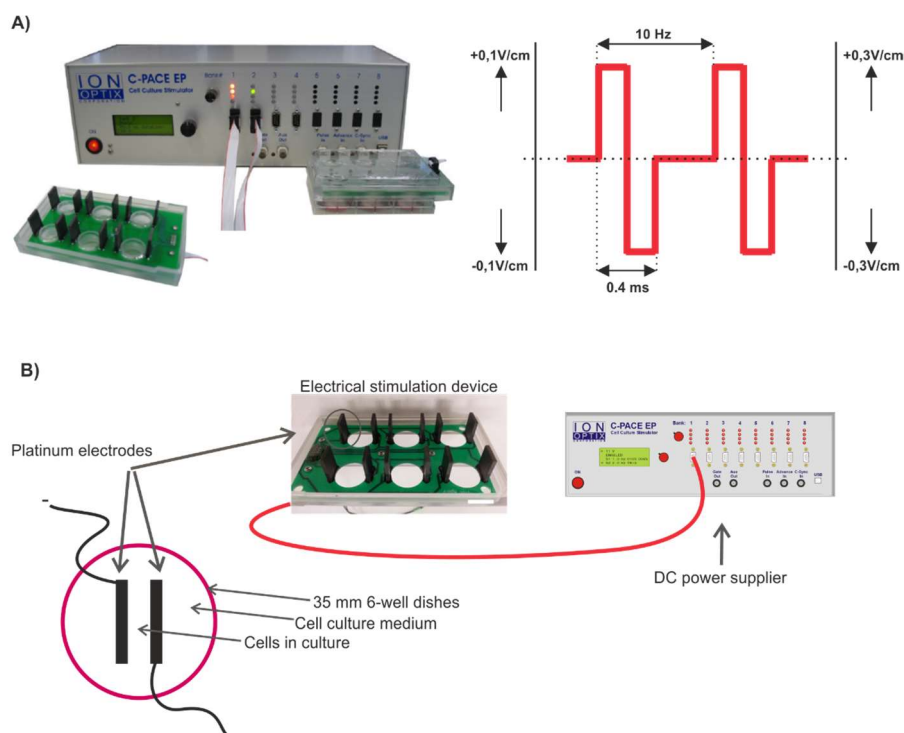
Figure 5.1. Setup for delivering electrical stimulation to the cells. U-shaped platinum electrodes, 22 mm apart, were secured to the lid of a 6-well cell-culture plate and connected to a standard DC power supply. The electrodes were in contact with the bottom of the cell culture plate and were fully covered by culture media.

The experimental design and set-up are shown in Figure 5.2. ASCs were pre-cultivated under standard conditions for 4 days and then the media was replaced with an osteogenic or adipogenic media. The control group was treated in fresh standard media. The cells were exposed to chronic stimulation for 30 min a day for 7, 14 or 21 days using a standard electrical power supply. The hypothesis was that ASCs

exposed to ES would stimulate characteristic alterations to improve osteogenic potential under osteogenic differentiation conditions. For 2D culture, a seeding density of 3×10^6 cells/3 mL were cultured in a 6-well, tissue-culture-treated, non-pyrogenic polystyrene plate (cell growth area of 9.5cm^2 approximately). For the 3D culture, ASCs at 1×10^5 cells/100 μL seeded in 0.2% aNFC were cultivated in TC cell culture inserts.
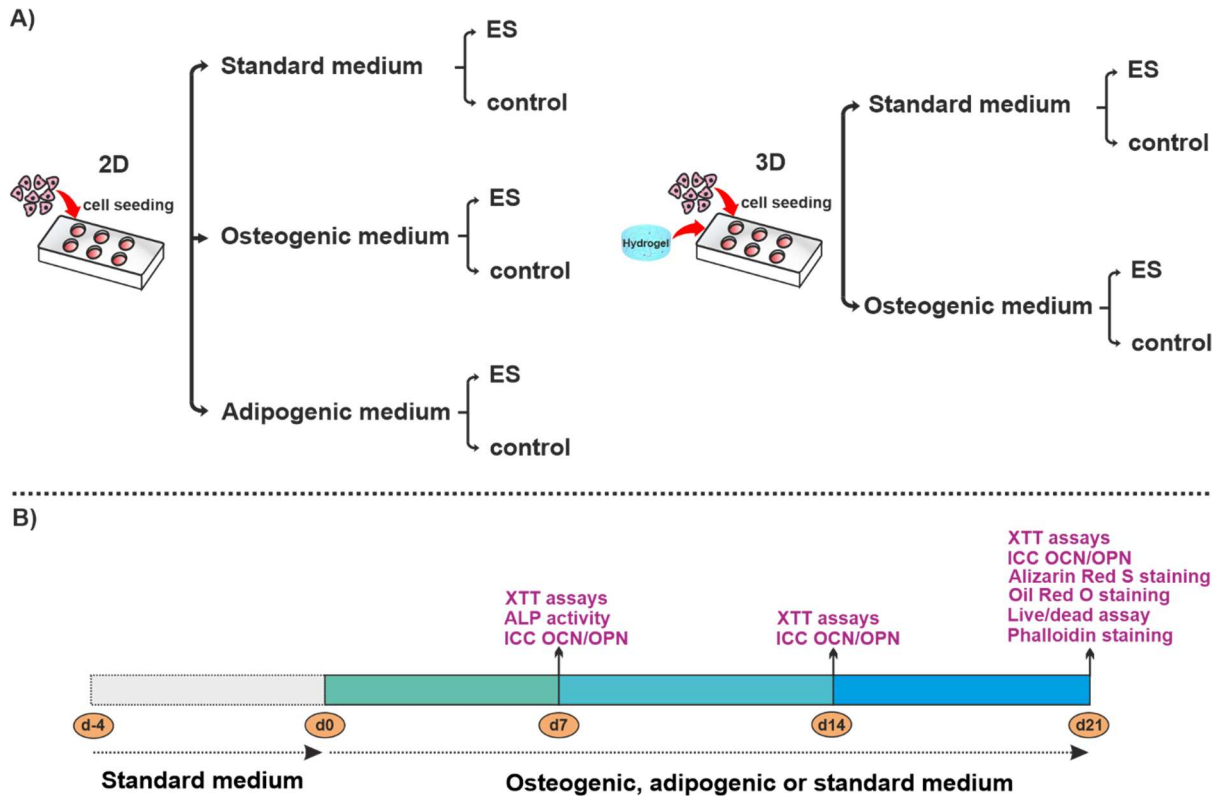
Figure 5.2. Schematic representation of the experimental design. (A) Experimental groups in 2D and 3D. In 2D and 3D, ASCs were differentiated into osteogenic or adipogenic medias under standard conditions with and without being exposed to ES. (B) ASCs were pre-cultivated in standard conditions for 4 days and then the media was replaced by an osteogenic, adipogenic or fresh standard media. XTT assays and immunocytochemical (ICC) staining against OCN and OPN were performed at day (d)7, d14 and d21. Alkaline phosphatase (ALP) activity was assessed on day 7, whilst Alizarin Red S staining, Oil Red O staining, live/dead assay and phalloidin staining were performed on day 21.

5.3. Results

5.3.1. ES improved the osteogenic differentiation potential of ASCs under 2D cell culture conditions

Electrical fields with different strengths were applied to the osteogenic differentiation of ASCs to determine optimal ES. The lower electrical field (0.1V/cm) showed no negative effect on cell viability at day 21 of culture compared with the control groups. ASCs were subjected to electric fields of 0.1V/cm at a 10 Hz frequency and a 0.4 ms pulse width alternating current signal. Cellular viability was measured by XTT viability analysis on days 7, 14 and 21 of osteogenic differentiation compared with cells in the control group. As shown in Figure 5.3A-C, ES evidently showed no adverse effect on cell viability after 21 days.
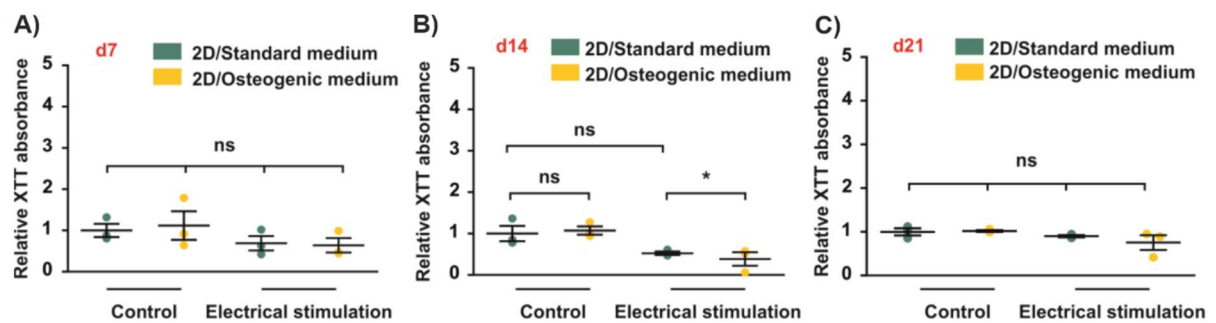
Figure 5.3. Long-term cultivation of ASCs in 2D cell culture did not affect their viability under standard and osteogenic differentiation conditions. (A-C) Cell viability in 2D was measured by XTT viability assay at an excitation wavelength of 490 nm and a reference wavelength of 650 nm. ASCs were exposed to ES in standard and osteogenic medias for up to 21 days followed by evaluation of viability using XTT assays. At days 7 and 21 ES, no significant differences in viability were detected. At day 14, ES of cells in the osteogenic media slightly decreased the viability compared with cells exposed to ES in a standard media. Values are shown as means ± standard errors (SEM) of three independent experiments using GraphPad Prism software (GraphPad, La Jolla, CA, USA), $^*P<0.05$, and a one-way ANOVA with Bonferroni correction (CI 95%).

Calcium deposition is a key indicator of the osteogenic differentiation of ASCs (Liu et al., 2014). After the assessment of Alizarin Red S fluorescence intensity, more extracellular mineral deposition of ASCs at day 21 of culture was observed in the osteogenic media when exposed to ES treatment (Figure 5.4A). The effect of ES with 0.1V/cm at a 10 Hz frequency for 30 min per day on the osteogenic differentiation of

ASCs was evaluated. As shown in Figure 5.4., cells exposed to ES with 0.1V/cm resulted in distinguishable changes in morphology in ASCs at day 21 compared with the control groups. Calcium deposition of ASCs stimulated to 0.1V/cm showed a significant difference despite slight morphological changes compared with cells without ES. Alizarin Red S fluorescence intensity was assessed in ASCs exposed to ES in the osteogenic media. When exposed to ES treatment, ASCs in the differentiation media showed a high level of Alizarin Red S fluorescence intensity compared with cells in the standard media (Figure 5.4B). As shown in Supplement 5.1., Appendix III, Alizarin Red S recovery values were determined using a standard curve ($y=0.0066x-0.0045$, $R^2=0.9729$). Overall, ES was able to accelerate the osteogenic differentiation of ASCs, which is consistent with the finding of a previous study by (Zhang et al., 2016).
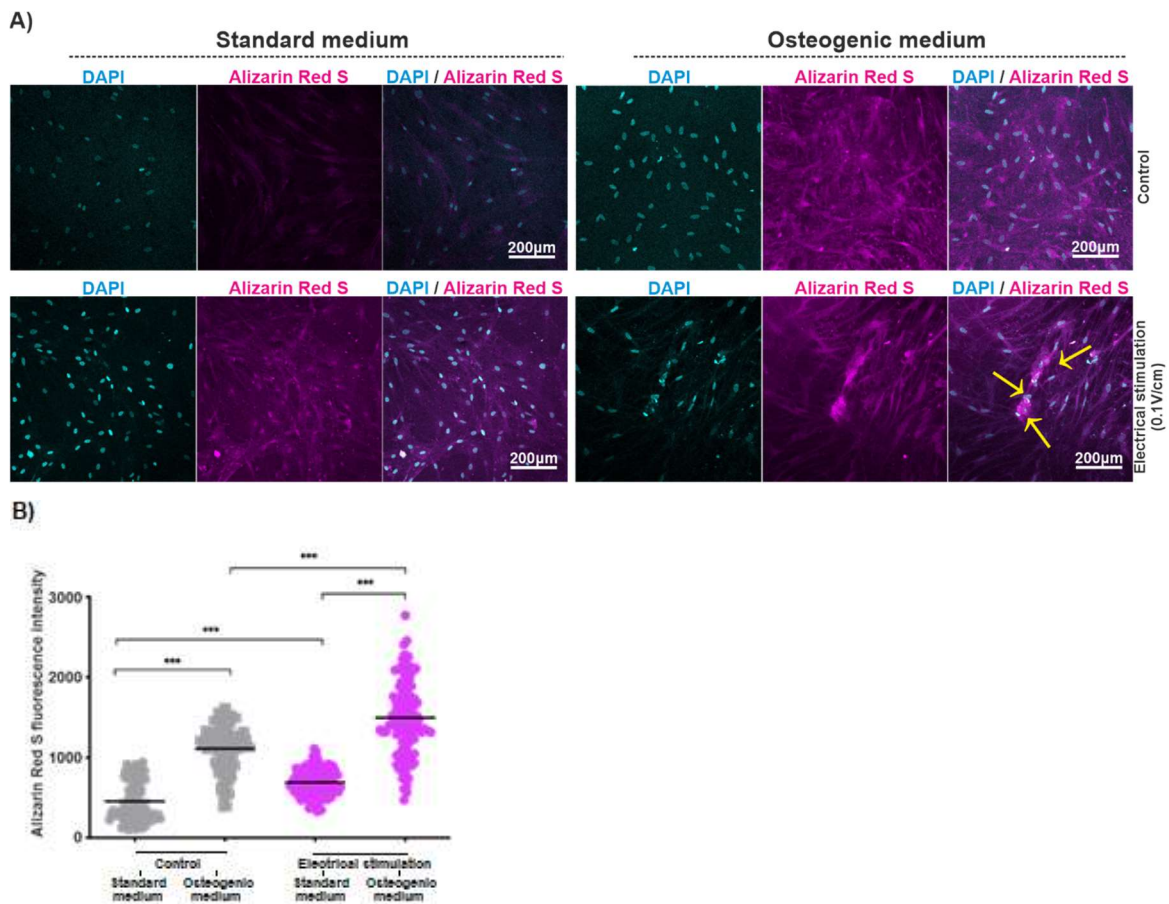
Figure 5.4. ES increased osteogenic differentiation potential of ASCs under 2D cell culture conditions. (A) ASCs were exposed to ES (0.1V/cm) in standard and osteogenic medias for up to 21 days followed by assessment of the Alizarin Red S fluorescence intensity. Confocal laser-scanning microscopy clearly revealed the

presence of nuclei in close proximity to the Alizarin Red S signal. ASCs exposed to ES showed an intense calcium deposition in the osteogenic media, as indicated by the arrows. Scale bar: 200µm. (B) Alizarin Red S fluorescence intensity was measured using confocal laser-scanning microscopy. Data were compared using a one-way ANOVA with Bonferroni correction (CI 95%). Error bars: SEM, [***]$P<0.0001$.

Calcein/ethidium homodimer-1 staining was used for live/dead assay. Cells were cultivated in 2D in standard and osteogenic differentiation medias with or without ES (0.1V/cm) for 21 days, followed by a calcein/ethidium homodimer-1 staining (Figure 5.5A). Assessment of live/dead assays at day 21 revealed no differences in viability between ASCs in the standard media and osteogenic medias without ES (Figure 5.5B). A significantly higher viability was demonstrated in ASCs in the osteogenic differentiation media treated with ES compared with cells in the standard media (Figure 5.5B). ASCs exposed to ES in the osteogenic differentiation media showed significantly higher ALP activity than cells with ES in the standard media and cells in the osteogenic differentiation media without ES whereas ALP activity at day 7 revealed no significantly higher ALP activity in cells under osteogenic conditions (Figure 5.5C). As shown in Supplement 5.3., Appendix III, activity in increases of absorbance was determined using a standard curve of ALP ($y=0.0563x+0.0027$, $R^2=0.9962$). To evaluate the levels of mineralisation, ASCs were cultivated at 21 days and the absorbance of Alizarin Red S was measured by photometry. Quantifying by colorimetric detection showed a higher level of Alizarin Red S absorbance in cells in the differentiation media with ES compared with cells in the standard media (Figure 5.5D). Cells exposed to ES in the osteogenic differentiation media showed the highest level of mineralisation compared with cells in the standard media (Figure 5.5D). In addition, ASCs exposed to ES displayed a significant increase in the osteogenic differentiation media compared with cells in the same media without ES.
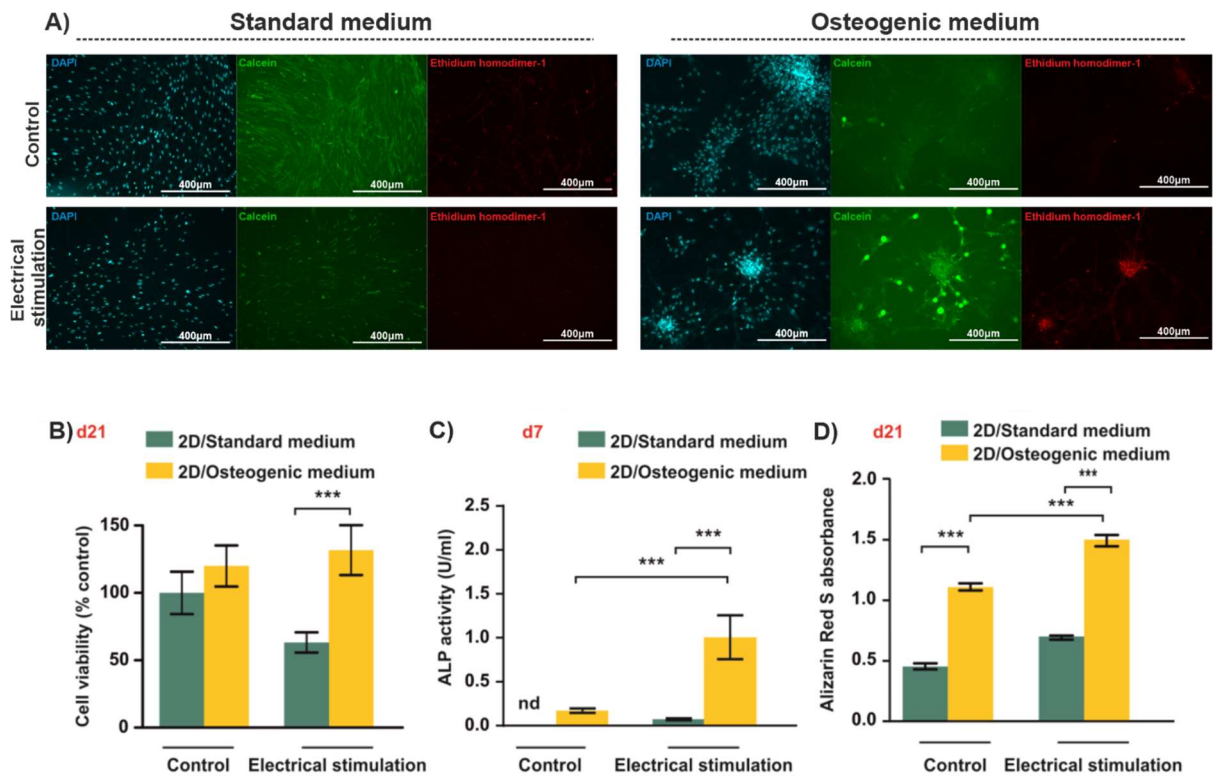
Figure 5.5. ES resulted in an increase of osteogenic differentiation potential in a 2D cell culture. (A) ASCs were exposed to ES in standard and osteogenic medias for up to 21 days followed by assessment of cell viability using live/dead assay. (B) Calcein/ethidium homodimer-1 based live/dead assay. Cells were cultivated in 2D in standard or osteogenic differentiation medias with or without ES for 21 days followed by a live/dead assay. Data analysis revealed no differences in relative viability in cells subjected to osteogenic differentiation and ES compared with cells in the standard media with ES. (C) After 7 days, cells were assayed for activity of ALP. A significant increase in ALP activity was observed in cells in the osteogenic media exposed to ES compared with non-stimulated cells under osteogenic conditions. (D) Colorimetric determination of calcium was assessed using Alizarin Red S dye recovery assay. Alizarin Red S absorbance of cells differentiated exposed to ES was measured at a wavelength of 405 nm using Spectra Max 340PC plate reader compared with cells by cultivation at 21 days with ES. ES resulted in significantly increased levels of mineralisation in the osteogenic media with ES compared with cells cultivated under osteogenic conditions without ES. Values are shown as means ± standard errors of three independent experiments using GraphPad Prism software (GraphPad, La Jolla, CA, USA). Data were compared using a one-way ANOVA with Bonferroni correction (CI 95%). At least three independent experiments were performed. Error bars: SEM, [***]$P<0.0001$.

Figure 5.6A-D shows that immunocytochemical analysis of the expression levels of OCN at days 7, 14 and 21 showed significantly higher expression levels in ASCs subjected to osteogenic differentiation with and without ES. At days 14 and 21, ES showed a high level of OCN expression in ASCs in the osteogenic media compared with cells subjected to an osteogenic media without ES (Figure 5.6C-D). The assessment of OPN expression showed increased levels of OPN in ASCs in the osteogenic differentiation media at days 7 and 14 (Figure 5.7A-C). In contrast, OPN expression showed no significant differences under ES treatment even though a higher expression was found in cells subjected to the osteogenic differentiation media at 21 days (Figure 5.7D). Immunocytochemical staining for OCN and OPN at day 14 and 7 was also shown in the supplement figure 5.8 and 5.9.
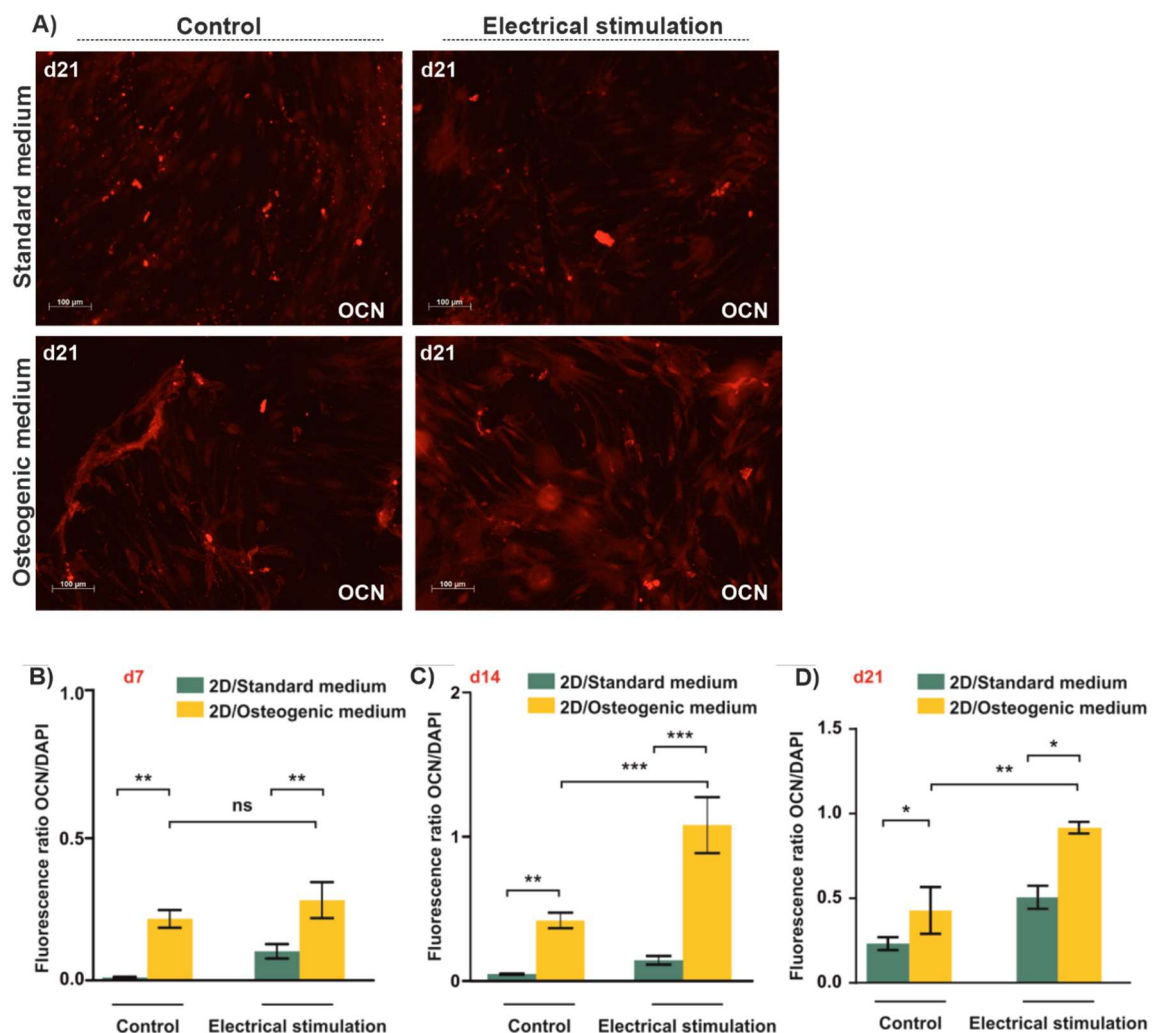
Figure 5.6. ES increased expression of OCN in the 2D cell culture on days 7, 14 and 21. (A) ASCs were exposed to ES in the osteogenic media for up to 21 days followed by immunocytochemical staining (OCN) and fluorescence microscopy.

Scale bar: 100μm. (B-D) Immunocytochemical analysis of OCN at days 7, 14 and 21. At days 14 and 21 significantly higher expression levels of OCN were observed in cells in the osteogenic differentiation media exposed to ES compared with osteogenically differentiated cells without ES. The fluorescence ratio was analysed using ImageJ software. Data were compared using a one-way ANOVA with Bonferroni correction (CI 95%). At least three independent experiments were performed. Error bars: SEM. $^{*}P<0.05$, $^{**}P<0.01$ $^{***}P<0.0001$. ns: not significant. nd: not detected.
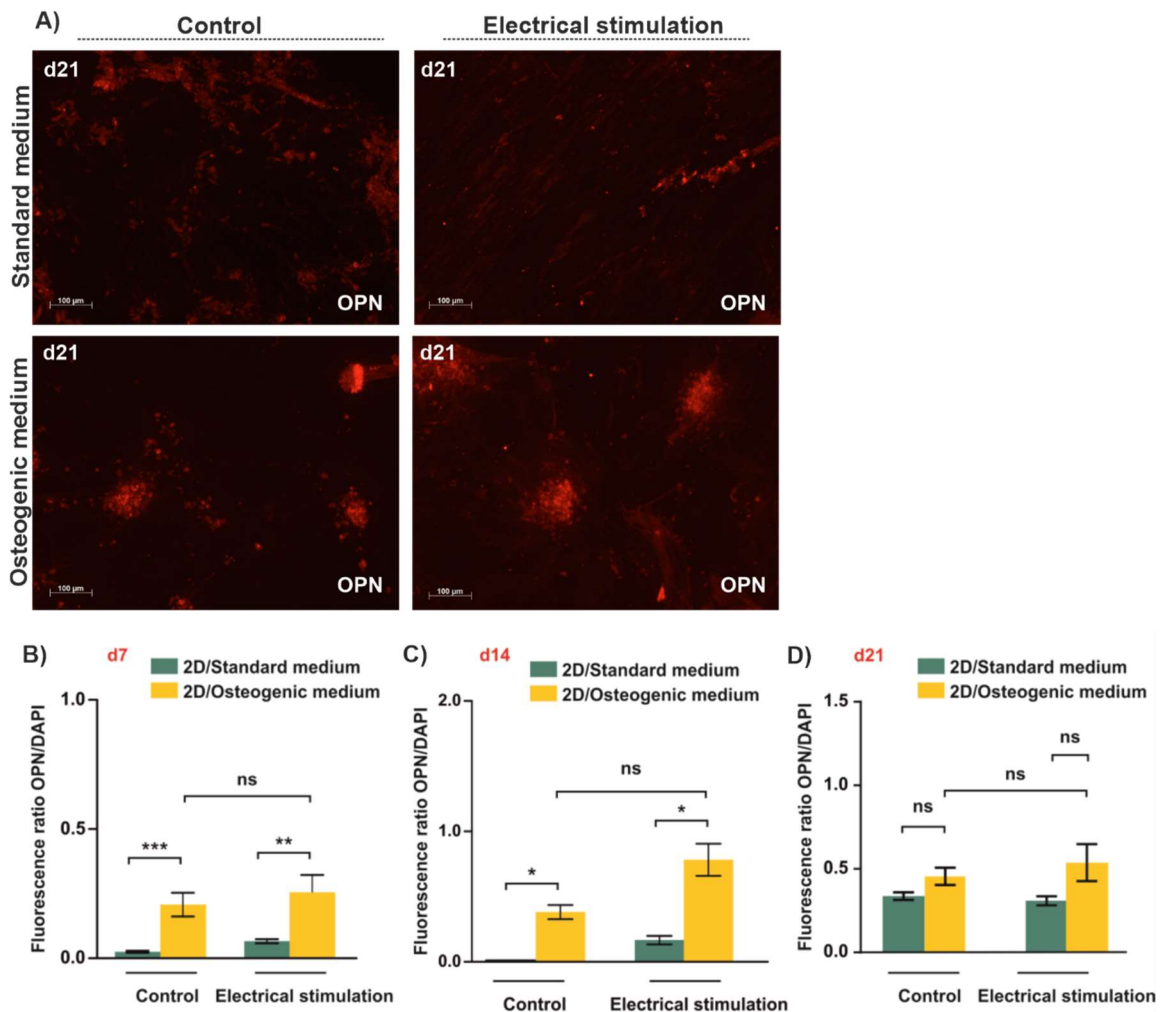
Figure 5.7. ES increased the levels of OPN in the 2D cell culture on days 7, 14 and 21. (A) ASCs were exposed to ES in the osteogenic media for up to 21 days followed by immunocytochemical staining (OPN) and fluorescence microscopy. Scale bar: 100μm. (B-D) Quantification of immunocytochemical analysis of OPN expression at days 7, 14 and 21. The expression level of OPN showed a significant increase in cells exposed to ES under osteogenic conditions at days 7 and 14 compared with the differentiated cells without ES. No significant differences were observed in OPN

expression at day 21 under ES conditions compared with the differentiated cells without ES. There were also no significant differences between cells in the osteogenic differentiation media with and without ES at all time points. The fluorescence ratio was analysed using ImageJ software. Data were compared using a one-way ANOVA with Bonferroni correction (CI 95%). At least three independent experiments were performed. Error bars: SEM. *P<0.05, **P<0.01 ***P<0.0001. ns: not significant. nd: not detected.

5.3.2. ES decreased the adipogenic differentiation of ASCs under 2D cell culture conditions

ES has been said to reduce the levels of adipogenic differentiation of human ASCs (Hernandez-Bule et al., 2016). To confirm their results in this chapter, ASCs were exposed to adipogenic differentiation with and without ES for 21 days. Assessment of adipogenic differentiation at day 21 revealed the absorbance of lipid droplets stained with Oil Red O and microscopy-based analysis of lipid droplet size. When ASCs were subjected to ES in an adipogenic differentiation media, a slight and non-significant decrease of Oil Red O absorbance was detected compared with cells in the adipogenic differentiation media without ES (Figure 5.8A). As Figure 5.8B shows, lipid droplets stained with Oil Red O were analysed using colour thresholding for lipid droplet signal only. The computational conversion yielded a consistent representation of the original image with a good separation of the clustered lipid droplets.

The quantitative analysis of ASCs stained with Oil Red O was performed at 540 nm (Figure 5.8C). Comparison of optical density of the ASCs subjected to chemical and electrical stimulation showed that ES resulted in a decrease of Oil Red O absorbance, as shown in Figure 5.8C. Changes in the relative frequency distribution of lipid droplets were also analysed and the results from ten different areas per condition were assessed in each experiment by the scatter line. ES resulted in a decrease in the size of lipid droplets (Figure 5.8D). As shown in Supplement 5.2., Appendix III, Oil Red stain recovery values was determined using a standard curve (y=0.0496x-0.0536, R^2=0.9672).
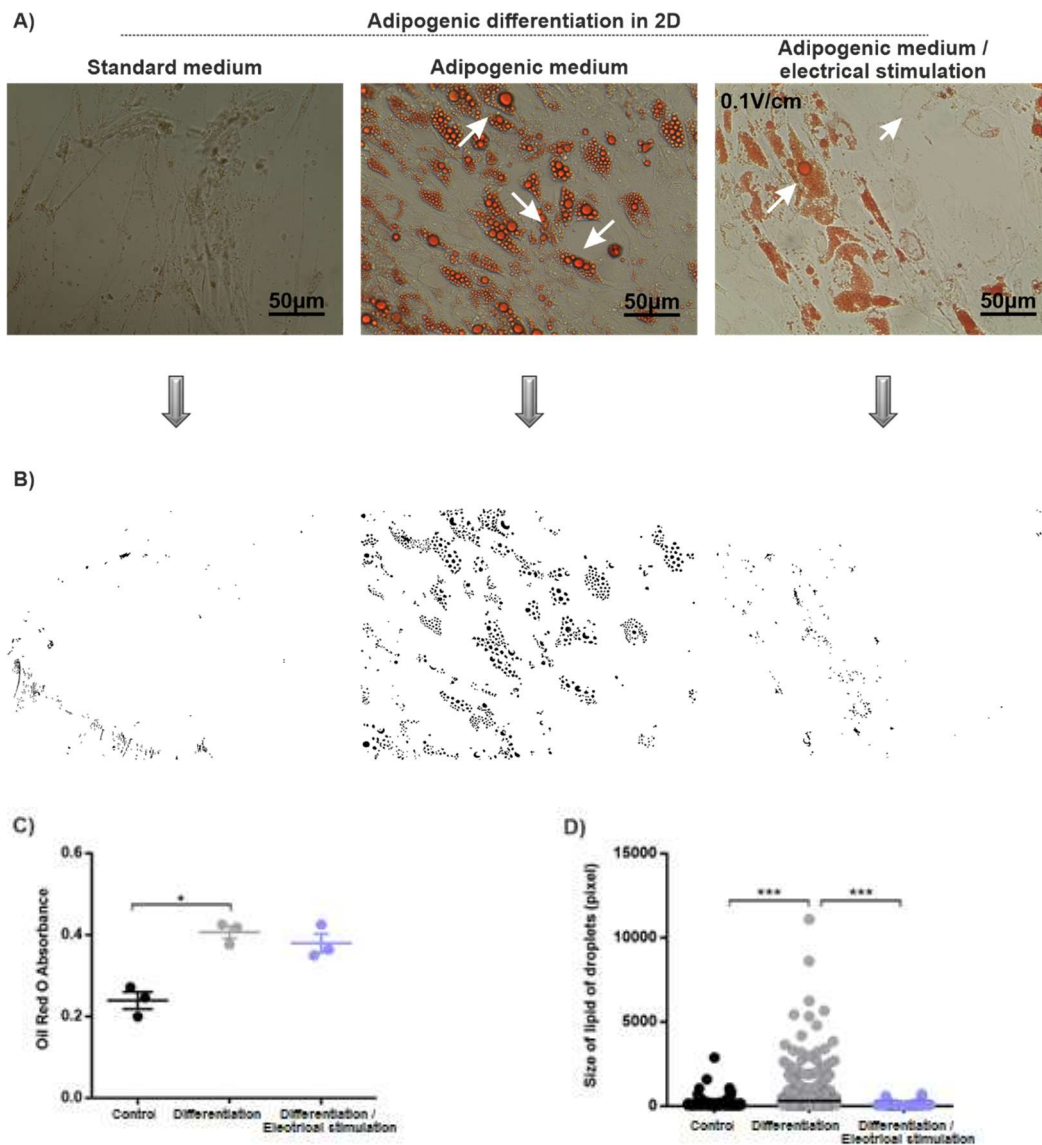
Figure 5.8. ES interfered with the adipogenic differentiation of ASCs. (A) ASCs were cultivated in an adipogenic or standard media for 21 days followed by staining of lipid droplets by Oil Red O, microscopy and image analysis. Microscopy revealed multiple large lipid droplets in ASCs in the adipogenic differentiation media without ES and only a few in cells exposed to 0.1V/cm of ES. Scale bar: 50µm. (B) Lipid droplets stained with Oil Red O were analysed using colour thresholding for lipid droplet signal only. The computational conversion yielded a consistent representation of the original image with a good separation of the clustered lipid droplets. (C-D) Image analysis revealed a slight but not significant decrease of Oil Red O absorbance and a highly significant decrease in the average size of the lipid droplets in cells cultivated under adipogenic conditions exposed to ES compared with cells in the adipogenic media without ES. Data were compared using a one-way ANOVA with Bonferroni correction (CI 95%). At least three independent experiments were

performed. Error bars: SEM. $^{*}P<0.05$, $^{***}P<0.0001$. ns: not significant. Diff: differentiation.

5.3.3. ES appeared no significant differences in cell viability of ASCs in 3D aNFC

Previous studies have reported that cells seeded in various biomaterials were more viable (measured by electrophysiology) and indicated an increased level of differentiation in earlier mature cells in cell culture compared with their 2D monolayer culture (measured using immunocytochemistry staining) (Frega et al., 2014, Yuan et al., 2015). ASCs in 3D aNFC hydrogels were evaluated to detect whether long-term cultivation of ASCs affects their viability. Under ES conditions, cellular viability was assessed in 3D aNFC hydrogels exposed to an osteogenic differentiation media and a standard media when cultivated for 7, 14 and 21 days (normalised to 3D control). Figure 5.9A-C shows that analysis of the XTT data revealed that ES showed no differences in cell viability at days 7 and 14 under osteogenic conditions with ES, but a slightly significant decrease in cell viability in the osteogenic differentiation media with ES at day 21 (Figures 5.9A-C). Electrical and chemical stress did not have a strong negative effect on viable cells normalised to 3D control cells, as shown in Figure 5.9A-C.
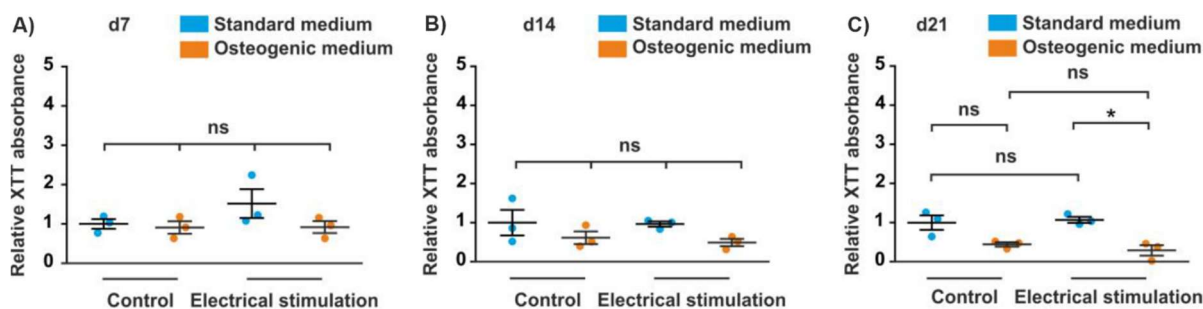
Figure 5.9. Long-term cultivation of ASCs in 3D aNFC showed a decrease in cell viability under standard and osteogenic differentiation conditions. (A-C) Assessment of cell viability in a 3D cell culture was measured by XTT viability assay at an excitation wavelength of 490 nm and a reference wavelength of 650 nm. ASCs embedded into 0.2% aNFC hydrogels were exposed to ES in standard and osteogenic medias for up to 21 days followed by assessment of cell viability using XTT assays. No significant differences in viability were detected at days 7 or 14, whereas a slight but significant decrease was observed in cells exposed to ES in the

osteogenic media at day 21 compared with cells in the standard media with ES. Error bars: SEM. $^*P<0.05$. ns: not significant, a one-way ANOVA with Bonferroni correction (CI 95%). Values are shown as means $\pm$ standard errors of three independent experiments using GraphPad Prism software (GraphPad, La Jolla, CA, USA).

To assess the proxy viability data obtained in the XTT assay, calcein/ethidium hoodimer-1 based on a live/dead assay was also performed (Figure 5.10A-B). Confocal laser-scanning microscopy and image analysis demonstrated higher relative cell viability in ASCs in 3D in the osteogenic differentiation media compared with cells in the standard media. Similarly, higher cell viability was determined in ASCs in 3D in the osteogenic media exposed to ES compared with cells in 3D in the standard media without ES (Figure 5.10C). Also, ES resulted in a significant decrease in cell viability in the standard media compared with cell viability in the standard media without ES. Similarly, ES showed a lower viability in differentiated cells subjected to ES compared with cells in the osteogenic media without ES (Figure 5.10C).
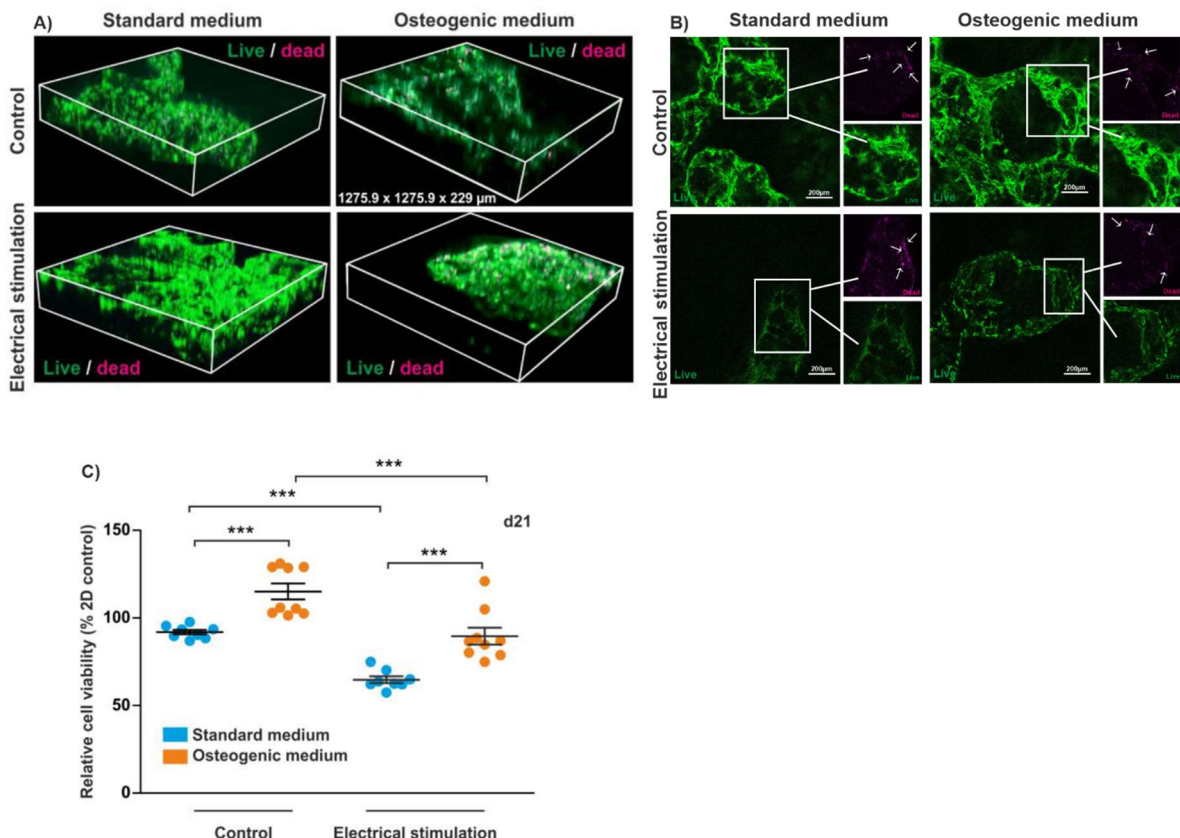
Figure 5.10. ES only moderately decreased the viability of ASCs in 3D aNFC under standard and osteogenic differentiation conditions. Calcein/ethidium homodimer-1 based-live/dead assay. (A-B) Cells were cultivated in standard or

osteogenic differentiation medias with or without ES for 21 days followed by a live/dead assay and confocal laser-scanning microscopy with subsequent 3D reconstruction. (C) Data analysis revealed higher relative viability in 3D cells in the osteogenic differentiation media compared with control cells in aNFC, and a higher relative viability in cells subjected to osteogenic differentiation, compared with cells in 3D with ES. The quotient mean fluorescence of live/dead cells was determined using GraphPad Prism software (GraphPad, La Jolla, CA, USA). Data were compared using a one-way ANOVA with Bonferroni correction (CI 95%). At least three independent experiments were performed. Error bars: SEM. $^*P<0.05$, $^{***}P<0.0001$. ns: not significant.

5.3.4. ASCs exposed to ES in 3D showed increased ALP activity and higher levels of calcium deposition during osteogenic differentiation

To further determine the effects of an electric field on 3D cell culture in the early osteogenic differentiation, ALP activity was evaluated at day 7 using ALP spectrophotometry. As shown in Figure 5.11A., ALP activity was upregulated with and without ES compared with cells in a standard media. As a marker of late osteogenesis, levels of mineralisation were determined using Alizarin Red S and confocal laser-scanning microscopy (Figure 5.11B-C). Alizarin Red S stained intensely calcium deposits in cells in the osteogenic differentiation media at day 21 when stimulated with 0.1V/cm. ES resulted in distinguishable changes in calcium-rich deposit of ASCs at day 21 compared with cells without chemical and electrical stimulation. Imaged-based analysis of Alizarin Red S autofluorescence showed a higher level of calcium deposition in cells in the osteogenic differentiation media under ES treatment compared with cells in the standard media with and without ES (Figure 5.11B-C). Significantly, ASCs subjected to the osteogenic differentiation media under ES conditions displayed a significantly higher fluorescence intensity of Alizarin Red S than cells in the osteogenic media without ES (Figure 5.11B).
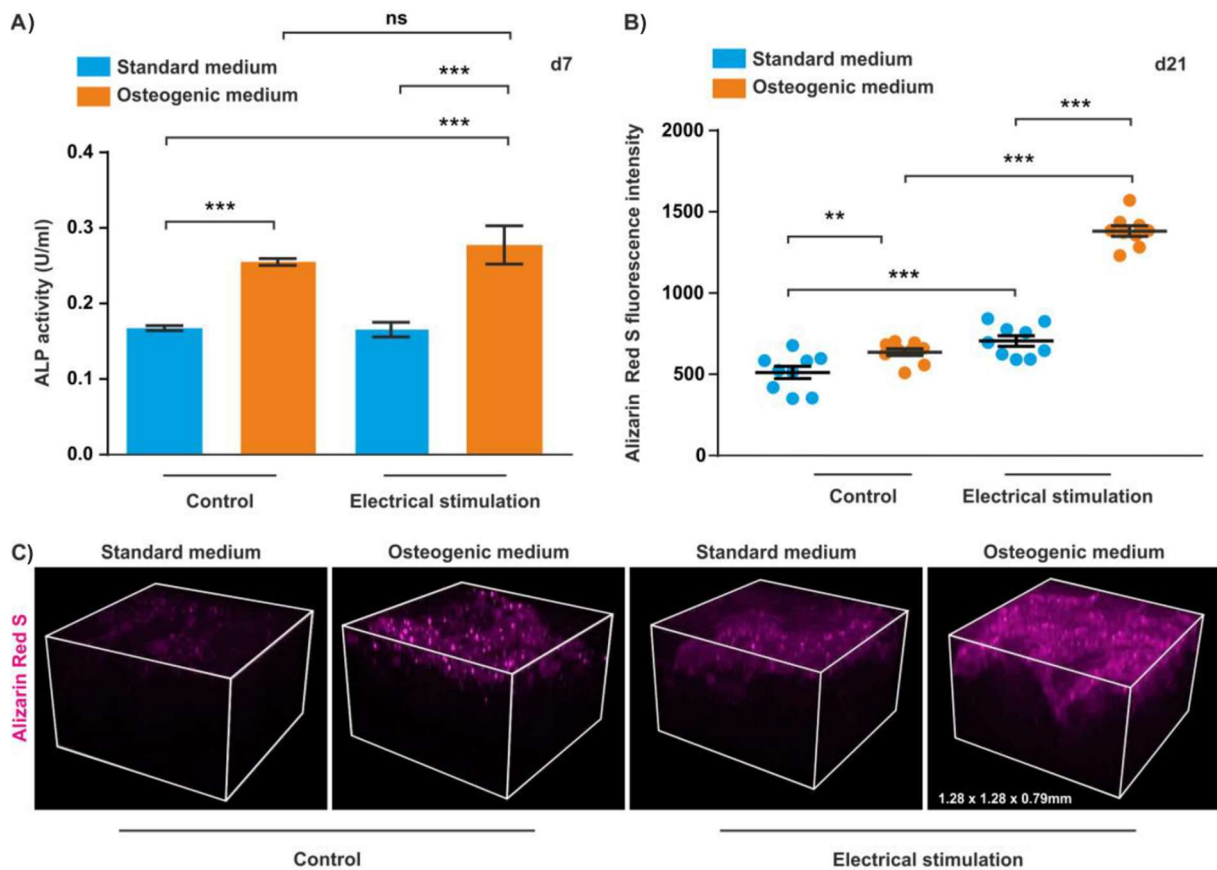
Figure 5.11. ES increased ALP activity and the level of mineralisation during osteogenic differentiation. (A) ALP activity in 3D. ASCs were exposed to ES in osteogenic and standard medias for 7 days followed by an assessment of ALP activity. Significantly higher ALP activities were observed in cells in the osteogenic differentiation media than in the standard media with and without ES. A significant difference was only seen between standard media and osteogenic media. Moreover, there are no additional effects on ALP activity in the osteogenic differentiation under ES conditions. (B-C) Calcium deposition in 3D. ASCs were cultivated in standard or osteogenic cultivation medias with and without ES. After 21 days, cells were subjected to Alizarin Red S staining and confocal laser-scanning microscopy. Osteogenic differentiation conditions led to an increase of mineralisation compared with cells in the control media both with and without ES. ES resulted in significantly higher levels of mineralisation in cells cultivated in the osteogenic media. The fluorescence intensity for Alizarin Red S was quantified using ImageJ software. Data in four different conditions were compared using a one-way ANOVA with Bonferroni correction (CI 95%). At least three independent experiments were performed. Error bars: SEM. $^{**}P<0.01$, $^{***}P<0.0001$. ns: not significant.

5.3.5. ES under osteogenic differentiation conditions in 3D increased the expression levels of OCN and OPN in ASCs

In order to determine the effects of ES on the expression of the late osteogenic markers OCN and OPN, ASCs in 3D aNFC hydrogels were cultivated for 21 days followed by immunocytochemical staining, confocal laser-scanning microscopy and image analysis. Confocal laser-scanning microscopy was used to visualise ASCs embedded in 0.2% aNFC with and without ES in response to late osteogenic markers (OCN and OPN) while quantifying by the fluorescence intensity of osteogenic markers (Figures 5.12A and 5.13A, respectively).

As shown in Figure 5.12(B-C-D) and Figure 5.13(B-C-D), the fluorescence ratio OCN/DAPI and the fluorescence ratio OPN/DAPI were measured by ImageJ software. The results obtained in 2D were familiar to the expression of OCN in ASCs embedded into 3D aNFC. ES resulted in a significant increase of OCN expression in cells in 3D subjected to ES in the osteogenic media compared with cells in the standard and osteogenic medias without ES at days 14 and 21 (Figure 5.12C-D). The expression level of OCN showed higher potential in ASCs subjected to ES compared with cells without ES under the osteogenic differentiation media in 3D aNFC at day 7. Moreover, ASCs in the osteogenic differentiation media at day 21 showed significantly higher levels of OCN under ES treatment compared with cells subjected to an osteogenic media without ES (Figure 5.12D).

In contrast to OCN, another late osteogenic marker, OPN, was evaluated in terms of its fluorescence intensity when ASCs were cultivated in 3D aNFC in the osteogenic differentiation media with ES compared with cells in the standard media with and without ES (Figure 5.13). ASCs exposed to ES exhibited higher levels of OPN expression in the osteogenic media at days 7 and 14 compared with cells subjected to the osteogenic media without ES (Figure 5.13B-C). Contrary to the results at days 7 and 14, ES showed no significant differences in the fluorescence intensity of OPN in cells in the osteogenic media compared with cells in the standard media with and without ES at day 21 (Figure 5.13D).
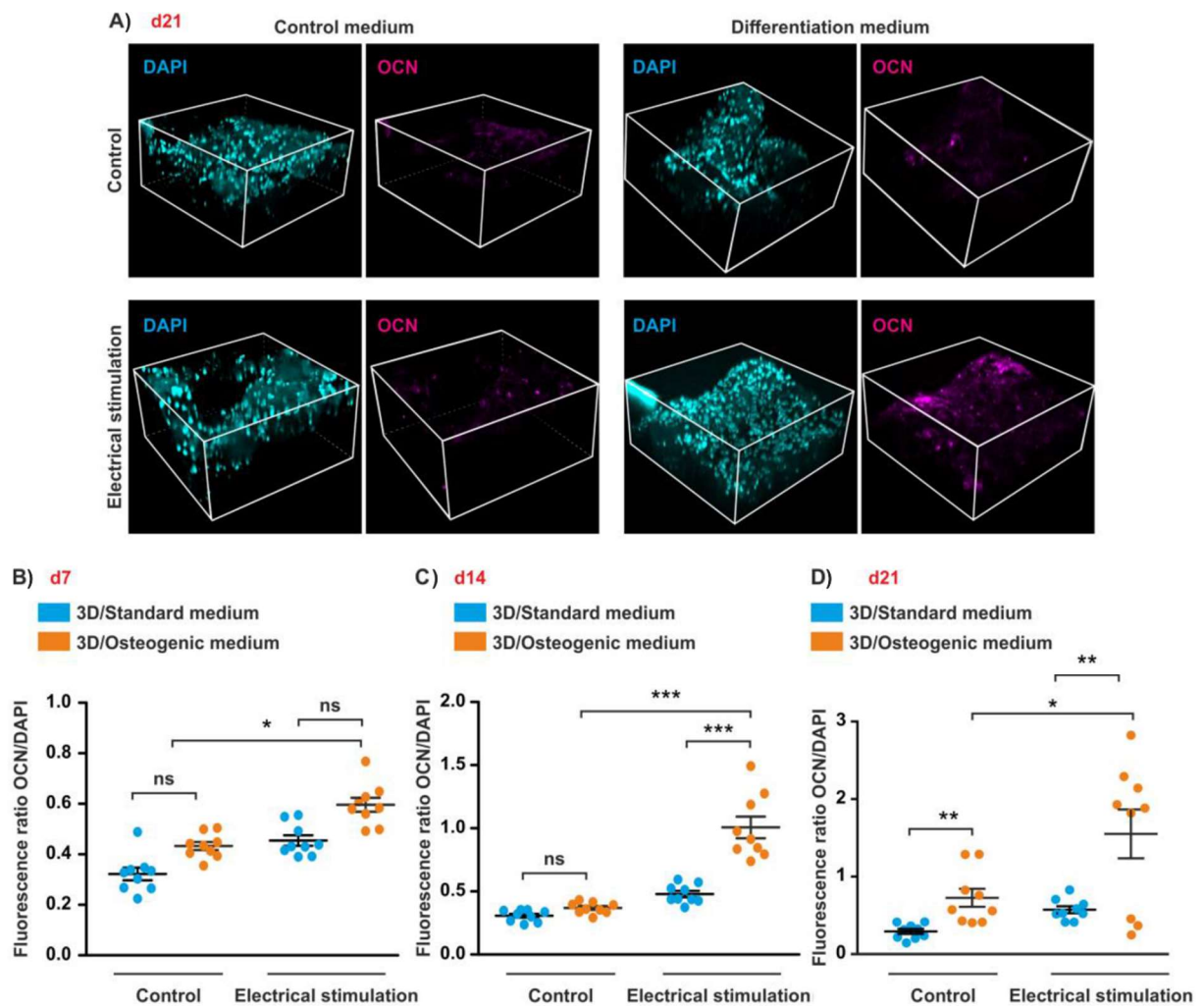
Figure 5.12. ES increased the expression of OCN in 3D at days 7, 14 and 21. (A) ES increased the expression of OCN in 3D. ASCs in osteogenic or standard medias were electrically stimulated for up to 21 days followed by immunocytochemical staining for OCN. Images were taken using confocal laser-scanning microscopy with subsequent 3D reconstruction. (B-D) ES significantly increased the expression of OCN in cells in the osteogenic media subjected to ES compared with cells in the standard and osteogenic medias not exposed to ES at days 7, 14 and 21. Data were compared using a one-way ANOVA with Bonferroni correction (CI 95%). At least three independent experiments were performed. Error bars: SEM. $^*P<0.05$, $^{**}P<0.01$, $^{***}P<0.0001$. ns: not significant.
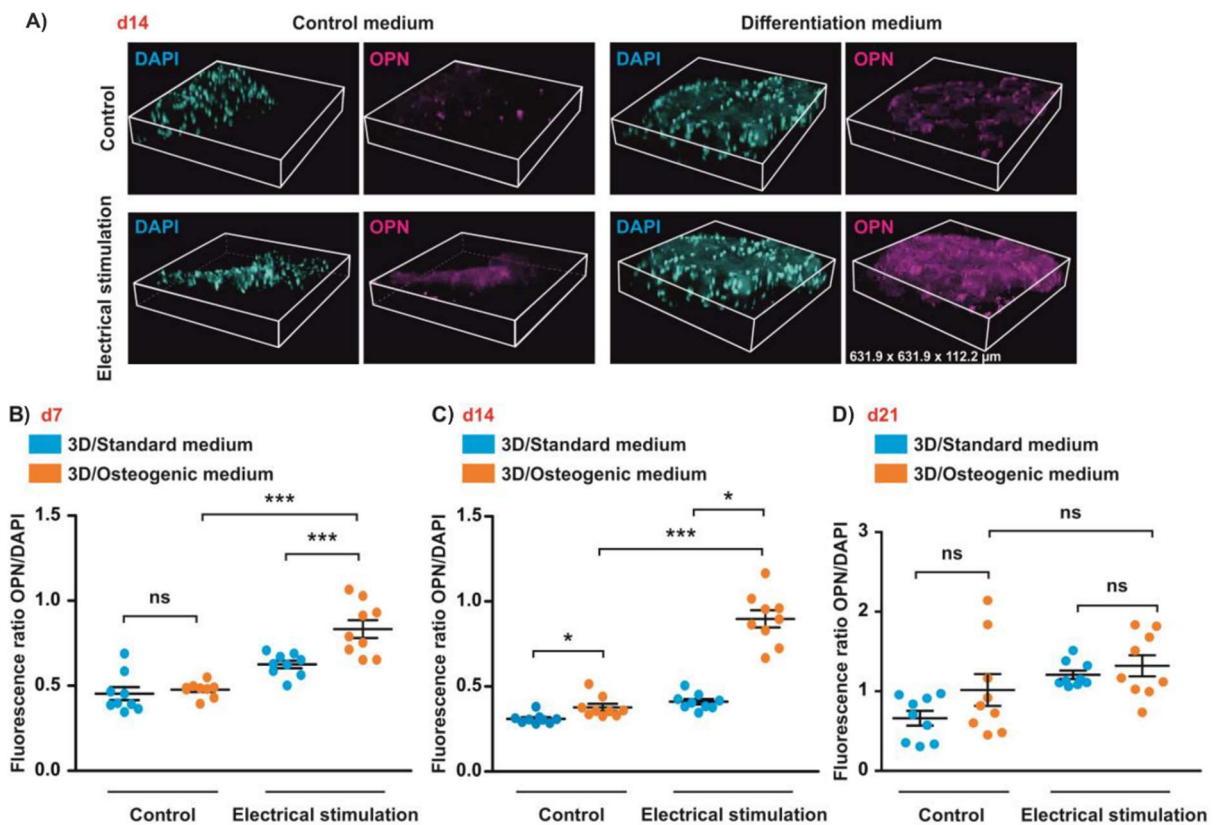
Figure 5.13. ES increased the expression of OPN in 3D at days 7 and 14 but did not affect it at day 21. (A) ASCs were cultivated in standard or osteogenic medias with and without ES for up to 14 days followed by immunocytochemical staining of OPN and confocal laser-scanning microscopy. (B-D) ES resulted in increased expression of OPN in cells under osteogenic conditions at days 7 and 14. At day 14, a higher expression level of OPN was observed in cells in the osteogenic media under ES exposure compared with cells under osteogenic conditions without ES. No significant differences in OPN expression were found at day 21 under ES conditions. Data were compared using a one-way ANOVA with Bonferroni correction (CI 95%). At least three independent experiments were performed. Error bars: SEM. $^*P<0.05$, $^{**}P<0.01$, $^{***}P<0.0001$. ns: not significant.

5.3.6. ASCs exposed to ES displayed a highly arranged actin cytoskeleton and formation of cell-free pores within the 3D aNFC hydrogel

When cells were cultivated into 3D aNFC, ASCs achieved homogenous growth under an electrical field. ASCs subjected to standard and osteogenic medias with and without ES were fixed and stained with phalloidin at day 21 in order to visualise the actin cytoskeleton. Confocal microscopy was performed to visualise actin filament in ASCs in 3D aNFC exposed to ES (Figure 5.14A). Image analysis showed a highly

arranged actin cytoskeleton in ASCs exposed to osteogenic differentiation with and without ES (Figure 5.14A-B). Notably, a denser actin cytoskeleton was exhibited in ASCs exposed to ES in standard and osteogenic differentiation medias (Figure 5.14A). The spread of the actin filament in cells exposed to ES was larger than in cells without ES. The arrangement of dense actin bundles is likely to imply increased osteogenic differentiation (Treiser et al., 2010).
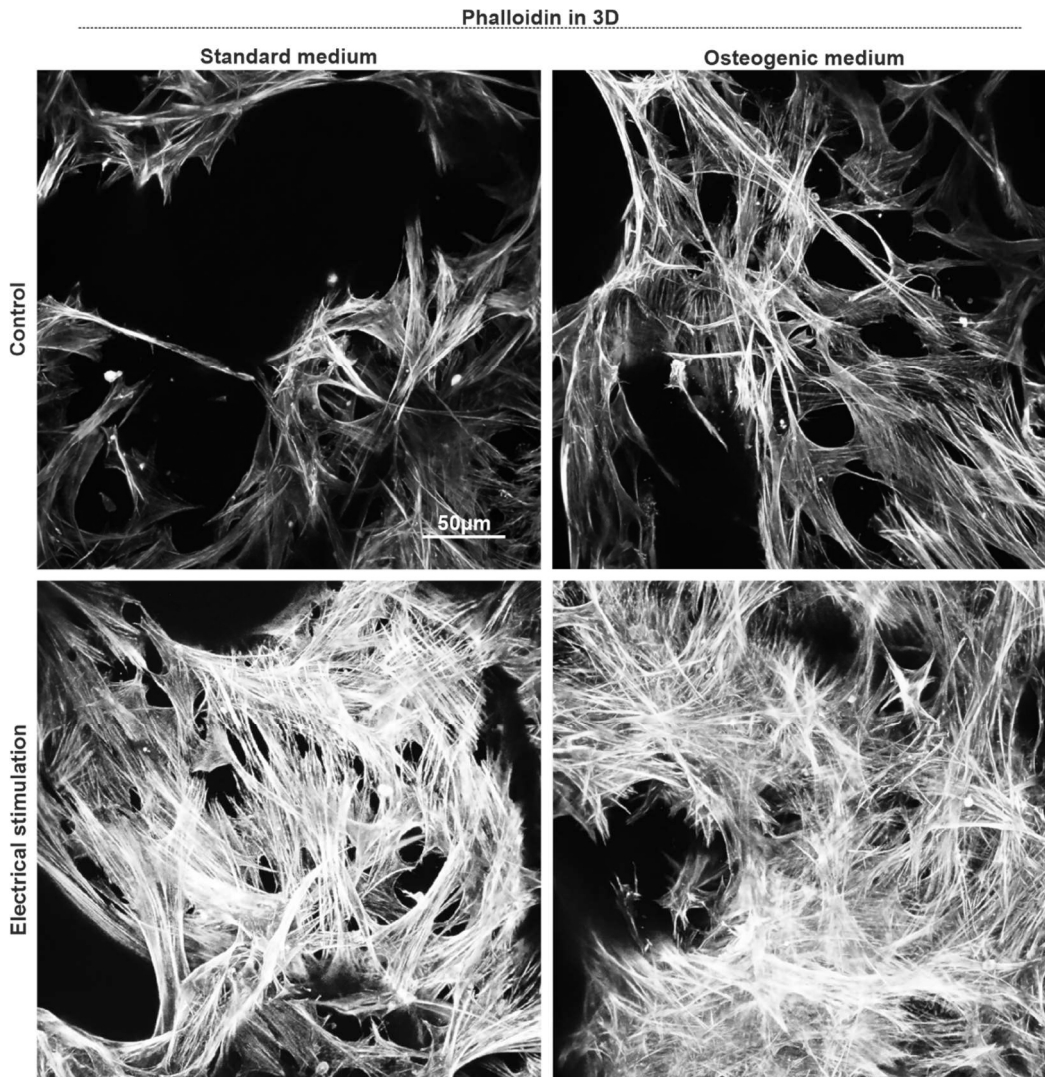
Figure 5.14. ES of ASCs induced profound re-arrangements of the actin cytoskeleton. (A) ASCs in aNFC were differentiated in an osteogenic differentiation media for 21 days with and without ES (0.1V/cm) followed by staining of the actin cytoskeleton using phalloidin with subsequent confocal microscopy. Image analysis revealed a highly aligned and dense network of F-actin fibres in cells in the osteogenic differentiation media and in cells exposed to ES independent of the culture condition. The images show maximum intensity projections of confocal z-stacks. Scale bar: 50μm. At least three independent experiments were performed.

5.4. Discussion

Nanoscale mechanical stimulation of MSCs has recently been performed to promote osteogenic differentiation in 2D and 3D cultures by two different methods, passive and active. Passive methods lead to substrate topography and stiffness (Kingham et al., 2013) whilst active methods comprise various forces from external sources such as vibration, centrifugation and shear flow (Zhao et al., 2014). Zhang et al. (2012a) found that vibration at 50 Hz with a peak acceleration of 3 g showed an increased level of osteogenic differentiation (Zhang et al., 2012a). In another study controlled with mechano-transductive stimuli, vibration of ASCs promoted with 50 and 100 Hz, with a peak acceleration of 3 g, resulted in increased ALP activity and calcium deposition (Tirkkonen et al., 2011). Campsie et al (2019) designed a novel bioreactor system using finite element analysis to measure the modal and harmonic motions, and increased osteogenic differentiation of MSCs embedded in 3D collagen gel was confirmed by using vibrational stimulation (Campsie et al., 2019).

ES treatment was optimized to promote cell viability and osteogenic differentiation in a 2D cell culture and found no strong negative effects on cell viability and an increase in the osteogenic potential of ASCs exposed to an electric field of 0.1 V/cm, at a frequency of 10Hz and 0.4ms pulse width alternating current. These results are consistent with those of Eischen-Loges et al. (2018) who found the optimal ES regimen to promote the osteogenic differentiation of BM-MSCs for 7 and 14 days. The cells treated with ES (0.1V/cm for 1 h per day) showed an increase in the RunX2 expression and calcium/calmodulin activity at 7 days (Eischen-Loges et al., 2018). Furthermore, exposure to ES resulted in an enhanced differentiation potential and an increase in the pro-osteogenic activity with RunX2 expression and ALP activity (Eischen-Loges et al., 2018). Another *in vitro* study showed a strong positive effect of ES on the osteogenic differentiation (Leppik et al., 2018).

The findings presented in this chapter have shown that imaged-based analysis of ASCs stained with Oil Red O revealed a slight but not significant decrease in Oil Red O absorbance and a highly significant decrease in the average size of the lipid droplets in cells cultivated under adipogenic conditions exposed to ES compared with cells in an adipogenic media without ES. ES with the 100 kHz-3 GHz frequency spectrum has been stated to be an effective treatment for reducing cytoplasmic lipid

content since such therapies promote tissue heating through molecular friction (Valentim da Silva et al., 2013). Among such therapies involving electromagnetic fields, capacitive-resistive electric transfer (CRET) has been used to treat tissues which are exposed to two different simultaneous stimuli: thermal electrically-induced and mechanical (Valentim da Silva et al., 2013). Hernandez-Bule et al. (2016) investigated the impact of CRET current at 448 kHz with *in vitro* exposure to short pulses, conducted at a subthermal density of 50 µA/ mm^2 on the adipogenic differentiation of human ASCs. Their results showed that decreased lipid synthesis was observed with the reduced expression of PPARγ and the activated MEK1/2 (mitogen-activated protein kinase kinases 1 and 2) by applying an electric stimulus (Hernandez-Bule et al., 2016). The data presented in this chapter have shown that a significant increase in ALP activity was observed in ASCs in 2D in an osteogenic media exposed to ES compared with cells without ES under osteogenic conditions. Furthermore, ES resulted in an increased fluorescence intensity of Alizarin Red S in ASCs in the osteogenic media with ES compared with cells cultivated under osteogenic conditions without ES. Most previous studies have shown that stem cells exposed to daily ES showed an increase in the osteogenic expression of bone-specific proteins such as OPN and ALP (Balint et al., 2013, Mobini et al., 2016). According to the findings of the current study, ES resulted in a high level of OCN expression in ASCs in osteogenic differentiation compared with cells subjected to an osteogenic media without ES at days 14 and 21. Similarly, the assessment of OPN expression demonstrated increased levels of OPN in ASCs in an osteogenic differentiation media at days 7 and 14.

Exogenous electrical fields with low voltage (10-150 mV/mm) are likely to induce bone cell migration, proliferation and differentiation (Mobini et al., 2017a). 3D cell culture seems to increase cell viability and osteogenic differentiation compared with conventional 2D culture in response to directly applied ES. There have been many reports suggesting that 3D cultivation with ES might have an impact on MSC viability and differentiation potential as a consequence of the optimized electrical current. In this current study, a high level of Alizarin Red S signal was observed after differentiation of ASCs in 2D and in 3D when exposed to ES. ASCs exposed to ES in 3D showed increased ALP activity and higher levels of calcium deposition during osteogenic differentiation. A more stringent test was applied by the additional determination of specific signals on the differentiated cells as the detection of Alizarin

Red S might lead to the risk of over-estimation because of false-positive signals caused by cell debris. Immunocytochemical staining of OCN and OPN have shown that ES resulted in higher levels of OCN and OPN in ASCs embedded into 3D aNFC when cultivated in an osteogenic media, whereas no expression in cells was observed in a standard media. These findings are consistent with those of Leppik et al. (2018) who reported that autologous bone marrow-derived mononuclear cells (BMC) embedded into β-tricalcium phosphate (β-TCP) showed an increase in osteogenic differentiation for eight weeks in ten rats. Their results showed that ES induced osteogenic differentiation *in vitro* and promoted greater amounts of bone cells and vessel formation *in vivo.* When the cells were combined with β-TCP scaffolds, ES promoted the osteogenic differentiation of MSCs (Leppik et al., 2018). Furthermore, Balikov et al. (2016) determined the impact of electric current on the differentiation of human MSCs without exogenous biochemicals. Using graphene with different patterned formats (for example, non-coated, pure monolayer graphene, and patterned formats with columnar and grid-like structures), they found higher expression of the early osteogenic marker RunX2 in all scaffolds tested under electric current with 0.3 V at 1 Hz, as well as the higher expression of OPN on grid and column graphene (Balikov et al., 2016).

By examining the impact of ES on cell viability and proliferation, some studies have reported an increase in viability and proliferation compared with the respective 3D controls whereas others have observed the opposite effects (reviewed in (Edmondson et al., 2014)). This can be at least partly attributed to the effect of electrical field on 3D cell culture method. In this study, cell viability of ASCs embedded within 0.2% aNFC hydrogels was measured under ES and in an osteogenic differentiation media at 7, 14 and 21 days. ES showed a slight decrease in the viability of ASCs cultured in 3D aNFC hydrogels for 7, 14 and 21 days. Analysis of the relationship between ES and chemical stimulation with differentiation potential showed that the viability of ASCs cultured in 3D was similar to those in both conditions. These results are in agreement with those of Li et al. (2020) which confirmed that a lower electrical field with 1V/cm did not show a negative effect on cell viability whilst a higher electrical voltage (10 and 20 V/cm) resulted in a higher incidence of dead cells (Li et al., 2020). Jing et al. (2016) reported that pulsed electromagnetic fields promoted an increase in osteogenic differentiation in a rabbit bone defect model after implantation into porous titanium (Jing et al., 2016).

The use of an electrical field has recently attracted attention as an approach to bone regeneration and endothelial tissue healing (McCaig et al., 2009). Titushkin and Cho (2007) found changes in stem cell behaviours with and without ES. Their results showed that the ability of MSCs to control changes in cytoskeleton structure was correlated with the osteogenic differentiation lineage (Titushkin and Cho, 2007, Titushkin and Cho, 2009). Some researchers have demonstrated the impact of an electrical field on the reorganisation of the cytoskeleton (Sun et al., 2006) and cell membrane receptors (Griffin and Bayat, 2011). The data presented in this chapter have shown a highly aligned and dense network of F-actin fibres in ASCs exposed to ES, which could be supported by osteogenic potential. ASCs embedded in 0.2% aNFC were treated with and without osteogenic differentiation supplementation for 21 days when exposed to 10 Hz at 0.1V/cm. The differentiated cells on stiff substrates showed extensive stress fibres under ES conditions, whilst the differentiated cells exposed to no ES had less spread and fewer stress fibres. The ES also induced thicker stress fibres in the undifferentiated cells embedded in 0.2% aNFC on stiff substrates compared with those exposed to no ES. This finding is consistent with previous data showing that the cytoskeleton reorganization in mouse ASCs showed morphological and functional changes in response to ES (Hammerick et al., 2010, Kim et al., 2006). Furthermore, the directly applied ES at 100 mV/mm showed modifications in the actin filament organisation in human MSCs (Mobini et al., 2017b).

Zhang et al. (2018) investigated the effect of ES on human ASCs and umbilical vein endothelial cell (HUVECs) co-cultures seeded in an electrically conductive poly-pyrrole (PPY)/chitosan (CS) scaffold and found that ASCs with and without ES (200 µA for 4 h per day) showed 346% and 139% higher calcium deposition respectively. Furthermore, the impact of ES and co-culture with HUVECs had synergistic effects on the osteogenic differentiation of ASCs. In this context, it is worth considering the impact of an electrical field on the paracrine effects, which is supported by the association between HUVECs and ASCs and which improved the cellular functions (Zhang et al., 2018a). Their findings also showed the potential therapeutic benefits of ASC/HUVEC in an electrically conductive scaffold for treating damaged bone (Zhang et al., 2018a).

5.5. Conclusion

The osteogenic differentiation of ASCs in 3D aNFC hydrogel has been shown to enable the formation of 3D bone-like constructs. It was found that an electrical field up to 0.1V/cm at 10 Hz did not result in a cytotoxic environment for cell viability compared with cells without ES. When stimulated at 10 Hz at 0.1V/cm, ES resulted in the enhanced osteogenic potential of ASCs under an osteogenic differentiation media. ES promoted an increase in the osteogenic potential of ASCs embedded into 3D aNFC including increased expression of osteogenesis-related proteins, high ALP activity and higher levels of mineralisation compared with cells in 3D without ES. The findings of this study suggest that ES could be a beneficial guide for applying to bone tissue engineering in the context of macroscopic bone formation in the future. The results reported and discussed in this chapter could be used for developing new therapies for osteoporosis on the grounds that ES on cells has appeared to have a profound effect on cellular proliferation and osteogenic differentiation. The data obtained from *in vitro* experiments suggest that 3D cell culture in combination with ES increased the osteogenic potential of ASCs. Future research could evaluate whether the ES of ASCs can promote similar effects in *in vivo* models of bone regeneration including the rodent model and in sheep. Such a large animal model can be proposed for a closer approximation to bone degeneration and regeneration in humans. ES could be a beneficial guide for applying to bone engineering in the future because the results presented in this chapter showed a positive effect of ES on cellular proliferation and osteogenic differentiation as well as re-arrangement of actin cytoskeleton. Follow-up *in vivo* data could enable the development of a novel therapy for osteoporosis and osteoporotic fractures in humans.

155

Chapter 6

Impact of 3D cell culture combined with electrical stimulation on the anti-Inflammatory potential of human mesenchymal stem cells and their secretome

155

6.1. Introduction

MSCs are widely believed to contribute to regeneration via paracrine factors, acting as 'bystander cells' and modulating endogenous regeneration. Indeed, there is a general consensus that the therapeutic benefit of MSCs in many conditions is paracrine; Arnold Caplan, who first coined the term `mesenchymal stem cells`, recommended referring to this cell type as `medicinal signalling cells` (Caplan, 2019). The current understanding of these `bystander effects` mediated by the secretome of MSCs is that it involves two main factors – immunomodulation and reduction of inflammation. In the context of immunomodulation, MSCs and their secretome can affect a wide variety of immune cells including but not limited to macrophages, dendritic cells, T-cells, B-cells and natural killer cells (reviewed in (Weiss and Dahlke, 2019) resulting in local immunosuppression. Notably, the anti-inflammatory action of the MSC secretome is not limited to immune cells as it can reduce the levels of pro-inflammatory markers in other tissues including cartilage (van Buul et al., 2012) and muscle tissue (Mitchell et al., 2019). In addition, bystander effects on the surrounding tissue include paracrine modulation of angiogenesis, anti-apoptosis, chemoattraction and the stimulation of resident cell proliferation (Caplan, 2017).

The immunomodulation of MSCs is mediated by cell-cell contact and contact-independent mechanisms, resulting in an immunosuppressive response (Gao et al., 2016). Herein, immunosuppressive responses are largely mediated soluble factors such as TGF-ß1, prostaglandin E2 (PGE2), hepatocyte growth factor (HGF), indoleamine-pyrrole 2,3-dioxygenase (IDO), nitric oxide (NO) and interleukin-10 (IL-10) as well as IL-6, galectins and leukaemia inhibitory factors (Gao et al., 2016). Proinflammatory cytokines interferon-γ (IFNγ) and tumour necrosis factor-α (TNF-α) produced by the damaged tissue during inflammation contribute to MSC migration to the damaged site, which in turn stimulates tissue repair and the resolution of inflammation (Kyurkchiev et al., 2014). Another immunomodulatory effect of MSCs is mediated by a contact-dependent mechanism that results in the decreased proliferation of T-cells and an increased percentage of Tregs (Han et al., 2011). Moreover, cell adhesion molecules (CD274, programmed death ligand 1), vascular cell adhesion molecule-1 and galectin-1 promote both cell-dependent contact and immunomodulation of MSC (Gao et al., 2016). IFNγ pre-treatment also increases the immunomodulatory effects of MSCs through the cell-cell contact mechanism and

secretion of soluble factors. The paracrine factors responsible for the effects described above are soluble factors including cytokines, growth factors and chemokines in addition to proteins and miRNAs embedded within extracellular vesicles (reviewed in (Eleuteri and Fierabracci, 2019).

A key factor playing a role in the lower osteogenic potential of osteoporotic MSCs is that in senile osteoporosis, MSCs undergo cellular senescence resulting in growth arrest and they have reduced proliferative, differentiation, anti-inflammatory and immunomodulatory potential (Bicer et al., 2021).
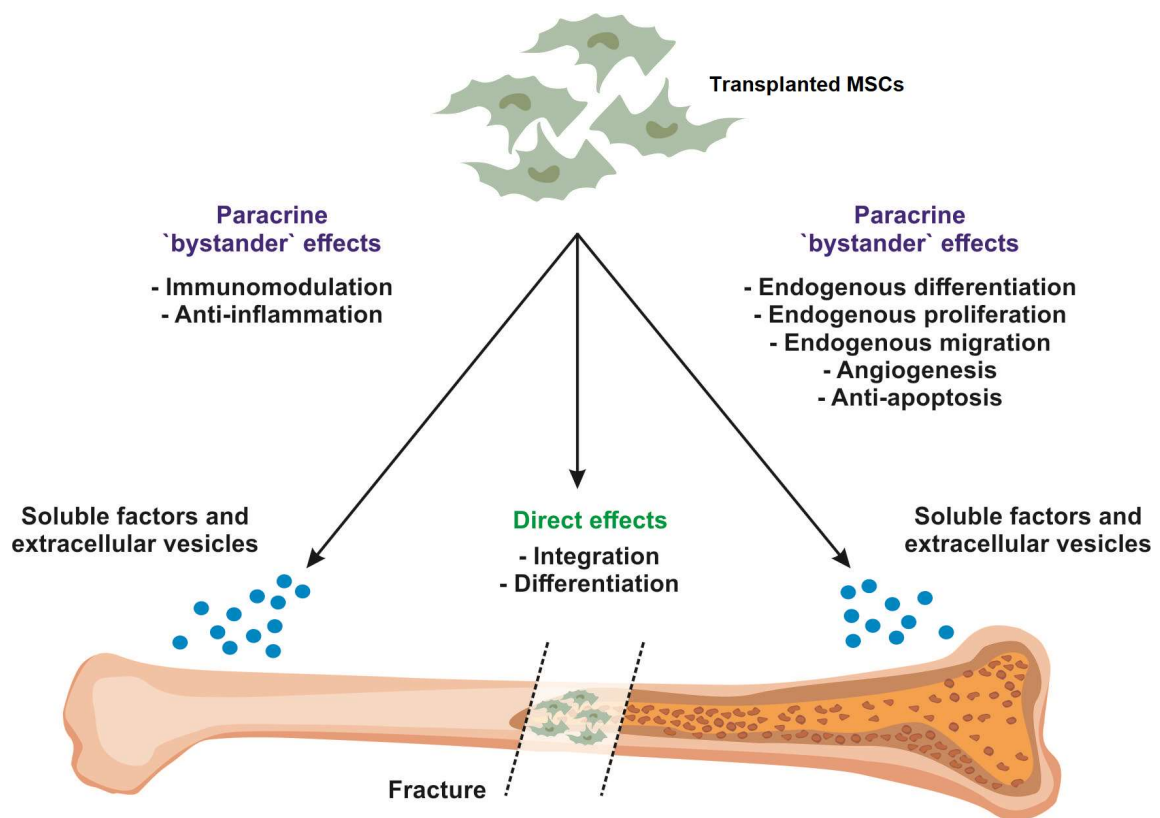
Figure 6.1. The contribution of MSCs to regeneration in bone fractures. In the acute phase after a bone fracture, resident transplanted MSCs release many paracrine factors, which in turn attract the migration of immune cells and additional MSCs to the site of the injury. The paracrine actions of MSCs also include modulating endogenous cell differentiation, proliferation and angiogenesis. In addition, they are able to integrate and undergo osteogenic differentiation thereby replacing lost bone material. Finally, in the late stage of bone regeneration, MSCs contribute to regeneration by releasing soluble and extracellular vesicle-embedded immunomodulatory and anti-inflammatory factors including proteins and miRNAs. The MSCs are transplanted MSCs (Bicer et al., 2021).

Increasing the viability as well as the proliferative and osteogenic differentiation capacity while retaining the anti-inflammatory and immunomodulatory potential of MSCs are therefore still essential steps required to deliver a successful and reliable autologous stem cell-based therapy for osteoporosis.

A better understanding of the effects of different 3D cell culture systems and ES on the immunomodulatory and anti-inflammatory potential of MSCs could therefore pave the way for more efficient MSC-based therapies.

6.2. Objectives

The results presented in Chapter 5 showed that ES in combination with 3D cultivation in aNFC does not negatively affect the viability of ASCs while boosting their osteogenic potential. The main objective in this chapter is to assess the impact of the combination of ES and 3D cell culture on the anti-inflammatory potential of ASC secretome.

The anti-inflammatory potential of secretomes released by ASCs cultivated in 2D and 3D with and without ES secretome was investigated by analysing the nuclear translocation of the pro-inflammatory transcription factor NFκB in human foreskin fibroblasts exposed to tumour necrosis factor alpha (TNF-α). Additionally, the TNF-α-induced activity levels of NFκB were explored in an established reporter cell line exposed to secretomes from ASCs cultivated with and without ES in 2D and 3D.

6.3. Results

6.3.1. TNF-α-induced nuclear translocation of the NFκB/p65 subunit showed a decrease in the presence of secretomes from ASCs cultivated in 2D and 3D

Using confocal microscopy, the nuclear translocation of the NFκB subunit p65 was monitored in fibroblasts exposed to TNF-α in combination with secretomes derived from ASCs with and without ES in 2D and 3D. Secretomes from ASCs cultivated in 2D and 3D were isolated. Fibroblasts were cultivated in the presence or absence of TNF-α in combination with the secretomes. If cells are activated with TNF-α, this

mimics inflammation in the dish and leads to the nuclear translocation of NFκB. If the secretomes have anti-inflammatory potential, they will reduce the level of p65 in the nucleus of fibroblasts exposed to TNF-α compared with cells in the presence of TNF-α alone.

Confocal imaging showed that NFκB/p65 (magenta) remained cytoplasmic with almost no nuclear staining in unstimulated fibroblasts whereas nuclear p65 was present in all cells exposed to TNF-α (Figure 6.2A-B). In contrast, fewer cells with nuclear p65 were observed when fibroblasts were co-exposed to 2D ASC secretome and TNF-α compared with cells with TNF-α alone (Figure 6.2C).
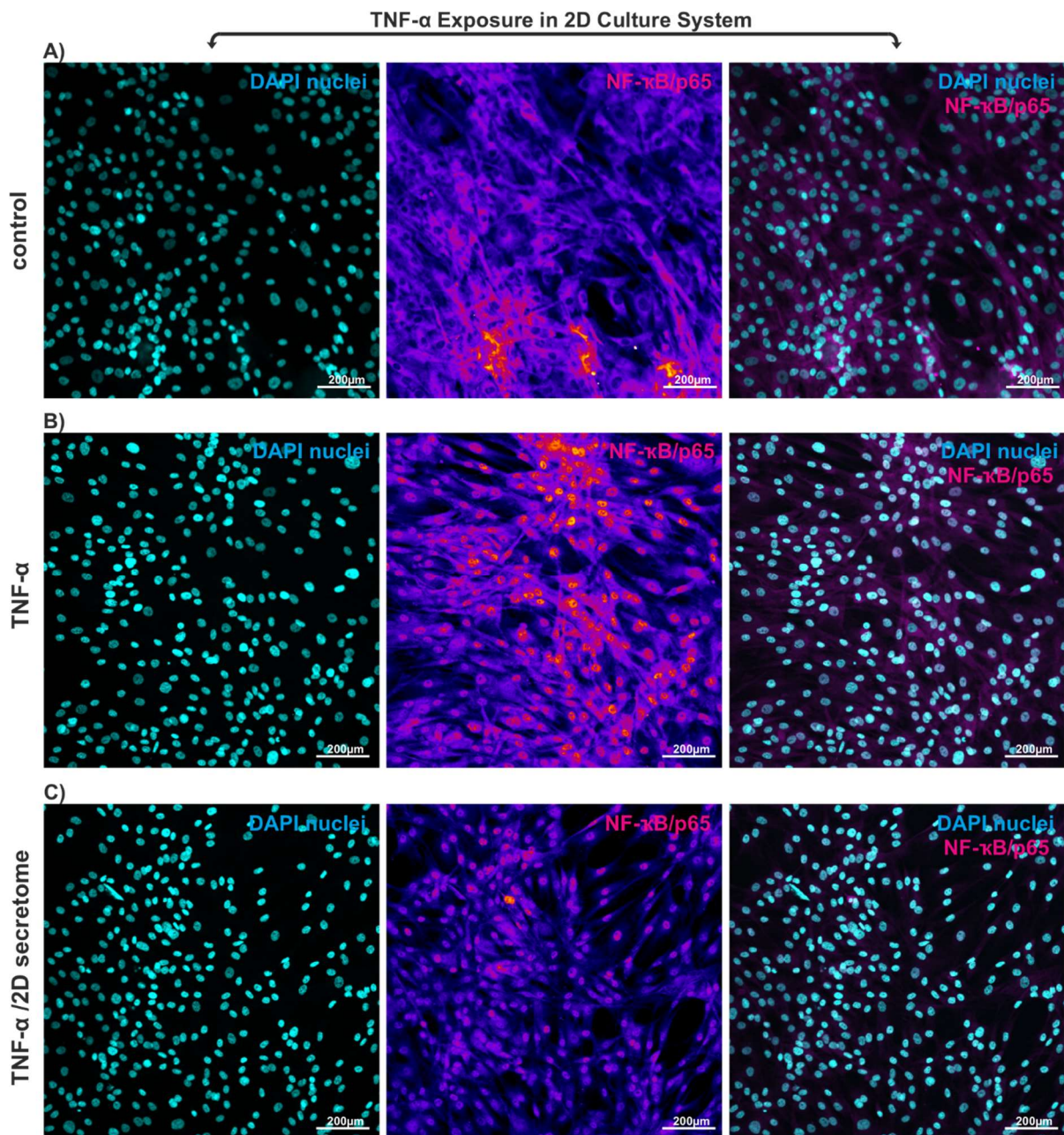
Figure 6.2. Secretome from ASCs cultivated in 2D reduced the nuclear translocation of p65 in fibroblasts exposed to TNF-α. (A-C) Fibroblasts were cultivated in the presence or absence of TNF-α (2ng/ml) (control) in combination with the secretomes generated in 2D. (A-C) Nuclear translocation of NFκB/p65 was detected by immunostaining (magenta colour, middle panels) and nuclei of fibroblasts were counterstained by DAPI (green colour, left panels). Cytoplasmic localization of NFκB/p65 in fibroblasts stimulated without TNF-α were compared with the nuclear localization of NFκB/p65 in fibroblasts stimulated with TNF-α. Scale bar: 200μm.

In order to assess the anti-inflammatory potential of the supernatant derived from ASCs cultivated in 3D, fibroblasts were cultivated in the presence or absence of TNF-α in combination with the secretomes from ASCs cultivated in 3D aNFC and NFC (Figure 6.3). The results shown in Figure 6.3B-C show that secretomes from ASCs cultivated in 3D NFC decreased the levels of nuclear translocation of p65 in fibroblasts exposed to TNF-α (Figure 6.3B-C) compared with fibroblasts with TNF-α alone (Figure 6.3A).

Figure 6.4 shows that the incubation of TNF-α exposed fibroblasts with secretomes released by ASCs seeded into 3D aNFC decreased the level of p65 in the nucleus compared with cells exposed to TNF-α alone. In addition to NFκB activation, a different morphology was observed in fibroblasts exposed to a combination of TNF-α and secretomes from ASCs cultivated in 2D and 3D.

Having visualised the data obtained by confocal laser-scanning microscopy, the nuclear translocation of p65 in fibroblasts was analysed in ImageJ to quantify the levels of nuclear translocation of NFκB p65. All of the results were compared with levels of p65 in control fibroblasts and cells cultivated in the presence of TNF-α. Notably, secretomes in 2D and 3D had a very different anti-inflammatory potential. Although the secretome from ASCs cultivated in 2D resulted in a decrease in the nuclear translocation of p65 in fibroblasts exposed to TNF-α, a stronger reduction was observed in the presence of secretomes of ASCs cultivated in 3D in both aNFC and NFC (Figure 6.5). The secretome from ASCs generated in 3D aNFC showed more reduction of the nuclear translocation of p65 in fibroblasts exposed to TNF-α, compared with the nuclear translocation of p65 in fibroblasts exposed to TNF-α in combination with the secretome from ASCs in 3D NFC (Figure 6.5).

Figure 6.3. Secretome from ASCs cultivated in 3D aNFC reduced the nuclear translocation of p65 in fibroblasts exposed to TNF-α. (A-C) Fibroblasts were cultivated in the presence or absence of TNF-α (2ng/ml) (control) in combination with the secretomes generated in 3D. (A-C) Translocation of NFκB/p65 was detected by immunostaining (magenta colour, middle panels) and nuclei of fibroblasts were localized by DAPI (green colour, left panels). Cytoplasmic localization of NFκB/p65 without TNF-α stimulation was compared with nuclear localization of NFκB/p65 in fibroblasts with TNF-α stimulation for 1 h (A-C). The nuclear localization of NFκB/p65 was counterstained by DAPI nuclear staining. Scale bar: 200μm.

Figure 6.4. Secretome from ASCs cultivated in 3D aNFC reduced the nuclear translocation of p65 in fibroblasts exposed to TNF-α, compared with secretome from ASCs cultivated in 2D. (A-D) Fibroblasts were cultivated in the presence or absence of TNF-α (2ng/ml) (control) in combination with the secretomes generated in

2D and 3D. (A-D) Translocation of NFκB/p65 was detected by immunostaining (magenta colour, middle panels) and nuclei of fibroblasts were localized by DAPI (green colour, left panels). Cytoplasmic localization of NFκB/p65 without TNF-α stimulation was compared with the nuclear localization of NFκB/p65 in fibroblasts with TNF-α stimulation for 1 h (A-D). Nuclei were counterstained by DAPI nuclear staining. Scale bar: 200μm.
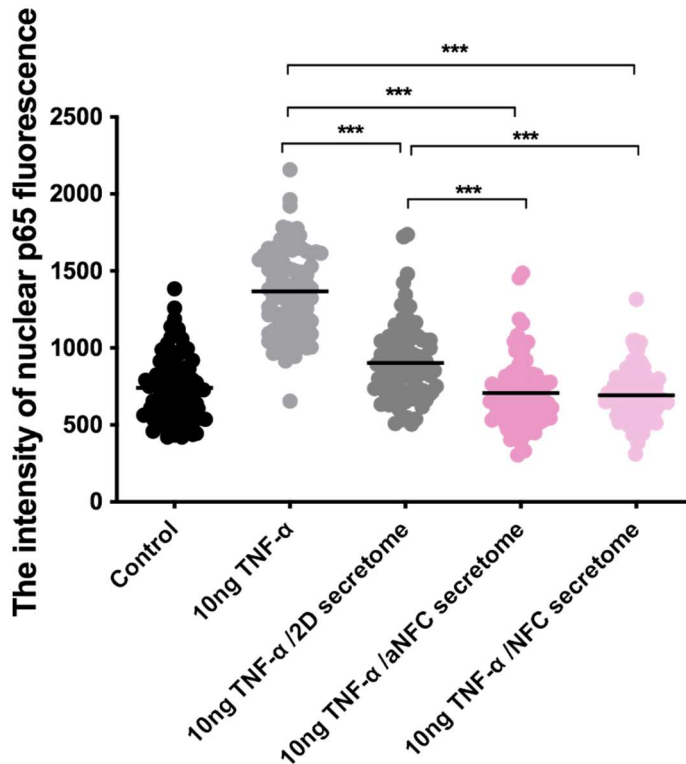
Figure 6.5. Quantification of nuclear p65 intensity showed a decrease in levels of inflammation in cells exposed to 2D and 3D ASC secretomes. Secretomes from ASCs cultivated in 3D aNFC reduced the nuclear translocation of p65 in fibroblasts exposed to TNF-α, compared with secretomes from ASCs in 2D. When the images from confocal laser-scanning microscopy were quantified, secretomes from ASCs cultivated in aNFC showed a higher anti-inflammatory potential than secretomes from ASCs in 2D. The intensity of nuclear p65 fluorescence was measured in Fiji Image J. Values are shown as means ± standard errors of three independent experiments using GraphPad Prism software (GraphPad, La Jolla, CA, USA). Data were compared using a one-way ANOVA with Bonferroni correction (CI 95%). At least three independent experiments were performed for each donor. [***]$P<0.0001$ was considered to be statistically significant.

6.3.2. 2D and 3D ASCs secretomes reduced NFκB activity in a cell reporter assay

2D and 3D ASCs secretomes resulted in a reduction in the nuclear translocation of p65 in fibroblasts exposed to TNF-α. In order to confirm these findings in an independent assay, a cell reporter assay was performed. Briefly, U251 NFκB-Luc-GFP reporter cell line (Zeuner et al., 2017) was used to monitor TNF-α and secretome-induced changes in NFκB-dependent luciferase expression and activity.

Secretomes were isolated from ASCs cultivated in 2D and 3D and then transferred onto the U251 NFκB-Luc-GFP reporter cells in the presence or absence of TNF-α. Figure 6.6 shows that the exposure of reporter cells to TNF-α alone resulted in high levels of NFκB activity. Notably, a combination of 2D secretome and TNF-α led to significantly decreased NFκB activity compared with cells exposed to TNF-α alone. Importantly, 3D secretomes from both NFC and aNFC further reduced the NFκB activity compared with cells exposed to both TNF-α alone and a combination of TNF-α and 2D secretome (Figure 6.6).
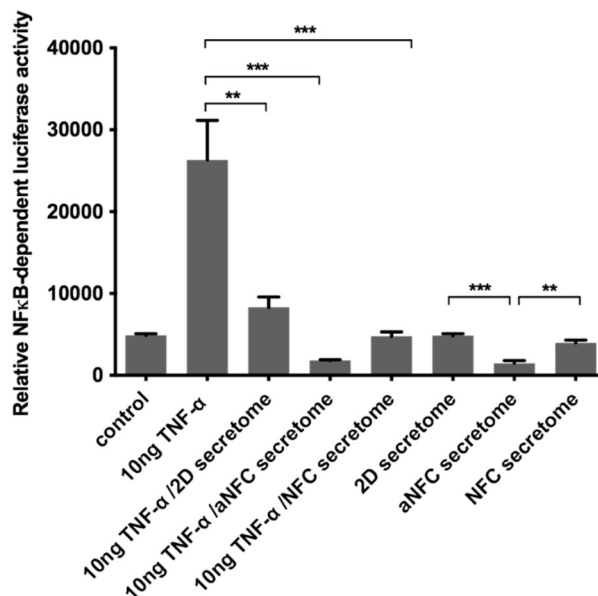
Figure 6.6.   The reporter cell assay showed a decreased level of NFκB dependent luciferase activity in cells co-exposed to 3D secretomes and TNF-α compared with a combination of TNF-α and 2D secretomes. A luciferase reporter assay was performed to compare TNF-α induced NFκB activation in reporter cells in the presence of secretomes from ASCs generated in 2D and 3D culture systems (three different donors). Values are shown as means ± standard errors of three

independent experiments using GraphPad Prism software (GraphPad, La Jolla, CA, USA). Data were compared using a one-way ANOVA with Bonferroni correction (CI 95%). At least three independent experiments were performed. [***]$P<0.0001$ and [**]$P<0.01$ were considered to be statistically significant.

6.3.3. ES resulted in a decrease in TNF-α-induced NFκB activation in 3D using NFκB/p65 nuclear translocation

Using confocal microscopy, the nuclear localization of the p65 subunit of NFκB was monitored in secretomes isolated from ASCs in 2D and 3D cultures with applied ES. In order to investigate NFκB activation in response to pro-inflammatory stimuli (TNF-α) under an electrical field, two detection systems based on nuclear localization of NFκB was performed: immunostaining for p65 subunits and a luciferase reporter assay. The secretomes from ASCs cultivated in 2D and 3D were isolated and then stimulated by fibroblasts with TNF-α either alone or with the 2D and 3D secretomes. The findings showed that the nuclear translocation of p65 in fibroblasts co-exposed to TNF-α and secretomes from ASCs in 2D cultures was higher than in cells in the presence of TNF-α and 3D secretomes. Interestingly, ES resulted in a decrease of NFκB activation in secretomes from ASCs cultivated in 2D and 3D cultures. The nuclear localization of the p65 subunit was monitored in the presence of secretomes from both 2D and 3D cultures with and without applied ES. Figures 6.7, 6.8 and 6.9 show the results of the immunocytochemical staining of images of fibroblasts grown in the presence of secretomes from ASCs cultivated in 2D and 3D cultures respectively. After overnight pre-cultivation with secretomes from ASCs cultivated in 3D and 2D with and without applied ES, fibroblasts were stimulated with TNF-α (2ng/ml) for 1 h. Confocal imaging showed that the NFκB/p65 in fibroblasts remained cytoplasmic in the control with almost no nuclear staining without TNF-α stimulation and high levels of nuclear p65 in TNF-α treated cells (Figure 6.7A-B). In contrast, the levels of nuclear p65 were reduced in the presence of 2D secretomes with and without ES (Figure 6.7C-D). Furthermore, the levels of nuclear p65 were reduced in the presence of 3D aNFC secretomes with and without ES (Figure 6.8C-D) and there was a substantial decrease in nuclear p65 in the presence of 3D NFC secretomes with and without ES (Figure 6.9C-D).
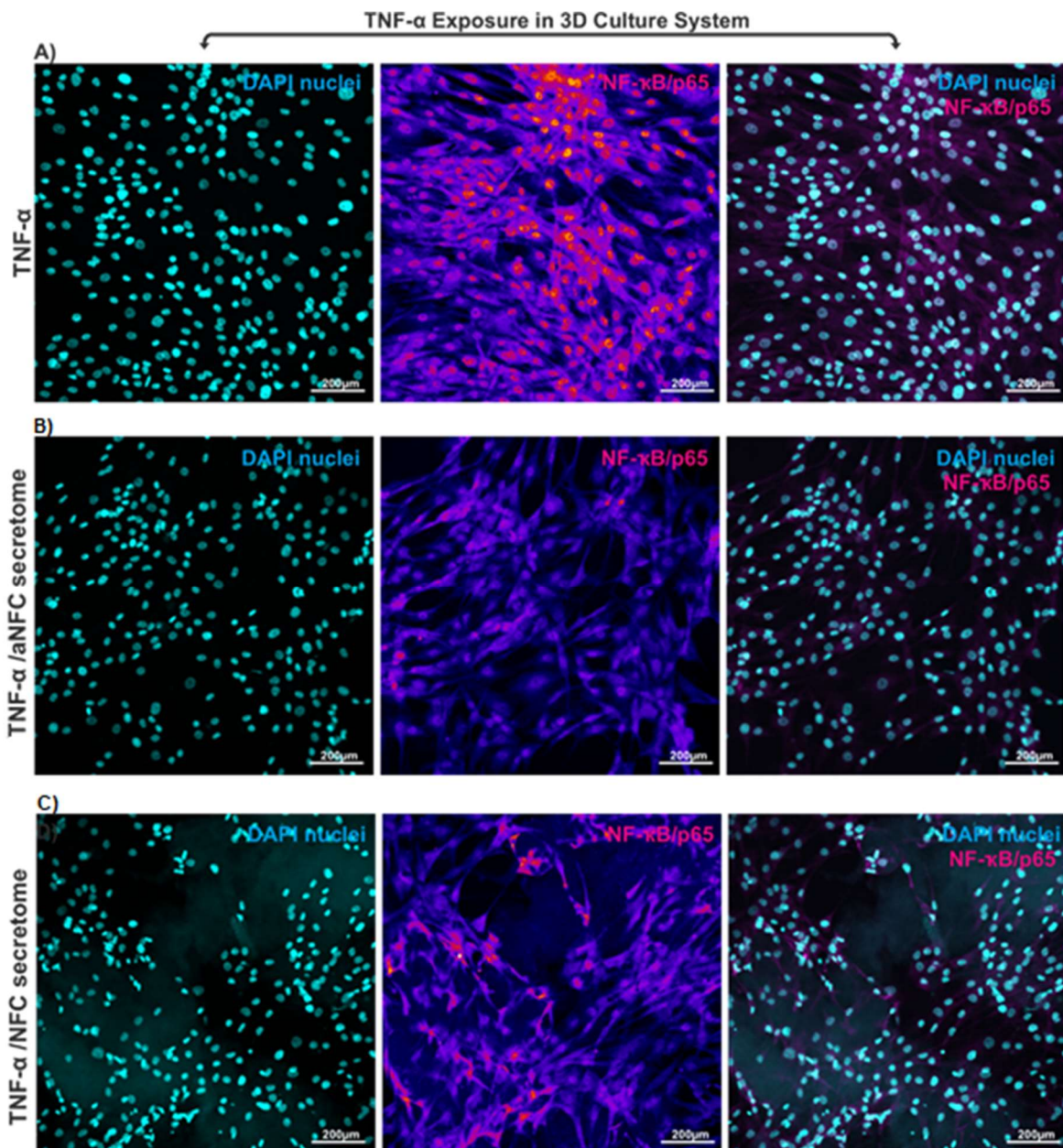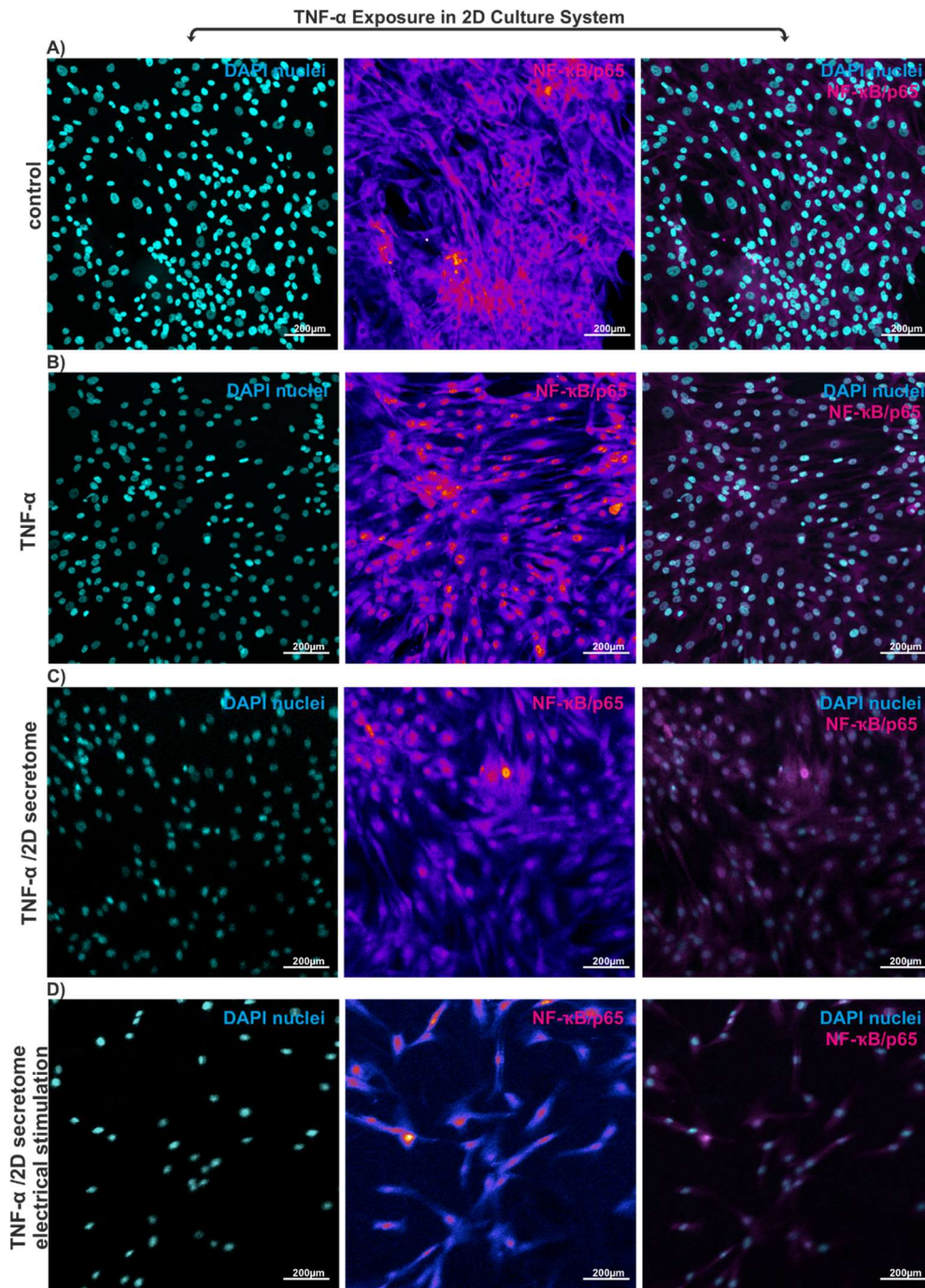
Figure 6.7. Secretome from ASCs cultivated in 2D with applied ES reduced the nuclear translocation of p65 in fibroblasts exposed to TNF-α. (A-D) Secretomes from ASCs were cultivated in 2D reduced the nuclear translocation of p65 in fibroblasts when exposed to ES. Fibroblasts were cultivated in the presence or absence of TNF-α (2ng/ml) (control) in combination with the secretomes generated in 2D with and without ES. (A-D) Nuclear translocation of NFκB/p65 was detected by immunostaining (magenta colour, middle panels) and nuclei of fibroblasts were counterstained by DAPI (green colour, left panels). Cytoplasmic localization of

167

NFκB/p65 in fibroblasts stimulated without TNF-α was compared with the nuclear localization of NFκB/p65 in fibroblasts stimulated with TNF-α. Scale bar: 200μm.
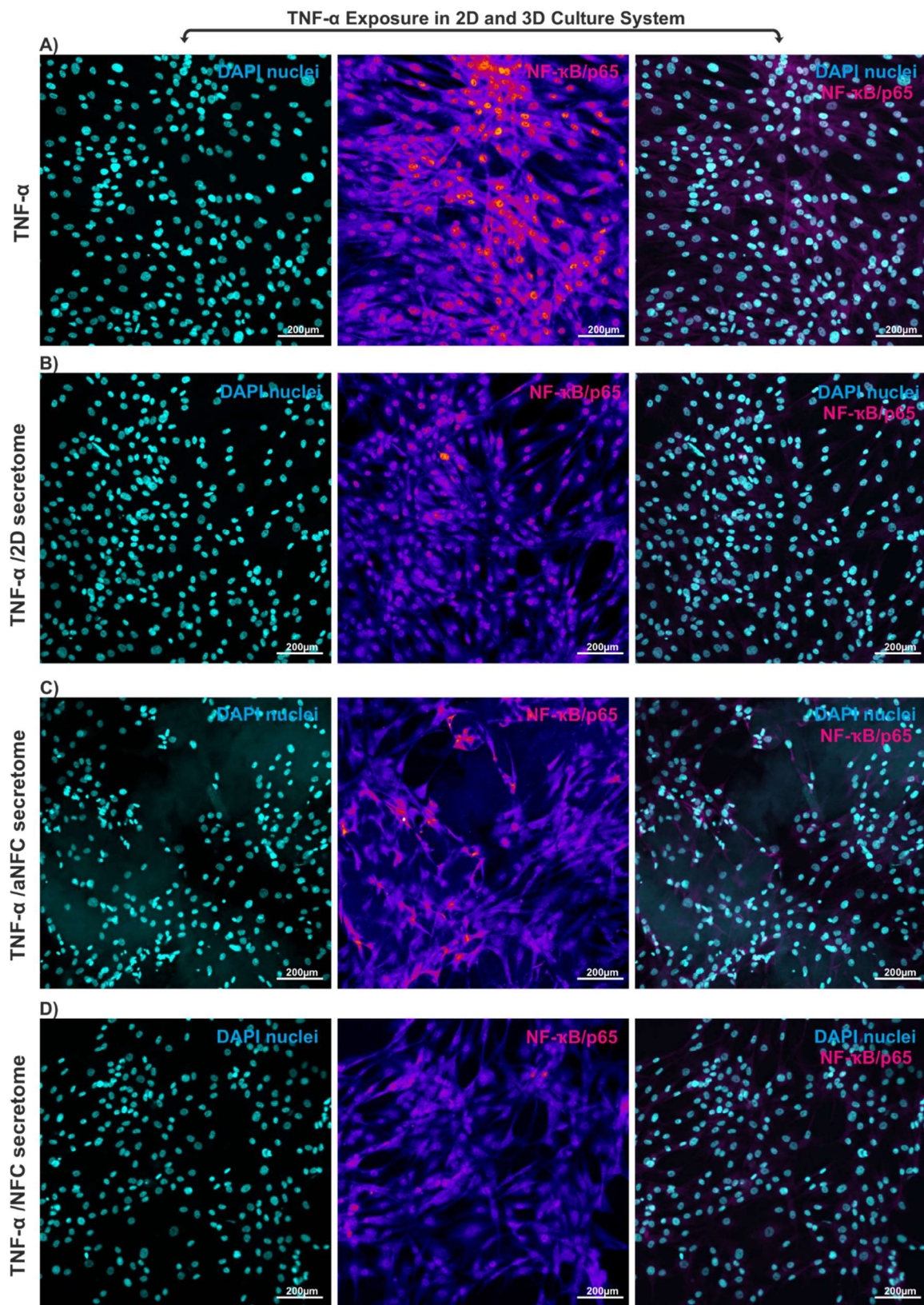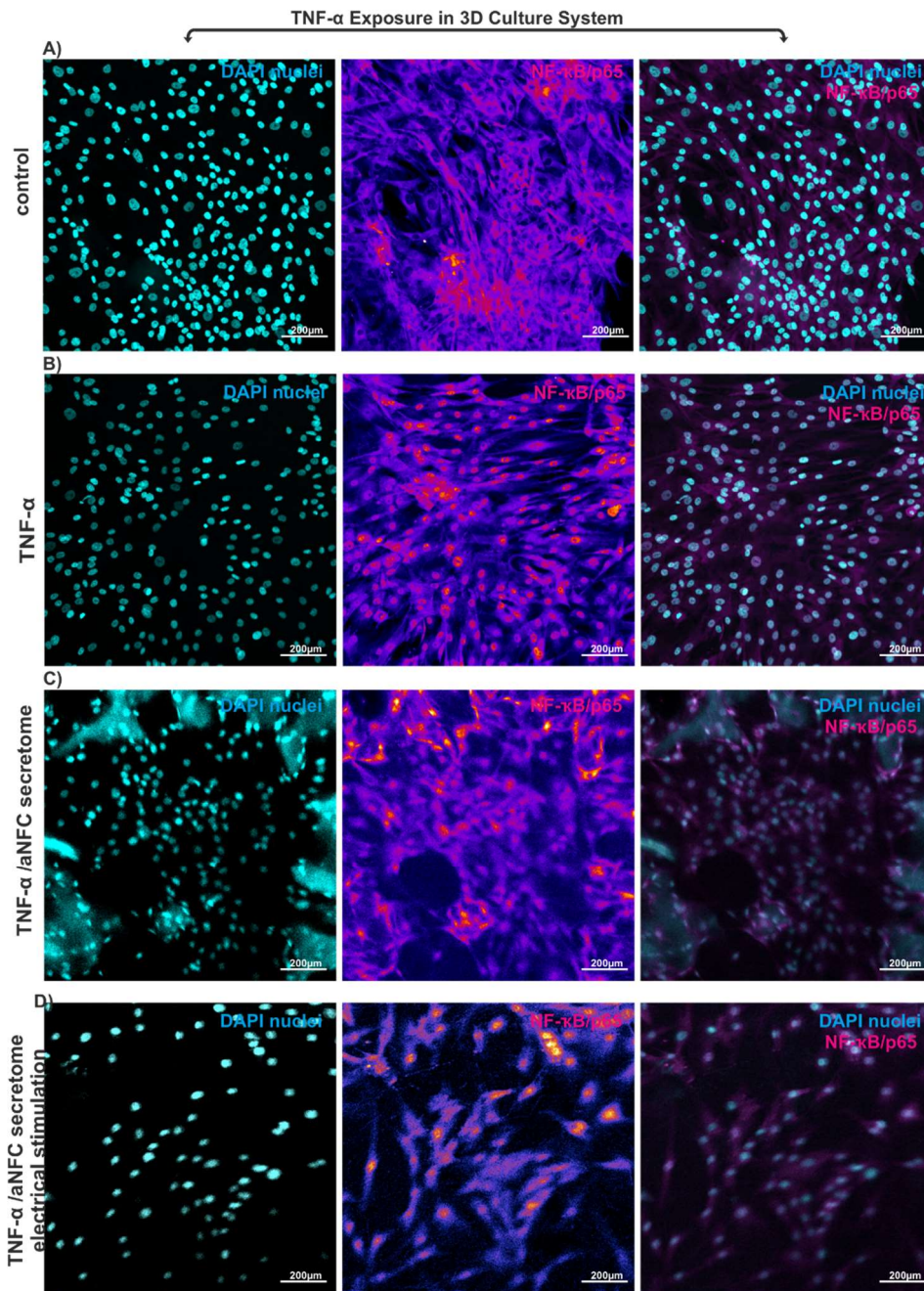

Figure 6.8. Secretome from ASCs cultivated in 3D aNFC with applied ES reduced the nuclear translocation of p65 in fibroblasts exposed to TNF-α. (A-D) Secretomes from ASCs were cultivated in 3D aNFC reduced the nuclear translocation of p65 in fibroblasts when exposed to ES. Fibroblasts were cultivated in the presence or absence of TNF-α (2ng/ml) (control) in combination with the secretomes generated in 3D aNFC with and without applied ES. (A-D) Nuclear translocation of NFκB/p65 was detected by immunostaining (magenta colour, middle

panels) and nuclei of fibroblasts were counterstained by DAPI (green colour, left panels). Cytoplasmic localization of NFκB/p65 in fibroblasts stimulated without TNF-α was compared with the nuclear localization of NFκB/p65 in fibroblasts stimulated with TNF-α. Scale bar: 200μm.
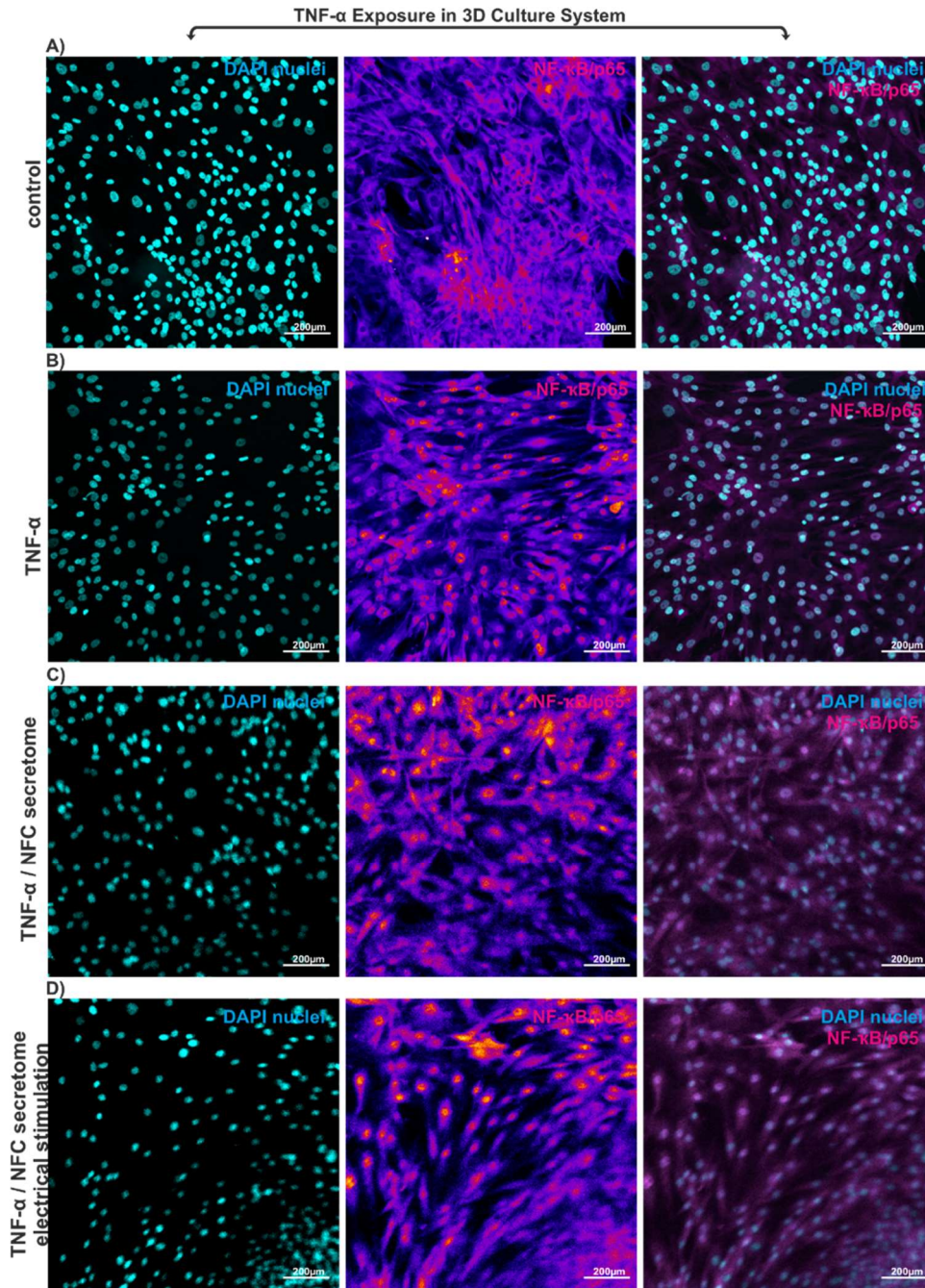
Figure 6.9. Secretome from ASCs cultivated in 3D NFC with applied ES reduced the nuclear translocation of p65 in fibroblasts exposed to TNF-α. (A-D) Secretomes from ASCs were cultivated in 3D NFC reduced the nuclear translocation of p65 in fibroblasts when exposed to ES. Fibroblasts were cultivated in the presence or absence of TNF-α (2ng/ml) (control) in combination with the secretomes

generated in 3D NFC with and without applied ES. (A-D) Nuclear translocation of NFκB/p65 was detected by immunostaining (magenta colour, middle panels) and nuclei of fibroblasts were counterstained by DAPI (green colour, left panels). Cytoplasmic localization of NFκB/p65 in fibroblasts stimulated without TNF-α was compared with the nuclear localization of NFκB/p65 in fibroblasts stimulated with TNF-α. Scale bar: 200μm.
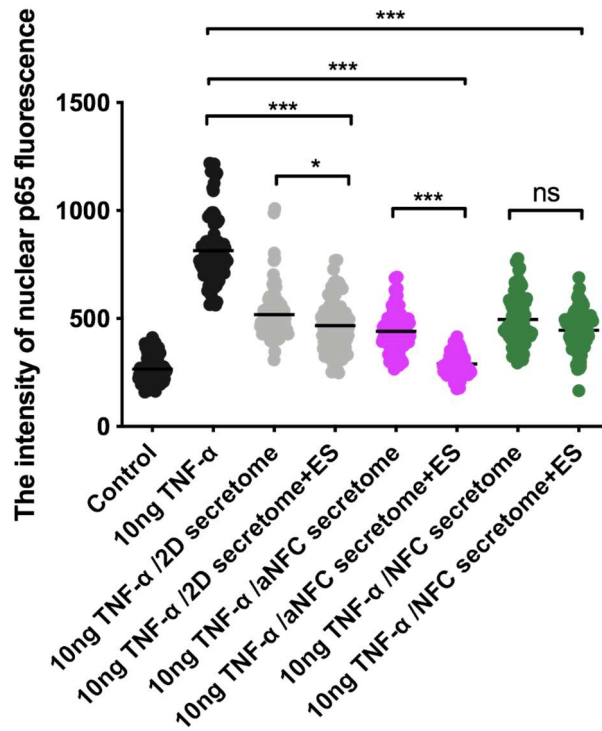
Figure 6.10. Quantification of nuclear p65 intensity showed a decrease in the inflammation of secretomes obtained from ASCs in 3D aNFC under ES conditions. Using ES conditions, secretomes from ASCs cultivated in 3D aNFC reduced the nuclear translocation of p65 in fibroblasts exposed to TNF-α compared with secretomes from ASCs in 3D NFC and in 2D. When the images from confocal laser-scanning microscopy were quantified, the secretomes from ASCs cultivated in aNFC and ES showed a higher anti-inflammatory potential than secretomes from ASCs in 3D without ES. Moreover, secretomes from ASCs cultivated in NFC exposed to ES showed a higher anti-inflammatory potential than secretomes from ASCs in 3D NFC applied without ES. The intensity of nuclear p65 fluorescence was measured in Fiji Image J. Values are shown as means $\pm$ standard errors of three independent experiments using GraphPad Prism software (GraphPad, La Jolla, CA, USA). Data were compared using a one-way ANOVA with Bonferroni correction (CI 95%). At least three independent experiments were performed for each donor. ***$P<0.0001$ was considered to be statistically significant.

6.3.4. ES resulted in a decrease in NFκB-dependent luciferase activity in reporter cells exposed to TNF-α and secretomes from ASCs generated in 2D and 3D cultures

In order to monitor the NFκB activation, the U251 NFκB-Luc-GFP reporter cell line (Zeuner et al., 2017) was used as described above and TNF-α was used to simulate inflammation. Having confirmed the nuclear translocation of p65 in fibroblasts exposed to TNF-α in combination with the secretome from ASCs in 3D aNFC by immunocytochemistry staining, a luciferase reporter assay was also carried out in order to quantify the NFκB activation. It was found that ES resulted in a decrease in the NFκB activation, which was monitored by the level of luciferase protein secreted in ASCs with stimulated TNF-α. Pre-cultured secretomes from ASCs in 2D and 3D under ES conditions were transferred onto the U251 NFκB-Luc-GFP reporter cell line, followed by an incubation for 48 h. The luminescence measurement showed active luciferase protein in the presence of secretomes from ASCs in both 2D and 3D cultures when exposed to TNF-α stimulation. Under ES conditions, 3D secretomes from aNFC reduced the NFκB activity exposed to both TNF-α alone and a combination of TNF-α and the respective conditions in 2D.

Figure 6.11 shows that the level of TNF-α-activated NFκB-dependent luciferase expression in presence of secretomes from ASCs in 3D aNFC culture showed a decrease under ES conditions compared with secretomes from ASCs in 3D aNFC without ES. NFκB activation in secretomes from ASCs in a 2D culture demonstrated a lower magnitude compared with the reporter cell line after TNF-α exposure. Furthermore, the pattern of NFκB activation in secretomes from ASCs in 3D cultures (aNFC and NFC) showed the lowest expression in response to TNF-α stimulation when ES was applied.
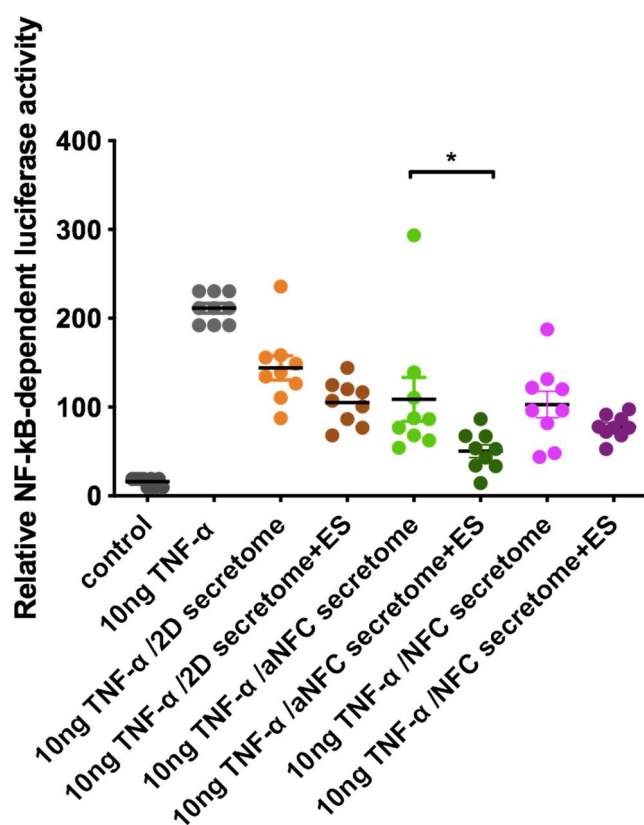
Figure 6.11. TNF-α-induced NFκB activation showed a decreased level of NFκB-dependent luciferase activity in secretomes from ASCs in 3D under ES conditions compared with secretomes in 3D without ES. The luciferase reporter assay was performed to compare the effect of ES treatment for TNF-α-induced NFκB activation in secretomes from ASCs generated in 2D and 3D culture systems for three different donors. Values are shown as means ± standard errors of three independent experiments using GraphPad Prism software (GraphPad, La Jolla, CA, USA). Data were compared using a one-way ANOVA with Bonferroni correction (CI 95%). At least three independent experiments were performed. $^{*}P<0.05$ was considered to be statistically significant.

6.4. Discussion

The impact of ES has been evaluated on the 3D cell culture in which the osteogenic differentiation potential of ASCs showed an increase in 3D cell culture in combination with ES (Bicer et al., 2020). Taken together, a combination of ES with 3D cell culture can improve the anti-inflammatory, immunomodulatory and regenerative potential of ASCs and their secretome. In this chapter, the impact of ASC secretomes on activity of the transcription factor NFκB has been evaluated. Notably, NFκB regulated the

level of a magnitude of pro-inflammatory cytokines including TNF-α, IL-1, IL-6, IL-8 and IL-4. Future studies could assess the effects of ASC secretomes on secretion of these cytokines and anti-inflammatory cytokine such as IL-10 using ELISA. Although there is some evidence that 3D cultivation as spheroids can reduce the anti-inflammatory and immunomodulatory potential of MSCs (Burand et al., 2020), most secretomes produced by MSCs cultivated in 3D scaffolds seem to have higher anti-inflammatory and immunomodulatory properties and an overall greater regenerative potential compared with conventionally cultivated SH-SY5Y neuroblastoma cells (Chierchia et al., 2017). Chierchia et al. (2017) found that MSC secretome-mediated neuroprotection of SH-SY5Y neuroblastoma cells after 6-hydroxydopamine treatment showed an increase when MSCs were cultivated in bovine collagen/polyethylene glycol and collagen/low-molecular weight hyaluronic acid hydrogels.

In accordance with these data, I have demonstrated in this chapter that secretomes from ASCs reduced the level of nuclear p65 in fibroblasts exposed to TNF-α and decreased the level of the nuclear translocation of p65 in fibroblasts exposed to TNF-α with stronger inhibition of the translocation when ASCs were cultivated in 3D. Additionally, ES further reduced the nuclear translocation of p65 in fibroblasts exposed to TNF-α when combined with secretome from ASCs generated in 2D compared with secretome from ASCs in 2D applied without ES. A luciferase reporter assay showed that TNF-α-induced NFκB activation was decreased in the U251 NFκB-Luc-GFP reporter cell line in combination with secretomes from ASCs cultivated in 3D aNFC (Figure 6.6). In this chapter, I have shown that both cultivation in 3D and ES increase the anti-inflammatory potential of ASC secretomes.

These findings are in accordance with those of Htwe et al. (2015) showing that fibroblasts have a higher anti-inflammatory potential in electrospun 3D scaffolds (Htwe et al., 2015). NFκB activation was at a higher level in 2D than in 3D. A higher regenerative potential of secretomes from 3D cultivated ASCs compared with 2D culture was reported by (Chierchia et al., 2017), who found that MSC secretome-mediated neuroprotection of SH-SY5Y neuroblastoma cells following 6-hydroxydopamine treatment was increased if the MSCs were cultivated in bovine collagen/polyethylene glycol and collagen/low-molecular weight hyaluronic acid hydrogels. However, to date, no molecular profiling of the secretomes has been reported. In 2018, it was also reported that 3D spheroid cultures of human BM-MSCs

secreted higher levels of vascular endothelial growth factor (VEGF) compared with 2D controls (Redondo-Castro et al., 2018). These findings are in line with several other reports demonstrating that 3D cultivation of ASCs results in an increased secretion of multiple growth factors including hepatocyte growth factor (HGF), VEGF, stromal cell-derived factor (SDF) and fibroblast growth factor-2 (FGF-2) (Lee et al., 2016, Kim et al., 2013b, Young et al., 2018).

More recently, Carter et al. (2019) studied the wound-healing potential of 2D and 3D cultivated human BM-MSCs *in vitro* and *ex vivo* and found that 3D cell culture of MSCs on electrospun gelatine/polycaprolactone fibres increased the secretion of FGF-2, IL-6, VEGF and HGF compared with 2D controls (Carter et al., 2019). In addition, 3D cell culture significantly improved secretome-mediated corneal wound healing in a rabbit corneal organ culture system (Carter et al., 2019). A comparative analysis of the secretomes of umbilical cord MSCs cultivated as spheroids and as an adherent monolayer showed that 3D cultivation significantly increases the secretion of IL-10, LIF, FGF-2, I-309, CSF and GM-CSF (Miranda et al., 2019) and that study also showed that secretome from 3D-cultivated MSCs had superior regenerative and anti-inflammatory potential in an *in vivo* model of arthritis in adult Wister rats.

Even so, the exact mechanism of increasing the anti-inflammatory potential of ASC secretomes is not known. It can be speculated that ES represents cellular stress which ASCs counterbalance by releasing a more potent secretome under ES (Bicer et al., 2021).
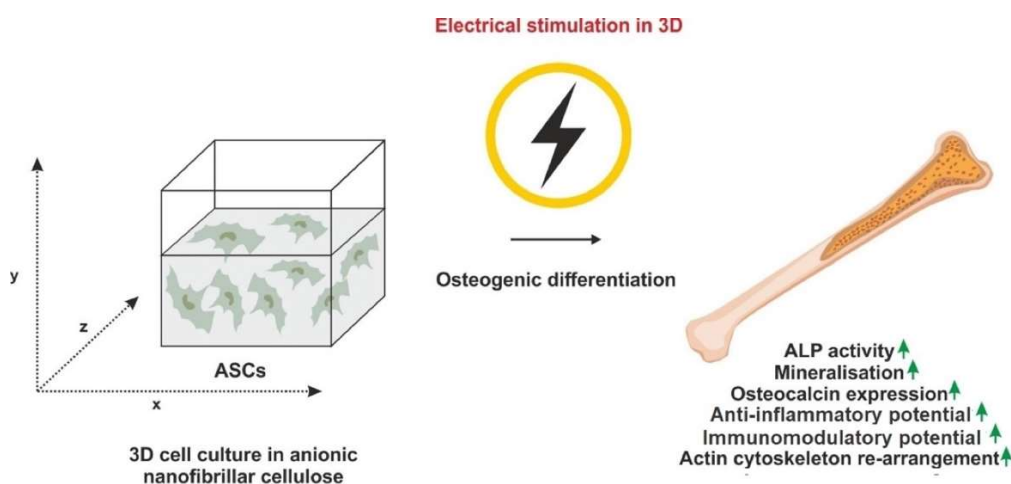
Figure 6.12. The effects of 3D cell culture in combination with ES on MSC properties relevant for bone regeneration. 3D cell culture in combination with ES

shows an increase in the osteogenic differentiation potential of ASCs for bone regeneration. This is related to the increased levels of ALP activity and mineralisation as well as an increase in the osteocalcin expression. The re-arrangement of the actin cytoskeleton of ASCs in 3D shows an increase when combined with ES conditions. In addition, secretomes from ASCs in 3D have more anti-inflammatory and immunomodulatory potential when in combination with ES conditions.

6.5. Conclusion

In this chapter I have explored the effect of 3D cell culture combined with ES on the regenerative, anti-inflammatory and immunomodulatory potential of ASCs and their secretome. It is apparent that 3D cell culture combined with ES increases the anti-inflammatory potential of ASCs secretomes. 3D cell culture combined with ES could indeed increase the levels of bone regeneration-relevant components within the MSC secretome. A rational design of 3D cell culture parameters could further improve the performance of MCSs in bone regeneration when exposed to ES. An additional and often neglected aspect of designing optimal scaffolds for MSC-mediated bone regeneration is their complex contribution to bone regeneration. Although ES shows an increase in bone regeneration of ASCs by integrating and differentiating into osteoblasts, it also plays an essential role in regulating the inflammation and modulating the immune system. Notably, a well-controlled inflammatory response can be effective for bone repair. Therefore, combining ES with 3D cell culture should be accepted as a promising amelioration for the immunomodulating paradigm because it is able to overcome the limitations of traditional 2D culture methods by the synergistic effects of ES. Further research will investigate the effect of 3D cell culture in combination with ES on the anti-inflammatory and regenerative potential of ASCs in *in vivo* models of bone regeneration including rodent models and in sheep as a large animal model. Increasing the anti-inflammatory and immunomodulatory potential of MSCs are key steps to promote a successful autologous stem cell-based therapy for osteoporosis. This chapter has established the potential of ES to decrease TNF-α-induced activation of NFκB, as shown by reduced nuclear translocation of p65 and lower NFκB-dependent luciferase activity in presence of secretomes of ASCs cultivated in 3D aNFC. Understanding the effect of secretomes of ASCs in 3D aNFC under ES conditions could pave the way for more efficient stem cell-based therapies for osteoporosis and bone fractures.

Chapter 7
General Discussion

7.1. Summary of the results

The experiments presented in this thesis have characterised optically transparent anionic nanofibrillar cellulose (aNFC) as the most suitable hydrogel for the 3D culture of adipose-derived MSCs (ASCs) in terms of cell viability, biocompatibility and compatibility with fluorescent imaging techniques (Chapter 3). The data have shown that culturing in aNFC increased the osteogenic differentiation potential of human ASCs in 3D as demonstrated by the higher expression of osteogenic differentiation markers (for example, OCN and OPN), increased ALP activity and higher levels of calcium deposition (Chapter 4). Furthermore, the results showed that ES in combination with 3D aNFC was able to further increase the osteogenic potential of ASCs in 3D (Chapter 5) and the anti-inflammatory potential of their secretomes (Chapter 6).

7.2. Significance of the current study for 3D cell culture

7.2.1. The spectral properties, biocompatibility and viability of 3D aNFC hydrogels

In order to determine the compatibility of aNFC with 3D imaging techniques, the optical properties of aNFC were evaluated using different wavelengths of light and compared with alginate and NFC hydrogel. All concentrations of aNFC exhibited a lower absorption over the whole spectrum compared with the other scaffolds. Furthermore, fluorescence emission was measured for each biomaterial with excitation wavelengths of 405 nm and 488 nm to determine the compatibility of aNFC with fluorescence-based techniques. The results showed that aNFC hydrogel was the best of those tested as aNFC had lower levels of autofluorescence compared with the other scaffolds investigated. These findings are in accordance with those of Bhattacharya et al. (2012) which showed the absorbance spectrum and fluorescence emission of NFC hydrogels. In that study, the UV-visible absorbance of 0.5% NFC was measured in the range 300-550 nm. NFC hydrogels exhibited no autofluorescence and also did not absorb visible or UV light (420 to 700 nm) (Bhattacharya et al., 2012). Although other scaffolds have been previously been investigated, the findings obtained in Figure 3.3 are novel and original since aNFC hydrogel has been examined for the first time in this study. A higher level of fluorescence emission was found in aNFC than those of other scaffolds.

The current study also investigated 3D aNFC hydrogels with regard to their biocompatibility with ASCs. In order to make hydrogels containing ASCs suitable for transplantation *in vivo*, the stiffness of the hydrogel should be increased by combining it with stiff materials, such as magnesium scaffolds. Therefore, the adhesion of aNFC when loaded onto magnesium was evaluated to further improve the biocompatibility of hydrogels (Figures 3.5 and 3.6). However, the hydrogels failed to adhere to the magnesium and so were not studied any further and it was decided to use aNFC alone for all future experimentation. Even so, combining aNFC hydrogels with stiff materials such as magnesium or titanium in future studies might further improve the osteogenic potential of adult stem cells. In this context, Oh et al. (2009) reported that MSC cultivation on titanium nanotubes (100 nm pores) had osteoinductive effects (Oh et al., 2009). These findings were confirmed by Schürmann et al. (2014) who investigated the effect of titanium with different pore sizes on cell viability and the osteogenic differentiation of neural crest-derived stem cells (NCSCs) (Schürmann et al., 2014). The results showed that titanium (30 nm pores) did not affect proliferation but increased the osteogenic differentiation of NCSCs without the need for additional cues. Chen et al. (2014) reported that magnesium scaffolds coated with ß-tricalcium phosphate were capable of stimulating the osteogenic differentiation of MSCs (Chen et al., 2014) and some researchers reported that the cultivation of MSCs on titanium nanotubes with lateral spacing of 15-30 nm increased mineralization after 4 days in culture (Park et al., 2007).

In order to assess the distribution of the cells in 3D, ASCs grown in 3D aNFC hydrogel were evaluated using a fluorescent staining assay with confocal laser-scanning and SEM microscopy. ASCs embedded into 0.2% aNFC were stained with PKH67 fluorescent dye and primary antibodies for nestin and beta-actin, followed by counter-staining with calcofluor white to examine the distribution of the cells in 3D (PKH67). Nestin was used as a stem cell marker and actin was used to assess the assembly of actin filaments. ASCs cultivated in 0.2% aNFC showed an homogeneous distribution and excellent biocompatibility (Figures 3.7 and 3.8). In addition, ASCs seeded into 0.2% aNFC were stained with cell tracker CMFDA, phalloidin to examine the structure of actin filaments in ASCs in 3D and counterstained with calcofluor white. Confocal laser-scanning microscopy showed an homogeneous morphological appearance of ASCs in aNFC (Figure 3.9). In addition, the viability of ASCs cultivated in different hydrogels (aNFC, NFC and alginate) and

in traditional 2D culture was assessed using a test for biocompatibility. This result showed that ASCs embedded in 0.2% aNFC had greater viability than ASCs grown in 0.2% NFC, 0.9% alginate and in traditional 2D culture (Figure 3.10). These findings are in accordance with those of a recent study from the Widera lab which showed that an anionic form of NFC significantly increased the viability of human ASCs (Sheard et al., 2019). Azoidis et al. (2017) also reported that low concentrations (0.2%) of NFC did not negatively affect the proliferation of bone marrow MSCs (BM-MSCs), ASCs or palatal MSCs. NFC at a higher concentration (0.5%), however, significantly reduced cellular viability and proliferation compared with 2D controls (Azoidis et al., 2017). Some researchers have reported that woven biodegradable composite fibres from poly-L-lactic acid substituted with hydroxyapatite had an overall positive effect on BM-MSC viability, whereas growth from poly-L-lactic acid alone reduced viability (Persson et al., 2018). Conversely, Nguyen et al. (2012) reported that electrospun scaffolds significantly reduced the proliferation of human MSCs as early as 7 days after seeding on nanofibrous scaffolds composed of poly-L-lactic acid and type I collagen (Nguyen et al., 2012). Some 3D scaffolds, including gelatin, poly lactic-co-glycolic acid and chitosan, had no effect on the viability or the proliferation of MSCs (Lo et al., 2016).

Although some studies have reported that 3D culture promotes an increase in viability and proliferation, others have observed the opposite effects (reviewed in (Edmondson et al., 2014). Cultivation of MSCs as spheroids often leads to a reduction in proliferation and viability (Tsai et al., 2015). This has been attributed to a reduced nutrient and oxygen supply and impaired waste product diffusion, particularly if a critical sphere size has been reached (reviewed in (Cesarz and Tamama, 2016). Although spheroid culture has often been associated with decreases in cellular proliferation and viability, 3D culture on scaffolds and in hydrogels often increases cell viability and proliferation compared with 2D cultures (reviewed in (Mirbagheri et al., 2019). Some researchers reported that 3D cultivation of minipig MSCs in electrospun 3D polycaprolactone increased both their proliferation and viability (Rampichova et al., 2013). Rat BM-MSCs have also been reported to increase their proliferation on collagen-based scaffolds (Han et al., 2012a). More recently, Yin et al. (2020) reported that 3D cultivation of ASCs in a nanofibrous polysaccharide hydrogel increased their proliferation and viability (Yin et al., 2020b). Interestingly, some reports have also shown that small differences in the scaffold

composition and even in the technique can be decisive for the outcome. For example, Brennan et al. (2015) showed that jet-sprayed micro-fibre polycaprolactone scaffolds increased human BM-MSC proliferation whilst electrospun variants of the same scaffold decreased proliferation compared with the 2D controls (Brennan et al., 2015). The studies referred to above are in general agreement with the results reported in Chapter 3, which demonstrated improved cellular proliferation and viability, an important feature for bone tissue engineering strategies. Because of the improved biocompatibility, biodegradability and bioactive properties of aNFC hydrogels, it is likely that they will be the subjects of future research as biomedical materials.

7.2.2. Impact of aNFC on the osteogenic potential of ASCs in 3D

Despite significant progress in developing efficient strategies for osteogenic differentiation in 2D, little has been achieved in establishing optimal conditions for osteogenic differentiation in 3D cell culture. One of the major problems with 2D cell culture is its lack of ability to create soluble factor gradients, a critical factor for cell differentiation (Tibbitt and Anseth, 2009). The aim of the current study was to investigate the potential improvement of osteogenic differentiation of ASCs in 3D cell culture (Chapter 4). The expression of osteoblast-related genes in ASCs in 3D aNFC was evaluated using conventional PCR analysis and compared with those in standard 2D culture. Osteogenic induction of ASCs cultured in 2D resulted in a higher expression of OCN and OPN at protein level for 21 days compared with undifferentiated cells (Figures 4.1 and 4.2). This is in general accordance with the findings of Castrén et al. (2015) who reported that OCN mRNA levels increase until day 21 in 2D culture (Castrén et al., 2015). For Runx2 mRNA, increased levels were only observed at day 14 (Figures 4.1 and 4.2). Another part of the same study, however, showed that the expression levels of Runx2 mRNA only increased at day 14 in MSCs cultivated in FCS in 2D culture and found low levels of Runx2 mRNA in human platelet lysate and plasma (PLP) cultures under osteogenic differentiation conditions (Castrén et al., 2015). In contrast, the higher level of Runx2 mRNA in PLP and FCS-differentiated cultures in 3D was shown on day 14 (Castrén et al., 2015). Interestingly the expression level of RunX2 was higher in ASCs in 3D aNFC under osteogenic media on day 21 (Figures 4.7 and 4.8). In addition, the high level of OCN and OPN expression in ASCs in 3D aNFC was found in an osteogenic media compared with a standard media on day 21 (Figures 4.7 and 4.8).

The differentiation potential of ASCs in 2D was evaluated by analysing calcium deposition as proof of mineralization using Alizarin Red S staining. ASCs grown in an osteogenic differentiation media showed significantly higher calcium deposition compared with cells in a control media (Figure 4.4). These findings are in general accordance with those of Castren et al. (2015) which showed that calcium deposition is higher in cells in an osteogenic differentiation media. OCN is secreted by mature osteoblasts to promote the mineralization of calcium deposits (Lian et al., 1998). In the current study, the expression of OCN and OPN was significantly increased in ASCs in aNFC under osteogenic differentiation conditions (Figures 4.9 and 4.10). This finding is in accordance with those of other reports exploring polycaprolactone-tricalcium phosphate scaffolds and jet sprayed microfibre polycaprolactone scaffolds, which have been suggested to possess similar osteoinductive effects in human foetal and adult BM-MSCs (Shekaran et al., 2015, Brennan et al., 2015). Another scaffold, an elastic 3D poly (ε-caprolactone), has been shown to increase the expression of bone sialoprotein and OCN in minipig BM-MSCs subjected to differentiation in 3D (Rampichova et al., 2013). Similarly, when gelatin and blends of gelatin and alginate were used as 3D scaffolds, increased osteogenic differentiation of ASCs and BM-MSCs was observed (Lo et al., 2016, Wang et al., 2016b).

In addition to the effects on the expression of osteogenic genes at mRNA level and the up-regulation of osteogenic markers at protein level, ASCs cultivated in 3D aNFC showed a higher level of mineral deposition in an osteogenic differentiation media at 21 days (Figure 4.11). A previous study by the Widera group reported high levels of calcium deposition after osteogenic induction in human MSCs seeded into aNFC (Sheard et al., 2019). This is consistent with the findings of an earlier study by Sefcik et al. (2008) who reported an increased calcification of ASCs on a 3D nanofibre matrix of type I rat tail collagen (Sefcik et al., 2008). In a further approach, some researchers used a blended scaffold composed of collagen and electrospun poly (L-lactic acid) to study the influence of 3D cell culture on the differentiation of human MSCs of undefined origin and found that differentiation in 3D significantly increased expression of OCN and OPN and increased the levels of calcification in human MSCs (Nguyen et al., 2012). Similar effects on the expression levels of OCN and OPN in rat BM-MSCs were observed if purified collagen was used to create a 3D scaffold: von Kossa staining revealed a statistically significant increase in calcification (Han et al., 2012a). Furthermore, the use of pure poly (l-lactic acid) scaffolds as a

substrate showed similar increases in the expression of pro-osteogenic markers in human BM-MSCs under osteogenic conditions (Persson et al., 2018), which was accompanied by a significant increase of Ca^{2+} deposition. By increasing the osteogenic differentiation potential, these scaffolds could be implemented in MSC-mediated bone regeneration therapy.

Calcium (Ca^{2+}) oscillation profiles in ASCs were evaluated in 2D following osteogenic differentiation to assess a frequency-dependent cell response. Unfortunately, Ca^{2+} oscillation patterns in 3D could not be assessed due to technical limitations. For example, the confocal laser-scanning microscopy did not have sufficient scanning speed or resolution in the *z*-axis to allow Ca^{2+} dynamics to be adequately visualised in the thick 3D hydrogel sections. The frequency of Ca^{2+} spikes in ASCs grown in 2D decreased following osteogenic differentiation compared with undifferentiated cells in 2D after 7, 14 and 21 days (Figure 4.5). These findings are in general accordance with those of Sun et al. (2007) who reported changes of Ca^{2+} oscillation in undifferentiated bone marrow MSC and exhibited unsynchronized Ca^{2+} oscillations in undifferentiated human MSCs (Sun et al., 2007). The same study also showed the effect on intracellular Ca^{2+} dynamics and the decreased frequency of Ca^{2+} spikes in the differentiated human osteoblasts in response to osteoinductive factors present in the osteogenic differentiation media (Sun et al., 2007). ASCs cultivated in aNFC hydrogels were assessed for potential differences in actin cytoskeleton architecture and formation of cell-free pores 21 days post-osteogenic induction. ASCs exposed to osteogenic differentiation exhibited a highly arranged actin cytoskeleton, denser actin bundles and formation of cell-free pores when cultivated in the 3D aNFC compared with undifferentiated cells (Figure 4.12). This finding is in accordance with those of Treiser et al. (2010) who showed that the osteogenic potential of cells was directly associated with the reorganization of actin cytoskeleton and dense actin bundles (Treiser et al., 2010). Some researchers also reported a rearrangement of the cytoskeleton during osteogenic differentiation (Chen and Jacobs, 2013) and others showed that osteogenic differentiation resulted in increased actin polymerization with perinuclear actin bundles framing the nucleus as well as dense actin fibres in the cell periphery (Titushkin and Cho, 2007) (reviewed in (Khan et al., 2020)). So as demonstrated in the current study and in other reports, osteogenic differentiation of MSCs is accompanied by the re-arrangement of actin filaments in 2D and 3D culture.

One study previously combined bone marrow-derived MSCs (BM-MSCs) and biomaterial scaffolds to investigate bone regeneration using a 3D platform (Quarto et al., 2001); after the implantation of custom-made porous hydroxyapatite scaffolds seeded with autologous BM-MSCs, a large bone defect (4-8 cm) was repaired in three patients. The use of 3D scaffolds has been supported by incorporating osteoconductive and osteoinductive biomaterials in order to improve the differentiation of stem cells (Iaquinta et al., 2019). Another recent study developed poly (2-hydroxyethyl methacrylate) cryogels which included hydroxyapatite to mimic an inorganic bone matrix, which supported an increase in the osteogenic differentiation potential (Haussling et al., 2019). ASCs cultured in collagen and platelet-rich plasma cryogels showed a higher osteogenic potential at 14 days compared with those with an arginine-glycine-aspartic acid peptide (Haussling et al., 2019). Interestingly, one study observed 3D interactions between cells and the extracellular matrix (ECM) without additional substrates and reported improved osteogenic differentiation and subsequent bone regeneration (Baraniak and McDevitt, 2012). These findings are consistent with those of a recent study in which the use of an artificial ECM as a scaffold model was also proposed for cellular therapy to improve the osteoconductive properties for bone formation (Egger et al., 2018). Another study found that ECM-scaffolds combined with MSCs showed excellent biocompatibility and promoted periodontal bone regeneration in dogs (Takewaki et al., 2017).

Biomaterials in combination with compliant stem cells can be surgically implanted at a lesion site of bone to promote bone regeneration. Kang et al. (2012) generated a matrigel scaffold combined with membrane proteins (similar to ECM) to support an appropriate environment for stem cells and the resulting scaffold improved bone healing *in vivo* (Kang et al., 2012b). Some researchers have reported that poly (polyethylene glycol citrate-co-N-isopropylacryl-amide) combined with gelatine was capable of delivering cells (for example, BMP9-transduced immortalized mouse embryonic fibroblasts and immortalized murine calvarial mesenchymal cells) to stimulate bone regeneration in murine critical-sized calvarial defects (Dumanian et al., 2017, Ye et al., 2016). Another *in vivo* study by Fu et al. (2019) showed that a matrigel scaffold combined with rat dental follicle stem/precursor cells promoted bone formation through BMP9 induction, and also demonstrated that BMP9 stimulated the osteogenic differentiation of rat dental follicle stem/precursor cells using matrigel as

an injectable scaffold (Fu et al., 2019). Overall, these studies indicate that ASCs combined with 3D aNFC could have a substantial potential to be an excellent therapeutic tool for bone recovery.

Although the exact mechanism for supporting osteogenic differentiation of ASCs in 3D is not known, aNFC hydrogel represents a promising therapy option for osteoporosis and osteoporotic fractures. Its use allows an effective bone recovery in MSC-based therapies.

7.2.3. Evaluating the effects of ES on the osteogenic potential of ASCs in 3D

To address the current limitations of bone fracture treatment using MSCs, techniques have focused on biophysical factors including nano- and macrotopology (Greiner et al., 2019a, Vordemvenne et al., 2020), substrate stiffness (Olivares-Navarrete et al., 2017), fluid shear stress (Yourek et al., 2010), nanovibration-induced displacement (Tsimbouri et al., 2017, Orapiriyakul et al., 2020) and ES have been investigated (Eischen-Loges et al., 2018, Chen et al., 2019). ES has been an attractive treatment to heal bone fractures for over 40 years (Aleem et al., 2016). A meta-analysis of randomized sham-controlled trials to assess the influence of ES in patients with fractures showed that patients experience lower pain levels and have decreased levels of radiographic non-union (Aleem et al., 2016).

The data presented in Chapter 5 showed that ES increased the osteogenic differentiation potential of ASCs under both 2D and 3D culture conditions and found no negative effects on cell viability at a frequency of 10Hz, 0.1 V/cm and 0.4 ms pulse width alternating current. This is in accordance with a study by Eischen-Loges et al. (2018) who found an increase in the osteogenic potential of BM-MSCs at 7 days and 14 days when the cells were treated with ES (0.1 V/cm for 1 h per day) (Eischen-Loges et al., 2018). Furthermore, ES resulted in an enhanced pro-osteogenic activity with RunX2 expression and ALP activity (Eischen-Loges et al., 2018). Another *in vitro* study showed a significant positive effect of ES on osteogenic differentiation (Leppik et al., 2018). In addition, ES increased the expression levels of OCN and OPN in 2D cell culture at days 7, 14 and 21 (Chapter 5). Moreover, ES resulted in a high level of calcium deposition in ASCs in 2D under osteogenic conditions. Contrary to the data in 2D, ASCs embedded into 3D aNFC exposed to ES moderately decreased their viability in both a standard and an osteogenic

differentiation media. ES also resulted in increased ALP activity and higher levels of calcium deposition in ASCs in 3D aNFC under osteogenic conditions. Similarly, ES resulted in an increase in the protein level of OCN in ASCs at day 21 whereas the protein level of OPN was unaffected. The major findings presented in Chapter 5 are in accordance with those of Wang et al. (2016a) who found that ES with a direct current (0.2 V/mm, 4 h) resulted in an increased osteogenic differentiation of rat BM-MSCs (Wang et al., 2016a). These observations are also supported by (Eischen-Loges et al., 2018) who reported on BM-MSCs exposed to 100 mV/mm of direct current ES for 3, 7 and 14 days. Their results showed that 3 days of ES treatment was insufficient to encourage a pro-osteogenic impact on the BM-MSCs, but when treated with ES for 7 and 14 days showed a significant increase in their osteogenic differentiation potential. The impact of osteogenic differentiation potential was higher at day 14 of culture after ES treatment, as evidenced by an increased expression of RunX2, OPN, osterix and calmodulin (Eischen-Loges et al., 2018). These findings confirmed those of Zhu et al. (2017) who found that BM-MSCs exposed to direct current ES for 7 days of culture showed higher amounts of calcium deposition (Zhu et al., 2017).

The data presented in Chapter 5 showed that ASCs exposed to ES and subjected to osteogenic differentiation displayed a highly aligned actin cytoskeleton and formed cell-free pores within the 3D aNFC hydrogel. Under ES conditions, ASCs in 3D aNFC were treated with and without an osteogenic differentiation media for 21 days. The differentiated cells in 2D showed extensive stress fibres under ES conditions, whilst the differentiated cells not exposed to ES had less spread and fewer stress fibres. The ES also induced thicker stress fibres in undifferentiated cells embedded in 0.2% aNFC, compared with those exposed to no ES. This is in accordance with the findings of some studies which have demonstrated the impact of an electrical field on the reorganisation of the cytoskeleton (Sun et al., 2006) and plasma membrane receptors (Griffin and Bayat, 2011). In those studies, ES was found to be an effective therapy for bone recovery. Furthermore, cytoskeleton reorganization in mouse ASCs resulted in morphological and functional changes in response to ES (Hammerick et al., 2010, Kim et al., 2006). Directly applied ES at 100 mV/mm also showed modifications in the actin filament organisation in human MSCs (Mobini et al., 2017b). Clinical studies have also reported that ES resulted in an effective treatment for osteoarthritis and bone defects (Maziarz et al., 2016) and that pulsed

electromagnetic stimulation promotes the osteogenic differentiation of MSCs (Schwartz et al., 2008, Teven et al., 2012, Kaivosoja et al., 2015, Ongaro et al., 2014). Other studies, however, reported that BM-MSCs and MC3T3-E1 cells have a lower cell viability and osteogenic differentiation potential when exposed to ES (Zhu et al., 2017, Kumar et al., 2016, Li et al., 2016b). These conflicting results could be explained by different experimental designs, including the frequency, strength and duration of ED. Optimal parameters for ES in 3D therefore still need to be identified.

Although many studies have focused on the impact of ES on MSCs, the mechanisms to explain how cells transform the electrical stimulus into an activated signalling pathway which generates a biological output are not clear. Cai et al. emphasised the impact of primary cilia to functionally modulate ES-induced calcium oscillations in order to enhance the osteogenic potential of ASCs (Cai et al., 2017), and Zhang et al. reported that a combination of stem cells and electrical current showed changes in the cell membrane via ion channels (Zhang et al., 2016). This is consistent with the findings of Sun et al. (2007) who studied the effects of ES on the Ca^{2+} oscillation in the hMSCs differentiation when exposed to 0.1 V/cm, 1 V/cm and 10 V/cm electrical stimulus for 30 min/day for 10 days and found that ES under osteogenic differentiation conditions for 10 days increased ALP activity and decreased Ca^{2+} spikes (Sun et al., 2007). Moreover, the Ca^{2+} spikes in human MSCs contribute to the Ca^{2+} flow via the inositol triphosphate receptors (IP_3R) and voltage-gated Ca^{2+} channels (Kawano et al., 2002). The potential effects of ES on the Ca^{2+} oscillation and downstream signalling in human MSCs are shown in Figure 7.1. Liu et al. (2017) reported that a stimulation time of 1 h/day was sufficient to cause a transient change in intracellular Ca^{2+} concentration, but that 0.5 h/day and 24 h/day did not cause a transient change in intracellular Ca^{2+} concentration (Liu et al., 2017).
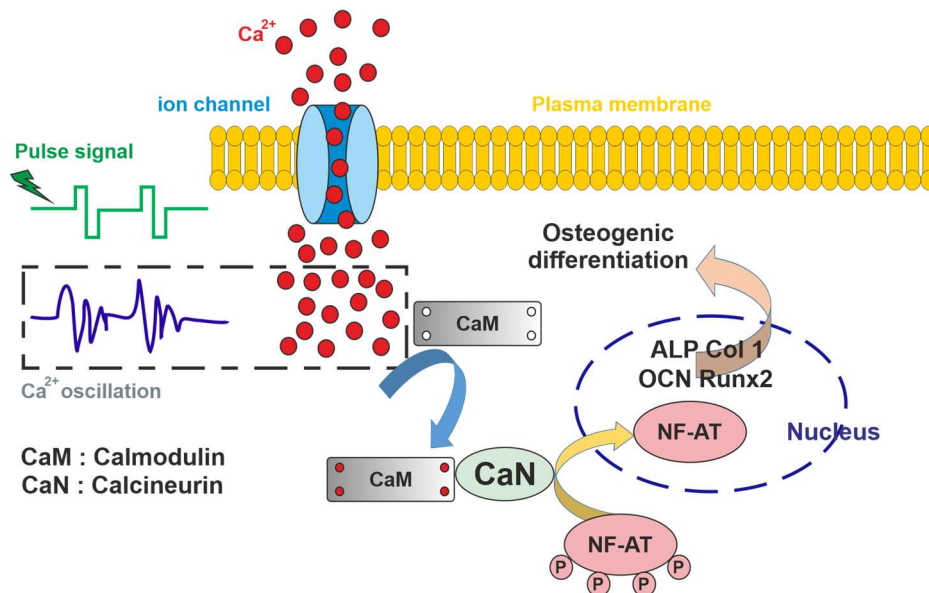
Figure 7.1. A model for the proposed effect of pulse signalling stimulation on Ca2+ oscillations and induction of osteogenic differentiation. A biphasic pulse signal promotes intracellular Ca^{2+} oscillation through calcium signalling pathways which bind four calcium ions to calmodulin (CaM). The entry of Ca^{2+} is sustained by the activation of the calcineurin (CaN)/nuclear factor of the activated T-cells (NF-AT) pathway, which is important for the regulatory T-cells. CaM activates CaN, which upregulates the expression of osteogenesis-related genes (such as ALP, Col1, OCN and RunX2) to promote osteogenic differentiation through the movement of NF-AT in the nucleus. CaM: calmodulin, CaN: calcineurin, NF-AT: nuclear factor of activated T cells, ALP: alkaline phosphatase, Col1: collagen type 1, OCN: osteocalcin, RunX2: runt-related transcription factor 2. (*Modified from* (Liu et al., 2017)).

Together with ES, calcium ion signalling supports the increased expression of osteogenesis-related genes for enhancing osteogenic differentiation (Liu et al., 2017). ES is also an effective mediator of Ca^{2+} oscillations and comprises three different activators: 1) cell surface receptors such as G-protein coupled receptors can generate the Ca^{2+} oscillations through activation of PLC (phospholipase C) and the generation of inositol-1,4,5-triphosphate (IP_3); 2) the activated ion channels: Ca^{2+} channels; and 3) important transducers such as integrins (Khatib et al., 2004). This was consistent with the current findings that Ca^{2+} oscillations in the undifferentiated ASCs showed higher amplitudes compared with differentiated cells (Chapter 4). Even though the effects of ES on Ca^{2+} oscillations in 3D were not studied, 3D aNFC hydrogel combined with ES in this current study could be a foundation for developing improved protocols for osteogenic differentiation in future *in vivo* experiments.

7.2.4. The effect of 3D cell culture combined with ES on the anti-inflammatory potential of ASCs and their secretomes

The results presented in this thesis have shown that 3D aNFC hydrogel has a significant impact on the regenerative and anti-inflammatory potential of human ASCs and their secretomes. As discussed in Chapter 6, 3D biomaterials have received attention for understanding the immune interactions between ASCs and 3D scaffolds. 3D aNFC hydrogels support the growth and differentiation of ASCs which, in combination with anti-inflammatory properties, makes aNFC hydrogel a next-generation osteoblast tissue scaffold. In the light of the facts discussed above, the regulation of inflammation is controlled through the regulation of NF-κB, which plays a central role in the expression of many genes, including pro-inflammatory cytokines (Barnes and Karin, 1997). Two important cytokines, TNF-α and IL-1β are secreted by inflammatory cells in the early inflammatory stage. These cytokines are regulated by NF-κB by means of a local inflammatory response and the activation of fibroblasts to synthesize inflammatory mediators (Jordana et al., 1994, Pang et al., 1994, Raines et al., 1989, Zucali et al., 1986, Dayer et al., 1985).

The findings presented in Chapter 6 showed that the TNF-α-induced nuclear translocation of p65 in fibroblasts was reduced when the stimulus was combined with secretomes from ASCs generated in 3D aNFC compared with secretomes from ASCs in 2D. Furthermore, a decreased level of NF-κB-dependent luciferase activity in the U251 NF-κB-Luc-GFP reporter cell line was observed when co-exposed to TNF-α and 3D secretomes compared with TNF-α and 2D secretomes. In addition, ES showed a decrease in the nuclear translocation of p65 in fibroblasts exposed to TNF-α when combined with secretomes from ASCs generated in 3D aNFC compared with secretomes from ASCs in 3D applied without an electric field. ES also resulted in a reduction in the level of NF-κB-dependent luciferase activity in reporter cells exposed to TNF-α and secretomes from ASCs generated in 2D and 3D cultures. The results presented in Chapter 6 are consistent with the result obtained from fibroblasts cultured in 3D by Htwe et al. (2015), who reported that electrospun polyethylene terephthalate scaffolds could be co-cultured with lung fibroblasts by activating NF-κB signalling with inflammatory conditions. By performing a luciferase reporter assay and immunostaining to monitor pro-inflammatory responses under *in*

vivo conditions, they also found a high level of anti-inflammatory response in 3D scaffolds (Htwe et al., 2015).

Green and Yamada found that human fibroblasts grown in a 3D cell-derived matrix showed higher proliferation compared with cells cultured in 2D (Green and Yamada, 2007). Furthermore, other studies have reported a higher regenerative potential of secretomes from 3D cultivated ASCs compared with a 2D culture (Chierchia et al., 2017) and have also reported an MSC secretome-mediated neuroprotection of SH-SY5Y neuroblastoma cells following 6-hydroxydopamine therapy when the MSCs were cultivated in bovine collagen/polyethylene glycol and collagen/low-molecular weight hyaluronic acid hydrogels. Redondo-Castro et al. (2018) showed that 3D spheroid cultures of human BM-MSCs secreted higher levels of vascular endothelial growth factor (VEGF) compared with 2D controls (Redondo-Castro et al., 2018). These findings are in accordance with those of several other studies demonstrating that 3D cultivation of ASCs results in an increased secretion of multiple growth factors including hepatocyte growth factor (HGF), VEGF, stromal cell-derived factor (SDF) and fibroblast growth factor-2 (FGF-2) (Lee et al., 2016, Kim et al., 2013b, Young et al., 2018).

Even though the exact mechanism for the increase of the anti-inflammatory potential of ASC-secretome is not known, ES could be incorporated in optimized therapy strategies for osteoporosis and osteoporotic fractures through the release of a more potent secretome. The follow-up *in vivo* data enable the development of more efficient MSC-based therapies.

7.2.5. Concluding remarks

aNFC hydrogel was used for *in vitro* 3D cell culture to assess the growth and osteogenic differentiation of ASCs. The results set out in this thesis have shown that not only are aNFC scaffolds suitable for the viability and biocompatibility of ASCs, but also that they support osteogenic differentiation of ASCs. The results obtained from this study have demonstrated that ES results in a significant increase in the osteogenic differentiation and anti-inflammatory potential of ASCs in 3D aNFC.

Consequently, this thesis contributes to new research avenues, which include the impact of ES on the osteogenic differentiation of ASCs. 3D aNFC hydrogels in

combination with ES could serve as a basis for next-generation therapies for osteoporosis and osteoporotic bone fractures. However, translating the preclinical results into the clinic will require an optimal design including both clinically compliant stem cells combined with biomaterials and optimised protocols for differentiation and ES. Future research should investigate whether ES of ASCs is able to promote similar effects in *in vivo* models, including rodent models and a large animal model (for example, sheep), which would reflect a better approximation of bone degeneration and regeneration in humans. Taken together, the preclinical data shown in this study and follow-up *in vivo* data could pave the way for new therapies for osteoporosis and osteoporotic bone fracture in humans.

7.2.6. Future directions

Even though this study and previous reports suggest that 3D cell culture in combination with ES promotes osteogenic differentiation of ASCs *in vitro*, it is yet to be determined whether similar effects can be observed in *in vivo* models of bone regeneration and in the human system. Follow-up *in vivo* experiments could include calvarial bone defect models in rodents (McGovern et al., 2018). In this scenario, bone defects would be introduced by creating a sagittal incision across the scalp of the animal. In an optimal experimental scenario, ASCs would be embedded in 3D aNFC and transplanted into the lesion site with SHAM surgery and aNFC alone serving as experimental controls. ES could be applied to the ASC-scaffold either prior to transplantation (*in vitro*) or post-transplantation (*in vivo*). More stringent *in vivo* experiments could include the transplantation of ASCs in 3D aNFC into critical-size defects in sheep models of osteoporosis. These ovine models of osteoporosis include a combination of oestrogen deficiency following ovariectomy plus a calcium-wasting diet resulting in a severely osteoporotic bone structure comparable to that seen in humans (Turner, 2002).

Although the focus of this study was on assessing the effects of ES on MSCs, it is believed that this technology is applicable to other areas of biotechnology. Other future directions could include the determination of the effect of various frequencies and amplitudes of ES on osteoclasts to examine whether this limit the rate of division and the activity of osteoclasts to reduce the levels of bone resorption. A large animal model could be used to assess this as such models represent a closer approximation to bone degeneration and regeneration in humans.

Chapter 8

References

ABEER, M., MOHD AMIN, M. C. I. & MARTIN, C. 2014. *A review of bacterial cellulose-based drug delivery systems: Their biochemistry, current approaches and future prospects*.

ABU-AMER, Y. 2013. NF-kappaB signaling and bone resorption. *Osteoporos Int,* 24**,** 2377-86.

ADEY, W. R. 1993. Biological effects of electromagnetic fields. *J Cell Biochem,* 51**,** 410-6.

AGGARWAL, S. & PITTENGER, M. F. 2005. Human mesenchymal stem cells modulate allogeneic immune cell responses. *Blood,* 105**,** 1815-22.

ALEEM, I. S., ALEEM, I., EVANIEW, N., BUSSE, J. W., YASZEMSKI, M., AGARWAL, A., EINHORN, T. & BHANDARI, M. 2016. Efficacy of Electrical Stimulators for Bone Healing: A Meta-Analysis of Randomized Sham-Controlled Trials. *Sci Rep,* 6**,** 31724.

ALMEIDA, M., AMBROGINI, E., HAN, L., MANOLAGAS, S. C. & JILKA, R. L. 2009. Increased lipid oxidation causes oxidative stress, increased peroxisome proliferator-activated receptor-gamma expression, and diminished pro-osteogenic Wnt signaling in the skeleton. *J Biol Chem,* 284**,** 27438-48.

AN, S. H., MATSUMOTO, T., MIYAJIMA, H., NAKAHIRA, A., KIM, K. H. & IMAZATO, S. 2012. Porous zirconia/hydroxyapatite scaffolds for bone reconstruction. *Dent Mater,* 28**,** 1221-31.

ASAGIRI, M. & TAKAYANAGI, H. 2007. The molecular understanding of osteoclast differentiation. *Bone,* 40**,** 251-64.

ASSIS-RIBAS, T., FORNI, M. F., WINNISCHOFER, S. M. B., SOGAYAR, M. C. & TROMBETTA-LIMA, M. 2018. Extracellular matrix dynamics during mesenchymal stem cells differentiation. *Developmental Biology,* 437**,** 63-74.

AZOIDIS, I., METCALFE, J., REYNOLDS, J., KEETON, S., HAKKI, S. S., SHEARD, J. & WIDERA, D. 2017. Three-dimensional cell culture of human mesenchymal stem cells in nanofibrillar cellulose hydrogels. *MRS Communications,* 7**,** 458-465.

AZUMA, Y., ITO, M., HARADA, Y., TAKAGI, H., OHTA, T. & JINGUSHI, S. 2001. Low-intensity pulsed ultrasound accelerates rat femoral fracture healing by acting on the various cellular reactions in the fracture callus. *J Bone Miner Res,* 16**,** 671-80.

BALIKOV, D. A., FANG, B., CHUN, Y. W., CROWDER, S. W., PRASAI, D., LEE, J. B., BOLOTIN, K. I. & SUNG, H.-J. 2016. Directing lineage specification of human mesenchymal stem cells by decoupling electrical stimulation and physical patterning on unmodified graphene. *Nanoscale,* 8**,** 13730-13739.

BALINT, R., CASSIDY, N., HIDALGO-BASTIDA, A. & CARTMELL, S. 2013. Electrical Stimulation Enhanced Mesenchymal Stem Cell Gene Expression for Orthopaedic Tissue Repair. *Journal of Biomaterials and Tissue Engineering,* 3**,** 212-221.

BARA, J. J., RICHARDS, R. G., ALINI, M. & STODDART, M. J. 2014. Concise review: Bone marrow-derived mesenchymal stem cells change phenotype following in vitro culture: implications for basic research and the clinic. *Stem Cells,* 32**,** 1713-23.

BARANIAK, P. R. & MCDEVITT, T. C. 2012. Scaffold-free culture of mesenchymal stem cell spheroids in suspension preserves multilineage potential. *Cell and Tissue Research,* 347**,** 701-711.

BARNES, P. J. & KARIN, M. 1997. Nuclear factor-kappaB: a pivotal transcription factor in chronic inflammatory diseases. *N Engl J Med,* 336**,** 1066-71.

BARONCELLI, M., VAN DER EERDEN, B. C. J., CHATTERJI, S., RULL TRINIDAD, E., KAN, Y. Y., KOEDAM, M., VAN HENGEL, I. A. J., ALVES, R. D. A. M., FRATILA-APACHITEI, L. E., DEMMERS, J. A. A., VAN DE PEPPEL, J. & VAN LEEUWEN, J. P. T. M. 2018. Human Osteoblast-Derived Extracellular Matrix with High Homology to Bone Proteome Is Osteopromotive. *Tissue Engineering Part A,* 24**,** 1377-1389.

BECKER, S. T., BOLTE, H., SCHÜNEMANN, K., SEITZ, H., BARA, J. J., BECK-BROICHSITTER, B. E., RUSSO, P. A. J., WILTFANG, J. & WARNKE, P. H. 2012. Endocultivation: the influence

of delayed vs. simultaneous application of BMP-2 onto individually formed hydroxyapatite matrices for heterotopic bone induction. *International Journal of Oral and Maxillofacial Surgery,* 41**,** 1153-1160.

BEHR, B., LEUCHT, P., LONGAKER, M. T. & QUARTO, N. 2010. Fgf-9 is required for angiogenesis and osteogenesis in long bone repair. *Proceedings of the National Academy of Sciences of the United States of America,* 107**,** 11853-11858.

BELLUCCI, D., VERONESI, E., STRUSI, V., PETRACHI, T., MURGIA, A., MASTROLIA, I., DOMINICI, M. & CANNILLO, V. 2019. Human Mesenchymal Stem Cell Combined with a New Strontium-Enriched Bioactive Glass: An ex-vivo Model for Bone Regeneration. *Materials (Basel),* 12.

BEN-DAVID, U., MAYSHAR, Y. & BENVENISTY, N. 2011. Large-scale analysis reveals acquisition of lineage-specific chromosomal aberrations in human adult stem cells. *Cell Stem Cell,* 9**,** 97-102.

BENTZ, A. T., SCHNEIDER, C. M. & WESTERLIND, K. C. 2005. The relationship between physical activity and 2-hydroxyestrone, 16alpha-hydroxyestrone, and the 2/16 ratio in premenopausal women (United States). *Cancer Causes Control,* 16**,** 455-61.

BERTOLDI, S., FARÈ, S., DENEGRI, M., ROSSI, D., HAUGEN, H. J., PAROLINI, O. & TANZI, M. C. 2010. Ability of polyurethane foams to support placenta-derived cell adhesion and osteogenic differentiation: preliminary results. *Journal of Materials Science: Materials in Medicine,* 21**,** 1005-1011.

BHATTACHARYA, M., MALINEN, M. M., LAUREN, P., LOU, Y.-R., KUISMA, S. W., KANNINEN, L., LILLE, M., CORLU, A., GUGUEN-GUILLOUZO, C., IKKALA, O., LAUKKANEN, A., URTTI, A. & YLIPERTTULA, M. 2012. Nanofibrillar cellulose hydrogel promotes three-dimensional liver cell culture. *Journal of Controlled Release,* 164**,** 291-298.

BICER, M., COTTRELL, G. S. & WIDERA, D. 2021. Impact of 3D cell culture on bone regeneration potential of mesenchymal stromal cells. *Stem Cell Research & Therapy,* 12**,** 31.

BICER, M., SHEARD, J., IANDOLO, D., BOATENG, S. Y., COTTRELL, G. S. & WIDERA, D. 2020. Electrical Stimulation of Adipose-Derived Stem Cells in 3D Nanofibrillar Cellulose Increases Their Osteogenic Potential. *Biomolecules,* 10.

BODLE, J. C., HANSON, A. D. & LOBOA, E. G. 2011. Adipose-derived stem cells in functional bone tissue engineering: lessons from bone mechanobiology. *Tissue Eng Part B Rev,* 17**,** 195-211.

BOEHNING, D., PATTERSON, R. & SNYDER, S. 2004. Apoptosis And Calcium: New Roles For Cytochrome c and Inositol 1,4,5-trisphosphate. *Cell cycle (Georgetown, Tex.),* 3**,** 252-4.

BOWERS, S. L., BANERJEE, I. & BAUDINO, T. A. 2010. The extracellular matrix: at the center of it all. *J Mol Cell Cardiol,* 48**,** 474-82.

BRADFORD, P. G., GERACE, K. V., ROLAND, R. L. & CHRZAN, B. G. 2010. Estrogen regulation of apoptosis in osteoblasts. *Physiol Behav,* 99**,** 181-5.

BRENNAN, M. A., RENAUD, A., GAMBLIN, A. L., D'ARROS, C., NEDELLEC, S., TRICHET, V. & LAYROLLE, P. 2015. 3D cell culture and osteogenic differentiation of human bone marrow stromal cells plated onto jet-sprayed or electrospun micro-fiber scaffolds. *Biomed Mater,* 10**,** 045019.

BURAND, A. J., JR., DI, L., BOLAND, L. K., BOYT, D. T., SCHRODT, M. V., SANTILLAN, D. A. & ANKRUM, J. A. 2020. Aggregation of Human Mesenchymal Stromal Cells Eliminates Their Ability to Suppress Human T Cells. *Front Immunol,* 11**,** 143.

CAI, S., BODLE, J. C., MATHIEU, P. S., AMOS, A., HAMOUDA, M., BERNACKI, S., MCCARTY, G. & LOBOA, E. G. 2017. Primary cilia are sensors of electrical field stimulation to induce osteogenesis of human adipose-derived stem cells. *The FASEB Journal,* 31**,** 346-355.

CAMACHO, P. M., PETAK, S. M., BINKLEY, N., CLARKE, B. L., HARRIS, S. T., HURLEY, D. L., KLEEREKOPER, M., LEWIECKI, E. M., MILLER, P. D., NARULA, H. S., PESSAH-POLLACK, R., TANGPRICHA, V., WIMALAWANSA, S. J. & WATTS, N. B. 2016. AMERICAN ASSOCIATION OF CLINICAL ENDOCRINOLOGISTS AND AMERICAN COLLEGE OF ENDOCRINOLOGY CLINICAL PRACTICE GUIDELINES FOR THE DIAGNOSIS AND TREATMENT OF POSTMENOPAUSAL OSTEOPOROSIS - 2016--EXECUTIVE SUMMARY. *Endocr Pract,* 22**,** 1111-8.

CAMPSIE, P., CHILDS, P. G., ROBERTSON, S. N., CAMERON, K., HOUGH, J., SALMERON-SANCHEZ, M., TSIMBOURI, P. M., VICHARE, P., DALBY, M. J. & REID, S. 2019. Design, construction and characterisation of a novel nanovibrational bioreactor and cultureware for osteogenesis. *Scientific Reports,* 9**,** 12944.

CAPLAN, A. I. 2010. What's in a name? *Tissue Eng Part A,* 16**,** 2415-7.

CAPLAN, A. I. 2017. Mesenchymal Stem Cells: Time to Change the Name! *Stem Cells Transl Med,* 6**,** 1445-1451.

CAPLAN, A. I. 2019. Medicinal signalling cells: they work, so use them. *Nature,* 566**,** 39.

CARTER, K., LEE, H. J., NA, K. S., FERNANDES-CUNHA, G. M., BLANCO, I. J., DJALILIAN, A. & MYUNG, D. 2019. Characterizing the impact of 2D and 3D culture conditions on the therapeutic effects of human mesenchymal stem cell secretome on corneal wound healing in vitro and ex vivo. *Acta Biomater,* 99**,** 247-257.

CASTRÉN, E., SILLAT, T., OJA, S., NORO, A., LAITINEN, A., KONTTINEN, Y. T., LEHENKARI, P., HUKKANEN, M. & KORHONEN, M. 2015. Osteogenic differentiation of mesenchymal stromal cells in two-dimensional and three-dimensional cultures without animal serum. *Stem Cell Research & Therapy,* 6**,** 167.

CESARZ, Z. & TAMAMA, K. 2016. Spheroid Culture of Mesenchymal Stem Cells. *Stem Cells Int,* 2016**,** 9176357.

CHANG, Y., CHO, B., KIM, S. & KIM, J. 2019. Direct conversion of fibroblasts to osteoblasts as a novel strategy for bone regeneration in elderly individuals. *Experimental & Molecular Medicine,* 51**,** 54.

CHAPARRO, O. & LINERO, I. 2016. Regenerative Medicine: A New Paradigm in Bone Regeneration. *Advanced Techniques in Bone Regeneration.*

CHARATCHAROENWITTHAYA, N., KHOSLA, S., ATKINSON, E. J., MCCREADY, L. K. & RIGGS, B. L. 2007. Effect of blockade of TNF-alpha and interleukin-1 action on bone resorption in early postmenopausal women. *J Bone Miner Res,* 22**,** 724-9.

CHAUDHURI, O., GU, L., KLUMPERS, D., DARNELL, M., BENCHERIF, S. A., WEAVER, J. C., HUEBSCH, N., LEE, H. P., LIPPENS, E., DUDA, G. N. & MOONEY, D. J. 2016. Hydrogels with tunable stress relaxation regulate stem cell fate and activity. *Nat Mater,* 15**,** 326-34.

CHEN, C., BAI, X., DING, Y. & LEE, I.-S. 2019. Electrical stimulation as a novel tool for regulating cell behavior in tissue engineering. *Biomaterials Research,* 23**,** 25.

CHEN, J. C. & JACOBS, C. R. 2013. Mechanically induced osteogenic lineage commitment of stem cells. *Stem Cell Research & Therapy,* 4**,** 107.

CHEN, Q., SHOU, P., ZHANG, L., XU, C., ZHENG, C., HAN, Y., LI, W., HUANG, Y., ZHANG, X., SHAO, C., ROBERTS, A. I., RABSON, A. B., REN, G., ZHANG, Y., WANG, Y., DENHARDT, D. T. & SHI, Y. 2014. An osteopontin-integrin interaction plays a critical role in directing adipogenesis and osteogenesis by mesenchymal stem cells. *Stem Cells,* 32**,** 327-37.

CHEN, Q., SHOU, P., ZHENG, C., JIANG, M., CAO, G., YANG, Q., CAO, J., XIE, N., VELLETRI, T., ZHANG, X., XU, C., ZHANG, L., YANG, H., HOU, J., WANG, Y. & SHI, Y. 2016. Fate decision of mesenchymal stem cells: adipocytes or osteoblasts? *Cell Death Differ,* 23**,** 1128-39.

CHIERCHIA, A., CHIRICO, N., BOERI, L., RAIMONDI, I., RIVA, G. A., RAIMONDI, M. T., TUNESI, M., GIORDANO, C., FORLONI, G. & ALBANI, D. 2017. Secretome released from hydrogel-embedded adipose mesenchymal stem cells protects against the Parkinson's disease related toxin 6-hydroxydopamine. *Eur J Pharm Biopharm,* 121**,** 113-120.

CHO, T. J., GERSTENFELD, L. C. & EINHORN, T. A. 2002. Differential temporal expression of members of the transforming growth factor beta superfamily during murine fracture healing. *J Bone Miner Res,* 17**,** 513-20.

COCHIS, A., GRAD, S., STODDART, M. J., FARÈ, S., ALTOMARE, L., AZZIMONTI, B., ALINI, M. & RIMONDINI, L. 2017. Bioreactor mechanically guided 3D mesenchymal stem cell chondrogenesis using a biocompatible novel thermo-reversible methylcellulose-based hydrogel. *Sci Rep,* 7**,** 45018.

COSMAN, F., DE BEUR, S. J., LEBOFF, M. S., LEWIECKI, E. M., TANNER, B., RANDALL, S. & LINDSAY, R. 2014. Clinician's Guide to Prevention and Treatment of Osteoporosis. *Osteoporos Int,* 25**,** 2359-81.

COSTA-PINTO, A. R., SALGADO, A. J., CORRELO, V. M., SOL, P., BHATTACHARYA, M., CHARBORD, P., REIS, R. L. & NEVES, N. M. 2008. Adhesion, proliferation, and osteogenic differentiation of a mouse mesenchymal stem cell line (BMC9) seeded on novel melt-based chitosan/polyester 3D porous scaffolds. *Tissue Eng Part A,* 14**,** 1049-57.

COUTU, D. L., FRANÇOIS, M. & GALIPEAU, J. 2012. Mesenchymal Stem Cells and Tissue Repair. *In:* ALLAN, D. S. & STRUNK, D. (eds.) *Regenerative Therapy Using Blood-Derived Stem Cells.* Totowa, NJ: Humana Press.

CRANNEY, A., PAPAIOANNOU, A., ZYTARUK, N., HANLEY, D., ADACHI, J., GOLTZMAN, D., MURRAY, T. & HODSMAN, A. 2006. Parathyroid hormone for the treatment of osteoporosis: a systematic review. *Cmaj,* 175**,** 52-9.

CUMMINGS, S. R., SAN MARTIN, J., MCCLUNG, M. R., SIRIS, E. S., EASTELL, R., REID, I. R., DELMAS, P., ZOOG, H. B., AUSTIN, M., WANG, A., KUTILEK, S., ADAMI, S., ZANCHETTA, J., LIBANATI, C., SIDDHANTI, S. & CHRISTIANSEN, C. 2009. Denosumab for prevention of fractures in postmenopausal women with osteoporosis. *N Engl J Med,* 361**,** 756-65.

DA SILVA LIMA, F., DA ROCHA ROMERO, A. B., HASTREITER, A., NOGUEIRA-PEDRO, A., MAKIYAMA, E., COLLI, C. & FOCK, R. A. 2018. An insight into the role of magnesium in the immunomodulatory properties of mesenchymal stem cells. *J Nutr Biochem,* 55**,** 200-208.

DA SILVA MEIRELLES, L., CAPLAN, A. I. & NARDI, N. B. 2008. In Search of the In Vivo Identity of Mesenchymal Stem Cells. *STEM CELLS,* 26**,** 2287-2299.

DA SILVA MEIRELLES, L., FONTES, A. M., COVAS, D. T. & CAPLAN, A. I. 2009. Mechanisms involved in the therapeutic properties of mesenchymal stem cells. *Cytokine & Growth Factor Reviews,* 20**,** 419-427.

DAS, S. & CROCKETT, J. C. 2013. Osteoporosis - a current view of pharmacological prevention and treatment. *Drug Des Devel Ther,* 7**,** 435-48.

DAY, A., FRANCIS, W., FU, K., PIEPER, I. L., GUY, O. J. & XIA, Z. 2018. Osteogenic Potential of Human Umbilical Cord Mesenchymal Stem Cells on Coralline Hydroxyapatite/Calcium Carbonate Microparticles. *Stem Cells International,* 2018**,** 1-9.

DAYER, J. M., BEUTLER, B. & CERAMI, A. 1985. Cachectin/tumor necrosis factor stimulates collagenase and prostaglandin E2 production by human synovial cells and dermal fibroblasts. *J Exp Med,* 162**,** 2163-8.

DE SALES LIMA, M. V., RIZZATO, J., GRACINDO MARQUES, D. V., KITAKAWA, D., DA SILVA PERALTA, F., PRADO SCHERMA, A. & CARVALHO, L. 2018. Denosumab Related Osteonecrosis of Jaw: a Case Report. *J Oral Maxillofac Res,* 9**,** e5.

DEL VALLE, L., DÍAZ, A. & PUIGGALÍ, J. 2017. Hydrogels for Biomedical Applications: Cellulose, Chitosan, and Protein/Peptide Derivatives. *Gels,* 3**,** 27.

DEMONTIERO, O., VIDAL, C. & DUQUE, G. 2012. Aging and bone loss: new insights for the clinician. *Ther Adv Musculoskelet Dis,* 4**,** 61-76.

DENG, J., PAN, J., HAN, X., YU, L., CHEN, J., ZHANG, W., ZHU, L., HUANG, W., LIU, S., YOU, Z. & LIU, Y. 2020. PDGFBB-modified stem cells from apical papilla and thermosensitive hydrogel scaffolds induced bone regeneration. *Chemico-Biological Interactions,* 316**,** 108931.

DI NICOLA, M., CARLO-STELLA, C., MAGNI, M., MILANESI, M., LONGONI, P. D., MATTEUCCI, P., GRISANTI, S. & GIANNI, A. M. 2002. Human bone marrow stromal cells suppress T-lymphocyte proliferation induced by cellular or nonspecific mitogenic stimuli. *Blood,* 99**,** 3838-43.

DIMITRIOU, R., JONES, E., MCGONAGLE, D. & GIANNOUDIS, P. V. 2011a. Bone regeneration: current concepts and future directions. *BMC Med,* 9**,** 66.

DIMITRIOU, R., JONES, E., MCGONAGLE, D. & GIANNOUDIS, P. V. 2011b. Bone regeneration: current concepts and future directions. *BMC Medicine,* 9**,** 66.

DOMINICI, M., LE BLANC, K., MUELLER, I., SLAPER-CORTENBACH, I., MARINI, F., KRAUSE, D., DEANS, R., KEATING, A., PROCKOP, D. & HORWITZ, E. 2006a. Minimal criteria for defining multipotent mesenchymal stromal cells. The International Society for Cellular Therapy position statement. *Cytotherapy,* 8**,** 315-7.

DOMINICI, M., LE BLANC, K., MUELLER, I., SLAPER-CORTENBACH, I., MARINI, F. C., KRAUSE, D. S., DEANS, R. J., KEATING, A., PROCKOP, D. J. & HORWITZ, E. M. 2006b. Minimal criteria for defining multipotent mesenchymal stromal cells. The International Society for Cellular Therapy position statement. *Cytotherapy,* 8**,** 315-317.

DRAKE, M. T., CLARKE, B. L. & KHOSLA, S. 2008. Bisphosphonates: mechanism of action and role in clinical practice. *Mayo Clin Proc,* 83**,** 1032-45.

DRURY, J. L. & MOONEY, D. J. 2003. Hydrogels for tissue engineering: scaffold design variables and applications. *Biomaterials,* 24**,** 4337-4351.

DUMANIAN, Z. P., TOLLEMAR, V., YE, J., LU, M., ZHU, Y., LIAO, J., AMEER, G. A., HE, T. C. & REID, R. R. 2017. Repair of critical sized cranial defects with BMP9-transduced calvarial cells delivered in a thermoresponsive scaffold. *PLoS One,* 12**,** e0172327.

DUONG LE, T., LEUNG, A. T. & LANGDAHL, B. 2016. Cathepsin K Inhibition: A New Mechanism for the Treatment of Osteoporosis. *Calcif Tissue Int,* 98**,** 381-97.

DUQUE, G., HUANG, D. C., DION, N., MACORITTO, M., RIVAS, D., LI, W., YANG, X. F., LI, J., LIAN, J., MARINO, F. T., BARRALET, J., LASCAU, V., DESCHENES, C., STE-MARIE, L. G. & KREMER, R. 2011. Interferon-gamma plays a role in bone formation in vivo and rescues osteoporosis in ovariectomized mice. *J Bone Miner Res,* 26**,** 1472-83.

DUTTA, R. C. & DUTTA, A. K. 2009. Cell-interactive 3D-scaffold; advances and applications. *Biotechnol Adv,* 27**,** 334-9.

EDMONDSON, R., BROGLIE, J. J., ADCOCK, A. F. & YANG, L. 2014. Three-dimensional cell culture systems and their applications in drug discovery and cell-based biosensors. *Assay Drug Dev Technol,* 12**,** 207-18.

EGGER, D., TRIPISCIANO, C., WEBER, V., DOMINICI, M. & KASPER, C. 2018. Dynamic Cultivation of Mesenchymal Stem Cell Aggregates. *Bioengineering (Basel),* 5.

EHNERT, S., FALLDORF, K., FENTZ, A. K., ZIEGLER, P., SCHRÖTER, S., FREUDE, T., OCHS, B. G., STACKE, C., RONNIGER, M., SACHTLEBEN, J. & NUSSLER, A. K. 2015. Primary human osteoblasts with reduced alkaline phosphatase and matrix mineralization baseline capacity are responsive to extremely low frequency pulsed electromagnetic field exposure - Clinical implication possible. *Bone Rep,* 3**,** 48-56.

EHNERT, S., FENTZ, A. K., SCHREINER, A., BIRK, J., WILBRAND, B., ZIEGLER, P., REUMANN, M. K., WANG, H., FALLDORF, K. & NUSSLER, A. K. 2017. Extremely low frequency pulsed electromagnetic fields cause antioxidative defense mechanisms in human osteoblasts via induction of •O(2)(-) and H(2)O(2). *Sci Rep,* 7**,** 14544.

EINHORN, T. A. 1998. The cell and molecular biology of fracture healing. *Clin Orthop Relat Res***,** S7-21.

EISCHEN-LOGES, M., OLIVEIRA, K. M. C., BHAVSAR, M. B., BARKER, J. H. & LEPPIK, L. 2018. Pretreating mesenchymal stem cells with electrical stimulation causes sustained long-lasting pro-osteogenic effects. *PeerJ,* 6**,** e4959.

EL-SHERBINY, I. M. & YACOUB, M. H. 2013. Hydrogel scaffolds for tissue engineering: Progress and challenges. *Glob Cardiol Sci Pract,* 2013**,** 316-42.

ELEUTERI, S. & FIERABRACCI, A. 2019. Insights into the Secretome of Mesenchymal Stem Cells and Its Potential Applications. *Int J Mol Sci,* 20.

ENGLER, A. J., SEN, S., SWEENEY, H. L. & DISCHER, D. E. 2006. Matrix elasticity directs stem cell lineage specification. *Cell,* 126**,** 677-89.

FAVI, P. M., BENSON, R. S., NEILSEN, N. R., HAMMONDS, R. L., BATES, C. C., STEPHENS, C. P. & DHAR, M. S. 2013. Cell proliferation, viability, and in vitro differentiation of equine mesenchymal stem cells seeded on bacterial cellulose hydrogel scaffolds. *Mater Sci Eng C Mater Biol Appl,* 33**,** 1935-44.

FERLIN, K. M., PRENDERGAST, M. E., MILLER, M. L., KAPLAN, D. S. & FISHER, J. P. 2016. Influence of 3D printed porous architecture on mesenchymal stem cell enrichment and differentiation. *Acta Biomaterialia,* 32**,** 161-169.

FERNANDEZ-YAGUE, M. A., ABBAH, S. A., MCNAMARA, L., ZEUGOLIS, D. I., PANDIT, A. & BIGGS, M. J. 2015. Biomimetic approaches in bone tissue engineering: Integrating biological and physicomechanical strategies. *Adv Drug Deliv Rev,* 84**,** 1-29.

FERRARI, S., REGINSTER, J.-Y., BRANDI, M. L., KANIS, J. A., DEVOGELAER, J.-P., KAUFMAN, J.-M., FÉRON, J.-M., KURTH, A. & RIZZOLI, R. 2016. Unmet needs and current and future approaches for osteoporotic patients at high risk of hip fracture. *Archives of Osteoporosis,* 11**,** 37.

FINKEMEIER, C. G. 2002. Bone-grafting and bone-graft substitutes. *J Bone Joint Surg Am,* 84-a**,** 454-64.

FLORENCIO-SILVA, R., SASSO, G. R., SASSO-CERRI, E., SIMOES, M. J. & CERRI, P. S. 2015. Biology of Bone Tissue: Structure, Function, and Factors That Influence Bone Cells. *Biomed Res Int,* 2015**,** 421746.

FREGA, M., TEDESCO, M., MASSOBRIO, P., PESCE, M. & MARTINOIA, S. 2014. Network dynamics of 3D engineered neuronal cultures: a new experimental model for in-vitro electrophysiology. *Sci Rep,* 4**,** 5489.

FRIEDENSTEIN, A. J., CHAILAKHYAN, R. K., LATSINIK, N. V., PANASYUK, A. F. & KEILISS-BOROK, I. V. 1974. Stromal cells responsible for transferring the microenvironment of the hemopoietic tissues. Cloning in vitro and retransplantation in vivo. *Transplantation,* 17**,** 331-40.

FU, T., LIANG, P., SONG, J., WANG, J., ZHOU, P., TANG, Y., LI, J. & HUANG, E. 2019. Matrigel Scaffolding Enhances BMP9-induced Bone Formation in Dental Follicle Stem/Precursor Cells. *Int J Med Sci,* 16**,** 567-575.

GALIEN, R. & GARCIA, T. 1997. Estrogen receptor impairs interleukin-6 expression by preventing protein binding on the NF-kappaB site. *Nucleic acids research,* 25**,** 2424-2429.

GAO, F., CHIU, S. M., MOTAN, D. A. L., ZHANG, Z., CHEN, L., JI, H. L., TSE, H. F., FU, Q. L. & LIAN, Q. 2016. Mesenchymal stem cells and immunomodulation: current status and future prospects. *Cell Death & Disease,* 7.

GARDINIER, J. D., MOHAMED, F. & KOHN, D. H. 2015. PTH Signaling During Exercise Contributes to Bone Adaptation. *J Bone Miner Res,* 30**,** 1053-63.

GAUTHIER, O., BOULER, J. M., AGUADO, E., PILET, P. & DACULSI, G. 1998. Macroporous biphasic calcium phosphate ceramics: influence of macropore diameter and macroporosity percentage on bone ingrowth. *Biomaterials,* 19**,** 133-9.

GENGTAO, Q., SHI, Z., XU, H., YANG, B., WEIR, M., LI, G., SONG, Y., WANG, J., HU, K., WANG, P. & ZHAO, L. 2017. Bone regeneration in minipigs via calcium phosphate cement scaffold delivering autologous BMSCs and platelet-rich plasma: Bone regeneration via BMSC-CPC in minipigs. *Journal of Tissue Engineering and Regenerative Medicine,* 12.

GOH, T. K., ZHANG, Z. Y., CHEN, A. K., REUVENY, S., CHOOLANI, M., CHAN, J. K. & OH, S. K. 2013. Microcarrier culture for efficient expansion and osteogenic differentiation of human fetal mesenchymal stem cells. *Biores Open Access,* 2**,** 84-97.

GRAYSON, W. L., BHUMIRATANA, S., CANNIZZARO, C. & VUNJAK-NOVAKOVIC, G. 2011. Bioreactor cultivation of functional bone grafts. *Methods Mol Biol,* 698**,** 231-41.

GREEN, J. A. & YAMADA, K. M. 2007. Three-dimensional microenvironments modulate fibroblast signaling responses. *Adv Drug Deliv Rev,* 59**,** 1293-8.

GREINER, J. F., GOTTSCHALK, M., FOKIN, N., BÜKER, B., KALTSCHMIDT, B. P., DREYER, A., VORDEMVENNE, T., KALTSCHMIDT, C., HÜTTEN, A. & KALTSCHMIDT, B. 2019a. Natural and synthetic nanopores directing osteogenic differentiation of human stem cells. *Nanomedicine : nanotechnology, biology, and medicine,* 17**,** 319-328.

GREINER, J. F., GOTTSCHALK, M., FOKIN, N., BÜKER, B., KALTSCHMIDT, B. P., DREYER, A., VORDEMVENNE, T., KALTSCHMIDT, C., HÜTTEN, A. & KALTSCHMIDT, B. 2019b. Natural and synthetic nanopores directing osteogenic differentiation of human stem cells. *Nanomedicine,* 17**,** 319-328.

GRIFFIN, M. & BAYAT, A. 2011. Electrical stimulation in bone healing: critical analysis by evaluating levels of evidence. *Eplasty,* 11**,** e34.

GUARINO, V., SCAGLIONE, S., SANDRI, M., ALVAREZ-PEREZ, M. A., TAMPIERI, A., QUARTO, R. & AMBROSIO, L. 2014. MgCHA particles dispersion in porous PCL scaffolds: in vitro mineralization and in vivo bone formation. *J Tissue Eng Regen Med,* 8**,** 291-303.

GUEX, A. G., PUETZER, J. L., ARMGARTH, A., LITTMANN, E., STAVRINIDOU, E., GIANNELIS, E. P., MALLIARAS, G. G. & STEVENS, M. M. 2017. Highly porous scaffolds of PEDOT:PSS for bone tissue engineering. *Acta Biomater,* 62**,** 91-101.

GUO, B. & MA, P. X. 2018. Conducting Polymers for Tissue Engineering. *Biomacromolecules,* 19**,** 1764-1782.

HAMMERICK, K. E., LONGAKER, M. T. & PRINZ, F. B. 2010. In vitro effects of direct current electric fields on adipose-derived stromal cells. *Biochemical and Biophysical Research Communications,* 397**,** 12-17.

HAN, K. H., RO, H., HONG, J. H., LEE, E. M., CHO, B., YEOM, H. J., KIM, M. G., OH, K. H., AHN, C. & YANG, J. 2011. Immunosuppressive mechanisms of embryonic stem cells and mesenchymal stem cells in alloimmune response. *Transplant Immunology,* 25**,** 7-15.

HAN, S., ZHAO, Y., XIAO, Z., HAN, J., CHEN, B., CHEN, L. & DAI, J. 2012a. The three-dimensional collagen scaffold improves the stemness of rat bone marrow mesenchymal stem cells. *J Genet Genomics,* 39**,** 633-41.

HAN, S., ZHAO, Y., XIAO, Z., HAN, J., CHEN, B., CHEN, L. & DAI, J. 2012b. The Three-Dimensional Collagen Scaffold Improves the Stemness of Rat Bone Marrow Mesenchymal Stem Cells. *Journal of Genetics and Genomics,* 39**,** 633-641.

HANNA, H., ANDRE, F. M. & MIR, L. M. 2017. Electrical control of calcium oscillations in mesenchymal stem cells using microsecond pulsed electric fields. *Stem Cell Res Ther,* 8**,** 91.

HANSON, A. D., MARVEL, S. W., BERNACKI, S. H., BANES, A. J., VAN AALST, J. & LOBOA, E. G. 2009. Osteogenic effects of rest inserted and continuous cyclic tensile strain on hASC lines with disparate osteodifferentiation capabilities. *Ann Biomed Eng,* 37**,** 955-65.

HAUSCHKA, P. V. & WIANS, F. H., JR. 1989. Osteocalcin-hydroxyapatite interaction in the extracellular organic matrix of bone. *Anat Rec,* 224**,** 180-8.

HAUSSLING, V., DENINGER, S., VIDONI, L., RINDERKNECHT, H., RUOSS, M., ARNSCHEIDT, C., ATHANASOPULU, K., KEMKEMER, R., NUSSLER, A. K. & EHNERT, S. 2019. Impact of Four Protein Additives in Cryogels on Osteogenic Differentiation of Adipose-Derived Mesenchymal Stem Cells. *Bioengineering (Basel),* 6.

HAYNESWORTH, S. E., BABER, M. A. & CAPLAN, A. I. 1996. Cytokine expression by human marrow-derived mesenchymal progenitor cells in vitro: effects of dexamethasone and IL-1 alpha. *J Cell Physiol,* 166**,** 585-92.

HENCH, L. L. & POLAK, J. M. 2002. Third-generation biomedical materials. *Science,* 295**,** 1014-7.

HEO, D. N., HOSPODIUK, M. & OZBOLAT, I. T. 2019. Synergistic interplay between human MSCs and HUVECs in 3D spheroids laden in collagen/fibrin hydrogels for bone tissue engineering. *Acta Biomaterialia,* 95**,** 348-356.

HEO, D. N., KO, W.-K., BAE, M. S., BOK LEE, J., LEE, D.-W., BYUN, W., HOON LEE, C., KIM, E., JUNG, B.-Y. & KWON, I. K. 2014. *Enhanced bone regeneration with a gold nanoparticle–hydrogel complex*.

HER, G. J., WU, H. C., CHEN, M. H., CHEN, M. Y., CHANG, S. C. & WANG, T. W. 2013. Control of three-dimensional substrate stiffness to manipulate mesenchymal stem cell fate toward neuronal or glial lineages. *Acta Biomater,* 9**,** 5170-80.

HERNANDEZ-BULE, M. L., MARTINEZ-BOTAS, J., TRILLO, M. A., PAINO, C. L. & UBEDA, A. 2016. Antiadipogenic effects of subthermal electric stimulation at 448 kHz on differentiating human mesenchymal stem cells. *Mol Med Rep,* 13**,** 3895-903.

HERNLUND, E., SVEDBOM, A., IVERGÅRD, M., COMPSTON, J., COOPER, C., STENMARK, J., MCCLOSKEY, E. V., JÖNSSON, B. & KANIS, J. A. 2013. Osteoporosis in the European Union: medical management, epidemiology and economic burden. A report prepared in collaboration with the International Osteoporosis Foundation (IOF) and the European Federation of Pharmaceutical Industry Associations (EFPIA). *Arch Osteoporos,* 8**,** 136.

HO, S. S., MURPHY, K. C., BINDER, B. Y., VISSERS, C. B. & LEACH, J. K. 2016. Increased Survival and Function of Mesenchymal Stem Cell Spheroids Entrapped in Instructive Alginate Hydrogels. *Stem Cells Transl Med,* 5**,** 773-81.

HOFMANN, A., RITZ, U., HESSMANN, M. H., ALINI, M., ROMMENS, P. M. & ROMPE, J. D. 2008. Extracorporeal shock wave-mediated changes in proliferation, differentiation, and gene expression of human osteoblasts. *J Trauma,* 65**,** 1402-10.

HOLICK, M. F. 2006. Resurrection of vitamin D deficiency and rickets. *J Clin Invest,* 116**,** 2062-72.

HTWE, S. S., HARRINGTON, H., KNOX, A., ROSE, F., AYLOTT, J., HAYCOCK, J. W. & GHAEMMAGHAMI, A. M. 2015. Investigating NF-κB signaling in lung fibroblasts in 2D and 3D culture systems. *Respir Res,* 16**,** 144.

HUANG, X., DAS, R., PATEL, A. & NGUYEN, T. D. 2018. Physical Stimulations for Bone and Cartilage Regeneration. *Regen Eng Transl Med,* 4**,** 216-237.

HUEBSCH, N., ARANY, P. R., MAO, A. S., SHVARTSMAN, D., ALI, O. A., BENCHERIF, S. A., RIVERA-FELICIANO, J. & MOONEY, D. J. 2010. Harnessing traction-mediated manipulation of the cell/matrix interface to control stem-cell fate. *Nature Materials,* 9**,** 518-526.

HUERTA, M., RIVNAY, J., RAMUZ, M., HAMA, A. & OWENS, R. 2015. Research Update: Electrical monitoring of cysts using organic electrochemical transistors. *APL Materials,* 3**,** 030701.

HUGHES, C. S., POSTOVIT, L. M. & LAJOIE, G. A. 2010. Matrigel: a complex protein mixture required for optimal growth of cell culture. *Proteomics,* 10**,** 1886-90.

HUNG, S. C., POCHAMPALLY, R. R., CHEN, S. C., HSU, S. C. & PROCKOP, D. J. 2007. Angiogenic effects of human multipotent stromal cell conditioned medium activate the PI3K-Akt pathway in hypoxic endothelial cells to inhibit apoptosis, increase survival, and stimulate angiogenesis. *Stem Cells,* 25**,** 2363-70.

HUSSEY, G. S., DZIKI, J. L. & BADYLAK, S. F. 2018. Extracellular matrix-based materials for regenerative medicine. *Nature Reviews Materials,* 3**,** 159-173.

HWANG, J. H., LEE, D. H., BYUN, M. R., KIM, A. R., KIM, K. M., PARK, J. I., OH, H. T., HWANG, E. S., LEE, K. B. & HONG, J. H. 2017. Nanotopological plate stimulates osteogenic differentiation through TAZ activation. *Sci Rep,* 7**,** 3632.

IANDOLO, D., SHEARD, J., KARAVITAS LEVY, G., PITSALIDIS, C., TAN, E., DENNIS, A., KIM, J.-S., MARKAKI, A. E., WIDERA, D. & OWENS, R. M. 2020. Biomimetic and electroactive 3D scaffolds for human neural crest-derived stem cell expansion and osteogenic differentiation. *MRS Communications,* 10**,** 179-187.

IAQUINTA, M. R., MAZZONI, E., BONONI, I., ROTONDO, J. C., MAZZIOTTA, C., MONTESI, M., SPRIO, S., TAMPIERI, A., TOGNON, M. & MARTINI, F. 2019. Adult Stem Cells for Bone Regeneration and Repair. *Front Cell Dev Biol,* 7**,** 268.

IHN, H. J., KIM, J. A., CHO, H. S., SHIN, H. I., KIM, G. Y., CHOI, Y. H., JEON, Y. J. & PARK, E. K. 2017. Diphlorethohydroxycarmalol from Ishige okamurae Suppresses Osteoclast Differentiation by Downregulating the NF-kappaB Signaling Pathway. *Int J Mol Sci,* 18.

ISAKSSON, E., WANG, H., SAHLIN, L., VON SCHOULTZ, B., MASIRONI, B., VON SCHOULTZ, E. & CLINE, J. M. 2002. Expression of estrogen receptors (alpha, beta) and insulin-like growth factor-I in breast tissue from surgically postmenopausal cynomolgus macaques after long-term treatment with HRT and tamoxifen. *Breast,* 11**,** 295-300.

ITO, M., AZUMA, Y., OHTA, T. & KOMORIYA, K. 2000. Effects of ultrasound and 1,25-dihydroxyvitamin D3 on growth factor secretion in co-cultures of osteoblasts and endothelial cells. *Ultrasound Med Biol,* 26**,** 161-6.

ITOH, S., NAKAMURA, S., NAKAMURA, M., SHINOMIYA, K. & YAMASHITA, K. 2006. Enhanced bone ingrowth into hydroxyapatite with interconnected pores by Electrical Polarization. *Biomaterials,* 27**,** 5572-9.

JAFAR, H., ABUARQOUB, D., ABABNEH, N., HASAN, M., AL-SOTARI, S., ASLAM, N., KAILANI, M., AMMOUSH, M., SHRAIDEH, Z. & AWIDI, A. 2019. hPL promotes osteogenic differentiation of stem cells in 3D scaffolds. *PLOS ONE,* 14**,** e0215667.

JANDT, K. D. 2007. Evolutions, Revolutions and Trends in Biomaterials Science – A Perspective. *Advanced Engineering Materials,* 9**,** 1035-1050.

JIANG, T., CARBONE, E. J., LO, K. W. H. & LAURENCIN, C. T. 2015. Electrospinning of polymer nanofibers for tissue regeneration. *Progress in Polymer Science,* 46**,** 1-24.

JIMI, E., HIRATA, S., OSAWA, K., TERASHITA, M., KITAMURA, C. & FUKUSHIMA, H. 2012. The current and future therapies of bone regeneration to repair bone defects. *Int J Dent,* 2012**,** 148261.

JING, D., ZHAI, M., TONG, S., XU, F., CAI, J., SHEN, G., WU, Y., LI, X., XIE, K., LIU, J., XU, Q. & LUO, E. 2016. Pulsed electromagnetic fields promote osteogenesis and osseointegration of porous titanium implants in bone defect repair through a Wnt/β-catenin signaling-associated mechanism. *Scientific Reports,* 6**,** 32045.

JOHNELL, O. & KANIS, J. A. 2006. An estimate of the worldwide prevalence and disability associated with osteoporotic fractures. *Osteoporos Int,* 17**,** 1726-33.

JORDANA, M., SÄRNSTRAND, B., SIME, P. J. & RAMIS, I. 1994. Immune-inflammatory functions of fibroblasts. *Eur Respir J,* 7**,** 2212-22.

KAIGLER, D., PAGNI, G., PARK, C. H., BRAUN, T. M., HOLMAN, L. A., YI, E., TARLE, S. A., BARTEL, R. L. & GIANNOBILE, W. V. 2013. Stem cell therapy for craniofacial bone regeneration: a randomized, controlled feasibility trial. *Cell Transplant,* 22**,** 767-77.

KAIVOSOJA, E., SARIOLA, V., CHEN, Y. & KONTTINEN, Y. T. 2015. The effect of pulsed electromagnetic fields and dehydroepiandrosterone on viability and osteo-induction of human mesenchymal stem cells. *Journal of Tissue Engineering and Regenerative Medicine,* 9**,** 31-40.

KAJIYA, H. 2012. Calcium signaling in osteoclast differentiation and bone resorption. *Adv Exp Med Biol,* 740**,** 917-32.

KANG, B.-J., RYU, H.-H., PARK, S. S., KIM, Y., WOO, H.-M., KIM, W. & KWEON, O. 2012a. Effect of Matrigel on the Osteogenic Potential of Canine Adipose Tissue-Derived Mesenchymal Stem Cells. *The Journal of veterinary medical science / the Japanese Society of Veterinary Science,* 74**,** 827-36.

KANG, B. J., RYU, H. H., PARK, S. S., KIM, Y., WOO, H. M., KIM, W. H. & KWEON, O. K. 2012b. Effect of matrigel on the osteogenic potential of canine adipose tissue-derived mesenchymal stem cells. *J Vet Med Sci,* 74**,** 827-36.

KARGOZAR, S., MOZAFARI, M., HASHEMIAN, S. J., BROUKI MILAN, P., HAMZEHLOU, S., SOLEIMANI, M., JOGHATAEI, M. T., GHOLIPOURMALEKABADI, M., KOROURIAN, A., MOUSAVIZADEH, K. & SEIFALIAN, A. M. 2018. Osteogenic potential of stem cells-seeded bioactive nanocomposite scaffolds: A comparative study between human mesenchymal stem cells derived from bone, umbilical cord Wharton's jelly, and adipose tissue. *J Biomed Mater Res B Appl Biomater,* 106**,** 61-72.

KARSENTY, G. 2001. Minireview: transcriptional control of osteoblast differentiation. *Endocrinology,* 142**,** 2731-3.

KATT, M. E., PLACONE, A. L., WONG, A. D., XU, Z. S. & SEARSON, P. C. 2016. In Vitro Tumor Models: Advantages, Disadvantages, Variables, and Selecting the Right Platform. *Front Bioeng Biotechnol,* 4**,** 12.

KAWANO, S., SHOJI, S., ICHINOSE, S., YAMAGATA, K., TAGAMI, M. & HIRAOKA, M. 2002. Characterization of Ca(2+) signaling pathways in human mesenchymal stem cells. *Cell Calcium,* 32**,** 165-74.

KEMPEN, D. H. R., CREEMERS, L. B., ALBLAS, J., LU, L., VERBOUT, A. J., YASZEMSKI, M. J. & DHERT, W. J. A. 2010. Growth Factor interactions in bone regeneration. *Tissue Engineering - Part B: Reviews,* 16**,** 551-566.

KENNEL, K. A. & DRAKE, M. T. 2009. Adverse effects of bisphosphonates: implications for osteoporosis management. *Mayo Clin Proc,* 84**,** 632-7; quiz 638.

KERSCHAN-SCHINDL, K. 2020. Romosozumab: a novel bone anabolic treatment option for osteoporosis? *Wien Med Wochenschr,* 170**,** 124-131.

KESELOWSKY, B. G., WANG, L., SCHWARTZ, Z., GARCIA, A. J. & BOYAN, B. D. 2007. Integrin alpha(5) controls osteoblastic proliferation and differentiation responses to titanium substrates presenting different roughness characteristics in a roughness independent manner. *J Biomed Mater Res A,* 80**,** 700-10.

KHAN, A. U., QU, R., FAN, T., OUYANG, J. & DAI, J. 2020. A glance on the role of actin in osteogenic and adipogenic differentiation of mesenchymal stem cells. *Stem Cell Research & Therapy,* 11**,** 283.

KHATIB, L., GOLAN, D. E. & CHO, M. 2004. Physiologic electrical stimulation provokes intracellular calcium increase mediated by phospholipase C activation in human osteoblasts. *Faseb j,* 18**,** 1903-5.

KHOSLA, S. 2001. Minireview: the OPG/RANKL/RANK system. *Endocrinology,* 142**,** 5050-5.

KHOSLA, S., MELTON, L. J., 3RD, ATKINSON, E. J. & O'FALLON, W. M. 2001. Relationship of serum sex steroid levels to longitudinal changes in bone density in young versus elderly men. *J Clin Endocrinol Metab,* 86**,** 3555-61.

KIM, H.-N., IYER, S., RING, R. & ALMEIDA, M. 2018. Chapter Six - The Role of FoxOs in Bone Health and Disease. *In:* GHAFFARI, S. (ed.) *Current Topics in Developmental Biology.* Academic Press.

KIM, I. L., KHETAN, S., BAKER, B. M., CHEN, C. S. & BURDICK, J. A. 2013a. Fibrous hyaluronic acid hydrogels that direct MSC chondrogenesis through mechanical and adhesive cues. *Biomaterials,* 34**,** 5571-5580.

KIM, I. S., SONG, J. K., ZHANG, Y. L., LEE, T. H., CHO, T. H., SONG, Y. M., KIM, D. K., KIM, S. J. & HWANG, S. J. 2006. Biphasic electric current stimulates proliferation and induces VEGF production in osteoblasts. *Biochimica et Biophysica Acta (BBA) - Molecular Cell Research,* 1763**,** 907-916.

KIM, J.-M., YANG, Y.-S., PARK, K. H., OH, H., GREENBLATT, M. B. & SHIM, J.-H. 2019. The ERK MAPK Pathway Is Essential for Skeletal Development and Homeostasis. *International Journal of Molecular Sciences,* 20**,** 1803.

KIM, J. H., PARK, I. S., PARK, Y., JUNG, Y., KIM, S. H. & KIM, S. H. 2013b. Therapeutic angiogenesis of three-dimensionally cultured adipose-derived stem cells in rat infarcted hearts. *Cytotherapy,* 15**,** 542-56.

KIM, T. H., OH, S. H., NA, S. Y., CHUN, S. Y. & LEE, J. H. 2012. Effect of biological/physical stimulation on guided bone regeneration through asymmetrically porous membrane. *J Biomed Mater Res A,* 100**,** 1512-20.

KINACI, A., NEUHAUS, V. & RING, D. C. 2014. Trends in bone graft use in the United States. *Orthopedics,* 37**,** e783-8.

KINGHAM, E., WHITE, K., GADEGAARD, N., DALBY, M. J. & OREFFO, R. O. C. 2013. Nanotopographical Cues Augment Mesenchymal Differentiation of Human Embryonic Stem Cells. *Small,* 9**,** 2140-2151.

KINNAIRD, T., STABILE, E., BURNETT, M. S., SHOU, M., LEE, C. W., BARR, S., FUCHS, S. & EPSTEIN, S. E. 2004. Local delivery of marrow-derived stromal cells augments collateral perfusion through paracrine mechanisms. *Circulation,* 109**,** 1543-9.

KIRSCH, M., BIRNSTEIN, L., PEPELANOVA, I., HANDKE, W., RACH, J., SELTSAM, A., SCHEPER, T. & LAVRENTIEVA, A. 2019. Gelatin-Methacryloyl (GelMA) Formulated with Human Platelet Lysate Supports Mesenchymal Stem Cell Proliferation and Differentiation and Enhances the Hydrogel's Mechanical Properties. *Bioengineering (Basel),* 6.

KLEIN-NULEND, J., BACABAC, R. G. & BAKKER, A. D. 2012. Mechanical loading and how it affects bone cells: the role of the osteocyte cytoskeleton in maintaining our skeleton. *Eur Cell Mater,* 24**,** 278-91.

KLUMPERS, D. D., ZHAO, X., MOONEY, D. J. & SMIT, T. H. 2013. Cell mediated contraction in 3D cell-matrix constructs leads to spatially regulated osteogenic differentiation. *Integr Biol (Camb),* 5**,** 1174-83.

KOHRT, W. M., BLOOMFIELD, S. A., LITTLE, K. D., NELSON, M. E. & YINGLING, V. R. 2004. Physical Activity and Bone Health. *Medicine & Science in Sports & Exercise,* 36**,** 1985-1996.

KOTOBUKI, N., KATSUBE, Y., KATOU, Y., TADOKORO, M., HIROSE, M. & OHGUSHI, H. 2008. In vivo survival and osteogenic differentiation of allogeneic rat bone marrow mesenchymal stem cells (MSCs). *Cell Transplant,* 17**,** 705-12.

KRAMPERA, M., GLENNIE, S., DYSON, J., SCOTT, D., LAYLOR, R., SIMPSON, E. & DAZZI, F. 2003. Bone marrow mesenchymal stem cells inhibit the response of naive and memory antigen-specific T cells to their cognate peptide. *Blood,* 101**,** 3722-9.

KRUM, S. A. 2011. Direct transcriptional targets of sex steroid hormones in bone. *J Cell Biochem,* 112**,** 401-8.

KUMAR, A., NUNE, K. C. & MISRA, R. D. K. 2016. Electric field-mediated growth of osteoblasts - the significant impact of dynamic flow of medium. *Biomaterials science,* 4**,** 136-144.

KWAK, H. B., KIM, J. Y., KIM, K. J., CHOI, M. K., KIM, J. J., KIM, K. M., SHIN, Y. I., LEE, M. S., KIM, H. S., KIM, J. W., CHUN, C. H., CHO, H. J., HONG, G. Y., JUHNG, S. K., YOON, K. H., PARK, B. H., BAE, J. M., HAN, J. K. & OH, J. 2009. Risedronate directly inhibits osteoclast differentiation and inflammatory bone loss. *Biol Pharm Bull,* 32**,** 1193-8.

KYURKCHIEV, D., BOCHEV, I., IVANOVA-TODOROVA, E., MOURDJEVA, M., ORESHKOVA, T., BELEMEZOVA, K. & KYURKCHIEV, S. 2014. Secretion of immunoregulatory cytokines by mesenchymal stem cells. *World J Stem Cells,* 6**,** 552-70.

LAM, A., SIM, E., SHEKARAN, A., LI, J., TEO, K.-L., GOGGI, J., SHAUL, R., BIRCH, W. & OH, S. 2019. Sub-confluent culture of human mesenchymal stromal cells on biodegradable polycaprolactone microcarriers enhances bone healing of rat calvarial defect. *Cytotherapy,* 21.

LANG, T., LEBLANC, A., EVANS, H., LU, Y., GENANT, H. & YU, A. 2004. Cortical and trabecular bone mineral loss from the spine and hip in long-duration spaceflight. *J Bone Miner Res,* 19**,** 1006-12.

LANGER, R. & TIRRELL, D. A. 2004. Designing materials for biology and medicine. *Nature,* 428**,** 487-492.

LANGHANS, S. A. 2018. Three-Dimensional in Vitro Cell Culture Models in Drug Discovery and Drug Repositioning. *Frontiers in Pharmacology,* 9.

LEE, J. H., HAN, Y. S. & LEE, S. H. 2016. Long-Duration Three-Dimensional Spheroid Culture Promotes Angiogenic Activities of Adipose-Derived Mesenchymal Stem Cells. *Biomol Ther (Seoul),* 24**,** 260-7.

LEE, S. Y., KOH, A., NIIKURA, T., OE, K., KOGA, T., DOGAKI, Y. & KUROSAKA, M. 2013. Low-intensity pulsed ultrasound enhances BMP-7-induced osteogenic differentiation of human fracture hematoma-derived progenitor cells in vitro. *J Orthop Trauma,* 27**,** 29-33.

LEI, T., LIANG, Z., LI, F., TANG, C., XIE, K., WANG, P., DONG, X., SHAN, S., JIANG, M., XU, Q., LUO, E. & SHEN, G. 2018. Pulsed electromagnetic fields (PEMF) attenuate changes in vertebral bone mass, architecture and strength in ovariectomized mice. *Bone,* 108**,** 10-19.

LENDECKEL, S., JODICKE, A., CHRISTOPHIS, P., HEIDINGER, K., WOLFF, J., FRASER, J. K., HEDRICK, M. H., BERTHOLD, L. & HOWALDT, H. P. 2004. Autologous stem cells (adipose) and fibrin glue used to treat widespread traumatic calvarial defects: case report. *J Craniomaxillofac Surg,* 32**,** 370-3.

LEPPIK, L., OLIVEIRA, K. M. C., BHAVSAR, M. B. & BARKER, J. H. 2020. Electrical stimulation in bone tissue engineering treatments. *Eur J Trauma Emerg Surg,* 46**,** 231-244.

LEPPIK, L., ZHIHUA, H., MOBINI, S., THOTTAKKATTUMANA PARAMESWARAN, V., EISCHEN-LOGES, M., SLAVICI, A., HELBING, J., PINDUR, L., OLIVEIRA, K. M. C., BHAVSAR, M. B., HUDAK, L., HENRICH, D. & BARKER, J. H. 2018. Combining electrical stimulation and tissue engineering to treat large bone defects in a rat model. *Scientific Reports,* 8**,** 6307.

LEVENTHAL, A., CHEN, G., NEGRO, A. & BOEHM, M. 2012. The benefits and risks of stem cell technology. *Oral Dis,* 18**,** 217-22.

LI, C., WANG, X., VAIS, H., THOMPSON, C. B., FOSKETT, J. K. & WHITE, C. 2007. Apoptosis regulation by Bcl-x$_L$ modulation of mammalian inositol 1,4,5-trisphosphate receptor channel isoform gating. *Proceedings of the National Academy of Sciences,* 104**,** 12565-12570.

LI, J., LIU, X., CROOK, J. M. & WALLACE, G. G. 2020. Electrical stimulation-induced osteogenesis of human adipose derived stem cells using a conductive graphene-cellulose scaffold. *Materials Science and Engineering: C,* 107**,** 110312.

LI, L., ZHANG, S., ZHANG, Y., YU, B., XU, Y. & GUAN, Z. 2009. Paracrine action mediate the antifibrotic effect of transplanted mesenchymal stem cells in a rat model of global heart failure. *Mol Biol Rep,* 36**,** 725-31.

LI, S., LIU, B., ZHANG, L. & RONG, L. 2014a. Amyloid beta peptide is elevated in osteoporotic bone tissues and enhances osteoclast function. *Bone,* 61**,** 164-75.

LI, S., YANG, B., TEGUH, D., ZHOU, L., XU, J. & RONG, L. 2016a. Amyloid β Peptide Enhances RANKL-Induced Osteoclast Activation through NF-κB, ERK, and Calcium Oscillation Signaling. *International Journal of Molecular Sciences,* 17**,** 1683.

LI, W., YEO, L. S., VIDAL, C., MCCORQUODALE, T., HERRMANN, M., FATKIN, D. & DUQUE, G. 2011. Decreased Bone Formation and Osteopenia in Lamin A/C-Deficient Mice. *Plos One,* 6.

LI, X., ZHAO, T., SUN, L., AIFANTIS, K. E., FAN, Y., FENG, Q., CUI, F. & WATARI, F. 2016b. The applications of conductive nanomaterials in the biomedical field. *Journal of Biomedical Materials Research Part A,* 104**,** 322-339.

LI, Y., LIU, M., YAN, Y. & YANG, S. T. 2014b. Neural differentiation from pluripotent stem cells: The role of natural and synthetic extracellular matrix. *World J Stem Cells,* 6**,** 11-23.

LI, Z. H., LIAO, W., ZHAO, Q., HUAN, T., FENG, P., WEI, X., YI, Y. & SHAO, N. S. 2014c. Effect of Cbfa1 on osteogenic differentiation of mesenchymal stem cells under hypoxia condition. *Int J Clin Exp Med,* 7**,** 540-8.

LIAN, J. B., STEIN, G. S., STEIN, J. L. & VAN WIJNEN, A. J. 1998. Osteocalcin gene promoter: Unlocking the secrets for regulation of osteoblast growth and differentiation. *Journal of Cellular Biochemistry***,** 62-72.

LIN, A. C., SEETO, B. L., BARTOSZKO, J. M., KHOURY, M. A., WHETSTONE, H., HO, L., HSU, C., ALI, A. S. & ALMAN, B. A. 2009. Modulating hedgehog signaling can attenuate the severity of osteoarthritis. *Nature Medicine,* 15**,** 1421-U11.

LIPS, P. 2001. Vitamin D deficiency and secondary hyperparathyroidism in the elderly: consequences for bone loss and fractures and therapeutic implications. *Endocr Rev,* 22**,** 477-501.

LIPS, P. & VAN SCHOOR, N. M. 2011. The effect of vitamin D on bone and osteoporosis. *Best Pract Res Clin Endocrinol Metab,* 25**,** 585-91.

LIU, H., LI, D., ZHANG, Y. & LI, M. 2018. Inflammation, mesenchymal stem cells and bone regeneration. *Histochemistry and Cell Biology,* 149**,** 393-404.

LIU, W., LIPNER, J., XIE, J., MANNING, C. N., THOMOPOULOS, S. & XIA, Y. 2014. Nanofiber scaffolds with gradients in mineral content for spatial control of osteogenesis. *ACS Appl Mater Interfaces,* 6**,** 2842-9.

LIU, Y., LIM, J. & TEOH, S.-H. 2013. Review: Development of clinically relevant scaffolds for vascularised bone tissue engineering. *Biotechnology Advances,* 31**,** 688-705.

LIU, Z., DONG, L., WANG, L., WANG, X., CHENG, K., LUO, Z. & WENG, W. 2017. Mediation of cellular osteogenic differentiation through daily stimulation time based on polypyrrole planar electrodes. *Scientific Reports,* 7**,** 17926.

LO, Y. P., LIU, Y. S., RIMANDO, M. G., HO, J. H., LIN, K. H. & LEE, O. K. 2016. Three-dimensional spherical spatial boundary conditions differentially regulate osteogenic differentiation of mesenchymal stromal cells. *Sci Rep,* 6**,** 21253.

LOESER, R. F., GOLDRING, S. R., SCANZELLO, C. R. & GOLDRING, M. B. 2012. Osteoarthritis: A disease of the joint as an organ. *Arthritis & Rheumatism,* 64**,** 1697-1707.

LOU, S., LV, H., YIN, P., LI, Z., TANG, P. & WANG, Y. 2019. Combination therapy with parathyroid hormone analogs and antiresorptive agents for osteoporosis: a systematic review and meta-analysis of randomized controlled trials. *Osteoporosis International,* 30**,** 59-70.

LUCA, A. C., MERSCH, S., DEENEN, R., SCHMIDT, S., MESSNER, I., SCHÄFER, K. L., BALDUS, S. E., HUCKENBECK, W., PIEKORZ, R. P., KNOEFEL, W. T., KRIEG, A. & STOECKLEIN, N. H. 2013. Impact of the 3D microenvironment on phenotype, gene expression, and EGFR inhibition of colorectal cancer cell lines. *PLoS One,* 8**,** e59689.

LUCULESCU, C. R., ACASANDREI, A. M., MUSTACIOSU, C. C., ZAMFIRESCU, M., DINESCU, M., CALIN, B. S., POPESCU, A., CHIOIBASU, D., CRISTIAN, D. & PAUN, I. A. 2018. Electrically responsive microstructured polypyrrole-polyurethane composites for stimulated osteogenesis. *Applied Surface Science,* 433**,** 166-176.

LUND, A. W., STEGEMANN, J. P. & PLOPPER, G. E. 2009. Mesenchymal Stem Cells Sense Three Dimensional Type I Collagen through Discoidin Domain Receptor 1. *Open Stem Cell J,* 1**,** 40-53.

MACLEAN, C., NEWBERRY, S., MAGLIONE, M., MCMAHON, M., RANGANATH, V., SUTTORP, M., MOJICA, W., TIMMER, M., ALEXANDER, A., MCNAMARA, M., DESAI, S. B., ZHOU, A., CHEN, S., CARTER, J., TRINGALE, C., VALENTINE, D., JOHNSEN, B. & GROSSMAN, J. 2008. Systematic review: comparative effectiveness of treatments to prevent fractures in men and women with low bone density or osteoporosis. *Ann Intern Med,* 148**,** 197-213.

MACNABB, C., PATTON, D. & HAYES, J. S. 2016. Sclerostin Antibody Therapy for the Treatment of Osteoporosis: Clinical Prospects and Challenges. *J Osteoporos,* 2016**,** 6217286.

MAJUMDAR, M. K., THIEDE, M. A., MOSCA, J. D., MOORMAN, M. & GERSON, S. L. 1998. Phenotypic and functional comparison of cultures of marrow-derived mesenchymal stem cells (MSCs) and stromal cells. *Journal of Cellular Physiology,* 176**,** 57-66.

MARTINO, M. M., MOCHIZUKI, M., ROTHENFLUH, D. A., REMPEL, S. A., HUBBELL, J. A. & BARKER, T. H. 2009. Controlling integrin specificity and stem cell differentiation in 2D and 3D environments through regulation of fibronectin domain stability. *Biomaterials,* 30**,** 1089-97.

MASON, C. & DUNNILL, P. 2009. Assessing the value of autologous and allogeneic cells for regenerative medicine. *Regen Med,* 4**,** 835-53.

MAZIARZ, A., KOCAN, B., BESTER, M., BUDZIK, S., CHOLEWA, M., OCHIYA, T. & BANAS, A. 2016. How electromagnetic fields can influence adult stem cells: positive and negative impacts. *Stem Cell Research & Therapy,* 7**,** 54.

MCCAIG, C., SONG, B. & RAJNICEK, A. 2009. Electrical dimensions in cell science. *Journal of cell science,* 122**,** 4267-76.

MCCLELLAND DESCALZO, D. L., EHNES, D. D. & ZUR NIEDEN, N. I. 2014. Stem cells for osteodegenerative diseases: current studies and future outlook. *Regen Med,* 9**,** 219-30.

MCCLUNG, M. R. 2017. Sclerostin antibodies in osteoporosis: latest evidence and therapeutic potential. *Therapeutic Advances in Musculoskeletal Disease,* 9**,** 263-270.

MCGOVERN, J. A., GRIFFIN, M. & HUTMACHER, D. W. 2018. Animal models for bone tissue engineering and modelling disease. *Dis Model Mech,* 11.

MCKEE, C. & CHAUDHRY, G. R. 2017. Advances and challenges in stem cell culture. *Colloids Surf B Biointerfaces,* 159**,** 62-77.

MEDHAT, D., RODRÍGUEZ, C. I. & INFANTE, A. 2019. Immunomodulatory Effects of MSCs in Bone Healing. *Int J Mol Sci,* 20.

MEHR, N. G., LI, X., CHEN, G., FAVIS, B. D. & HOEMANN, C. D. 2015. Pore size and LbL chitosan coating influence mesenchymal stem cell in vitro fibrosis and biomineralization in 3D porous poly(epsilon-caprolactone) scaffolds. *Journal of Biomedical Materials Research Part A,* 103**,** 2449-2459.

MEIRELLES LDA, S., FONTES, A. M., COVAS, D. T. & CAPLAN, A. I. 2009. Mechanisms involved in the therapeutic properties of mesenchymal stem cells. *Cytokine Growth Factor Rev,* 20**,** 419-27.

MERRYWEATHER, D. & ROACH, P. 2017. The need for advanced three-dimensional neural models and developing enabling technologies. *MRS Communications,* 7**,** 309-319.

MIRANDA, J. P., CAMOES, S. P., GASPAR, M. M., RODRIGUES, J. S., CARVALHEIRO, M., BARCIA, R. N., CRUZ, P., CRUZ, H., SIMOES, S. & SANTOS, J. M. 2019. The Secretome Derived From 3D-Cultured Umbilical Cord Tissue MSCs Counteracts Manifestations Typifying Rheumatoid Arthritis. *Front Immunol,* 10**,** 18.

MIRBAGHERI, M., ADIBNIA, V., HUGHES, B. R., WALDMAN, S. D., BANQUY, X. & HWANG, D. K. 2019. Advanced cell culture platforms: a growing quest for emulating natural tissues. *Materials Horizons,* 6**,** 45-71.

MISCH, C. M. 2010. Autogenous bone: is it still the gold standard? *Implant Dent,* 19**,** 361.

MITCHELL, R., MELLOWS, B., SHEARD, J., ANTONIOLI, M., KRETZ, O., CHAMBERS, D., ZEUNER, M. T., TOMKINS, J. E., DENECKE, B., MUSANTE, L., JOCH, B., DEBACQ-CHAINIAUX, F., HOLTHOFER, H., RAY, S., HUBER, T. B., DENGJEL, J., DE COPPI, P., WIDERA, D. & PATEL, K. 2019. Secretome of adipose-derived mesenchymal stem cells promotes skeletal muscle regeneration through synergistic action of extracellular vesicle cargo and soluble proteins. *Stem Cell Res Ther,* 10**,** 116.

MITNICK, M. A., GREY, A., MASIUKIEWICZ, U., BARTKIEWICZ, M., RIOS-VELEZ, L., FRIEDMAN, S., XU, L., HOROWITZ, M. C. & INSOGNA, K. 2001. Parathyroid hormone induces hepatic production of bioactive interleukin-6 and its soluble receptor. *Am J Physiol Endocrinol Metab,* 280**,** E405-12.

MIZUNO, H. 2009. Adipose-derived stem cells for tissue repair and regeneration: ten years of research and a literature review. *J Nippon Med Sch,* 76**,** 56-66.

MOBINI, S., LEPPIK, L. & BARKER, J. 2016. Direct current electrical stimulation chamber for treating cells in vitro. *BioTechniques,* 60**,** 95-98.

MOBINI, S., LEPPIK, L., THOTTAKKATTUMANA PARAMESWARAN, V. & BARKER, J. H. 2017a. In vitro effect of direct current electrical stimulation on rat mesenchymal stem cells. *PeerJ,* 5**,** e2821.

MOBINI, S., TALTS, Ü.-L., XUE, R., CASSIDY, N. & CARTMELL, S. 2017b. Electrical Stimulation Changes Human Mesenchymal Stem Cells Orientation and Cytoskeleton Organization. *Journal of Biomaterials and Tissue Engineering,* 7**,** 829-833.

MODDER, U. I., ACHENBACH, S. J., AMIN, S., RIGGS, B. L., MELTON, L. J., 3RD & KHOSLA, S. 2010. Relation of serum serotonin levels to bone density and structural parameters in women. *J Bone Miner Res,* 25**,** 415-22.

MOGHADDAM, M. M., BONAKDAR, S., SHARIATPANAHI, M. R., SHOKRGOZAR, M. A. & FAGHIHI, S. 2019. The Effect of Physical Cues on the Stem Cell Differentiation. *Curr Stem Cell Res Ther,* 14**,** 268-277.

MOHAMMED, E., EL-ZAWAHRY, M., FARRAG, A. R., ABDEL AZIZ, N., SHARAF-ELDIN, W., ABU-SHAHBA, N., MAHMOUD, M., GABER, K., ISMAIL, T., MOSSAAD, M. & ABDELALEEM, A. 2019. Osteogenic Differentiation Potential of Human Bone Marrow and Amniotic Fluid-Derived Mesenchymal Stem Cells in Vitro & in Vivo. *Open Access Macedonian Journal of Medical Sciences,* 7.

MOUNTZIARIS, P. M., TZOUANAS, S. N. & MIKOS, A. G. 2010. Dose effect of tumor necrosis factor-alpha on in vitro osteogenic differentiation of mesenchymal stem cells on biodegradable polymeric microfiber scaffolds. *Biomaterials,* 31**,** 1666-75.

MULLER, S., NICHOLSON, L., AL HARBI, N., MANCUSO, E., JONES, E., DICKINSON, A., WANG, X. N. & DALGARNO, K. 2019. Osteogenic potential of heterogeneous and CD271-enriched mesenchymal stromal cells cultured on apatite-wollastonite 3D scaffolds. *BMC Biomed Eng,* 1**,** 16.

MUNOZ-PINTO, D. J., JIMENEZ-VERGARA, A. C., HOU, Y., HAYENGA, H. N., RIVAS, A., GRUNLAN, M. & HAHN, M. S. 2012. Osteogenic potential of poly(ethylene glycol)-poly(dimethylsiloxane) hybrid hydrogels. *Tissue Eng Part A,* 18**,** 1710-9.

MUÑOZ-TORRES, M., ALONSO, G. & RAYA, M. P. 2004. Calcitonin therapy in osteoporosis. *Treat Endocrinol,* 3**,** 117-32.

MURUGAN, R. & RAMAKRISHNA, S. 2005. Development of nanocomposites for bone grafting. *Composites Science and Technology,* 65**,** 2385-2406.

NAKAMURA, M., NAGAI, A., TANAKA, Y., SEKIJIMA, Y. & YAMASHITA, K. 2010. Polarized hydroxyapatite promotes spread and motility of osteoblastic cells. *J Biomed Mater Res A,* 92**,** 783-90.

NAM, S.-S., LEE, J. C., KIM, H. J., PARK, J.-W., LEE, J.-M., SUH, J.-Y., UM, H.-S., KIM, J.-Y., LEE, Y. & KIM, Y.-G. 2016. Serotonin Inhibits Osteoblast Differentiation and Bone Regeneration in Rats. *Journal of Periodontology,* 87**,** 461-469.

NGUYEN, L. T., LIAO, S., CHAN, C. K. & RAMAKRISHNA, S. 2012. Enhanced osteogenic differentiation with 3D electrospun nanofibrous scaffolds. *Nanomedicine (Lond),* 7**,** 1561-75.

NISHIKAWA, M., AKATSU, T., KATAYAMA, Y., YASUTOMO, Y., KADO, S., KUGAI, N., YAMAMOTO, M. & NAGATA, N. 1996. Bisphosphonates act on osteoblastic cells and inhibit osteoclast formation in mouse marrow cultures. *Bone,* 18**,** 9-14.

OFFICE OF THE SURGEON, G. 2004. Reports of the Surgeon General. *Bone Health and Osteoporosis: A Report of the Surgeon General.* Rockville (MD): Office of the Surgeon General (US).

OH, S., BRAMMER, K. S., LI, Y. S. J., TENG, D., ENGLER, A. J., CHIEN, S. & JIN, S. 2009. Stem cell fate dictated solely by altered nanotube dimension. *Proceedings of the National Academy of Sciences,* 106**,** 2130-2135.

OH, S.-A., LEE, H.-Y., LEE, J., KIM, T.-H., JANG, J.-H., KIM, H.-W. & WALL, I. 2011. Collagen Three-Dimensional Hydrogel Matrix Carrying Basic Fibroblast Growth Factor for the Cultivation of Mesenchymal Stem Cells and Osteogenic Differentiation. *Tissue engineering. Part A,* 18**,** 1087-100.

OHAB, J. J., FLEMING, S., BLESCH, A. & CARMICHAEL, S. T. 2006. A neurovascular niche for neurogenesis after stroke. *J Neurosci,* 26**,** 13007-16.

OKUMURA, A., GOTO, M., GOTO, T., YOSHINARI, M., MASUKO, S., KATSUKI, T. & TANAKA, T. 2001. Substrate affects the initial attachment and subsequent behavior of human osteoblastic cells (Saos-2). *Biomaterials,* 22**,** 2263-2271.

OLIVARES-NAVARRETE, R., LEE, E. M., SMITH, K., HYZY, S. L., DOROUDI, M., WILLIAMS, J. K., GALL, K., BOYAN, B. D. & SCHWARTZ, Z. 2017. Substrate Stiffness Controls Osteoblastic and Chondrocytic Differentiation of Mesenchymal Stem Cells without Exogenous Stimuli. *PLoS One,* 12**,** e0170312.

OLIVARES-NAVARRETE, R., RAZ, P., ZHAO, G., CHEN, J., WIELAND, M., COCHRAN, D. L., CHAUDHRI, R. A., ORNOY, A., BOYAN, B. D. & SCHWARTZ, Z. 2008. Integrin alpha2beta1 plays a critical role in osteoblast response to micron-scale surface structure and surface energy of titanium substrates. *Proc Natl Acad Sci U S A,* 105**,** 15767-72.

OMINSKY, M. S., BOYCE, R. W., LI, X. & KE, H. Z. 2017. Effects of sclerostin antibodies in animal models of osteoporosis. *Bone,* 96**,** 63-75.

ONGARO, A., PELLATI, A., BAGHERI, L., FORTINI, C., SETTI, S. & DE MATTEI, M. 2014. Pulsed electromagnetic fields stimulate osteogenic differentiation in human bone marrow and adipose tissue derived mesenchymal stem cells. *Bioelectromagnetics,* 35**,** 426-436.

ORAPIRIYAKUL, W., TSIMBOURI, P. M., CHILDS, P. G., CAMPSIE, P., WELLS, J., FERNANDEZ-YAGUE, M., BURGESS, K., TANNER, K. E., TASSIERI, M., MEEK, R. M. D., VASSALLI, M., BIGGS, M. J., SALMERÓN-SÁNCHEZ, M., OREFFO, R. O. C., REID, S. & DALBY, M. J. 2020. Nanovibrational stimulation of mesenchymal stem cells induces therapeutic reactive oxygen species and inflammation for 3D bone tissue engineering. *bioRxiv***,** 2020.04.10.035568.

ORRENIUS, S., ZHIVOTOVSKY, B. & NICOTERA, P. 2003. Regulation of cell death: the calcium–apoptosis link. *Nature Reviews Molecular Cell Biology,* 4**,** 552-565.

PADIAL-MOLINA, M., O'VALLE, F., LANIS, A., MESA, F., DOHAN EHRENFEST, D. M., WANG, H. L. & GALINDO-MORENO, P. 2015. Clinical Application of Mesenchymal Stem Cells and Novel Supportive Therapies for Oral Bone Regeneration. *Biomed Res Int,* 2015**,** 341327.

PAJEROWSKI, J. D., DAHL, K. N., ZHONG, F. L., SAMMAK, P. J. & DISCHER, D. E. 2007. Physical plasticity of the nucleus in stem cell differentiation. *Proceedings of the National Academy of Sciences of the United States of America,* 104**,** 15619-15624.

PANG, G., COUCH, L., BATEY, R., CLANCY, R. & CRIPPS, A. 1994. GM-CSF, IL-1 alpha, IL-1 beta, IL-6, IL-8, IL-10, ICAM-1 and VCAM-1 gene expression and cytokine production in human duodenal fibroblasts stimulated with lipopolysaccharide, IL-1 alpha and TNF-alpha. *Clin Exp Immunol,* 96**,** 437-43.

PAPE, H. C., EVANS, A. & KOBBE, P. 2010. Autologous bone graft: properties and techniques. *J Orthop Trauma,* 24 Suppl 1**,** S36-40.

PARK, H., KIM, J. S., OH, E. J., KIM, T. J., KIM, H. M., SHIM, J. H., YOON, W. S., HUH, J. B., MOON, S. H., KANG, S. S. & CHUNG, H. Y. 2018. Effects of three-dimensionally printed polycaprolactone/beta-tricalcium phosphate scaffold on osteogenic differentiation of

adipose tissue- and bone marrow-derived stem cells. *Arch Craniofac Surg,* 19**,** 181-189.

PARK, J., BAUER, S., VON DER MARK, K. & SCHMUKI, P. 2007. Nanosize and Vitality: TiO2 Nanotube Diameter Directs Cell Fate. *Nano Letters,* 7**,** 1686-1691.

PARK, M. H., YU, Y., MOON, H. J., KO DU, Y., KIM, H. S., LEE, H., RYU, K. H. & JEONG, B. 2014. 3D culture of tonsil-derived mesenchymal stem cells in poly(ethylene glycol)-poly(L-alanine-co-L-phenyl alanine) thermogel. *Adv Healthc Mater,* 3**,** 1782-91.

PEK, Y. S., WAN, A. C. A. & YING, J. Y. 2010. The effect of matrix stiffness on mesenchymal stem cell differentiation in a 3D thixotropic gel. *Biomaterials,* 31**,** 385-391.

PERSSON, M., LEHENKARI, P. P., BERGLIN, L., TURUNEN, S., FINNILA, M. A. J., RISTELI, J., SKRIFVARS, M. & TUUKKANEN, J. 2018. Osteogenic Differentiation of Human Mesenchymal Stem cells in a 3D Woven Scaffold. *Sci Rep,* 8**,** 10457.

POLDERVAART, M. T., GOVERSEN, B., DE RUIJTER, M., ABBADESSA, A., MELCHELS, F. P. W., ONER, F. C., DHERT, W. J. A., VERMONDEN, T. & ALBLAS, J. 2017. 3D bioprinting of methacrylated hyaluronic acid (MeHA) hydrogel with intrinsic osteogenicity. *PLoS One,* 12**,** e0177628.

POURNAQI, F., GHIAEE, A., VAKILIAN, S. & ARDESHIRYLAJIMI, A. 2017. Improved proliferation and osteogenic differentiation of mesenchymal stem cells on polyaniline composited by polyethersulfone nanofibers. *Biologicals,* 45**,** 78-84.

QU, H., FU, H., HAN, Z. & SUN, Y. 2019. Biomaterials for bone tissue engineering scaffolds: a review. *RSC Advances,* 9**,** 26252-26262.

QUARTO, R., MASTROGIACOMO, M., CANCEDDA, R., KUTEPOV, S. M., MUKHACHEV, V., LAVROUKOV, A., KON, E. & MARCACCI, M. 2001. Repair of large bone defects with the use of autologous bone marrow stromal cells. *N Engl J Med,* 344**,** 385-6.

RAINES, E. W., DOWER, S. K. & ROSS, R. 1989. Interleukin-1 mitogenic activity for fibroblasts and smooth muscle cells is due to PDGF-AA. *Science,* 243**,** 393-6.

RAMPICHOVA, M., CHVOJKA, J., BUZGO, M., PROSECKA, E., MIKES, P., VYSLOUZILOVA, L., TVRDIK, D., KOCHOVA, P., GREGOR, T., LUKAS, D. & AMLER, E. 2013. Elastic three-dimensional poly (epsilon-caprolactone) nanofibre scaffold enhances migration, proliferation and osteogenic differentiation of mesenchymal stem cells. *Cell Prolif,* 46**,** 23-37.

RAMPICHOVÁ, M., CHVOJKA, J., BUZGO, M., PROSECKÁ, E., MIKEŠ, P., VYSLOUŽILOVÁ, L., TVRDÍK, D., KOCHOVÁ, P., GREGOR, T., LUKÁŠ, D. & AMLER, E. 2013. Elastic three-dimensional poly (ε-caprolactone) nanofibre scaffold enhances migration, proliferation and osteogenic differentiation of mesenchymal stem cells. *Cell Proliferation,* 46**,** 23-37.

RATH, S. N., NOOEAID, P., ARKUDAS, A., BEIER, J. P., STROBEL, L. A., BRANDL, A., ROETHER, J. A., HORCH, R. E., BOCCACCINI, A. R. & KNESER, U. 2016. Adipose- and bone marrow-derived mesenchymal stem cells display different osteogenic differentiation patterns in 3D bioactive glass-based scaffolds. *J Tissue Eng Regen Med,* 10**,** E497-e509.

RATNER, B. D., HOFFMAN, A., SCHOEN, F. J. & LEMONS, J. E. 2013. *Biomaterials Science: An Introduction to Materials: Third Edition*.

RAY, L. B. 2018. RANKL in bone homeostasis. *Science,* 362**,** 42-43.

REDONDO-CASTRO, E., CUNNINGHAM, C. J., MILLER, J., BROWN, H., ALLAN, S. M. & PINTEAUX, E. 2018. Changes in the secretome of tri-dimensional spheroid-cultured human mesenchymal stem cells in vitro by interleukin-1 priming. *Stem Cell Res Ther,* 9**,** 11.

REILLY, D. T. & BURSTEIN, A. H. 1975. The elastic and ultimate properties of compact bone tissue. *J Biomech,* 8**,** 393-405.

REZWAN, K., CHEN, Q. Z., BLAKER, J. J. & BOCCACCINI, A. R. 2006. Biodegradable and bioactive porous polymer/inorganic composite scaffolds for bone tissue engineering. *Biomaterials,* 27**,** 3413-31.

RHO, J. Y., KUHN-SPEARING, L. & ZIOUPOS, P. 1998. Mechanical properties and the hierarchical structure of bone. *Med Eng Phys,* 20**,** 92-102.

RICKERT, D., SAUERBIER, S., NAGURSKY, H., MENNE, D., VISSINK, A. & RAGHOEBAR, G. M. 2011. Maxillary sinus floor elevation with bovine bone mineral combined with either autogenous bone or autogenous stem cells: a prospective randomized clinical trial. *Clin Oral Implants Res,* 22**,** 251-8.

RODRIGUES, G. H. D., TAMEGA, I. D., DUQUE, G. & NETO, V. S. D. 2002. Severe bone changes in a case of Hutchinson-Gilford syndrome. *Annales De Genetique,* 45**,** 151-155.

ROMERO-LÓPEZ, M., LI, Z., RHEE, C., MARUYAMA, M., PAJARINEN, J., O'DONNELL, B., LIN, T.-H., LO, C.-W., HANLON, J., DUBOWITZ, R., YAO, Z., BUNNELL, B. A., LIN, H., TUAN, R. & GOODMAN, S. B. 2020. Macrophage Effects on Mesenchymal Stem Cell Osteogenesis in a Three-Dimensional in vitro Bone Model. *Tissue Engineering Part A*.

ROSETTI, E. P., MARCANTONIO, R. A., CIRELLI, J. A., ZUZA, E. P. & MARCANTONIO, E., JR. 2009. Treatment of gingival recession with collagen membrane and DFDBA: a histometric study in dogs. *Braz Oral Res,* 23**,** 307-12.

ROSS, P. D. 1996. Osteoporosis. Frequency, consequences, and risk factors. *Arch Intern Med,* 156**,** 1399-411.

ROZMAN, B., GASPERLIN, M., TINOIS-TESSONEAUD, E., PIROT, F. & FALSON, F. 2009. Simultaneous absorption of vitamins C and E from topical microemulsions using reconstructed human epidermis as a skin model. *European Journal of Pharmaceutics and Biopharmaceutics,* 72**,** 69-75.

RUMINSKI, S., OSTROWSKA, B., JAROSZEWICZ, J., SKIRECKI, T., WLODARSKI, K., SWIESZKOWSKI, W. & LEWANDOWSKA-SZUMIEL, M. 2018. Three-dimensional printed polycaprolactone-based scaffolds provide an advantageous environment for osteogenic differentiation of human adipose-derived stem cells. *J Tissue Eng Regen Med,* 12**,** e473-e485.

RUTHERFORD, R. B., MOALLI, M., FRANCESCHI, R. T., WANG, D., GU, K. & KREBSBACH, P. H. 2002. Bone morphogenetic protein-transduced human fibroblasts convert to osteoblasts and form bone in vivo. *Tissue Engineering,* 8**,** 441-452.

SAITO, A., NAGAISHI, K., IBA, K., MIZUE, Y., CHIKENJI, T., OTANI, M., NAKANO, M., OYAMA, K., YAMASHITA, T. & FUJIMIYA, M. 2018. Umbilical cord extracts improve osteoporotic abnormalities of bone marrow-derived mesenchymal stem cells and promote their therapeutic effects on ovariectomised rats. *Scientific Reports,* 8**,** 1161.

SAITO, T., FUKAI, A., MABUCHI, A., IKEDA, T., YANO, F., OHBA, S., NISHIDA, N., AKUNE, T., YOSHIMURA, N., NAKAGAWA, T., NAKAMURA, K., TOKUNAGA, K., CHUNG, U. I. & KAWAGUCHI, H. 2010. Transcriptional regulation of endochondral ossification by HIF-2alpha during skeletal growth and osteoarthritis development. *Nat Med,* 16**,** 678-86.

SANCHEZ, A. R., SHERIDAN, P. J. & KUPP, L. I. 2003. Is platelet-rich plasma the perfect enhancement factor? A current review. *Int J Oral Maxillofac Implants,* 18**,** 93-103.

SANDOR, G. K., NUMMINEN, J., WOLFF, J., THESLEFF, T., MIETTINEN, A., TUOVINEN, V. J., MANNERSTROM, B., PATRIKOSKI, M., SEPPANEN, R., MIETTINEN, S., RAUTIAINEN, M. & OHMAN, J. 2014. Adipose stem cells used to reconstruct 13 cases with cranio-maxillofacial hard-tissue defects. *Stem Cells Transl Med,* 3**,** 530-40.

SAUERBIER, S., STRICKER, A., KUSCHNIERZ, J., BUHLER, F., OSHIMA, T., XAVIER, S. P., SCHMELZEISEN, R. & GUTWALD, R. 2010. In vivo comparison of hard tissue

regeneration with human mesenchymal stem cells processed with either the FICOLL method or the BMAC method. *Tissue Eng Part C Methods,* 16**,** 215-23.

SCHINDELIN, J., ARGANDA-CARRERAS, I., FRISE, E., KAYNIG, V., LONGAIR, M., PIETZSCH, T., PREIBISCH, S., RUEDEN, C., SAALFELD, S., SCHMID, B., TINEVEZ, J. Y., WHITE, D. J., HARTENSTEIN, V., ELICEIRI, K., TOMANCAK, P. & CARDONA, A. 2012. Fiji: an open-source platform for biological-image analysis. *Nat Methods,* 9**,** 676-82.

SCHNEIDER, C. A., RASBAND, W. S. & ELICEIRI, K. W. 2012. NIH Image to ImageJ: 25 years of image analysis. *Nat Methods,* 9**,** 671-5.

SCHÜRMANN, M., WOLFF, A., WIDERA, D., HAUSER, S., HEIMANN, P., HÜTTEN, A., KALTSCHMIDT, C. & KALTSCHMIDT, B. 2014. Interaction of adult human neural crest-derived stem cells with a nanoporous titanium surface is sufficient to induce their osteogenic differentiation. *Stem Cell Res,* 13**,** 98-110.

SCHWARTZ, Z., SIMON, B. J., DURAN, M. A., BARABINO, G., CHAUDHRI, R. & BOYAN, B. D. 2008. Pulsed electromagnetic fields enhance BMP-2 dependent osteoblastic differentiation of human mesenchymal stem cells. *Journal of Orthopaedic Research,* 26**,** 1250-1255.

SEFCIK, L. S., NEAL, R. A., KASZUBA, S. N., PARKER, A. M., KATZ, A. J., OGLE, R. C. & BOTCHWEY, E. A. 2008. Collagen nanofibres are a biomimetic substrate for the serum-free osteogenic differentiation of human adipose stem cells. *J Tissue Eng Regen Med,* 2**,** 210-20.

SEIB, F. P., PREWITZ, M., WERNER, C. & BORNHÄUSER, M. 2009. Matrix elasticity regulates the secretory profile of human bone marrow-derived multipotent mesenchymal stromal cells (MSCs). *Biochemical and Biophysical Research Communications,* 389**,** 663-667.

SHAMIR, E. R. & EWALD, A. J. 2014. Three-dimensional organotypic culture: experimental models of mammalian biology and disease. *Nat Rev Mol Cell Biol,* 15**,** 647-64.

SHANG, Q., WANG, Z., LIU, W., SHI, Y., CUI, L. & CAO, Y. 2001. Tissue-engineered bone repair of sheep cranial defects with autologous bone marrow stromal cells. *J Craniofac Surg,* 12**,** 586-93; discussion 594-5.

SHEARD, J. J., BICER, M., MENG, Y., FRIGO, A., AGUILAR, R. M., VALLANCE, T. M., IANDOLO, D. & WIDERA, D. 2019. Optically Transparent Anionic Nanofibrillar Cellulose Is Cytocompatible with Human Adipose Tissue-Derived Stem Cells and Allows Simple Imaging in 3D. *Stem Cells Int,* 2019**,** 3106929.

SHEKARAN, A., SIM, E., TAN, K. Y., CHAN, J. K., CHOOLANI, M., REUVENY, S. & OH, S. 2015. Enhanced in vitro osteogenic differentiation of human fetal MSCs attached to 3D microcarriers versus harvested from 2D monolayers. *BMC Biotechnol,* 15**,** 102.

SHIN, Y., HAN, S., JEON, J. S., YAMAMOTO, K., ZERVANTONAKIS, I. K., SUDO, R., KAMM, R. D. & CHUNG, S. 2012. Microfluidic assay for simultaneous culture of multiple cell types on surfaces or within hydrogels. *Nat Protoc,* 7**,** 1247-59.

SHYU, K. G., WANG, B. W., WU, G. J., LIN, C. M. & CHANG, H. 2013. Mechanical stretch via transforming growth factor-β1 activates microRNA208a to regulate endoglin expression in cultured rat cardiac myoblasts. *Eur J Heart Fail,* 15**,** 36-45.

SIMÃO, A. M. S., YADAV, M. C., NARISAWA, S., BOLEAN, M., PIZAURO, J. M., HOYLAERTS, M. F., CIANCAGLINI, P. & LUIS MILLA, J. 2010. Proteoliposomes harboring alkaline phosphatase and nucleotide pyrophosphatase as matrix vesicle biomimetics. *Journal of Biological Chemistry,* 285**,** 7598-7609.

SIMS, N. A. & MARTIN, T. J. 2015. Coupling Signals between the Osteoclast and Osteoblast: How are Messages Transmitted between These Temporary Visitors to the Bone Surface? *Front Endocrinol (Lausanne),* 6**,** 41.

SINGH, J., ONIMOWO, J. O. & KHAN, W. S. 2015. Bone marrow derived stem cells in trauma and orthopaedics: a review of the current trend. *Curr Stem Cell Res Ther,* 10**,** 37-42.

SONG, J. K., CHO, T. H., PAN, H., SONG, Y. M., KIM, I. S., LEE, T. H., HWANG, S. J. & KIM, S. J. 2009. An electronic device for accelerating bone formation in tissues surrounding a dental implant. *Bioelectromagnetics,* 30**,** 374-84.

SONG, Y., JU, Y., SONG, G. & MORITA, Y. 2013. In vitro proliferation and osteogenic differentiation of mesenchymal stem cells on nanoporous alumina. *Int J Nanomedicine,* 8**,** 2745-56.

SPIN-NETO, R., MARCANTONIO, E., JR., GOTFREDSEN, E. & WENZEL, A. 2011. Exploring CBCT-based DICOM files. A systematic review on the properties of images used to evaluate maxillofacial bone grafts. *J Digit Imaging,* 24**,** 959-66.

STIEHLER, M., BUNGER, C., BAATRUP, A., LIND, M., KASSEM, M. & MYGIND, T. 2009. Effect of dynamic 3-D culture on proliferation, distribution, and osteogenic differentiation of human mesenchymal stem cells. *J Biomed Mater Res A,* 89**,** 96-107.

STOCKMANN, P., PARK, J., VON WILMOWSKY, C., NKENKE, E., FELSZEGHY, E., DEHNER, J. F., SCHMITT, C., TUDOR, C. & SCHLEGEL, K. A. 2012. Guided bone regeneration in pig calvarial bone defects using autologous mesenchymal stem/progenitor cells - a comparison of different tissue sources. *J Craniomaxillofac Surg,* 40**,** 310-20.

SUGA, H., ETO, H., SHIGEURA, T., INOUE, K., AOI, N., KATO, H., NISHIMURA, S., MANABE, I., GONDA, K. & YOSHIMURA, K. 2009. IFATS collection: Fibroblast growth factor-2-induced hepatocyte growth factor secretion by adipose-derived stromal cells inhibits postinjury fibrogenesis through a c-Jun N-terminal kinase-dependent mechanism. *Stem Cells,* 27**,** 238-49.

SUN, S., LIU, Y., LIPSKY, S. & CHO, M. 2007. Physical manipulation of calcium oscillations facilitates osteodifferentiation of human mesenchymal stem cells. *Faseb j,* 21**,** 1472-80.

SUN, S., TITUSHKIN, I. & CHO, M. 2006. Regulation of mesenchymal stem cell adhesion and orientation in 3D collagen scaffold by electrical stimulus. *Bioelectrochemistry,* 69**,** 133-141.

TABOAS, J. M., MADDOX, R. D., KREBSBACH, P. H. & HOLLISTER, S. J. 2003. Indirect solid free form fabrication of local and global porous, biomimetic and composite 3D polymer-ceramic scaffolds. *Biomaterials,* 24**,** 181-94.

TAKEWAKI, M., KAJIYA, M., TAKEDA, K., SASAKI, S., MOTOIKE, S., KOMATSU, N., MATSUDA, S., OUHARA, K., MIZUNO, N., FUJITA, T. & KURIHARA, H. 2017. MSC/ECM Cellular Complexes Induce Periodontal Tissue Regeneration. *Journal of Dental Research,* 96**,** 984-991.

TAN, J., XU, X., TONG, Z., LIN, J., YU, Q., LIN, Y. & KUANG, W. 2015. Decreased osteogenesis of adult mesenchymal stem cells by reactive oxygen species under cyclic stretch: a possible mechanism of age related osteoporosis. *Bone Research,* 3**,** 15003.

TARAFDER, S., BALLA, V. K., DAVIES, N. M., BANDYOPADHYAY, A. & BOSE, S. 2013. Microwave-sintered 3D printed tricalcium phosphate scaffolds for bone tissue engineering. *J Tissue Eng Regen Med,* 7**,** 631-41.

TEIXEIRA, G. Q., BARRIAS, C. C., LOURENCO, A. H. & GONCALVES, R. M. 2014. A multicompartment holder for spinner flasks improves expansion and osteogenic differentiation of mesenchymal stem cells in three-dimensional scaffolds. *Tissue Eng Part C Methods,* 20**,** 984-93.

TEVEN, C. M., GREIVES, M., NATALE, R. B., SU, Y., LUO, Q., HE, B. C., SHENAQ, D., HE, T. C. & REID, R. R. 2012. Differentiation of osteoprogenitor cells is induced by high-frequency pulsed electromagnetic fields. *J Craniofac Surg,* 23**,** 586-93.

THOMAS, T., GORI, F., KHOSLA, S., JENSEN, M. D., BURGUERA, B. & RIGGS, B. L. 1999. Leptin acts on human marrow stromal cells to enhance differentiation to osteoblasts and to inhibit differentiation to adipocytes. *Endocrinology,* 140**,** 1630-8.

TIBBITT, M. W. & ANSETH, K. S. 2009. Hydrogels as extracellular matrix mimics for 3D cell culture. *Biotechnology and Bioengineering,* 103**,** 655-663.

TIRKKONEN, L., HALONEN, H., HYTTINEN, J., KUOKKANEN, H., SIEVANEN, H., KOIVISTO, A. M., MANNERSTROM, B., SANDOR, G. K., SUURONEN, R., MIETTINEN, S. & HAIMI, S. 2011. The effects of vibration loading on adipose stem cell number, viability and differentiation towards bone-forming cells. *J R Soc Interface,* 8**,** 1736-47.

TITUSHKIN, I. & CHO, M. 2007. Modulation of cellular mechanics during osteogenic differentiation of human mesenchymal stem cells. *Biophys J,* 93**,** 3693-702.

TITUSHKIN, I. & CHO, M. 2009. Regulation of cell cytoskeleton and membrane mechanics by electric field: role of linker proteins. *Biophys J,* 96**,** 717-28.

TORTELLI, F., TASSO, R., LOIACONO, F. & CANCEDDA, R. 2010. The development of tissue-engineered bone of different origin through endochondral and intramembranous ossification following the implantation of mesenchymal stem cells and osteoblasts in a murine model. *Biomaterials,* 31**,** 242-9.

TOSTESON, A. N., BURGE, R. T., MARSHALL, D. A. & LINDSAY, R. 2008. Therapies for treatment of osteoporosis in US women: cost-effectiveness and budget impact considerations. *Am J Manag Care,* 14**,** 605-15.

TOUPADAKIS, C. A., GRANICK, J. L., SAGY, M., WONG, A., GHASSEMI, E., CHUNG, D. J., BORJESSON, D. L. & YELLOWLEY, C. E. 2013. Mobilization of endogenous stem cell populations enhances fracture healing in a murine femoral fracture model. *Cytotherapy,* 15**,** 1136-47.

TREISER, M. D., YANG, E. H., GORDONOV, S., COHEN, D. M., ANDROULAKIS, I. P., KOHN, J., CHEN, C. S. & MOGHE, P. V. 2010. Cytoskeleton-based forecasting of stem cell lineage fates. *Proc Natl Acad Sci U S A,* 107**,** 610-5.

TSAI, A. C., LIU, Y., YUAN, X. & MA, T. 2015. Compaction, fusion, and functional activation of three-dimensional human mesenchymal stem cell aggregate. *Tissue Eng Part A,* 21**,** 1705-19.

TSIMBOURI, P. M., CHILDS, P. G., PEMBERTON, G. D., YANG, J., JAYAWARNA, V., ORAPIRIYAKUL, W., BURGESS, K., GONZÁLEZ-GARCÍA, C., BLACKBURN, G., THOMAS, D., VALLEJO-GIRALDO, C., BIGGS, M. J. P., CURTIS, A. S. G., SALMERÓN-SÁNCHEZ, M., REID, S. & DALBY, M. J. 2017. Stimulation of 3D osteogenesis by mesenchymal stem cells using a nanovibrational bioreactor. *Nature Biomedical Engineering,* 1**,** 758-770.

TURINETTO, V., VITALE, E. & GIACHINO, C. 2016. Senescence in Human Mesenchymal Stem Cells: Functional Changes and Implications in Stem Cell-Based Therapy. *Int J Mol Sci,* 17.

TURNER, A. S. 2002. The sheep as a model for osteoporosis in humans. *Vet J,* 163**,** 232-9.

URQUIA EDREIRA, E. R., HAYRAPETYAN, A., WOLKE, J. G., CROES, H. J., KLYMOV, A., JANSEN, J. A. & VAN DEN BEUCKEN, J. J. 2016a. Effect of calcium phosphate ceramic substrate geometry on mesenchymal stromal cell organization and osteogenic differentiation. *Biofabrication,* 8**,** 025006.

URQUIA EDREIRA, E. R., HAYRAPETYAN, A., WOLKE, J. G. C., CROES, H. J. E., KLYMOV, A., JANSEN, J. A. & VAN DEN BEUCKEN, J. J. P. 2016b. Effect of calcium phosphate ceramic substrate geometry on mesenchymal stromal cell organization and osteogenic differentiation. *Biofabrication,* 8**,** 025006.

VALDES, A. M., SPECTOR, T. D., TAMM, A., KISAND, K., DOHERTY, S. A., DENNISON, E. M., MANGINO, M., TAMM, A., KERNA, I., HART, D. J., WHEELER, M., COOPER, C., LORIES,

R. J., ARDEN, N. K. & DOHERTY, M. 2010. Genetic variation in the SMAD3 gene is associated with hip and knee osteoarthritis. *Arthritis Rheum,* 62, 2347-52.

VALENTIM DA SILVA, R. M., BARICHELLO, P. A., MEDEIROS, M. L., DE MENDONCA, W. C., DANTAS, J. S., RONZIO, O. A., FROES, P. M. & GALADARI, H. 2013. Effect of capacitive radiofrequency on the fibrosis of patients with cellulite. *Dermatol Res Pract,* 2013, 715829.

VAN BUUL, G. M., VILLAFUERTES, E., BOS, P. K., WAARSING, J. H., KOPS, N., NARCISI, R., WEINANS, H., VERHAAR, J. A., BERNSEN, M. R. & VAN OSCH, G. J. 2012. Mesenchymal stem cells secrete factors that inhibit inflammatory processes in short-term osteoarthritic synovium and cartilage explant culture. *Osteoarthritis Cartilage,* 20, 1186-96.

VISWANATHAN, P., ONDECK, M. G., CHIRASATITSIN, S., NGAMKHAM, K., REILLY, G. C., ENGLER, A. J. & BATTAGLIA, G. 2015. 3D surface topology guides stem cell adhesion and differentiation. *Biomaterials,* 52, 140-7.

VORDEMVENNE, T., WÄHNERT, D., KOETTNITZ, J., MERTEN, M., FOKIN, N., BECKER, A., BÜKER, B., VOGEL, A., KRONENBERG, D., STANGE, R., WITTENBERG, G., GREINER, J. F., HÜTTEN, A., KALTSCHMIDT, C. & KALTSCHMIDT, B. 2020. Bone Regeneration: A Novel Osteoinductive Function of Spongostan by the Interplay between Its Nano- and Microtopography. *Cells,* 9, 654.

VULCANO, E., MURENA, L., FALVO, D. A., BAJ, A., TONIOLO, A. & CHERUBINO, P. 2013. Bone marrow aspirate and bone allograft to treat acetabular bone defects in revision total hip arthroplasty: preliminary report. *Eur Rev Med Pharmacol Sci,* 17, 2240-9.

WANG, J. R., AHMED, S. F., GADEGAARD, N., MEEK, R. M., DALBY, M. J. & YARWOOD, S. J. 2014a. Nanotopology potentiates growth hormone signalling and osteogenesis of mesenchymal stem cells. *Growth Horm IGF Res,* 24, 245-50.

WANG, P., ZHAO, L., CHEN, W., LIU, X., WEIR, M. D. & XU, H. H. K. 2014b. Stem Cells and Calcium Phosphate Cement Scaffolds for Bone Regeneration. *Journal of dental research,* 93, 618-625.

WANG, Q., ZHAO, B., LI, C., RONG, J.-S., TAO, S.-Q. & TAO, T.-Z. 2014c. Decreased proliferation ability and differentiation potential of mesenchymal stem cells of osteoporosis rat. *Asian Pacific Journal of Tropical Medicine,* 7, 358-363.

WANG, X., GAO, Y., SHI, H., LIU, N., ZHANG, W. & LI, H. 2016a. Influence of the intensity and loading time of direct current electric field on the directional migration of rat bone marrow mesenchymal stem cells. *Front Med,* 10, 286-96.

WANG, X. F., SONG, Y., LIU, Y. S., SUN, Y. C., WANG, Y. G., WANG, Y. & LYU, P. J. 2016b. Osteogenic Differentiation of Three-Dimensional Bioprinted Constructs Consisting of Human Adipose-Derived Stem Cells In Vitro and In Vivo. *PLoS One,* 11, e0157214.

WATTS, N. B., ADLER, R. A., BILEZIKIAN, J. P., DRAKE, M. T., EASTELL, R., ORWOLL, E. S. & FINKELSTEIN, J. S. 2012. Osteoporosis in men: an Endocrine Society clinical practice guideline. *J Clin Endocrinol Metab,* 97, 1802-22.

WEGST, U. G., BAI, H., SAIZ, E., TOMSIA, A. P. & RITCHIE, R. O. 2015. Bioinspired structural materials. *Nat Mater,* 14, 23-36.

WEISS, A. R. R. & DAHLKE, M. H. 2019. Immunomodulation by Mesenchymal Stem Cells (MSCs): Mechanisms of Action of Living, Apoptotic, and Dead MSCs. *Front Immunol,* 10, 1191.

WOHL, G. R., BOYD, S. K., JUDEX, S. & ZERNICKE, R. F. 2000. Functional adaptation of bone to exercise and injury. *J Sci Med Sport,* 3, 313-24.

WU, L., MAGAZ, A., WANG, T., LIU, C., DARBYSHIRE, A., LOIZIDOU, M., EMBERTON, M., BIRCHALL, M. & SONG, W. 2018. Stiffness memory of indirectly 3D-printed elastomer

nanohybrid regulates chondrogenesis and osteogenesis of human mesenchymal stem cells. *Biomaterials,* 186**,** 64-79.

XIN, X., HUSSAIN, M. & MAO, J. J. 2007. Continuing differentiation of human mesenchymal stem cells and induced chondrogenic and osteogenic lineages in electrospun PLGA nanofiber scaffold. *Biomaterials,* 28**,** 316-25.

XING, L. & BOYCE, B. F. 2005. Regulation of apoptosis in osteoclasts and osteoblastic cells. *Biochemical and Biophysical Research Communications,* 328**,** 709-720.

XUE, R., LI, J. Y.-S., YEH, Y., YANG, L. & CHIEN, S. 2013. Effects of matrix elasticity and cell density on human mesenchymal stem cells differentiation. *Journal of Orthopaedic Research,* 31**,** 1360-1365.

YAMAGUCHI, Y., OHNO, J., SATO, A., KIDO, H. & FUKUSHIMA, T. 2014. Mesenchymal stem cell spheroids exhibit enhanced in-vitro and in-vivo osteoregenerative potential. *BMC Biotechnol,* 14**,** 105.

YANG, C., HAN, B., CAO, C., YANG, D., QU, X. & WANG, X. 2018. Injectable double-network hydrogel for co-culture of vascular endothelial cells and bone marrow mesenchymal stem cells for simultaneously enhancing vascularization and osteogenesis. *Journal of Materials Chemistry B,* 6.

YANG, J., ANDRE, P., YE, L. & YANG, Y. Z. 2015. The Hedgehog signalling pathway in bone formation. *Int J Oral Sci,* 7**,** 73-9.

YANG, S., KIM, J., RYU, J. H., OH, H., CHUN, C. H., KIM, B. J., MIN, B. H. & CHUN, J. S. 2010. Hypoxia-inducible factor-2alpha is a catabolic regulator of osteoarthritic cartilage destruction. *Nat Med,* 16**,** 687-93.

YANG, X., CHEN, L., XU, X., LI, C., HUANG, C. & DENG, C. X. 2001. TGF-beta/Smad3 signals repress chondrocyte hypertrophic differentiation and are required for maintaining articular cartilage. *J Cell Biol,* 153**,** 35-46.

YE, J., WANG, J., ZHU, Y., WEI, Q., WANG, X., YANG, J., TANG, S., LIU, H., FAN, J., ZHANG, F., FARINA, E. M., MOHAMMED, M. K., ZOU, Y., SONG, D., LIAO, J., HUANG, J., GUO, D., LU, M., LIU, F., LIU, J., LI, L., MA, C., HU, X., HAYDON, R. C., LEE, M. J., REID, R. R., AMEER, G. A., YANG, L. & HE, T. C. 2016. A thermoresponsive polydiolcitrate-gelatin scaffold and delivery system mediates effective bone formation from BMP9-transduced mesenchymal stem cells. *Biomed Mater,* 11**,** 025021.

YEHYA, N., YERRAPUREDDY, A., TOBIAS, J. & MARGULIES, S. S. 2012. MicroRNA modulate alveolar epithelial response to cyclic stretch. *BMC Genomics,* 13**,** 154.

YIN, Q., XU, N., XU, D., DONG, M., SHI, X., WANG, Y., HAO, Z., ZHU, S., ZHAO, D., JIN, H. & LIU, W. 2020a. Comparison of senescence-related changes between three- and two-dimensional cultured adipose-derived mesenchymal stem cells. *Stem Cell Research & Therapy,* 11**,** 226.

YIN, Q., XU, N., XU, D., DONG, M., SHI, X., WANG, Y., HAO, Z., ZHU, S., ZHAO, D., JIN, H. & LIU, W. 2020b. Comparison of senescence-related changes between three- and two-dimensional cultured adipose-derived mesenchymal stem cells. *Stem Cell Res Ther,* 11**,** 226.

YONEMORI, K., MATSUNAGA, S., ISHIDOU, Y., MAEDA, S. & YOSHIDA, H. 1996. Early effects of electrical stimulation on osteogenesis. *Bone,* 19**,** 173-80.

YOUNG, S. A., SHERMAN, S. E., COOPER, T. T., BROWN, C., ANJUM, F., HESS, D. A., FLYNN, L. E. & AMSDEN, B. G. 2018. Mechanically resilient injectable scaffolds for intramuscular stem cell delivery and cytokine release. *Biomaterials,* 159**,** 146-160.

YOUREK, G., MCCORMICK, S. M., MAO, J. J. & REILLY, G. C. 2010. Shear stress induces osteogenic differentiation of human mesenchymal stem cells. *Regen Med,* 5**,** 713-24.

YOUSEFI, A. M., JAMES, P. F., AKBARZADEH, R., SUBRAMANIAN, A., FLAVIN, C. & OUDADESSE, H. 2016. Prospect of Stem Cells in Bone Tissue Engineering: A Review. *Stem Cells Int,* 2016**,** 6180487.

YU, L., WU, Y., LIU, J., LI, B., MA, B., LI, Y., HUANG, Z., HE, Y., WANG, H., WU, Z. & QIU, G. 2018. 3D Culture of Bone Marrow-Derived Mesenchymal Stem Cells (BMSCs) Could Improve Bone Regeneration in 3D-Printed Porous Ti6Al4V Scaffolds. *Stem Cells Int,* 2018**,** 2074021.

YU, X., TANG, X., GOHIL, S. V. & LAURENCIN, C. T. 2015. Biomaterials for Bone Regenerative Engineering. *Adv Healthc Mater,* 4**,** 1268-85.

YUAN, X., ZHOU, M., GOUGH, J., GLIDLE, A. & YIN, H. 2015. A novel culture system for modulating single cell geometry in 3D. *Acta Biomaterialia,* 24**,** 228-240.

YUAN, Y., CHEN, X., ZHANG, L., WU, J., GUO, J., ZOU, D., CHEN, B., SUN, Z., SHEN, C. & ZOU, J. 2016. The roles of exercise in bone remodeling and in prevention and treatment of osteoporosis. *Prog Biophys Mol Biol,* 122**,** 122-130.

YUAN, Y., ZHANG, L., TONG, X., ZHANG, M., ZHAO, Y., GUO, J., LEI, L., CHEN, X., TICKNER, J., XU, J. & ZOU, J. 2017. Mechanical Stress Regulates Bone Metabolism Through MicroRNAs. *J Cell Physiol,* 232**,** 1239-1245.

ZEUNER, M. T., VALLANCE, T., VAIYAPURI, S., COTTRELL, G. S. & WIDERA, D. 2017. Development and Characterisation of a Novel NF-κB Reporter Cell Line for Investigation of Neuroinflammation. *Mediators Inflamm,* 2017**,** 6209865.

ZHANG, C., LI, J., ZHANG, L., ZHOU, Y., HOU, W., QUAN, H., LI, X., CHEN, Y. & YU, H. 2012a. Effects of mechanical vibration on proliferation and osteogenic differentiation of human periodontal ligament stem cells. *Arch Oral Biol,* 57**,** 1395-407.

ZHANG, J., LI, M., KANG, E.-T. & NEOH, K. G. 2016. Electrical stimulation of adipose-derived mesenchymal stem cells in conductive scaffolds and the roles of voltage-gated ion channels. *Acta Biomaterialia,* 32**,** 46-56.

ZHANG, J., NEOH, K. G. & KANG, E.-T. 2018a. Electrical stimulation of adipose-derived mesenchymal stem cells and endothelial cells co-cultured in a conductive scaffold for potential orthopaedic applications. *Journal of Tissue Engineering and Regenerative Medicine,* 12**,** 878-889.

ZHANG, K., WANG, S., ZHOU, C., CHENG, L., GAO, X., XIE, X., SUN, J., WANG, H., WEIR, M. D., REYNOLDS, M. A., ZHANG, N., BAI, Y. & XU, H. H. K. 2018b. Advanced smart biomaterials and constructs for hard tissue engineering and regeneration. *Bone Res,* 6**,** 31.

ZHANG, Y., BOSE, T., UNGER, R. E., JANSEN, J. A., KIRKPATRICK, C. J. & VAN DEN BEUCKEN, J. 2017. Macrophage type modulates osteogenic differentiation of adipose tissue MSCs. *Cell Tissue Res,* 369**,** 273-286.

ZHANG, Z. Y., TEOH, S. H., HUI, J. H., FISK, N. M., CHOOLANI, M. & CHAN, J. K. 2012b. The potential of human fetal mesenchymal stem cells for off-the-shelf bone tissue engineering application. *Biomaterials,* 33**,** 2656-72.

ZHAO, L.-G., CHEN, S.-L., TENG, Y.-J., AN, L.-P., WANG, J., MA, J.-L. & XIA, Y.-Y. 2014. The MEK5/ERK5 pathway mediates fluid shear stress promoted osteoblast differentiation. *Connective Tissue Research,* 55**,** 96-102.

ZHENG, G., XIE, Z., WANG, P., LI, J., LI, M., CEN, S., TANG, S. A., LIU, W., YE, G., LI, Y., WANG, S., WU, X., SU, H., WU, Y. & SHEN, H. 2019. Enhanced osteogenic differentiation of mesenchymal stem cells in ankylosing spondylitis: a study based on a three-dimensional biomimetic environment. *Cell Death & Disease,* 10**,** 350.

ZHENG, P., YAO, Q., MAO, F., LIU, N., XU, Y., WEI, B. & WANG, L. 2017. Adhesion, proliferation and osteogenic differentiation of mesenchymal stem cells in 3D printed

poly-epsilon-caprolactone/hydroxyapatite scaffolds combined with bone marrow clots. *Mol Med Rep,* 16**,** 5078-5084.

ZHU, M., TANG, D., WU, Q., HAO, S., CHEN, M., XIE, C., ROSIER, R. N., O'KEEFE, R. J., ZUSCIK, M. & CHEN, D. 2009. Activation of beta-catenin signaling in articular chondrocytes leads to osteoarthritis-like phenotype in adult beta-catenin conditional activation mice. *J Bone Miner Res,* 24**,** 12-21.

ZHU, S., JING, W., HU, X., HUANG, Z., CAI, Q., AO, Y. & YANG, X. 2017. Time-dependent effect of electrical stimulation on osteogenic differentiation of bone mesenchymal stromal cells cultured on conductive nanofibers. *Journal of Biomedical Materials Research Part A,* 105**,** 3369-3383.

ZUCALI, J. R., DINARELLO, C. A., OBLON, D. J., GROSS, M. A., ANDERSON, L. & WEINER, R. S. 1986. Interleukin 1 stimulates fibroblasts to produce granulocyte-macrophage colony-stimulating activity and prostaglandin E2. *J Clin Invest,* 77**,** 1857-63.

Appendices

Appendix I

Supplement 2.1. Antibodies and fluorescent dyes

Primary antibodies

Antibody	Source	Working dilution	Supplier	Catalogue No.
Osteocalcin (G-5)	Mouse	1:100	Santa Cruz Biotechnology	SC-365797
Osteopontin (AKm2A1)	Mouse	1:100	Santa Cruz Biotechnology	SC-21742
NFκB p65 (monoclonal) (IgG1) (anti-human)	Mouse	1:100	Santa Cruz Biotechnology	SC·8008

Secondary antibodies

Antibody	Source	Working dilution	Supplier	Catalogue No.
AlexaFluor 488 IgG (goat anti-mouse)	Goat	1:300	Life Technologies Ltd.	A-11029
AlexaFluor 488 IgG (donkey anti-mouse)	Donkey	1:300	Life Technologies Ltd.	A-11034
AlexaFluor 555 IgG (goat anti-mouse)	Goat	1:300	Life Technologies Ltd.	A-11032
AlexaFluor 555 IgG (donkey anti-mouse)	Donkey	1:300	Life Technologies Ltd.	A-11037

Fluorescent dyes

Fluorescent dyes	Source	Working dilution	Supplier	Catalogue No.
Phalloidin Atto 555	N/A	1:300	Sigma-Aldrich	A-19083
AlexaFluor 647 (Phalloidin)	N/A	1:300	Thermo Fisher Scientific	A-22287
Fluorescein Isothiocyanate Isomer I (FITC/dextran)	N/A	-	Sigma-Aldrich	F7250-100MG
4',6-diamidino-2-phenylindole (DAPI)	N/A	1:2000	Sigma-Aldrich	-

Supplement 2.2. Primers and PCR reagents

PCR reagents

Taq DNA Polymerase with Standard Taq Buffer (New England Biolabs M0273). Deoxynucleotide Triphosphates (dNTPs) (Promega, dATP U1205, dCTP U1225, dGTP U1215, dTTP U1235). 100 bp DNA ladder (Promega G2101). SYBR™ Safe DNA Gel Stain (Thermo Fisher Scientific S33102).

Details of conventional real-time (RT) primers

Primer	Forward (5'-3')	Reverse (5'-3')
Bmp2	AGACCTGTATCGCAGGCACT	AAACTCCTCCGTGGGGATAG
GAPDH	CATGAGAAGTATGACAACAGCCT	AGTCCTTCCACGATACCAAAGT
RunX2	TCGCCAGGCTTCATAGCAAA	GGCCTTGGGTAAGGCAGATT
Osteocalcin	GTGCAGCCTTTGTGTCCAAG	TCAGCCAACTCGTCACAGTC
Osteopontin	GACCAGAGTGCTGAAACCCA	AGGGAGTTTCCATGAAGCCA
Osterix	CAGAGCAGGTTCCTCCACTG	CTTGAGACAGCAGGGGACAG
Vimentin	GACAATGCGTCTCTGGCACGTCTT	TCCTCCGCCTCCTGCAGGTTCTT

Size of bands and annealing temperature of conventional RT primers

Primer	Size of bands	Annealing temperature
Bmp2	193 bp	64
GAPDH	113 bp	59
RunX2	170 bp	66.1
Osteocalcin	143 bp	58.9
Osteopontin	199 bp	58.9
Osterix	187 bp	58
Vimentin	236 bp	65.6

Appendix II

Supplement 3.1. No primary antibody controls for Alexa Fluor 488 and Alexa Fluor 555 (Scale bars are the same as the other 3D images)

A) No primary Alexa 488 / max intensity projection   B) No primary Alexa 555 / max intensity projection
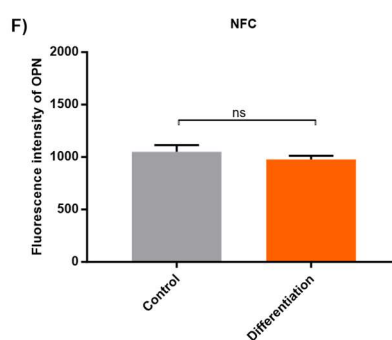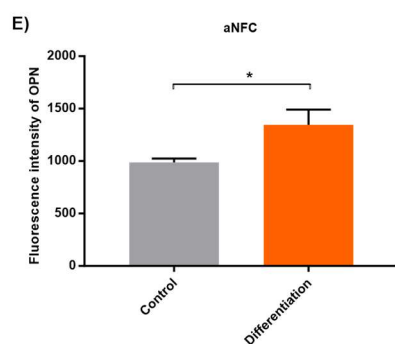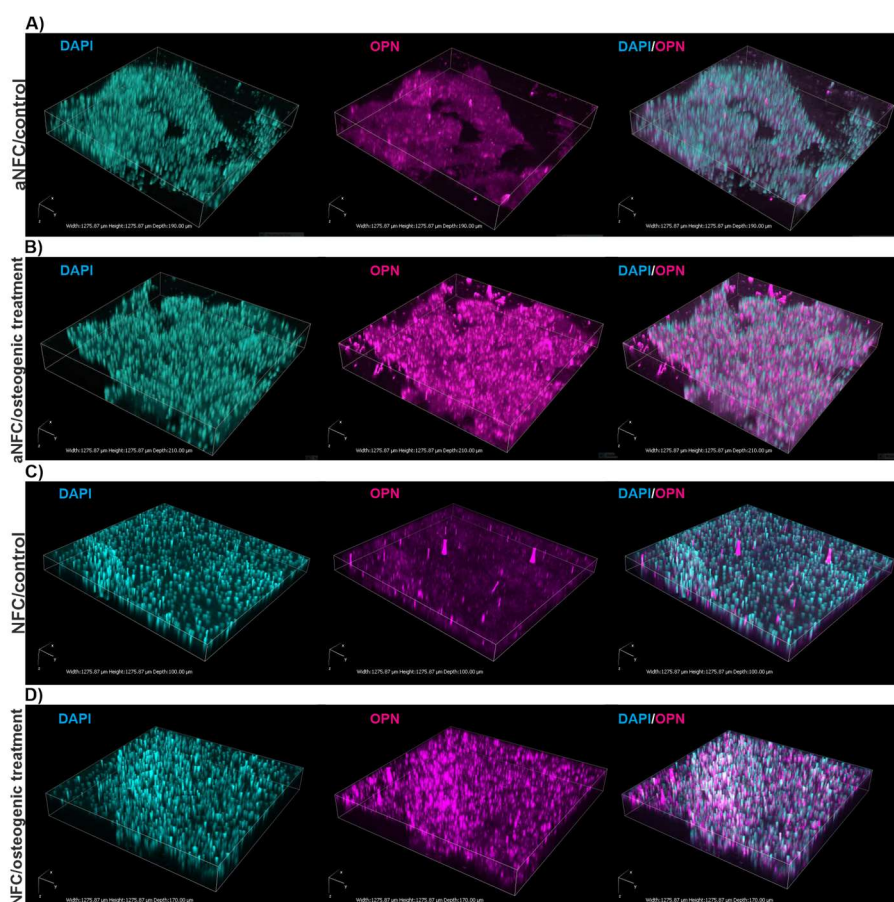
Appendix II

Appendix III

Supplement 4.1. ASCs cultivated in an adipogenic differentiation media at 21 days showed intense lipid droplets stained with Oil Red O compared with cells in a standard media. (A) Chemically stimulated ASCs in an adipogenic differentiation media showed a higher level of lipid droplets when cultivated at 21 days compared with cells in the cultivation media at 21 days. Scale bar: 50µm. (B) Changes in the relative frequency distribution of lipid droplets were analysed and the results of ten different areas per condition were assessed in each experiment by the scatter line. The average size of lipid droplets also increased in cells subjected to adipogenic differentiation. The data showed more intense lipid droplets in the differentiated cells in an adipogenic media. Data were compared using student t-test with unpaired t test Welch's correction. At least three independent experiments were performed. ***P<0.0001 was considered to be statistically significant. The differentiated cells in the adipogenic and osteogenic lineage were proof of multipotency.

A)

B)
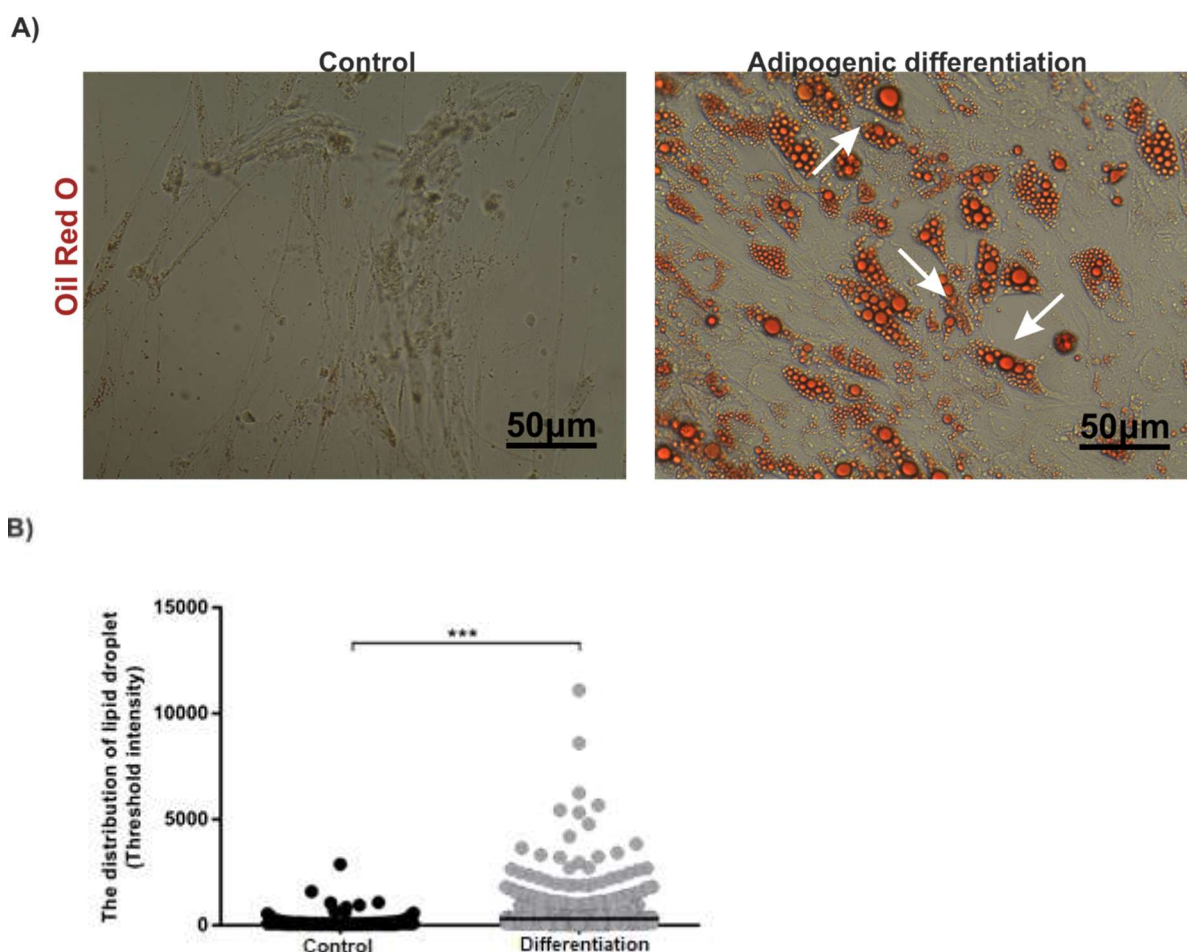
Supplement 4.2. Image-based analysis revealed a higher level of OCN expression in ASCs in 3D under osteogenic conditions for 21 days. (A-B-E) Confocal microscopy was used to visualise and quantify the OCN in the differentiated ASCs embedded in 0.2% aNFC compared with the undifferentiated cells. (C-D-F) Confocal microscopy was used to visualise and quantify the OCN in the differentiated ASCs embedded in 0.2% NFC compared with the undifferentiated cells. OCN expression in ASCs in aNFC showed a higher signal than cells in NFC exposed to osteogenic differentiation.
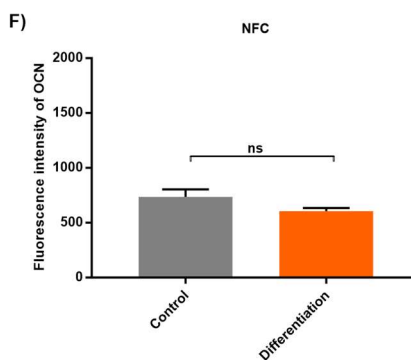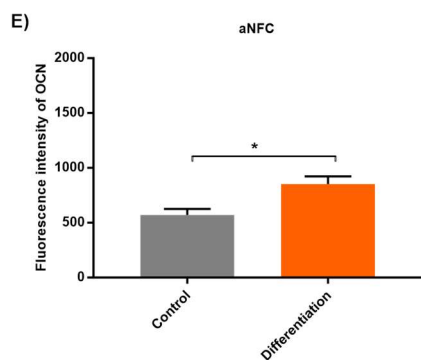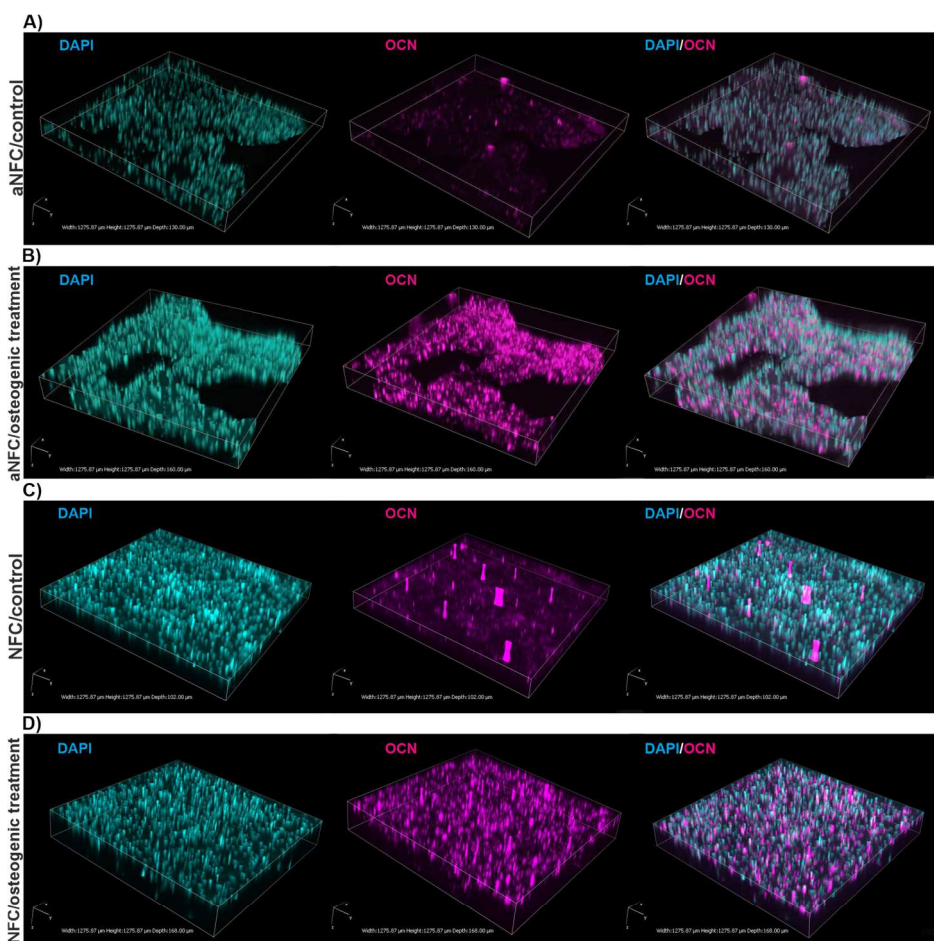
Supplement 4.3. Image-based analysis revealed a higher level of OPN expression in ASCs in 3D under osteogenic conditions for 21 days. (A-B-E) Confocal microscopy was used to visualise and quantify the OPN in the differentiated ASCs embedded in 0.2% aNFC compared with the undifferentiated cells. (C-D-F) Confocal microscopy was used to visualise and quantify the OPN in the differentiated ASCs embedded in 0.2% NFC compared with the undifferentiated cells. Comparison with the results shown in Figure 4.9E-F shows that aNFC works obviously better than NFC in the differentiated cells.
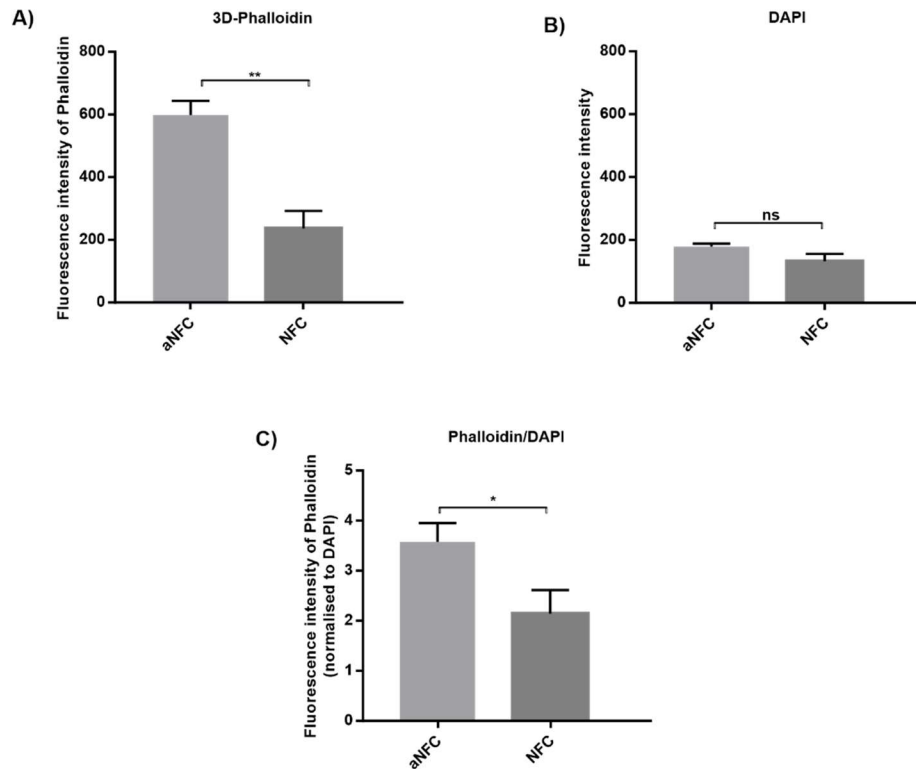
Supplement 4.4. ASCs cultivated in 3D aNFC exhibited intense lipid droplets stained with Oil Red O subjected to adipogenic differentiation media for 21 days compared with cells in the standard media. Chemically stimulated ASCs in an adipogenic differentiation media showed a higher level of lipid droplets when cultivated at 21 days compared with cells in a standard media at 21 days. ASCs in 3D aNFC could be accepted as proof of multipotency when cultivated in adipogenic conditions. Scale bar: 200-50µm.
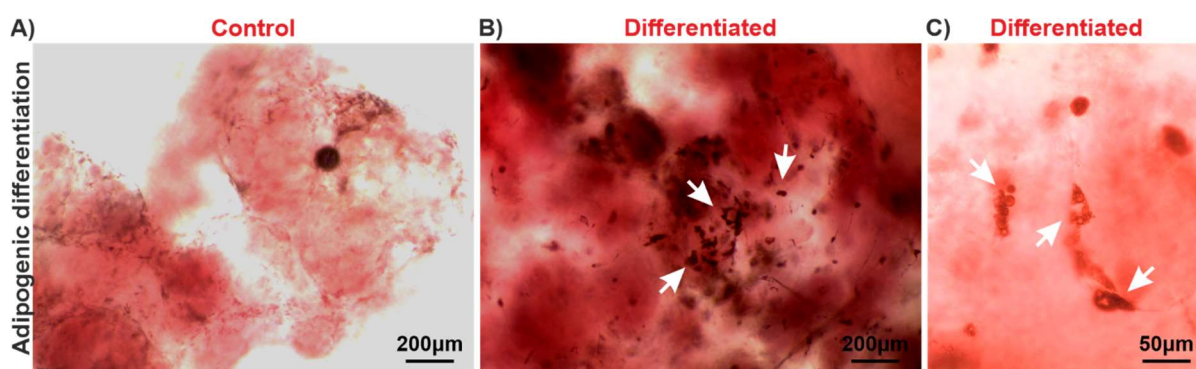
Supplement 4.5. ASCs exposed to osteogenic differentiation display a highly arranged actin cytoskeleton and formation of cell-free pores within the 3D hydrogels. The fluorescence intensity of phalloidin normalised to DAPI was assessed to indicate the increased actin polymerization.
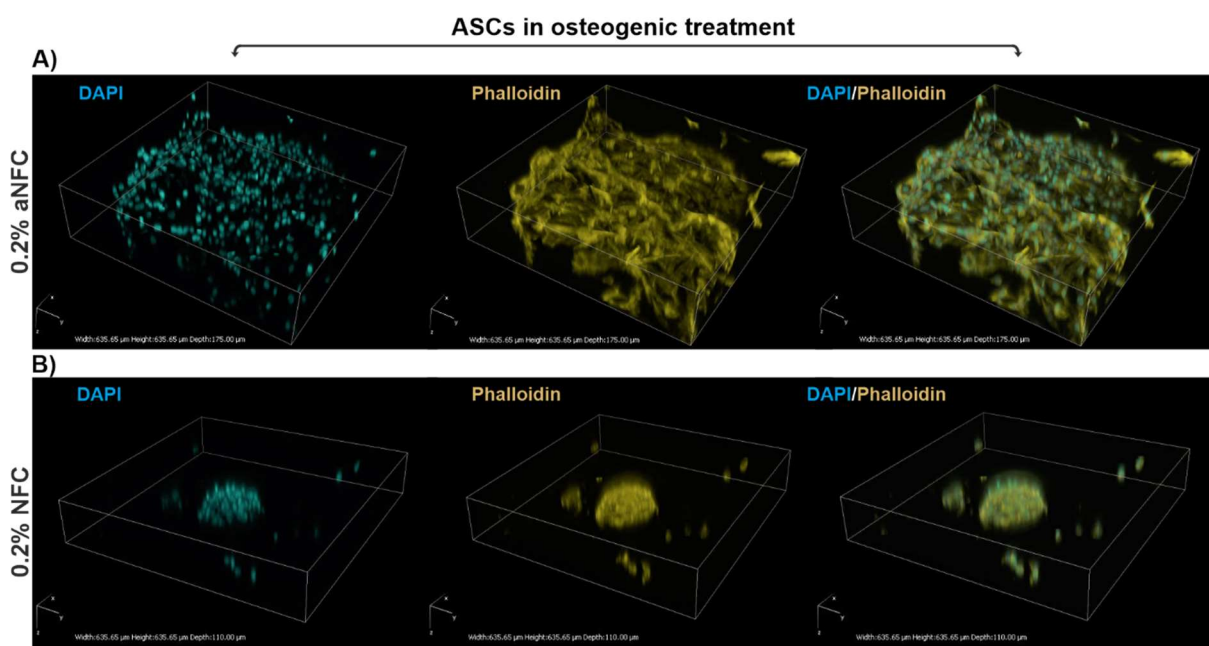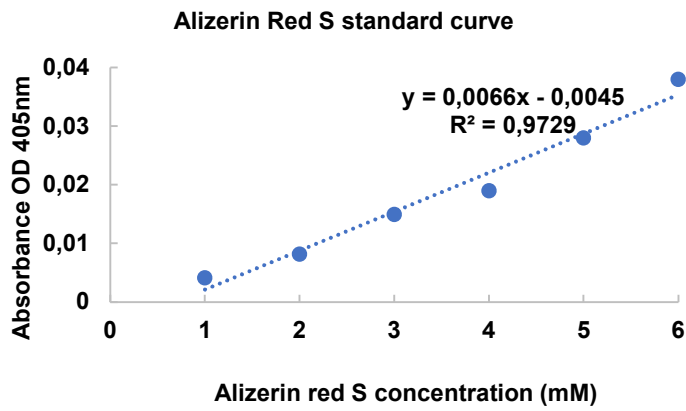
Supplement 4.6. ASCs exposed to osteogenic differentiation display a highly arranged actin cytoskeleton and formation of cell-free pores within the 3D hydrogels. The fluorescence intensity of phalloidin normalised to DAPI was assessed to indicate the increased actin polymerization. The quantification of F-actin filament was determined to detect the fluorescence intensity of phalloidin using Image J software.
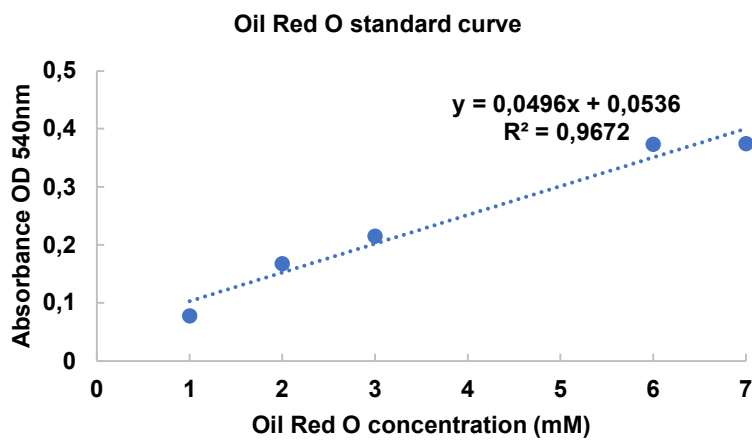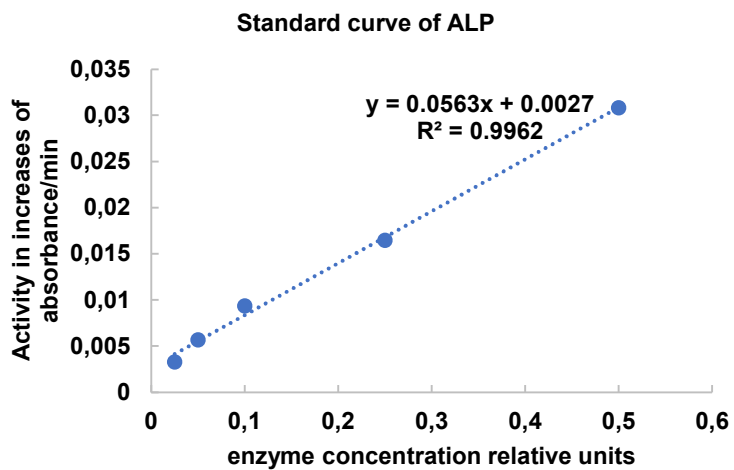
Appendix IV

### Supplement 5.1. Alizarin Red S standard curve

Alizerin Red S standard curve

$y = 0,0066x - 0,0045$
$R^2 = 0,9729$

Absorbance OD 405nm

Alizerin red S concentration (mM)

Supplement 5.2. Oil Red O standard curve

Oil Red O standard curve

$y = 0,0496x + 0,0536$
$R^2 = 0,9672$

Absorbance OD 540nm

Oil Red O concentration (mM)

Supplement 5.3. Alkaline Phosphatase (ALP) standard curve

Standard curve of ALP

$y = 0.0563x + 0.0027$
$R^2 = 0.9962$

Activity in increases of absorbance/min

enzyme concentration relative units

Supplement 5.4. ES increased the osteogenic differentiation potential of ASCs under 2D cell culture conditions. (A) ASCs were exposed to ES (0.1V/cm and 0.3V/cm) in standard and osteogenic medias for up to 21 days followed by assessment of Alizarin Red S fluorescence intensity. Confocal laser-scanning microscopy clearly revealed the presence of nuclei in close proximity to the Alizarin Red S signal. Scale bar: 200µm.
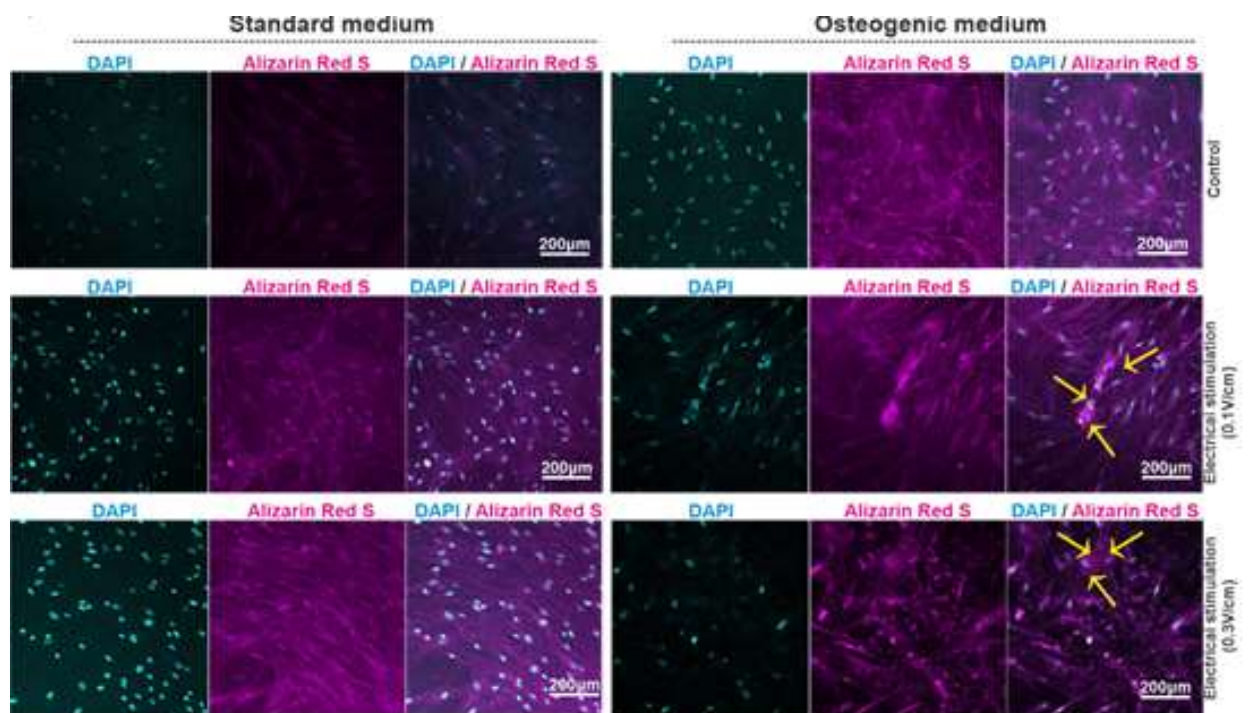
Supplement 5.5. Immunocytochemistry staining of ASCs in 2D performed using a monoclonal antibody (for example OCN) in standard and osteogenic medias when exposed to no ES, 0.1V/cm of ES and 0.3V/cm of ES at day 21.
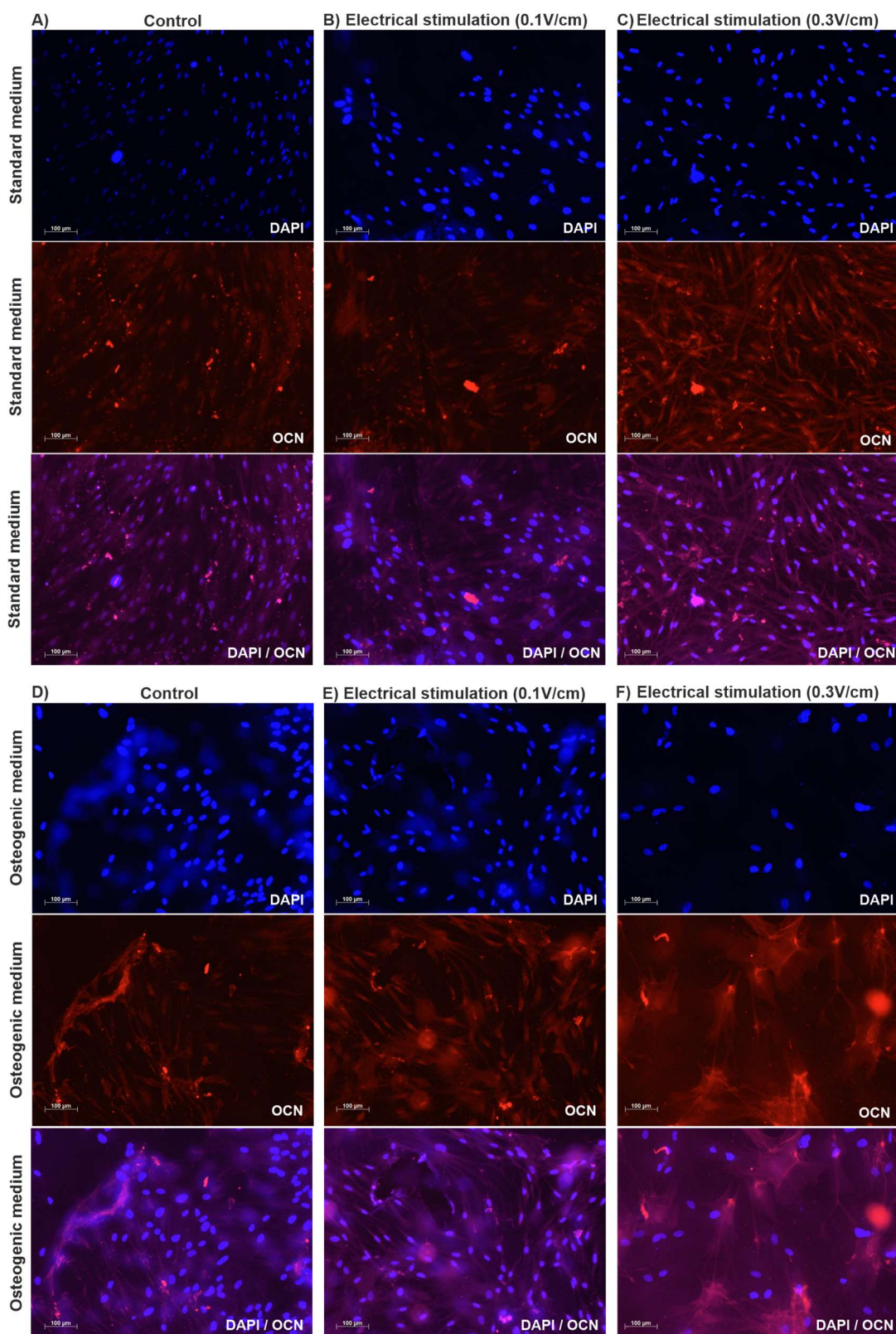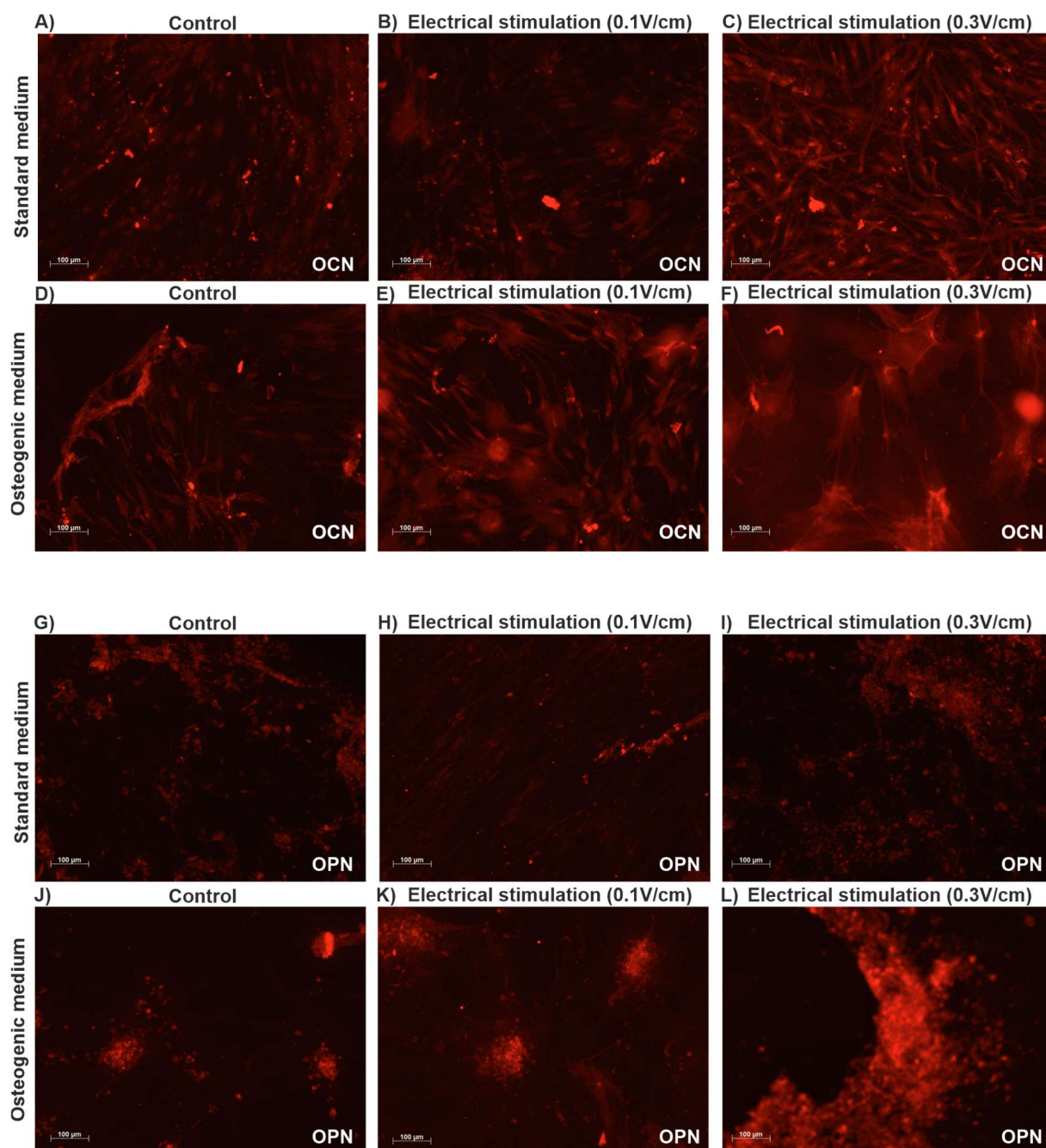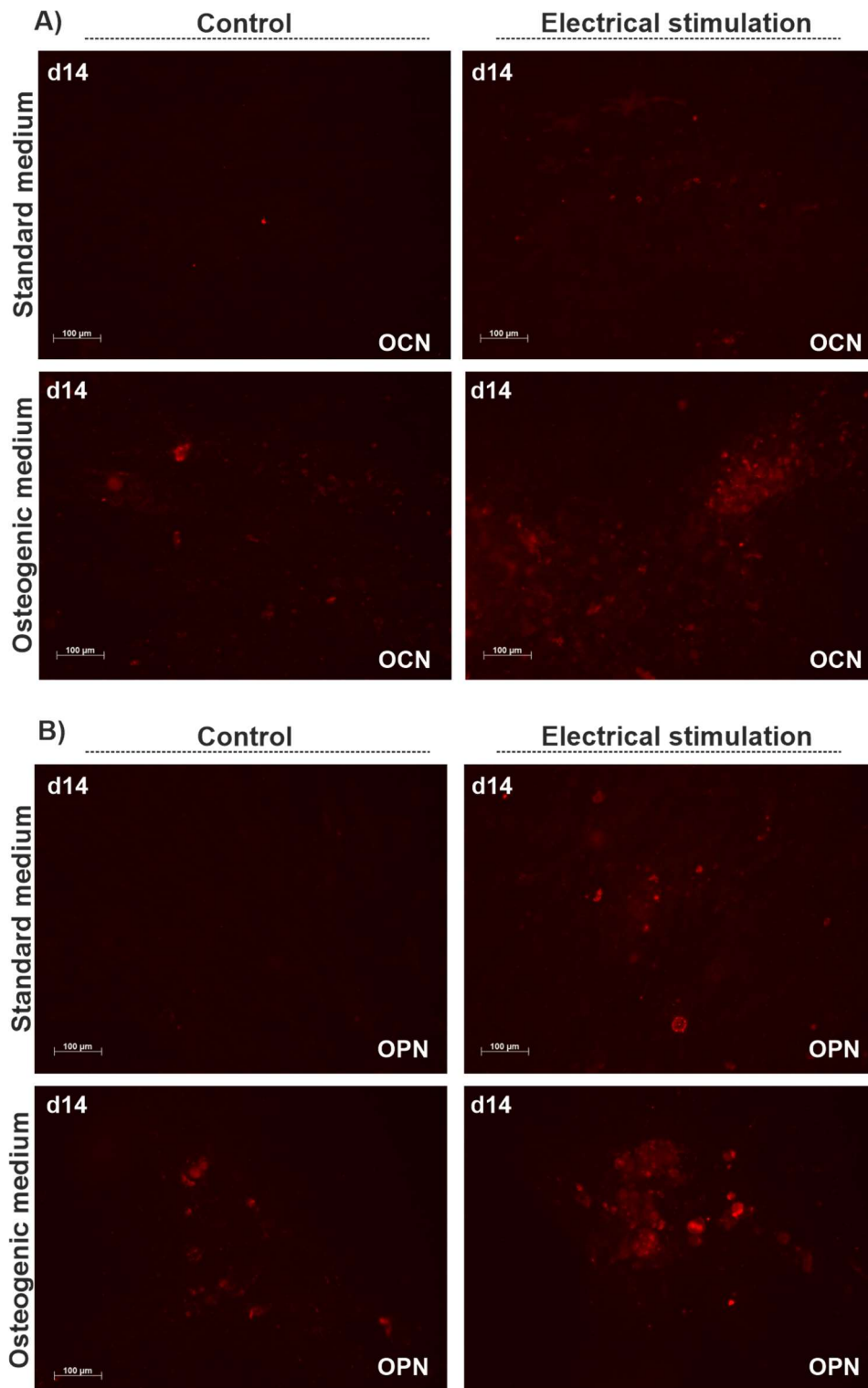
Supplement 5.6. Immunocytochemistry staining of ASCs in 2D performed using a monoclonal antibody (for example OPN) in standard and osteogenic medias when exposed to no ES, 0.1V/cm of ES and 0.3V/cm of ES at day 21.
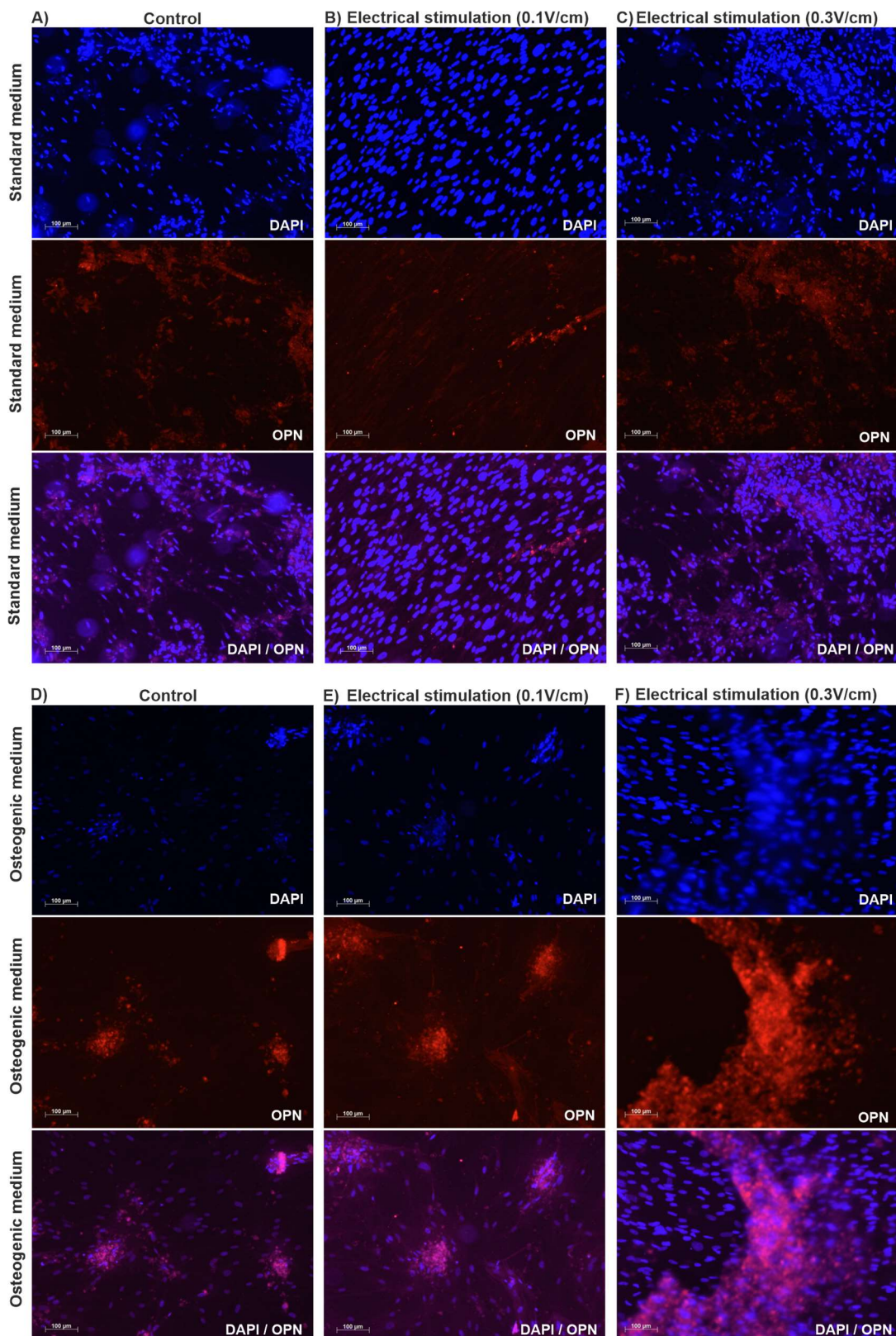
Supplement 5.7. Immunocytochemistry staining of ASCs in 2D performed using a monoclonal antibody (for example OCN and OPN) in standard and osteogenic medias when exposed to no ES, 0.1V/cm of ES and 0.3V/cm of ES at day 21.

Supplement 5.8. Immunocytochemistry staining of ASCs in 2D performed using a monoclonal antibody (for example OCN and OPN) in standard and osteogenic medias when exposed to ES (0.1V/cm) at day 14.

Supplement 5.9. Immunocytochemistry staining of ASCs in 2D performed using a monoclonal antibody (for example OCN and OPN) in standard and osteogenic medias when exposed to ES (0.1V/cm) at day 7.

Supplement 5.10. Immunocytochemistry staining of ASCs in 3D performed using a monoclonal antibody (for example OCN and OPN) in standard and osteogenic medias when exposed to 0.1V/cm of ES at day 14.

Supplement 5.11. Immunocytochemistry staining of ASCs in 3D performed using a monoclonal antibody (for example OCN and OPN) in standard and osteogenic medias when exposed to 0.1V/cm of ES at day 7.